

University of Windsor

Scholarship at UWindor

Electronic Theses and Dissertations

Theses, Dissertations, and Major Papers

3-10-2021

Soybean Peroxidase Catalyzed Oligomerization of Acetaminophen and Selected Parabens for Wastewater Treatment

Baturh Yarkwan
University of Windsor

Follow this and additional works at: <https://scholar.uwindsor.ca/etd>

Recommended Citation

Yarkwan, Baturh, "Soybean Peroxidase Catalyzed Oligomerization of Acetaminophen and Selected Parabens for Wastewater Treatment" (2021). *Electronic Theses and Dissertations*. 8582.
<https://scholar.uwindsor.ca/etd/8582>

This online database contains the full-text of PhD dissertations and Masters' theses of University of Windsor students from 1954 forward. These documents are made available for personal study and research purposes only, in accordance with the Canadian Copyright Act and the Creative Commons license—CC BY-NC-ND (Attribution, Non-Commercial, No Derivative Works). Under this license, works must always be attributed to the copyright holder (original author), cannot be used for any commercial purposes, and may not be altered. Any other use would require the permission of the copyright holder. Students may inquire about withdrawing their dissertation and/or thesis from this database. For additional inquiries, please contact the repository administrator via email (scholarship@uwindsor.ca) or by telephone at 519-253-3000ext. 3208.

**Soybean Peroxidase Catalyzed Oligomerization of Acetaminophen and Selected
Parabens for Wastewater Treatment**

By

Baturh Yarkwan

A Dissertation

**Submitted to the Faculty of Graduate Studies
through the Department of Chemistry and Biochemistry
In Partial Fulfillment of the Requirements for
the Degree of Doctor of Philosophy
at the University of Windsor**

Windsor, Ontario, Canada

2021

© 2021 Baturh Yarkwan

Soybean Peroxidase Catalyzed Oligomerization of Acetaminophen and Selected Parabens for
Wastewater Treatment

by Baturh Yarkwan

APPROVED BY:

A. Bassi, External Examiner
Western University

K. Drouillard
Great Lakes Institute for Environmental Research

J. Trant
Department of Chemistry and Biochemistry

S. Mundle
Department of Chemistry and Biochemistry

N. Biswas, Co-Advisor
Department of Civil and Environmental Engineering

K. Taylor, Co-Advisor
Department of Chemistry and Biochemistry

January 20, 2021

DECLARATION OF ORIGINALITY

I hereby certify that I am the sole author of this thesis and that no part of this thesis has been published or submitted for publication.

I certify that, to the best of my knowledge, my thesis does not infringe upon anyone's copyright nor violate any proprietary rights and that any ideas, techniques, quotations, or any other material from the work of other people included in my thesis, published or otherwise, are fully acknowledged in accordance with the standard referencing practices. Furthermore, to the extent that I have included copyrighted material that surpasses the bounds of fair dealing within the meaning of the Canada Copyright Act, I certify that I have obtained a written permission from the copyright owner(s) to include such material(s) in my thesis and have included copies of such copyright clearances to my appendix.

I declare that this is a true copy of my thesis, including any final revisions, as approved by my thesis committee and the Graduate Studies office, and that this thesis has not been submitted for a higher degree to any other University or Institution.

ABSTRACT

Esters of *para*-hydroxybenzoic acid (parabens) commonly used as universal preservatives, *para*-hydroxybenzoic acid, the degradation intermediate of parabens and the common analgesic/antipyretic pharmaceutically active ingredient, acetaminophen have been detected in the environment around the world largely because they are inefficiently removed by conventional wastewater treatment processes. These compounds are emerging contaminants, thus necessitating research for an alternative treatment regimen for their efficient removal from wastewater treatment plants effluent before discharge into receiving water bodies. Soybean peroxidase-catalyzed reaction in the presence of peroxide at appropriate pH was employed to treat these contaminants in synthetic wastewater with compound removal monitored using high performance liquid chromatography. Oligomers formed were determined with the aid of mass spectroscopy, using appropriate ionization techniques. The parameters influencing the removal process were optimized, both for single-compound treatment and in a mixture of the five compounds (mix-5), targeting $\geq 95\%$ removal efficiency under both study conditions. Optimal pH for four single compounds was 6.5 while that for acetaminophen was 8.0; mix-5 showed optimal removal at pH 6.5. SBP requirement varied between 0.006 U/mL and 2.3 U/mL in the increasing order of Acetaminophen < propyl paraben < butyl paraben < *para*-hydroxybenzoic acid < methyl paraben in single-compound (1.0 mM) treatment while 1.43 U/mL was optimal for the mixture treatment (0.2 mM each). Optimal peroxide was in the order of propyl paraben = butyl paraben < acetaminophen < methyl paraben < *para*-hydroxybenzoic acid which correspond to the peroxide-substrate ratio and ranging from 1.15 mM to 2.0 mM. Step-feeding of peroxide was able to achieve the target removal efficiency for poorly removed single compounds and those in mix-5. Time course studies for single-compounds showed initial pseudo-first-order kinetics for all the compounds, with the normalized rate constants in the order acetaminophen > butyl paraben \approx propyl paraben > *para*-hydroxybenzoic acid \approx methyl paraben but followed the order of acetaminophen > butyl paraben > *para*-hydroxybenzoic acid > propyl paraben \approx methyl paraben in mix-5. Mass spectroscopic analysis for single compounds showed the formation of oligomers of varying

sizes ranging from dimers of *para*-hydroxybenzoic acid, to pentamers of acetaminophen, hexamers of propyl paraben and heptamers of methyl paraben and butyl paraben. Mass spectral analysis of mix-5 showed evidence of homo- and hetero-oligomers up to pentamers. The results support the possibility of soybean peroxidase-catalyzed treatment of the contaminants of emerging concern, both as single compounds and as a mixture. The possibility of mixture treatment is important for dealing with real wastewater effluents. These results show prospects for scaled-up processes with potential applications to hospital, industrial and pharmaceutical company wastes where these compounds may be predominantly found, before discharging such wastewaters to municipal treatment plants and thence receiving water bodies.

DEDICATION

The trio by whom my life was formed – Yamasa Baturh, Yarkwan S. Baturh, both of blessed memory and Kpennan H. Yarkwan; and the second trio, who are at the center of my daily life – Sylvia, Mhoonom and An-Alu. To you, I joyfully dedicate this dissertation.

Thus says the LORD:

“Let not the wise *man* glory in his wisdom,
Let not the mighty *man* glory in his might,
Nor let the rich *man* glory in his riches;
But let him who glories glory in this,
That he understands and knows Me,
That I *am* the LORD, exercising lovingkindness, judgment, and
righteousness in the earth.
For in these I delight,” says the LORD.

Jeremiah 9: 23-24 (NKJV)

ACKNOWLEDGEMENT

The choice to mention names is often a decision to the unavoidable mistake of skipping some key persons. Though I cannot shy away from mentioning some, I apologize in advance to those who should be here but may not be included. Even though my heart deeply acknowledges and appreciates your love and care.

My profound gratitude goes to my Supervisors, Drs. K.E. Taylor and Nihar Biswas for graciously taking me into their research group and nursing these fluidic ideas which have become a tangible substance embodied in this dissertation. Your patience and mentoring prowess will ever be appreciated. Thanks to Dr. J.K. Bewtra, whose incisive contributions at our team meetings have remained very insightful. Thanks to my committee members – Drs. John Trant, Scott Mundle and Ken Drouillard for their availability and constructive criticisms. I am very grateful to Dr. Bassi, for accepting to serve as my external examiner.

Thanks to the several professors and staff I had the opportunity to learn from during my training. Special thanks to Dr. H.S. Eichhorn in this regard. Marlene Bezaire deserves special accolades for her personal commitment to the success of my stay in Windsor. To the several colleagues in graduate school, your warmth of friendship is highly appreciated. Thanks to all colleagues, past and present in Taylor-Biswas group – Miao, Laura, Neda, Debjani, Kayven, June, Amanpreet, Negin, Samira, Stefano, Victoria, Maxim, Thomas, Lily, Nicola. You have been incredibly awesome in your unique ways.

To these amazing people I extend my profound gratitude – Joe Lichaa, who is always “happy to help”, Dr. Auld, who taught me the use of MassLynx, and Tina and the CCC team. Thanks to Bill for servicing our lab instruments.

Thanks to the Nigerian government through Federal University of Agriculture, Makurdi for providing part funding for my Ph.D. training. I appreciate the University of Windsor for International Doctoral entrance scholarship. I am grateful to NSERC through the research grants of my supervisors for consumables used during this training.

The Campbell Baptist Church family had been more than home for us. Thanks to Larry and Doreen Cheshire, Ken and Ann-Marie Dundas, David and Cristina Lahoud – in whose

basement part of this dissertation was written, Carolyn and David Doerkson, John and Linda Corrente, Dr. John and Meline Guy, Gabrielle Desjarlin and the several other brethren who labored along with us to ensure I sail through all the hurdles. You made us feel at home, when we were thousands of kilometers away from our native home.

The love from our Nigerian community in Windsor have been overwhelming. Sis Chi, the Afolabi's, Sabageh's, Anagor's,... may God bless you richly. Thanks to Sunday Akande, who made the great sacrifice of allowing me work in his home while the lockdown came in effect. Thank you, Bonaventure Molokwu, for freely designing the program that helped do all the combinational patterns of mix-5, which I needed to interpret mass spectrometry data. Thanks to Amos Iorliam and Oliver Iorhemem, for the encouragements and advises.

Special thanks to my VC, Prof. R.A. Kimbir and Registrar, Mrs. Helen Nyitse. Thanks to Prof. E.I Kucha, the immediate past VC who approved my foreign training. I am indebted to my HOD and Dean, Prof. (Mrs.) RAI Ega and Prof. Amah, respectively, for all the assistance. To the several colleagues at Dept. of Biochemistry, FUAM, I deeply appreciate your sacrifices during my study leave. Special gratitude is reserved to HRH Prof. J.O.I. Ayatse, Tor Tiv V, by whose signature, God enlisted me among the academics at UAM.

I am eternally indebted to my family and in-laws for their support. Thanks to my wife Sylvia, who endured protracted hours tending our little ones while I “fought” with all the instruments of the lab. Thanks especially for your moral support during times I was at the verge of tipping off over the cliff into irrecoverable despair. God bless you richly, my wife. You made me know the unconditional love of a father and your sweet words “Daddy” have always resonated in my ears...thanks, Mhoonom and An-Alu. You such great daughters.

To my disciplers, Dr. and Mrs Adegorite, the TRINA brethren, especially Mr. and Mrs. Zach Akinkuade, for your spiritual care and generosity, I say thanks to all of you.

Finally, if not for life, how could I be here today. Unto God, the creator and giver of life, I return all thanks for everything I am, and will ever be, for I know, a man has nothing except it is given of him from above. Thanks, O Lord for giving me even this one.

TABLE OF CONTENTS

DECLARATION OF ORIGINALITY	iii
ABSTRACT	iv
DEDICATION	vi
ACKNOWLEDGEMENTS	vii
LIST OF TABLES	xiv
LIST OF FIGURES	xvi
LIST OF APPENDICES	xxvii
LIST OF ABBREVIATIONS	xxviii
CHAPTER 1: INTRODUCTION	1
1.0 Background	1
1.1 Sources of CECs in the environment.....	1
1.2 Effects of CECs	3
1.3 Wastewater treatment technologies	4
1.3.1 Enzymatic treatment of CECs	5
1.4 Research objectives	7
CHAPTER 2: LITERATURE REVIEW	8
2.0 Viewing an ancient problem through new lenses	8
2.1 A broad class of pollutants	9
2.2 Environmental burden of PPCPs	9
2.2.1 Environmental pollutants exist in mixture.....	12
2.3. Transformation of parent CECs	13
2.3.1 Environmental transformations	13
2.3.2. Transformation during wastewater disinfection	14

2.4 Occurrence of CECs	15
2.4.1 Parabens in humans – factors and occurrences	15
2.4.2 Acetaminophen in the environment	20
2.5 Effects of the CECs in humans and aquatic organisms	21
2.6 Environmental transformation of phenolics	23
2.6.1. Biotransformation of phenolics – the example of acetaminophen	23
2.6.3 Environmental transformation of phenolics through CDOM	25
2.7 Brief overview of conventional wastewater treatment processes	28
2.8 Advanced Oxidation Processes (AOPs)	29
2.8.1 Ozonation	30
2.8.2. Fenton and Electro-Fenton (EF) AOPs	32
2.8.3 Electrochemical oxidation as an AOP	35
2.8.4 Other AOPs	36
2.9. Oxidoreductases in wastewater treatment	37
2.9.1 Tyrosinases	37
2.9.2. Laccases	38
2.9.3 Peroxidases	39
2.9.3.1 Structural features and properties of HRP C and SBP	40
2.9.3.2. Amino acids involved in catalysis	42
2.9.3.3. Catalysis in peroxidases	44
2.9.3.3.1 Formation of compound I	44
2.9.3.3.2 Compound II	45

2.9.3.3.3 Compound III	45
2.9.3.4 Applications of peroxidases in treatment of CECs	46
2.9.3.5 Apparent inactivation of HRP/SBP during catalysis	46
2.9.3.6 SBP catalyzed phenolic oligomerization	47
2.9.3.7 Selling points of SBP	48
2.9.3.8 Effects of dissolved substances on peroxidase-catalyzed removal of phenolics	50
2.10 Mass Spectrometry (MS) in environmental studies	52
2.11 Summary of literature as related to dissertation	52
CHAPTER 3: MATERIALS AND METHODS	54
3.0 Chemicals and enzymes	54
3.1.0 Buffer salts and standard buffers	54
3.1.1 Buffers: choice and preparation	55
3.1.2. Preparation of compound stock solutions	55
3.2 HPLC solvents and Accessories	55
3.3 Instruments	56
3.3.1 UV-Vis spectrophotometer	56
3.3.2 HPLC and HPLC protocols	56
3.4 SBP Activity assay	58
3.4.1 SBP extraction	58
3.4.2 Preparation of 10x Phenol reagent	58
3.4.3 SBP activity assay	58

3.5 Hydrogen peroxide assay	59
3.5.1 Effects of incremental addition of hydrogen peroxide on substrate Removal	60
3.6 Batch reactor protocol	60
3.7 Mass spectrometry analysis	62
3.8 Sources of error	63
CHAPTER 4: RESULTS and DISCUSSION	64
4.0 SBP reaction parameters optimization: an overview.....	64
4.1 pH optimization	65
4.1.1 Range-finding experiments	65
4.1.2 pH optimization – narrow-range experiments	70
4.2 SBP optimization for the oligomerization of CECs	74
4.2.1 Range finding	74
4.2.2 SBP optimization for the oligomerization of CECs – narrow range.....	78
4.3 Hydrogen peroxide optimization	84
4.4 Mixed existence demands mixed treatment – exploring possibilities	90
4.4.1 Optimizations for mix-5 treatment	92
4.5 Time Course Studies – Single-Compound and Mix-5.....	107
4.6 Mass spectral evidence for formation of oligomers following SBP treatment	116
4.6.1 Acetaminophen	117
4.6.2 Structural isomerism in acetaminophen oligomerization	127
4.6.3 Mass spectral analysis of PHBA	131
4.6.4 Mass spectral analysis of parabens – methyl paraben.....	132
4.6.5 Mass spectral analysis of PP.....	142
4.6.6 Mass spectral analysis of butyl paraben	149

4.7 Effect of desolvation gas temperature on molecular ions	158
4.8 Mass spectral analysis of mix-5 precipitates	160
4.8.1 Dimers from mix-5 precipitate	162
4.8.2 Trimers from mix-5 precipitate	171
4.8.3 Tetramers from mix-5 precipitate	187
4.8.4 Pentamers from mix-5 precipitate	194
CHAPTER 5: SUMMARY, CONCLUSIONS AND RECOMMENDATIONS	203
5.0 Summary	203
5.1 Conclusions	205
5.2 Recommendations for future studies	206
REFERENCES	208
APPENDICES	241
VITA AUCTORIS	261

LIST OF TABLES

Table 2.1 Physicochemical parameters of the studied CECs	11
Table 2.2: Concentrations of CECs in different environmental matrices	12
Table 2.3 Concentration (ng/g of indoor air) of PB in indoor air and estimated daily intakes (ng/kg bw/day)	16
Table 2.4 Parabens in human samples	18
Table 3.1: HPLC analytical conditions for the analysis of the CECs (flow rate 1.0 mL/min)	57
Table 4.1: Summary of parameter optimization and removals of studied CECs	90
Table 4-2: Summary of % remaining of MP, PP and BP under three different treatment conditions	104
Table 4-3: Summary of % improvements in parabens removal efficiency between different treatment processes	105
Table 4-4 Summary of chemical reaction kinetics for single-compound studies ...	112
Table 4-5 Summary of reaction kinetics for mix-5 under optimized conditions	115
Table 4-6 Acetaminophen monomer and oligomers following SBP treatment	120
Table 4-7 PHBA and oligomers following SBP treatment as observed from supernatant using ASAP(+)	132
Table 4-8 MP and oligomers following SBP treatment as observed from precipitate using ASAP(-)	134
Table 4-9 PP and oligomers following SBP treatment as observed from precipitate and supernatant	144
Table 4-10 BP and oligomers following SBP treatment as	

observed from precipitate and supernatant.....	151
Table 4-11 Effects of ionization temperature on detection of molecular ions in ASAP(-)	160
Table 4-12 Dimers detected from mix-5 precipitate under optimized conditions using ASAP(+)	162
Table 4-13 Trimers detected from mix-5 precipitate under optimized conditions using ASAP(+)	172
Table 4-14 Tetramers detected from mix-5 precipitate under optimized conditions using ASAP(+)	187
Table 4-15 Pentamers detected from mix-5 precipitate under optimized conditions using ASAP(+)	195
Table C-1 Summary of analytical parameters for single-compound analysis of studied CECs	247
Table D-1 Summary of retention times and calibration curves' properties of CECs in mix-5 at 247 nm	250
Table G-1 Recovery of compounds in mix-5 following SPE	260

LIST OF FIGURES

Fig.2.1: Proposed mechanism for transformation of acetaminophen in soil	24
Fig. 2.2: Mechanism of ³ CDOM* generation and quenching	26
Fig. 2.3: Proposed initial steps in the indirect photodegradation of Acetaminophen	28
Fig. 2. 4: Fenton reaction scheme (Raoudi <i>et al.</i> 2018, Deng and Zhao 2015)	33
Figure 2.5 Three-dimensional crystal structure of HRP C.	41
Fig.2.6 Peroxidase cycle	43
Fig.2.7 Resonance pattern of phenol	48
Fig. 2.8. Annual soybean production in Ontario and Canada	50
Fig. 4-1: pH optimization of acetaminophen – range finding.....	66
Fig. 4-2. pH optimization of PHBA – range finding	67
Fig. 4-3. pH optimization of MP – range finding	68
Fig. 4-4. pH optimization of PP – range finding	69
Fig. 4-5. pH optimization of BP – range finding	69
Fig. 4-6. pH optimization for acetaminophen – narrow-range	70
Fig. 4-7. pH optimization for PHBA – narrow-range	71
Fig. 4-8. pH optimization for MP narrow-range	72
Fig. 4-9. pH optimization for PP – narrow-range	72
Fig. 4-10. pH optimization for BP – narrow-range	73
Fig. 4-11. SBP optimization of acetaminophen – range finding	74
Fig. 4-12. SBP optimization of PHBA – range finding	75
Fig. 4-13. SBP optimization for MP – range finding	77
Fig. 4-14. SBP optimization for PP – range finding	77
Fig. 4-15. SBP optimization of BP –range finding	78
Fig. 4-16. SBP optimization of acetaminophen – narrow range	79
Fig. 4-17. SBP optimization for PHBA – narrow range	79
Fig. 4-18. SBP optimization for MP – narrow range	81

Fig. 4-19. SBP optimization for PP – narrow range	81
Fig. 4-20. SBP optimization for BP –narrow range	82
Fig. 4-21. Hydrogen peroxide optimization of acetaminophen	85
Fig. 4-22. Hydrogen peroxide optimization for PHBA	86
Fig. 4-23. Hydrogen peroxide optimization for MP	86
Fig. 4-24. Hydrogen peroxide optimization for PP	87
Fig. 4.25. Hydrogen peroxide optimization for BP	88
Fig. 4-26. pH optimization for removal of mix-5 – range finding	93
Fig.4-27 pH optimization of mix-5 – narrow range	94
Fig.4-28 pH optimization of mix-5: Narrow range with reduced amount of SBP ...	95
Fig. 4-29 pH optimization of mix-5 – narrow range with further reduced amount of SBP	96
Fig. 4-30 SBP optimization of mix-5 – range finding	98
Fig. 4-31 SBP optimization of mix-5 – narrow range	98
Fig. 4-32 Hydrogen peroxide optimization of mix-5 – range finding	99
Fig. 4-33 Hydrogen optimization of mix-5 – narrow range	100
Fig.4-34 Effects of extended incubation time on mix-5 removal	101
Fig.4-35 Effect of centrifugation, extended incubation time, and additional SBP and H ₂ O ₂ on removal of mix-5	102
Fig.4-36 Effect of incremental addition of hydrogen peroxide at about the longest half of the individual mix-5 component	103
Fig. 4-37 Effect of incremental addition of hydrogen peroxide at about twice of the longest half of the individual mix-5 component	104
Fig. 4-38 Time course for acetaminophen under optimized conditions	109
Fig. 4-39 Time course for PHBA under optimized conditions	110
Fig. 4-40 Time course for MP under optimized conditions	110
Fig.4-41 Time course for PP under optimized conditions	111
Fig.4-42 Time course for BP under optimized conditions	111
Fig.4-43 Time course for mix-5 under optimized for first 2 minutes	113

Fig.4-44 Time course for mix-5 under optimized conditions	114
Fig.4-45 ESI(+) mass spectrum of acetaminophen	118
Fig. 4-46 ESI(+) mass spectrum of acetaminophen supernatant	119
Fig. 4-47 ESI(+) mass spectrum of acetaminophen precipitate under optimized conditions	119
Fig. 4-48 ESI(+) mass spectrum of acetaminophen supernatant under optimized conditions	122
Fig. 4-49 ESI(+) mass spectrum of acetaminophen precipitate under optimized conditions showing dimer and its sodium salt	123
Fig. 4-50 ESI(+) mass spectrum of acetaminophen supernatant under optimized conditions showing dimer and its sodium salt	123
Fig. 4-51 ESI(+) mass spectrum of acetaminophen precipitate under optimized conditions showing trimer and its sodium salt	123
Fig. 4-52 ESI(+) mass spectrum of acetaminophen supernatant under optimized conditions showing trimer	123
Fig. 4-53 ESI(+) mass spectrum of acetaminophen precipitate under optimized conditions showing tetramer and its sodium salt	125
Fig. 4-54 ESI(+) mass spectrum of acetaminophen supernatant under optimized conditions showing tetramer and its sodium salt	125
Fig. 4-55 ESI(+) mass spectrum of acetaminophen precipitate under optimized conditions showing pentamer and its sodium salt	126
Fig.4-56 Proposed structures of acetaminophen modified monomer and oligomers formed following SBP treatment under optimized conditions	127
Fig.4-57 Oxidative coupling pattern of acetaminophen molecules under enzyme catalyzed reactions	128
Fig.4-58 Semiempirical calculations of the distribution of spin and charge densities in an acetaminophen radical	130
Fig. 4-59 Proposed mechanism of SBP-catalyzed oligomerization of Acetaminophen	130

Fig. 4-60 ASAP(+) mass spectrum of PHBA supernatant under optimized conditions	131
Fig. 4-61 ASAP(+) mass spectrum of PHBA supernatant under optimized conditions showing dimer.....	131
Fig. 4-62 proposed structure of PHBA dimer formed under optimized conditions ...	132
Fig. 4-63 ASAP(-) full scan mass spectrum of MP	133
Fig. 4-64 ASAP(-) full scan mass spectrum of MP precipitate	135
Fig. 4-65 ASAP(-) mass spectrum of MP precipitate between 110 and 175 m/z	135
Fig. 4-66 ASAP(-) mass spectrum of MP precipitate under optimized conditions showing dimer and oxygenated dimer	136
Fig. 4-67 ASAP(-) mass spectrum of MP precipitate under the optimized conditions showing trimer and oxygenated trimer	137
Fig. 4-68 ASAP(-) mass spectrum of MP precipitate	138
Fig. 4-69 ASAP(-) mass spectrum of MP precipitate at the optimized conditions showing pentamer and oxygenated pentamer	138
Fig. 4-70 ASAP(-) mass spectrum of MP precipitate under optimized conditions showing hexamer and oxygenated hexamer	139
Fig. 4-71 ASAP(-) mass spectrum of MP precipitate under optimized conditions showing heptamer and oxygenated heptamer	140
Fig. 4-72 proposed structures for the oligomers of MP found in precipitate under optimized conditions	142
Fig. 4-73 ASAP(-) mass spectrum showing PP standard between 50 and 1200 m/z ...	143
Fig.4-74 ASAP(-) mass spectrum showing PP precipitate	144
Fig.4-75 ASAP(-) mass spectrum of PP under optimized conditions showing dimer and oxygenated dimer	145
Fig. 4-76 ASAP(-) mass spectrum of PP precipitate under optimized conditions showing trimer and oxygenated trimer	146
Fig. 4-77 ASAP(-) mass spectrum of PP precipitate under optimized conditions	

showing tetramer and oxygenated tetramer	146
Fig. 4-78 ASAP(-) mass spectrum of PP precipitate under optimized conditions showing pentamer and oxygenated pentamer	147
Fig. 4-79 ASAP(-) mass spectrum of PP precipitate under optimized conditions showing hexamer and oxygenated hexamer	148
Fig.4-80 Proposed structures for oligomers of PP	149
Fig. 4-81 ASAP(-) mass spectrum of BP	150
Fig.4-82 ASAP(-) mass spectrum of BP precipitate showing entire pane	151
Fig.4-83 ASAP(-) mass spectrum of BP precipitate showing dimer and oxygenated dimer	152
Fig.4-84 ASAP(-) mass spectrum of BP precipitate showing trimer and oxygenated trimer	153
Fig. 4-85 ASAP(-) mass spectrum of BP precipitate showing tetramer and oxygenated tetramer	153
Fig.4-86 ASAP(-) mass spectrum of BP precipitate showing pentamer and oxygenated pentamer	154
Fig. 4-87 ASAP(-) mass spectrum of BP precipitate showing hexamer and oxygenated hexamer	154
Fig. 4-88 ASAP(-) mass spectrum of BP precipitate showing heptamer and oxygenated heptamers	155
Fig. 4-89 Proposed structural formula for the oligomers of BP (R=C ₄ H ₉)	156
Fig.4-90 Proposed reaction pathway for oligomerization of Parabens following SBP treatment	157
Fig. 4-91 ASAP(-) mass spectrum of MP at three different desolvation gas temperatures	159
Fig. 4-92 Full scan ASAP(+) mass spectrum of mix-5 precipitate under optimized conditions	163

Fig. 4-93 ASAP(+) mass spectrum of mix-5 precipitate under optimized conditions showing a homo-dimer of Acetaminophen	164
Fig. 4-94 ASAP(+) mass spectrum of mix-5 precipitate under optimized conditions showing a dimer of PHBA-PHBA	164
Fig. 4-95 ASAP(+) mass spectrum of mix-5 precipitate under optimized conditions showing a dimer of PHBA-MP	165
Fig. 4-96 ASAP(+) mass spectrum of mix-5 precipitate under optimized conditions showing a dimer of PHBA-PP	166
Fig.4-97 ASAP(+) mass spectrum of mix-5 precipitate under optimized conditions showing a dimer of PHBA-BP	167
Fig.4-98 ASAP(+) mass spectrum of mix-5 precipitate under optimized conditions showing a dimer of MP-MP	167
Fig. 4-99 ASAP(+) mass spectrum of mix-5 precipitate under optimized conditions showing a dimer of MP-PP	168
Fig. 4-100 ASAP(+) mass spectrum of mix-5 precipitate under optimized conditions showing a dimer of MP-BP	168
Fig. 4-101 ASAP(+) mass spectrum of mix-5 precipitate under optimized conditions showing a dimer of PP-PP	169
Fig. 4-102 ASAP(+) mass spectrum of mix-5 precipitate under optimized conditions showing a dimer of PP-BP	169
Fig. 4-103 ASAP(+) mass spectrum of mix-5 precipitate under optimized conditions showing a dimer of BP-BP	170
Fig.4-104 Proposed structural formulae for the dimers of mix-5 under optimized conditions	171
Fig. 4-105 ASAP(+) mass spectrum of mix-5 precipitate under optimized conditions showing a trimer of PHBA-PHBA-MP	173
Fig. 4-106 ASAP(+) mass spectrum of mix-5 precipitate under optimized conditions showing a trimer of PHBA-PHBA-PP	173
Fig. 4-107 ASAP(+) mass spectrum of mix-5 precipitate under	

optimized conditions showing a trimer of PHBA-PHBA-BP	174
Fig. 4-108 ASAP(+) mass spectrum of mix-5 precipitate under optimized conditions showing a trimer of PHBA-MP-MP	175
Fig. 4-109 ASAP(+) mass spectrum of mix-5 precipitate under optimized conditions showing a trimer of PHBA-MP-PP	175
Fig. 4-110 ASAP(+) mass spectrum of mix-5 precipitate under optimized conditions showing a trimer of PHBA-MP-BP	176
Fig. 4-111 ASAP(+) mass spectrum of mix-5 precipitate under optimized conditions showing a trimer of PHBA-PP-PP	177
Fig. 4-112 ASAP(+) mass spectrum of mix-5 precipitate under optimized conditions showing a trimer of PHBA-PP-BP	177
Fig. 4-113 ASAP(+) mass spectrum of mix-5 precipitate under optimized conditions showing a trimer of PHBA-BP-BP	178
Fig. 4-114 ASAP(+) mass spectrum of mix-5 precipitate under optimized conditions showing a trimer of MP-MP-MP	179
Fig. 4-115 ASAP(+) mass spectrum of mix-5 precipitate under optimized conditions showing a trimer of MP-MP-PP	179
Fig. 4-116 ASAP(+) mass spectrum of mix-5 precipitate under optimized conditions showing a trimer of MP-MP-BP	180
Fig. 4-117 ASAP(+) mass spectrum of mix-5 precipitate under optimized conditions showing a trimer of MP-PP-PP	181
Fig. 4-118 ASAP(+) mass spectrum of mix-5 precipitate under optimized conditions showing a trimer of MP-PP-BP	181
Fig. 4-119 ASAP(+) mass spectrum of mix-5 precipitate under optimized conditions showing a trimer of MP-BP-BP	182
Fig. 4-120 ASAP(+) mass spectrum of mix-5 precipitate under optimized conditions showing a trimer of PP-PP-PP	182
Fig. 4-121 ASAP(+) mass spectrum of mix-5 precipitate under optimized conditions showing a trimer of PP-PP-BP	183
Fig. 4-122 ASAP(+) mass spectrum of mix-5 precipitate under	

optimized conditions showing a trimer of PP-BP-BP	184
Fig. 4-123 ASAP(+) mass spectrum of mix-5 precipitate under optimized conditions showing a trimer of BP-BP-BP	184
Fig. 4-124. Proposed structural formulae for the trimers of mix-5 under optimized conditions	186
Fig.4-125 ASAP(+) mass spectrum of mix-5 precipitate under optimized conditions showing a tetramer of PHBA-PHBA-PHBA-PP	188
Fig.4-126 ASAP(+) mass spectrum of mix-5 precipitate under optimized conditions showing a tetramer matching PHBA-PHBA-PHBA-BP	189
Fig.4-127 ASAP(+) mass spectrum of mix-5 precipitate under optimized conditions showing a tetramer matching PHBA-PHBA-MP-BP	190
Fig. 4-128 ASAP(+) mass spectrum of mix-5 precipitate under optimized conditions showing tetramer matching to PHBA-PHBA-PP-PP	190
Fig.4-129 ASAP(+) mass spectrum of mix-5 precipitate under optimized conditions showing a tetramer of PHBA-PHBA-PP-BP	191
Fig. 4-130 ASAP(+) mass spectrum of mix-5 precipitate under optimized conditions showing a tetramer of PHBA-PHBA-BP-BP	191
Fig. 4-131 ASAP(+) mass spectrum of mix-5 precipitate under optimized conditions showing a tetramer of PHBA-PP-PP-BP	192
Fig. 4-132 ASAP(+) mass spectrum of mix-5 precipitate under optimized conditions showing a tetramer matching MP-PP-PP-BP	192
Fig.4-133. Proposed structural formulae for plausible tetramers combinations of mix-5 under optimized conditions	193
Fig. 4-134 ASAP(+) mass spectrum of mix-5 precipitate under optimized	

conditions showing a pentamer matching PHBA-PHBA-MP-MP-BP.....	193
Fig.4-135 ASAP(+) mass spectrum of mix-5 precipitate under optimized conditions showing a pentamer of PHBA-PHBA-MP-PP-PP	196
Fig. 4-136 ASAP(+) mass spectrum of mix-5 precipitate under optimized conditions showing a pentamer matching PHBA-PHBA-MP-PP-BP	197
Fig. 4-137 ASAP(+) mass spectrum of mix-5 precipitate under optimized conditions showing a pentamer of PHBA-PHBA-PP-PP-PP	198
Fig. 4-138 ASAP(+) mass spectrum of mix-5 precipitate under optimized conditions showing a pentamer of PHBA-PHBA-PP-PP-BP	198
Fig. 4-139 ASAP(+) mass spectrum of mix-5 precipitate under optimized conditions showing a pentamer matching PHBA-PHBA-PP-BP-BP	199
Fig.4-140 ASAP(+) mass spectrum of mix-5 precipitate under optimized conditions showing pentamer matching PHBA-PHBA-BP-BP-BP	199
Fig. 4-141 ASAP(+) mass spectrum of mix-5 precipitate under optimized conditions showing a pentamer of PHBA-PP-PP-PP-BP	200
Fig. 4-142 ASAP(+) mass spectrum of mix-5 precipitate under optimized conditions showing a pentamer of PHBA-PP-PP-BP-BP	200
Fig. 4-143 ASAP(+) mass spectrum of mix-5 precipitate under optimized conditions showing a pentamer of PHBA-PP-BP-BP-BP	201
Fig. 4-144 Proposed structural formulae for plausible pentamer combinations (but not permutations) of mix-5 under optimized conditions	202
Fig. A-1: SBP catalyzed formation of quinoneimine chromophore From phenol and SBP	242

Fig. B-1 Calibration Curve for Hydrogen Peroxide	244
Fig. C-1 Calibration curve for acetaminophen for single-compound analysis	245
Fig. C-2 Calibration curve for PHBA for single-compound analysis	245
Fig. C-3 Calibration curve of MP for single-compound analysis	246
Fig. C-4 Calibration curve of PP for single-compound analysis	246
Fig. C-5 Calibration curve of BP for single-compound analysis	247
Fig. D-1 Calibration curve of Acetaminophen in mix-5	248
Fig. D-2 Calibration curve of PHBA in mix-5	248
Fig. D-3 Calibration curve of MP in mix-5	249
Fig. D-4 Calibration curve of PP in mix-5	249
Fig. D-5 Calibration curve of BP in mix-5	250
Fig. E-1 Effect of Varying amount of SBP and H ₂ O ₂ concentrations on removal of contaminants for 3 h	251
Fig. E-2 Effect of Varying amount of SBP and H ₂ O ₂ concentrations on removal of contaminants for 5 h	251
Fig. F-1 ASAP(-) mass spectrum of MP supernatant showing dimer and oxygenated dimer	252
Fig. F-2 ASAP(-) mass spectrum of MP supernatant showing trimer and oxygenated trimer	252
Fig. F-3 ASAP(-) mass spectrum of MP supernatant showing tetramer and oxygenated tetramer	253
Fig. F-4 ASAP(-) mass spectrum of MP supernatant showing pentamer and oxygenated pentamer	253
Fig. F-5 ASAP(-) mass spectrum of MP supernatant showing hexamer and oxygenated hexamer	254
Fig. F-6 ASAP(-) mass spectrum of PP supernatant showing dimer at m/z 357.1337	254
Fig. F-7 ASAP(-) mass spectrum of PP supernatant showing trimer and oxygenated trimer	255

Fig. F-8 ASAP(-) mass spectrum of PP supernatant showing tetramer and oxygenated tetramer	255
Fig. F-9 ASAP(-) mass spectrum of BP supernatant showing dimer and oxygenated dimer	256
Fig. F-10 ASAP(-) mass spectrum of BP supernatant under optimized conditions showing trimer and oxygenated trimer	256
Fig. F-11 ASAP(-) mass spectrum of BP supernatant under optimized conditions showing tetramer and oxygenated tetramer	257
Fig. F-12 ASAP(-) mass spectrum of BP supernatant under optimized conditions showing pentamer and oxygenated pentamer	257
Fig. F-13 ASAP(-) mass spectrum of BP supernatant under optimized conditions showing hexamer and oxygenated	258
Fig. F-14 ASAP(-) mass spectrum of BP supernatant under optimized conditions showing heptamer	258

LIST OF APPENDICES

Appendix A: SBP Assay – reagents, procedure and SBP activity calculation.....	241
Appendix B: Hydrogen peroxide assay	243
Appendix C: Calibration curves for single-compound analysis	245
Appendix D: Calibration curves for compounds analysis in mix-5	248
Appendix E: Effects of varying SBP and peroxide on compounds removal in mix-5	251
Appendix F: ASAP(-) mass spectra of MP, PP and BP detected in supernatants of single-compound SBP treatments	252
Appendix G: SPE protocol and recoveries	259

LIST OF ABBREVIATIONS/SYMBOLS

ABTS	2,2'-azino-bis-(3-ethylbenzthiazoline-6-sulphonate)
Acet/APAP	Acetaminophen/ <i>N</i> -acetyl p-aminophenol
AgNP	Silver nanoparticle
Amu	Atomic mass units
AOP	Advanced oxidation process
ASAP	Atmospheric solids analysis probe
BBA	Benzylbutyl phthalate
BP	Butyl paraben
BPA	Bisphenol A
BzP	Benzyl paraben
CDOM/NOM	Chromophoric dissolved organic matter/ Nitrogenous organic matter
CEC	Contaminant of emerging concern
DBP	Disinfection by-products
DGT	Desolvation gas temperature
diBrE2	2,4-dibromo-17 β -estradiol
DOC	Dissolved organic carbon
DOM	Dissolved organic matter
DT ₅₀	Dissipation time in water or water sediment compartment
E1	Estrone
E2	17 β -estradiol
E3	Estriol
EC	Emerging contaminants
EDC	Endocrine disruption chemicals
EE2	17 α -ethinyl estradiol
EP	Ethyl paraben
ER $_{\alpha}$	Estrogen receptor α

ESI	Electrospray ionization
GAC	Granular activated carbon
GlcNac	N-acetyl glucosamine
HPLC	High performance liquid chromatography
HRP	Horseradish peroxidase
HRP C	Horseradish peroxidase isoenzyme C
K _{ow}	Octanol water partition coefficient
LOD	Limit of detection
LOQ	Limit of quantitation
MP	Methyl paraben
MS	Mass spectrometry
NABQI	N-acetyl-benzoquinine imine
NP	Nonyl phenol
PAC	Powdered activated carbon
PHBA	<i>para</i> -hydroxybenzoic acid
PP	Propyl paraben
PPCP	Pharmaceuticals and personal care products
SBP	Soybean peroxidase
TCS	Triclosan
TOC	Total organic carbon
TRI	Toxics Release Inventory
UV-Vis	Ultra-Violet Visible
WWTP	Wastewater treatment plant

CHAPTER 1

INTRODUCTION

1.0 Background

Contaminants of emerging concern (CECs) are widely distributed and have been reported across the continents of the world (Bradley *et al.* 2020, Fang *et al.* 2019, K'Oreje *et al.* 2018). Owing to the increase in the analytical capabilities of modern analytical instruments, this class of chemical compounds which was previously elusive can be largely detected and quantified. Basically, these could be broadly divided into pharmaceuticals and personal care products, (PPCPs), pesticides and industrial chemicals (Ouda *et al.* 2021). Since these compounds are known, or reasonably suspected to be toxic (summarized below) but are unregulated, this scenario creates suspicions and health associated uncertainties.

1.1 Sources of CECs in the environment

Two cardinal factors are driving the increase of CECs in surface waters, namely human population growth and the inability of the wastewater treatment plants in removing these compounds before the effluents are being discharged. The United Nations, Department of Economic and Social Affairs (2019) reported an estimated global human population of 7.7 billion in 2019, and projected an increase to 8.5 billion, 9.7 billion and 10.9 billion persons by 2030, 2050 and 2100, respectively. This implies an ever-increasing demand for PPCPs and other related chemicals mentioned above to sustain human lifestyles and feed the growing global community. Moreover, increasing human population translates to growing demand on shrinking freshwater resources, partly contributed by global warming and its attendant negative effects on global freshwater bodies.

The advances in earnings and per capita income across the world, mostly from the developing nations has increased the PPCPs and industrial products consumption capabilities of many individuals (Klein *et al.* 2018). The result is the increased demand for processed products, of which the technological advances of the developed nations are available to meet such demands, a major way of enhancing their economic sustenance and growth. Hence, more industrial activities are going on, utilizing raw materials to create finished products. Some of these raw materials are treated with chemicals which often end

up in the sewer lines. The production processes may also require the use of chemical additives or modifiers in a manner to improve the desirable qualities of raw materials. Similarly, the finished products may also contain chemical preservatives in order to improve the shelf life of the products. For example, parabens are used as preservatives in foods and pharmaceuticals. Pharmaceutical companies incorporating Acetaminophen in analgesic/antipyretic formulations may tend to generate wastewater containing this CEC in the discharge from the production process. Although industries treat wastewater before discharge, there is evidence of exceptionally high CECs in such effluents (Kleywegt *et al.* 2019). All these collectively form constituents of the industrial discharges which end up in the sewage line heading for the wastewater treatment plants (WWTPs). Since most conventional treatment plants are unable to remove many of these compounds, they find their way into the receiving water and create pollution.

On the other hand, the need to feed the estimated 7.7 billion humans on earth necessitates the adaptation of mechanized agriculture as the only way to produce enough food. Moreover, rearing animals - terrestrial or aquatic- requires the inputs of feed and health management that calls for the application of antibiotics. This has made the application of pesticides not just an option, but a necessity. These may create residues on plants and plant products as well as cultivated soils, while substantial fractions may enter water bodies, collectively tagged agricultural runoff. For animals, tissue accumulation of antibiotics (Han *et al.* 2020) and PPCPs (Yang *et al.* 2020) in fish harvested for human consumption has been reported, while animal droppings have also been found to be contaminated with the pharmaceuticals and feed additives (Gros *et al.* 2019). Water released from aquaculture to surface waters may also contain the residual chemicals which were administered to enhance the health and productivity of the aquatic organisms (Han *et al.* 2020).

Industrial release of pharmaceutically active ingredients such as Acetaminophen to the environment has been shown to be at concentrations above those commonly observed in wastewater treatment plant effluent (Kleywegt *et al.* 2019), not to mention influents. Similarly, hospitals which usually consume large quantities of Acetaminophen and other pharmaceutical products of all kinds make substantial contributions to the inventory of pharmaceuticals released into the environment (Afsa *et al.* 2020).

These chemicals are primarily collected by the WWTP via the sewer system, from manufacturing plants, hospitals, and residences. However, WWTP were by nature designed to provide water conservation and maintain public health, and not necessarily removal of CECs. Therefore, Acetaminophen, parabens and other CECs are often found at concentrations of ng/L to $\mu\text{g/L}$ in the WWTP effluents (Bradley *et al.* 2020, Ghoshdastidar *et al.* 2015, Blair *et al.* 2013). In addition, it is also reported that agricultural runoff from agricultural fields may contain hydrophilic CECs at concentrations comparable with those found in WWTP effluents (Spahr *et al.* 2020). Both sources constitute indiscriminate disposal of PPCPs in the environment.

Ingested pharmaceuticals may be released partly in their original parent or metabolized forms. Any chemical in the environment may be converted to other forms by microbial activities, photodegradation, hydrolysis or sorption onto appropriate medium. For example, they are commonly found in the sludge of WWTPs (Heidler *et al.* 2006). Similarly, during wastewater treatment, the parent chemicals may be partly converted to other products, especially during the disinfection phase, hence forming a class of compounds generally described as disinfection by-products (DBPs). These show the tendency of other chemicals to arise from one parent compound, which may have different structural complexity, concentration, persistence, toxic effects other than their by-products. Another complicating factor associated with such intermediates is that even when their molecular structure is inferred from modern analytical instruments such as mass spectrometry (MS) or gas-chromatography mass spectrometry (GC-MS), one may only be able to do qualitative analysis or relative quantitative estimates on them, since there may not be standards to accurately quantify them (Bradley *et al.* 2020).

1.2 Effects of CECs

The effects of CECs on organisms has been widely documented (Celente *et al.* 2020, Yang *et al.* 2020, Guiloski *et al.* 2017, Yamamoto *et al.* 2011). Either antimicrobials are causing the development of antimicrobial resistant strains of microorganisms, there is the endocrine disrupting effect creating intersex in fishes, tadpoles, or other aquatic organisms or biofilms are being disturbed in a manner that alters ecological dynamics in well-established aquatic bacterial communities. Other effects are the oxidative stress associated with some

chemicals. In order to elucidate these effects, the trio assessment battery of algae, crustaceans and fish, with ascending trophic level hierarchy, have always been used in elucidating the toxicity of CECs. Factors usually considered are environmental persistence of a chemical and its ability to bioaccumulate in organism tissues such as muscles and blood. Advances in molecular sciences have opened a doorway and redefined toxicity assessment beyond the organismic level to the molecular level, which made possible the tracking of alterations in the DNA, or abnormal expression of proteins, to studies on tissue histology and biochemistry (Guiloski *et al.* 2017). These developments have substantially helped our understanding of CECs at certain environmental concentrations which were formerly reported as not posing any threat to organismic population (Ramos *et al.* 2014) and are now being redefined (Guiloski *et al.* 2017). Thus, improvements to toxicity assessment strategies coupled with environmental monitoring provide a risk framework. The final step is removing sources by either replacement of these compounds with more inert forms in commercial processes or enhancing removal technologies from the waste stream. The objectives of this dissertation address the latter.

The rising body of knowledge suggesting toxic effects of CECs on the aquatic biota, and hence the suspicion that these chemicals may also be hazardous to humans makes it necessary for research in order to develop new and effective technologies which can minimize the release of CECs into the receiving water bodies. These may at least conserve the available water resources to be readily available for human use in drinking, meeting other domestic and industrial needs, agricultural purposes and recreational activities, without any detrimental effects on aquatic habitats and livestock and, by extension, human beings.

1.3 Wastewater treatment technologies

Conventional WWTPs are known to operate basically with preliminary/primary and secondary treatment stages. In the preliminary/primary treatment stage, usually employing physical unit processes, the emphasis is to remove grit, solid suspended particles, some organic matter, oils and grease and prepare the water for the next stage. The secondary treatment stage uses biological treatment unit processes, which sometimes enlist chemical addition to achieve the removal of biodegradable organic matter and suspended solids. Most common secondary treatment processes require the use of activated sludge systems.

Treatment is achieved through use of microbial oxidation of organic compounds, hence enabling a partial removal of CECs depending on their characteristic physical-chemical properties. Different removal pathways exist, including microbial mediated decomposition, sorption to suspended solids and microbial utilization as a source of biomass development (Burch *et al.* 2019). Processes other than employed in traditional primary and secondary treatment are usually described as tertiary or advanced treatment (Quach-Cu *et al.* 2018).

The essence of tertiary treatment is to ensure effluents that can be safely discharged into receiving water bodies without posing any ecotoxic threat to aquatic biota and may also be used as a source of water for municipal supply (Angeles *et al.* 2020). Among the tertiary treatment processes, advanced oxidation processes (AOPs) have received much research attention and some pilot studies or even full-scale WWTP implementation with one or more of such techniques in sequence (Angeles *et al.* 2020). The underlying common point in AOPs is the generation of a hydroxyl radical, which attacks the CECs in a non-selective manner and eventually mineralizes them, due to its strong oxidizing capabilities (Villegas *et al.* 2016, Ribeiro *et al.* 2015). Different approaches employing ultraviolet (UV) radiation, hydrogen peroxide, ozone and/or molecular oxygen have been adapted for wastewater treatment. Some notable examples here include Fenton process, ozonation, catalytic wet peroxide oxidation, electrochemical oxidation, heterogenous photocatalysis and some may even be combined such as photo-Fenton process (Rizo *et al.* 2019). Different approaches have been employed to generate the required hydroxyl radicals based upon which AOPs are used may be divided into photo-chemical, chemical, electro-chemical and sono-chemical processes (Ribeiro *et al.* 2015) among others.

1.3.1 Enzymatic treatment of CECs

The bio-catalytic approach to CECs treatment employs the use of either peroxidases or laccases to produce aryl radicals of phenolic or anilino compounds which in turn couple non-enzymatically to form dimers, and if soluble, they would return to the cycle again and form dimer radicals which can combine in a similar manner to form higher molecular weight oligomers. This sequence of reactions will continue each time an aryl substrate goes

through the peroxidase catalytic cycle until the oligomer being formed becomes hydrophobic enough to precipitate out of solution.

Peroxidases are sourced from plants, bacteria and fungi. By far the most extensively studied peroxidase is the horseradish peroxidase (HRP), which has very high catalytic efficiency for the conversion of its aryl substrates to oligomer products. However, it is processed from roots of the plant which is cultivated in limited quantities, hence very expensive, making soybean peroxidase (SBP) a viable alternative. It has a wide catalytic pH range, high thermostability, efficiency at low substrate concentration, is very abundant as a by-product of agricultural industry. It is sourced from the seed hulls of soybeans, a very abundant crop cultivated *en masse* here in North America and other continents of the world. Moreover, the crude extract is usually employed in this treatment process, thereby saving cost associated with enzyme purification. In contrast with the other AOPs and other advanced treatment processes, the superior qualities of SBP based enzymatic treatment stand out.

Although some of the AOPs (photo-Fenton, UV/TiO₂, ozonation, powdered and granular activated carbons, (PAC and GAC) have high EC removal and, in some instances, some or strong disinfection capability, the associated drawbacks with many of them include, production of disinfection by-products (DBPs) of unknown but suspected toxicity, high operational costs and uncertainty of range of efficiency that can be covered (Rizzo *et al.* 2019). These disadvantages form the basis upon which a biocatalytic process employing SBP can leverage upon. For instance, the primary essence of a treatment is to remove suspected toxic ECs. However, if a process itself produces DBPs of unknown toxic nature, then it may not be appropriate. For instance, the mineralization of acetaminophen by an electro-Fenton process produced intermediates including 1,4-benzoquinone and 2-hydroxy-4-(N-acetyl) aminophenol, compounds whose toxicity exceeds the parent compound (Le *et al.* 2017).

Therefore, my research aims at using a crude extract of SBP for the treatment of five ECs: acetaminophen, methylparaben (MP), propylparaben (PP), butylparaben (BP) and the common paraben hydrolysis intermediate, *para*-hydroxybenzoic acid (PHBA). These parabens were chosen based on their relative abundance in environmental water samples.

Removal feasibility shall be targeted at 95% of 1 mM concentrations of single substrates and an equimolar mixture of the five (mix-5) CECs. These choices are based on analytical conveniences and ease of comparison with previous studies in the lab. It is recognized subsequent study would have to extend the feasibility to much lower concentrations reflective of obtainable situations in WWTP effluents.

1.4 Research objectives

This study intends to employ SBP in the treatment of selected emerging contaminants in synthetic wastewater. The specific objectives are:

a). **Optimization of parameters**

The reaction parameters which include crude enzyme (SBP) activity, hydrogen peroxide concentration and pH required to attain the highest removal, targeting 95% of the initial substrate concentration will be determined

b). **Determine the initial rate of removal of the CECs**

The reaction time course will be determined under the optimum conditions, from which the initial stage will be fit to a first-order model to derive initial rate constant and half-life of the respective CECs.

c). **Determine product formation in supernatant and precipitate**

It is hypothesized that the reaction produces oligomers, therefore mass spectrometry (MS) will be employed using either electrospray ionization (ESI) or atmospheric solid analysis probe (ASAP) to determine the oligomeric products formed.

d). **Mechanism of reactions**

Oligomeric products are expected to be formed; therefore, the pathway of coupling will be elucidated.

e). **Carry out mixture treatment studies**

In nature, CEC will exist in a mixture of other compounds, therefore the selected 5 CECs in this study will be mixed (mix-5) and studied against objectives a – c above.

CHAPTER 2

LITERATURE REVIEW

2.0 Viewing an ancient problem through new lenses

The absence of enough literature before now on the presence of chemical substances in our environment does not mean an environment devoid of these pollutants. Recent advances in analytical technologies have introduced instrumentations capable of detecting chemical concentrations down to parts per trillion (Noguera-Oviedo and Aga 2016, Beausse 2004, Koplín *et al.* 2002), existing in different and complex environmental matrices (Sedlak *et al.* 2000). This has improved our awareness of the presence of chemicals which have been there all along without our knowledge and their effects could not be ascertained, due to our previous inability to quantify and monitor them (Noguera-Oviedo and Aga 2016). Our knowledge of their presence in different environmental matrices and the suspicion surrounding their effects on organisms has created an emerging concern (Philip *et al.* 2018). The Toxics Release Inventory (TRI), a registry of the United States (US) Environmental Protection Agency (EPA) in 2020 added 158 chemicals to its previous listing (<https://www.epa.gov/toxics-release-inventory-tri-program/list-pfas-added-tri-ndaa>) and further updated it bringing the listing to 767 chemicals in the inventory in early 2021. This substantiates the growing nature of information around emerging contaminants.

On a general note, it may be more appropriate then to consider such chemical substances as contaminants of emerging concern, (CEC) which Sauve and Desrosiers (2014) defined as natural or synthetic chemicals, which have been detected in environmental matrices, and are reasonably suspected to elicit metabolic alterations in organisms upon contact with such organisms. Enough information on CECs make them to be regulated. For instance, TRI listing highlights carcinogens or chemicals capable of eliciting chronic human health effects, or substantial adverse acute human health problems and considerable environmental effects.

2.1 A broad class of pollutants

CECs are known to arise from pharmaceuticals and their metabolites (Li *et al.* 2019, Brown & Wong, 2018, Sanganyado *et al.* 2017, Maeng *et al.* 2011), personal care products (Xie, *et al.* 2019, Juliano & Magrini, 2017, Lu *et al.* 2018, Galindo-Miranda *et al.* 2019), artificial sweeteners (Arbelaez *et al.* 2015) and hormones, either natural (such as estradiol, estriol, estrone and testosterone) or synthetic hormones (ethinylestradiol) (Barel-Cohen *et al.* 2006, Weizel *et al.* 2018, Amin *et al.* 2018, Mina *et al.* 2018, Shargil *et al.* 2015, Yarahmada *et al.* 2018). Other classes of CECs are flame retardants and plasticizers, (Chokwe & Mporetji 2019, Zha *et al.* 2018, Shi *et al.* 2016), biocides, such as pesticides, fungicides, herbicides, rodenticides, insecticides (Corcoran *et al.* 2020, Shalaby *et al.* 2018, Zhao *et al.* 2018).

The disinfection of treated wastewater before discharge into the environment, mostly employs chlorine, chloramines, or in some wastewater treatment plants (WWTPs), ultraviolet (UV) light (Ding *et al.* 2013, Alvarez-Rivera *et al.* 2014). Chlorination and chloramination have been known to produce compounds collectively described as disinfection by products, (DBPs), which constitute another class of CECs. Trihalomethanes (THMs) and haloacetic acids (HAA) are earlier identified classes of DBPs which have been regulated in municipal water supplies, owing to established toxicity reports (Postigo *et al.* 2018, Narotsky *et al.* 2015). Like any other class of CECs, more compounds are being identified which fit into this group (Gong & Zhang 2015, Ding *et al.* 2013), more so that with varying treatment conditions, different kinds of DBPs may be identified (Zhong *et al.* 2019, Li *et al.* 2017).

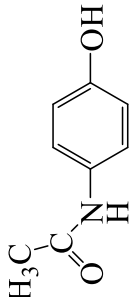
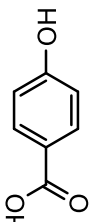
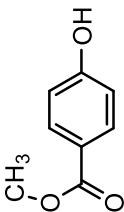
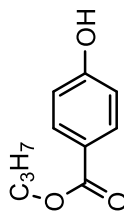
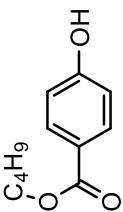
2.2 Environmental burden of PPCPs

The presence of PPCP in the environment was first reported in 1976 in Kansas City, US, where WWTP effluents were reported to have contained clofibric acid between 0.8 to 2 µg/L (Ebele *et al.* 2017). Since then a surge in research interest has arisen into PPCPs in the environment (Fang *et al.* 2019, Noguera-Oviedo & Aga 2016), largely due to the perceived associated ecotoxicological effects (Celente *et al.* 2020, Ginebreda *et al.* 2014) and perceived human health hazards (de Garcia *et al.* 2017, Cizmas *et al.* 2015) linked to these classes of compounds. PPCPs are often found in ng/L to few mg/L in the environment

(Koplin *et al.* 2002). The physicochemical properties and environmental abundance of some of the CECs employed in this study are listed (Tables 2.1 and 2.2) respectively

Several reports have been published on the existence of PPCPs in the environment, for example (Ouda *et al.* 2021, Aryal *et al.* 2020, Keerthanan, *et al.* 2020, Ohoro *et al.* 2019, Padri and Tamzir, 2019, Ebele *et al.* 2020 Brown and Wong, 2018, Ebele *et al.* 2017). Therefore, more information can be obtained from these cited literatures.

Table 2.1 Physicochemical parameters of the studied CECs

CEC	Molecular formula	Structural formula	Mwt (g/mol)	pKa	Log K_{ow}	Melting Point (°C)	Boiling Point (°C)	Appearance
Acet	$C_8H_9NO_2$		151.16	9.38	0.314	168-172	-	White crystalline powder
PHBA	$C_7H_6O_3$		138.12	4.54	1.39	214-215	336.2	White powder
MP	$C_8H_8O_3$		152.15	8.17 ^a	1.96	125-128	280	White crystalline powder
PP	$C_{10}H_{12}O_3$		180.20	8.64 ^b	2.98	95-98	294.3	White crystalline powder
BP	$C_{11}H_{14}O_3$		194.23	8.49 ^b	3.47	67-71	309.2	White crystals

a= Soni *et al.* (2005), b = Gomes *et al.* (2018b)

Table 2.2: Concentrations of CECs in different environmental matrices

Matrix/compound	MP	PP	BP	PHBA	Acet	Source
Surface water(streams)(ng/L)	49-676	7.5-207	10-163	NR	NR	Yamamoto <i>et al.</i> 2011
WWTP Effluents* (ng/L)	4.4-41	2.80-19.3	ND-2.10	500-2590	NR	Karthikraj <i>et al.</i> (2017)
Sludge (ng/g dry wt)	16.0-172	82.0-910	ND-1.0	389-31500	NR	Karthikraj <i>et al.</i> (2017)
Wastewater effluents (µg/L)*					28.9	Ghoshdastidar <i>et al.</i> (2015)

*molar concentrations (nM) MP =0.03-0.3, PP =0.02-0.1, BP =ND-0.01, PHBA = 3.6-19 and Acet = 190

Pharmaceuticals are substances employed for diagnosis, prevention, or cure of a disease and for restoring, modifying or correcting processes in living things (Monteiro and Boxall 2010, Daughton and Ternes 1990), and comprises at least 4000 known compounds (Beausse 2004). Many of these have been identified in the environment across the continents of the globe (Tran *et al.* 2018, Ebele *et al.* 2017, Cizmas *et al.* 2015, Howard and Muir 2011). Between 2010 and 2016 at least 2638 different chemical compounds have been detected in surface waters around the world and 819 of these were detected in more than one location (Fang *et al.* 2019). Fang *et al.* (2019) categorized these chemicals under three main groups of PPCPs, pesticides and industrial chemicals and reported more than 90% of these were detected among EU and Asian member states and the US.

2.2.1 Environmental pollutants exist in mixture

The first national study in the US surveyed 139 streams across 30 states with a bias towards downstream points where WWTP effluent and large-scale animal husbandry activities

were located, with a pre-set target for 95 PPCPs (Koplin *et al.* 2002). The study reported 82 PPCPs were detected in 80% of sampled locations, with a median of 7 PPCPs and maximum of 38 PPCPs detected per sampling point. The commonly identified chemicals were grouped under several classes, including fecal steroids, plant and animal steroids, insect repellants, stimulants, antimicrobial disinfectants, fire retardants, and non-ionic detergent metabolites. These fit into the three classes of PPCPs, pesticides and industrial chemicals reported elsewhere (Fang *et al.* 2019). The frequency, lowest and highest detection values for acetaminophen were 23.8%, 0.009 µg/L and 10.0 µg/L, respectively. In a related recent study, Bradley *et al.* (2020) surveyed 308 headstreams across 4 regions in the US, targeting 111 pharmaceuticals. From the studied locations, 88 pharmaceuticals were identified and 91% of sampled locations had more than 1 pharmaceutical compound present, with cumulative highest concentrations of 36.1 µg/L per site. Acetaminophen at 68% was the 5th most frequently detected pharmaceutical in the south-eastern states of the US. The cumulative analyte concentrations were reported to have a positive correlation with land use and presence of WWTP effluent discharge point sources, while in some cases pharmaceutical mixtures were prevalent in 75% of streams without any upstream WWTP effluent discharge point source. For a sampled location with very high mixture aggregate as demonstrated in this study, synergistic or antagonistic studies need to elucidate the effects of such mixtures on aquatic organisms. Moreover, most studies focus on parent compounds ignoring the metabolites (Beausse 2004) or degradates that might arise from the parent PPCPs, hence underestimating the actual ecotoxic effects (Bradley *et al.* 2020, Ginebreda *et al.* 2014). With increased urbanization and modern lifestyle, there is no end in view to abating the release of CECs into the environment, rather a feasible technique of removing them from WWTPs must be devised to safeguard aquatic resources, environmental biota and consequently humans.

2.3. Transformation of parent CECs

2.3.1 Environmental transformations

CECs are known to undergo different transformations in the environment such as oxidation, adsorption, photolysis or biodegradation, generally taking the form of a conjugation reaction, or a deconjugation processes (Parezanovic *et al.* 2019, Patel *et al.*

2019, Li *et al.* 2016). CECs undergo attenuation along the course of flow in a river, depending on the chemical properties of the compound and environmental characteristics of the river. Li *et al.* (2016) compared the attenuation of the specific compounds between a German river and three Swedish rivers, and reported 80% attenuation of acetaminophen in the German river, but $\leq 5\%$ and between 18-46% for two Swedish rivers, respectively. The attenuation of CECs is determined by the characteristics of the river (depth, turbidity, sandy sediments), sunshine and sunlight penetration which may help enhance photo-degradation as well as established bacterial communities capable of degrading the CECs (Kunkel and Radke 2012). Stability of a CEC under such factors as temperature, pH, matrix interaction, light, humidity, also determines its transformation in the environment (Parezanovic *et al.* 2019).

2.3.2. Transformation during wastewater disinfection

The chlorination of water containing parabens has been shown to produce chloro-derivatives, 3-chloro-paraben and 3,5-dichloro-paraben of the corresponding parent parabens (Mao *et al.* 2016). These DBPs are suspected to be more toxic than the parent compounds (Zavala and Estrada. 2016). Since an aerobic process is often employed in WWTP, microbial mineralization could be achieved, as in the case of aspirin, producing water and carbon dioxide as final products (Richardson and Bowron, 1985). Yet, some CECs are transformed into hydrophilic intermediates, which may pass through WWTPs without undergoing further change, and end up in the receiving water bodies as surface water pollutants (Halling-Sørensen *et al.* 1998). Some compounds partition into the sludge, an occurrence Jones *et al.* (2005) reported is fairly correlated with the log K_{ow} values of the individual compounds. This demonstrates a clear situation where some poorly removed CECs in influent wastewaters may eventually return into the environment through the sludge or as transformed chemicals. Therefore, the disappearance of CECs from influents along the stages of conventional WWTPs may not necessarily be removal, but transformation and or partition into solid phase.

2.4 Occurrence of the CECs

2.4.1 Parabens in humans – factors and occurrence

Use of parabens as food preservatives constitutes a major route of exposure, following the consumption of such preserved foods. Total parabens in human foods is up to 16 ng/g fresh weight, composed mostly of MP, EP, PP and minute concentrations of BP and benzyl paraben (BzP) (Karthikraj, *et al.* 2018). In the US, the estimated daily dietary intake of total parabens is in the order of infants (< 1 year old) > toddlers (1-6) > children (6-10) > adults (more than 21) > teenagers (11-21) and corresponds to the orders of: (940, 879, 470, 307 and 273) ng/kg bw/day, respectively (Liao *et al.* 2013a). Indoor dust could also be another source of human exposure to parabens (Table 2.3). Since the concentration varies, it is also expected the estimated daily intakes will vary as well. Children are more susceptible to PBs intake from inhalation and dermal absorption (Table 2.3) due to their relatively lighter skin membrane and the subcutaneous tissues.

Table 2.3 Concentration (ng/g of indoor air) of PB in indoor air and estimated daily intakes (ng/kg bw/day)

Country	Compound/concentration (ng/g)				
	MP	EP	PP	BP	PHBA
US	587	22	640	20	76
China	226	8.9	123	1.5	1130
Korea	1380	49	761	49	275
Japan	1670	91	268	42	33
Estimated daily Intakes of parabens from breathing (ng/kg bw/day)					
US Children	1.40	0.05	1.52	0.05	3.32
US Adults	0.22	0.08	0.24	0.007	0.52
China Children	0.53	0.02	0.29	0.004	0.98
China Adult	0.11	0.004	0.06	0.007	0.20
Korea Children	3.24	0.12	1.78	0.11	5.42
Korea Adult	0.66	0.02	0.36	0.02	1.11
Japan Children	3.90	0.21	0.63	0.10	5.38
Japan Adult	0.86	0.047	0.14	0.02	1.18

*source: Wang *et al.* (2012). Children (4-11 years), Adults (>21 years)

There is a strong positive correlation between gender, PPCPs use, and age on urinary total parabens concentrations (Fisher *et al.* 2017, Meeker *et al.* 2013, Wang *et al.* 2015). The most important factor determining the distribution of parabens among humans being gender (Smith *et al.* 2012). Moos *et al.* (2014) reported the highest levels of parabens were

detected in females of all ages, compared to males of similar ages. In a cross-sectional study in the US, female adolescents had at least 3 times higher total urinary parabens than their male counterparts (Scinicariello and Buser 2016). This is due to the behavioral differences associated with the genders. Most females may opt for a range of lotions and cosmetics which have been implicated in increasing urinary paraben concentrations (Meeker *et al.* 2013). For instance, BP is especially higher in women who have reported use of shampoo and conditioners than women who did not (Fisher *et al.* 2017).

Parabens have been identified in human urine and breast milk (Fisher *et al.* 2017, Meeker *et al.* 2013), placenta fluid (Fernandez *et al.* 2015), human adipose tissue (Wang *et al.* 2015), serum (Hines *et al.* 2015), normal and cancerous breast tissue (Shanmugam *et al.* 2010), as illustrated in Table 2.3. Parabens are the most abundant environmental phenolics present in adipose tissue (Wang *et al.* 2015) arising from environmental exposure such as indoor dust inhalation (Wang *et al.* 2012), consumption of foods (Karthikraj *et al.* 2018, Liao *et al.* 2013a) and PPCPs (Melo and Queiroz 2010) preserved with parabens. They have been observed to accumulate in urine as conjugated substances in less than 24 hours following dermal application and decline steadily thereafter (Fisher *et al.* 2017) in a manner portraying ease of dermal absorption and rapid metabolism of the parent parabens (Liao *et al.* 2013). Oral administration of PP in humans showed rapid absorption and elimination within three hours producing metabolites such as glucuronide and sulphate conjugates, PHBA, and *para*-hydroxyhippuric acid and the unconjugated parent compound in urine

Table 2.4 Parabens in human samples

Sample/Name	PHBA	MP	EP	PP	BP	Source	Country/Continent
Adipose fat (ng/g wet wt)	<LOQ-17400	<LOQ-22.3	<LOQ-30.6	<LOQ-18.2	<LOQ-1.05	Wang <i>et al.</i> (2015)	US/North America
Urine(ng/mL)*	NR	140	NR	30.0	1.0	Meeker <i>et al.</i> (2013)	Puerto Rico/North America
Urine (ug/L)	NR	94.9	15.13	25.50	3.28	Fisher <i>et al.</i> (2017)	Canada/North America
Breast Milk (ug/L)	NR	0.99	0.12	0.33	N/A	Fisher <i>et al.</i> (2017)I	Canada/North America
Urine(ng/mL)*	1.80E3±3460	6.77±25.9	0.220±1.71	0.860±50.8	NR	Xue <i>et al.</i> (2015)	India/Asia
Urine (ng/mL) Mothers	NR	57	8.4	10	1.8	Frederiksen <i>et al.</i> (2013)	Denmark/Europe
Urine (ng/mL) children	NR	18	1.0	2.0	0.19	Frederiksen <i>et al.</i> (2013)	Denmark/Europe
Urine (ng/mL) (Female adults)	NR	232	33.5	60.6	4.32	Heffeman <i>et al.</i> (2015)	Australia/Oceania
Tumour breast tissue (ng/g wet wt)+	NR	802	2657	1136	5199	Shanmugam <i>et al.</i> (2010)	India/Asia

+ arithmetic mean values *represents geometric means of study population or GM+/-SD

NR=Not reported, N/A=Not available

(Shin *et al.* 2019). Oral administration at a dose of 0.6 mg/kg body weight produced urinary excretion of 8.6% of free and conjugated PP, 23.2% of *p*-hydroxyhippuric acid, while PHBA accounted for 7.0% (Shin *et al.* 2019). The intermediate of parabens metabolism, PHBA at 17,400 ng/g wet weight, has been detected in adipose tissues in quantities surpassing total paraben concentration in similar tissues, evidently showing PHBA is counter-intuitively retained in human adipose tissue (Table 2.3) (Wang *et al.* 2015). Since the epidermal covering tissue hosts esterase producing bacteria, this esterase facilitates the hydrolysis of the parabens releasing PHBA, which could be absorbed through the epidermal cortex to accumulate in the adipose tissue.

Although parabens are used as a mixture in preparations, their presence in human tissues and urine varies substantially, albeit in direct reflection to the concentration used in PPCPs. Commonly detected parabens include MP, EP, PP and BP. Among human subjects, Meeker *et al.* (2011) reported a prevalence rate of 100%, 92% and 32% of MP, PP and BP, respectively in urine samples with a positive correlation between MP and PP, in the sampled population. A similar positive correlation between MP and PP was observed in a Chinese study (Wang *et al.* 2013). This can be traced to the co-formulation of MP and PP in products to enhance effective antimicrobial activity. A survey of 2548 samples in the US in 2005-2006 showed the occurrence of commonly observed parabens ranked in order, as MP, PP, BP and EP by 99.1%, 92.7%, 47.2% and 42.4%, respectively (Calafat *et al.* 2010). However, in a German study, the predominant urinary parabens were in the descending order of MP, EP, PP and BP (Moos *et al.* 2014).

As adjudged from Table 2.4, the burden of human exposure to paraben cuts across several continents. Though urinary levels may differ depending on several factors, it is obvious exposure is a common phenomenon and, social class does not create a consumption divide among members of the populace (Fisher *et al.* 2017, Xue *et al.* 2015). Of all the matrices, urine is the most effective in determining the presence of free and conjugated parabens in humans because it is subjected to show very high detection rate for the target compounds and provides the highest and reproducible detection, unlike breast milk and serum (Hines *et al.* 2015).

The EU directive for parabens use in cosmetics allows an upper limit of 0.8% by weight for total parabens, while for MP and EP the upper limit is capped at 0.4%; 0.19% is the recommended upper limit for the sum of PP and BP (SCCS 2011). However, the Danish government in consideration of the endocrine disruption effect of PBs prohibited the use of normal and isomers of PP and BP in products intended for children under 3 years of age (EU 2011). A survey of products in the EU showed adherence to this, but also observations of PBs use without appropriate quantity labelling was reported (Melo and Queiroz 2010). Urinary presence of parabens in pregnant women and breast milk has been summarized in Table 2.4. Since the predominant PBs in the foregoing are MP and PP, removal of these warrants further study along with BP as a representative of the longer alkyl group PBs. An effective alternative method to address their treatment will help keep our environment clean.

2.4.2 Acetaminophen in the environment

As an antipyretic and analgesic drug of first choice (Perumalla *et al.* 2012) Acetaminophen is consumed among an estimated 30 million people around the world each day (Ding *et al.* 2020) since it is largely tolerated among humans with very little side effects. It is also one of the commonly abused drugs (Tran *et al.* 2018). Due to this large daily consumption and even abuse, it is not strange it is among the top 10 most frequently detected pharmaceuticals from different study locations around the world (Bradley *et al.* 2020, Ebele *et al.* 2017, Koplín *et al.* 2002). Although acetaminophen has a short half-life (Yamamoto *et al.* 2009), its continuous replenishment from WWTPs effluent, and release from other methods of fecal material disposal makes it to pseudo-persist in the environment (Laurentiis *et al.* 2014) in a manner that raises suspicion over its possible toxic health effects on aquatic organisms and the environment.

Acetaminophen have been detected in surface water, ground water, WWTP effluents and even drinking water samples (Ebele *et al.* 2020, Bradley *et al.* 2020, Kleywegt *et al.* 2019, Archer *et al.* 2017, Ghoshdastidar *et al.* 2015) worldwide (Tran *et al.* 2018). In WWTP effluents, Ghoshdastidar *et al.* (2015) reported 28.9 µg/L of the CEC in Nova Scotia, Canada. Ebele *et al.* (2020) examined the concentration of acetaminophen in surface water, ground water and treated drinking water in Lagos, Nigeria and reported concentrations

were between 1-12430 ng/L, 1-188 ng/L and 1-11 ng/L, respectively for the three sources of water they sampled. Similarly, Archer *et al.* (2017) studied effects of WWTP discharges on the receiving water and reported a steep concentration gradient of 20.8 ng/L and 63.7 ng/L, between upstream and downstream, respectively, of the discharge point source. Petrie *et al.* (2014) have reported the WWTP effluent acetaminophen concentration range of <20-11733 ng/L and surface water concentration of <1.5-1388 ng/L. Pharmaceutical companies may appear to be the highest sole contributor of Acetaminophen to receiving waters. Kleywegt *et al.* (2020) surveyed several wastewater effluents released from pharmaceutical industries in Ontario, Canada and reported the concentration of acetaminophen to be 136,506 ng/L and downstream concentration of the chemical in the receiving water body was found to be between 74,700 – 94,700 ng/L. Based on these findings, it was recommended pharmaceutical companies should improve on the treatment of their wastewater effluents before discharge. The availability of alternative treatment technologies as articulated in this study will be helpful especially to such companies which release high quantities of pharmaceutically active CECs which may be harmful to microbial organisms employed during biological treatment of wastewater.

2.5 Effects of the CECs in humans and aquatic organisms

The use of parabens in PPCPs has remained a controversial topic to date (Barabasz *et al.* 2019) owing to safety concerns. This is because some observed effects in animal models are not noticed in humans (Nowak *et al.* 2018). Paraben use in adult males does not affect human serum testosterone levels nor semen quality parameters (Scinicariello and Buser 2016) whereas BP is strongly implicated in facilitating sperm DNA damage (Meeker *et al.* 2011). However, in male rat models, *in utero* and during lactation, exposure to BP causes a significant decrease in serum testosterone, reduced sperm count as well as daily sperm production in a dose-dependent manner, at doses of 400 mg/kg/day and 1000 mg/kg/day (Zhang *et al.* 2014). Moreover, parabens initiate estrogen and progesterone production via the estrogen receptor alpha (ER- α), a phenomenon which depends on concentration and alkyl chain length, in a GH3 rat pituitary cancer cell line (Vo *et al.* 2011). When tested in cell culture broth at 250 $\mu\text{g/mL}$ and 500 $\mu\text{g/mL}$, parabens caused chromosomal aberration and DNA damage in human lymphocytes *in vitro* (Bayulken *et al.* 2019). Environmental

concentrations of MP obstruct human neutrophil oxygen-dependent functions which could affect human innate immune responses upon exposure to xenoestrogens (Nowak *et al.* 2020). For aquatic organisms, paraben mixtures strongly inhibit bioluminescence in *Aliivibrio fischeri* more than individual compounds at similar concentrations, and elicit strong toxicity to *Daphnia magna*, at concentrations at least four-fold higher than average environmental concentrations (Lee *et al.* 2018). This illustrates the synergistic effect of PB mixtures on the model organism. Zebrafish (*Danio rerio*) embryos exposed solutions of MP at sub-lethal doses of 10 ppb and 100 ppb demonstrated reduced hatchability and heart rate, besides reduced acetylcholinesterase (AChE) activity (Raja *et al.* 2019). MP affects growth, reproduction and survival of several soil micro-organisms at concentrations above 22 mg/kg dry soil (Kim *et al.* 2018).

While it is obvious these compounds pose a threat due to their molecular interaction with human cells and aquatic organisms, many have argued the concentration needed to elicit an observable physical effect is too large compared to the concentrations used in PPCPs and as detected in environmental matrices. A comprehensive review of the toxicity of parabens has been covered elsewhere (Jamal *et al.* 2019, Barabasz *et al.* 2018, Nowak *et al.* 2018, Darbre and Harvey 2008).

Acetaminophen toxicity in humans is associated with liver injury and renal impairment at when overdoses are taken (Vrbova *et al.* 2016). It is the most common cause of acute liver failure in the US (Ramachandran and Jaeschke, 2018). However, because the doses at which toxicity is noticed in humans are very high (Vrbova *et al.* 2016) human exposure will not be considered here, but effects on named aquatic organisms will be reviewed.

The occurrence of acetaminophen in aquatic environments raises the concern of its toxicity to the inhabiting organisms and consequently the established aquatic food chain. Improvements in molecular assays have moved toxicology to molecular assessment, where exposure can be monitored beyond whole-organism responses, as previously obtainable. For instance, Ayabahan *et al.* (2020) demonstrated biomarkers identified and quantified with the help of proteomic tools could be useful in providing strong evidences to establish and distinguish between hepatic toxicity and endocrine disruption, based upon which risk assessment decisions could be established. Ding *et al.* (2020) reported at 50 µg/L,

Acetaminophen induced upregulation of genes associated with detoxification and metabolism and altered several physiological parameters in the model invertebrate *Daphnia magna*. At 250 ng/L, Rhamdia quelen were observed to have reduced testosterone levels, while at 2500 ng/L, the fish displayed increased estradiol levels and reduced hemoglobin and hematocrit values (Guiloski *et al.* 2017). Choi *et al.* (2019) reported at 30 µg/L, acetaminophen altered the histological parameters in exposed rainbow trout kidney and gills, caused poor resorption of ions, and lowered oxygen consumption. Therefore, while effluents from WWTPs may be considered to be lower than the levels based upon which toxic effects were reported (Archer *et al.* 2017), increased water concentrations due to discharges from pharmaceuticals pose threatening health effects, being detected in concentrations higher than those reported for eliciting aquatic toxic effects (Kleywegt *et al.* 2019).

2.6 Environmental transformation of phenolics

Phenolics undergo several changes in the aquatic and soil environments such as adsorption/absorption, bioaccumulation, biotransformation and oxidation/reduction (Zhou *et al.* 2019). Of these transformation pathways, the most substantial in the aquatic/soil environment are microbial transformation and an interplay of abiotic factors as illustrated by the action of chromophoric dissolved organic matter (CDOM) (Parezanovic *et al.* 2019). Biotransformation is usually occasioned by microbial communities inherent in the respective environments in a way that degrades phenolics to lower molecular weight intermediates and/or oligomerizes them.

2.6.1. Biotransformation of phenolics – the example of acetaminophen

Figure 2.1 shows the proposed biotransformation pathway for acetaminophen by Lang *et al.* (2016). At lower concentrations (26.5 µM), it predominantly formed dimers and trimers by oxidative coupling via C-C bond formation between carbon atoms *ortho* to the hydroxyl group. Contrariwise, higher concentrations (530 µM) yielded lower proportions of the oligomers, while *para*-aminophenol was predominantly formed. Other intermediates observed from the degradation pathway include *p*-benzoquinone imine, *p*-benzoquinone, 1,4-hydroquinone, 3-hydroxyacetaminophen, 1,4-benzoquinone, 1,4-dimethoxybenzene,

4-methoxyphenol, 2-hexenoic acid, hydroquinone, N-acetyl-*p*-benzoquinone and *p*-acetanimide. (Liang *et al.* 2016, Zhou *et al.* 2017, Li *et al.* 2017). The toxicities of *p*-aminophenol and *p*-benzoquinone are more than the substrate (Bedner and Macrehamn 2006, Harada *et al.* 2008), which leaves much room for concern over the safety of aquatic organisms and the microbial community where the biotransformation occurs. Also, the

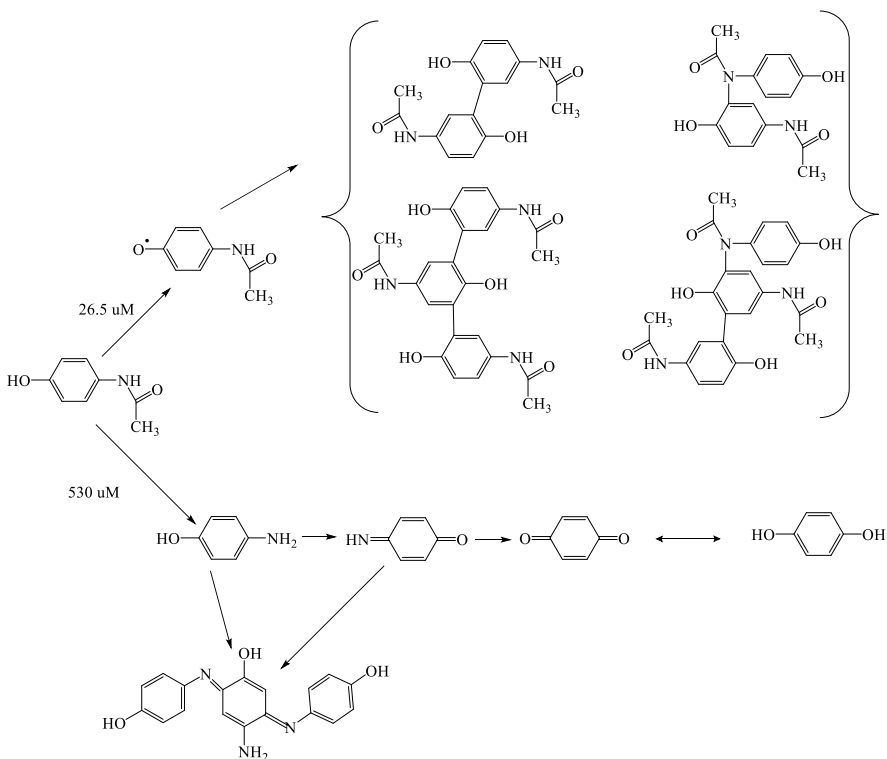


Fig.2.1: Proposed mechanism for transformation of acetaminophen in soil (Adapted from Liang *et al.* 2016).

possibility of uptake of these transformation by-products into plants cultivated on such contaminated soils may result in the bioaccumulation, and subsequent transfer to higher organisms (Pam *et al.* 2014). Liang *et al.* (2019) reported the decline in microbial count following biotransformation of large concentrations of acetaminophen.

Biotransformation of acetaminophen in water and soil is affected by soil type, seasonal/spatial variations, pH, intensity of solar radiation and concentrations of acetaminophen present in the environment (Liang *et al.* 2016, Zhou *et al.* 2016, Li *et al.* 2017). The transformation was observed to be 8.9%, 17.0% and 15.4% for medium loam,

sandy clay and silty clay soils, respectively (Li *et al.* 2014). Zhou *et al.* (2019) reported varied microbial community structures between different lakes; season of the year under consideration and even time of the day when the water was drawn for microbial analysis. They also observed high solar radiance affected the rate of microbial biotransformation of acetaminophen, which might be through the production of colored dissolved organic matter (CDOM), whose higher production rate with high solar radiance may exert a lethal effect on the microbial community. However, Song and Jiang (2020) reported enhanced microbial (*Treponema*, *Magnetospirillum* and *Aspergillus*) growth which favored degradation of organic matter following solar irradiation. Liang *et al.* (2016) reported three species of bacteria linked to acetaminophen biotransformation in soils, while fifteen bacterial and fungal species were characterized from different lakes studied in China (Zhou *et al.* 2019) and linked to the biotransformation of phenolics.

The rate of removal may vary from one location to the other, because the prevailing environmental factors may not be similar amongst locations. Transformation studies have been reported at 70 hours (Zhou *et al.* 2019), 11 days (Zhang *et al.* 2016) and even 120 days (Li *et al.* 2013), with varying degrees of removal. Acetaminophen is classified as a low persistent CEC and has a dissipation time for 90% of its initial concentration (DT₉₀) for 11 days in water/sediment compartments (Löffler *et al.* 2005).

2.6.3 Environmental transformation of phenolics through CDOM

Dissolved organic carbon (DOC) is a usual feature of surface waters and is predominantly made up of allochthonous organic matter described as chromophoric dissolved organic matter (CDOM). CDOM consists of 50-90% humic substances, lignin and plant pigments which are biologically recalcitrant but can be degraded through photochemical reactions releasing inorganic carbon, nitrogen and phosphorus besides low-molecular weight organic compounds (Vähätalo 2009).

Solar radiation initiates both photosynthetic activities in plants and photodegradation reactions on the incident environment. Photodegradation may proceed either through the direct absorption of solar radiation, or indirectly through highly reactive chemical species such as free radicals and electronically excited molecular species (McNeill and Canonica

2016). Effecting solar radiation ranges are primarily the photolytic UV and short wavelength visible radiations, approximately 290-500 nm (Vähätalo 2009, Faust and Hoigne 1987).

Zhou *et al.* (2019) surveyed the origin and chemical reactivity of different sources of $^3\text{CDOM}^*$ and classified them into high-energy triplet states (>250 kJ/mol) and low-energy triplet states (<250 kJ/mol). The former were found to be associated with the autochthonous-origin dissolved organic matter, effluent and wastewater organic matter while the latter originated from terrestrial dissolved organic matter. The efficiency of $^3\text{CDOM}^*$ formation is independent of DOC concentration but is strongly related with the source of DOM, as algal and microbial DOM tends to show higher quantum yields, while the rate of light absorption, depends on the quantity of DOC (McCabe and Arnold 2017), which is in agreement with basic principles. Differences based on source properties, quantum yield, molecular weight contribution, aromaticity of composite heterocyclics, optical properties have also been reported (Marchisio *et al.* 2015, Su *et al.* 2015, Loisel *et al.* 2012, Bracchini *et al.* 2010).

Upon solar irradiation, CDOM absorbs a photon to become excited, forming the singlet state of excited CDOM, ($^1\text{CDOM}^*$) which is converted to the $^3\text{CDOM}^*$, either through oxygen-dependent deactivation or oxygen-independent deactivation (Figure 2.2.). At oxygen-saturated surface water levels, oxygen dependence dominates over oxygen

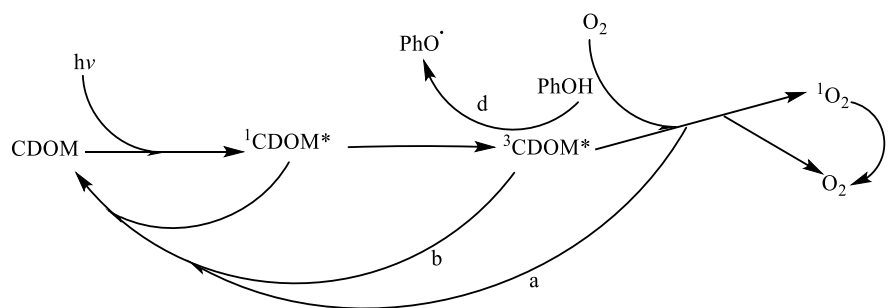


Fig. 2.2: Mechanism of $^3\text{CDOM}^*$ generation and quenching. Quenching of $^3\text{CDOM}^*$ is either (a) oxygen-dependent or (b) oxygen-independent; (c) singlet oxygen relaxes to molecular oxygen; (d) phenol is oxidized to phenoxyl radical

independence leading to the production of singlet oxygen $^1\text{O}_2$ (Golanoski *et al.* 2012) which undergoes unimolecular deactivation to become molecular oxygen, O_2 . The pollutant-transformation effect of $^3\text{CDOM}^*$ is exerted by either electron transfer or energy transfer (Zhou *et al.* 2017).

Several compounds, derivatives of phenol and aniline, are susceptible to environmental transformation through $^3\text{CDOM}^*$, a comprehensive list of which was reviewed (McNeill and Canonica, 2016). Milstead *et al.* (2018) reported the indirect photolytic degradation of 2,4-dibromo-17 β -estradiol (diBrE2) facilitated substantially by surface water $^3\text{CDOM}^*$ as the intermediate. Phenolic transformation proceeds largely (>65% of initial concentration, with 24% degraded by direct photolysis) via a $^3\text{CDOM}^*$ mediated pathway, producing phenoxylphenol, dihydroxybiphenyl, and other lower molecular weight monomers (Li *et al.* 2017), Figure 2.3. A similar reaction pathway and intermediates were reported elsewhere (Chen *et al.* 2018). The half-life of the reaction which varies with the kind of $^3\text{CDOM}^*$ used was 6.7 – 17.5 h. Although reactive oxygen species (ROS) such as $^1\text{O}_2$, HO^\bullet , O_2^- were present, their combined chemical transformation effect on acetaminophen was minimal, and the rate of the reaction was dependent on the amount of dissolved oxygen present. It was also reported elsewhere (Loiselle *et al.* 2012) that HO^\bullet is less likely to play a significant role in photo-transformation. Consequently, any factor that reduces the presence of dissolved oxygen in surface water may lead to decreased rate of removal of phenolic contaminants (Golanoski *et al.* 2012).

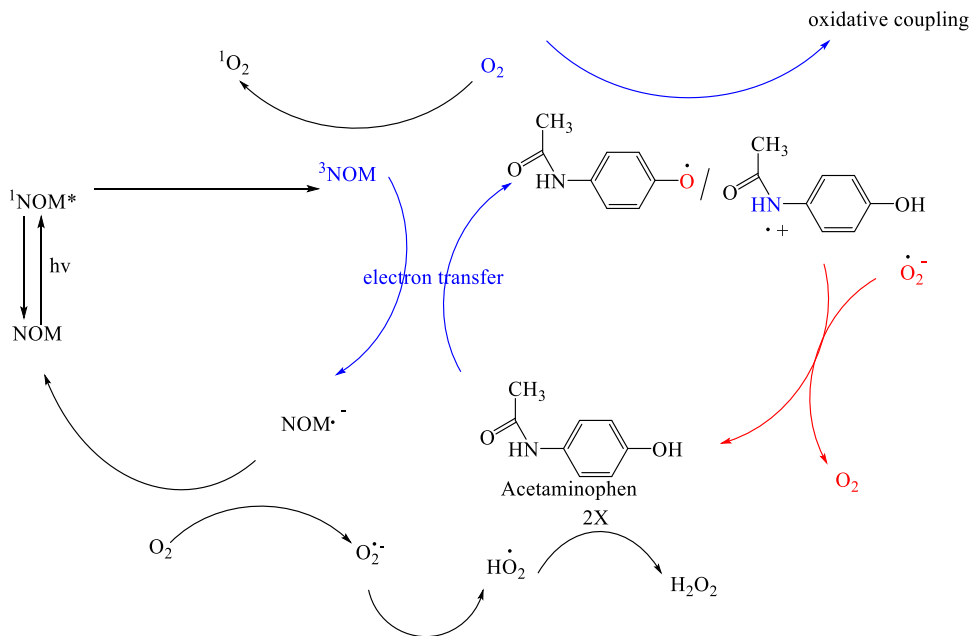


Fig. 2.3: Proposed initial step in the indirect photodegradation of acetaminophen in NOM-enriched solutions modified from Li *et al.* (2017). (Note: NOM is used here to retain the originality of the author's presentation).

The pathway shown above follows the pattern of the general sequence of reactions presented in Fig.2.2. The regeneration of CDOM (NOM) in the surface water is to ensure the continual replenishment of the reactant, in order to foster the photochemical transformation process.

2.7 Brief overview of conventional wastewater treatment processes

A wastewater treatment plant is a set of sequential unit operations where influent wastewater moves through the respective process units, receives treatment and then discharged as effluent. The aim of a WWTP is to produce water that meets acceptable environmental discharge standards (Saleh *et al.* 2019, Bustillo-Lecompte *et al.* 2016, US EPA 1998) into receiving water bodies. Quality standards are set based on physico-chemical parameters such as pH, chemical oxygen demand (COD), biochemical oxygen demand, (BOD), BOD incubation at 20 °C for five days (BOD₅), total suspended solids (TSS), total nitrogen (TN), ammonia expressed as NH_4^+ and NH_3 , and total phosphorus (Liu *et al.* 2019, Metcalf and Eddy 2014). Above a threshold presence of these parameters show positive correlation with toxicity of WWTP effluents (Ma *et al.* 2016). The lack of

regulatory parameters for the existing array of organic compounds in the effluents further underscores the omission of discharge standards for this class of pollutants.

Conventional wastewater treatment goes through three stages of treatment, namely screening or pre-treatment, primary treatment and secondary treatment. The secondary treatment stage mostly employs activated sludge because it produces effluent that meet regulatory standards at reasonable operating and maintenance costs (Jelic *et al.* 2012).

Wastewater effluents arising at the end of the last treatment stage, constitutes the focus of our research work, since this point serves as the gateway through which all unremoved CECs present in sewage enters the environment.

2.8 Advanced Oxidation Processes (AOPs)

Although natural degradation of phenolics (CECs) occur in the environment, the process is so slow to remove a majority of the dissolved CECs in a manner to sustain environmental health, considering the half-lives of the CECs, the pseudo-persistence and the effluent concentrations emanating from conventional WWTPs. This calls for an artificial process to improve the rate of conversion making AOPs an important option to explore.

AOPs are chemical reactions that produce strong oxidants, hydroxyl radicals ($\cdot\text{OH}$) or sulphate radicals ($\text{SO}_4^{\cdot-}$) which are able to oxidize refractory organic pollutants, to intermediates such as carboxylic acids, carbon dioxide and halide ions (Bartolomeu *et al.* , 2018, Salimi *et al.* 2017). Radicals have unpaired electrons and react with aromatic pollutants by addition to unsaturated bonds and aromatic rings, abstraction of hydrogen from aliphatic carbons and electron transfer (Bauer and Fallman 1997). AOPs were initially employed for the treatment of drinking water in the 1980s, however their application has increased over the years to cover wastewater treatment (Deng and Zhao 2015, Glaze 1987). Theoretically, pollutants are degraded without creating a secondary waste stream requiring any further treatment, thereby minimizing the operational process cost, in contrast to other processes such as adsorption, stripping and ion exchange (Fast *et al.* 2017, Metcalf and Eddy 2014).

Common approaches employed in AOPs include ozone, Fenton chemistry, and hydrogen peroxide (Fast *et al.* 2017), and some of these have been employed in the treatment of CECs such as parabens: ozone (Pipolo *et al.* 2017, Tay *et al.* 2010), ozone/UV and ozone/UV/ZnO (Asgari *et al.* 2019), UV and UV/H₂O₂ (Bledzka *et al.* 2012, Hansen and Anderson 2012). Others are photo-Fenton and Fenton (Orak *et al.* 2017, Lucas and Peres 2015) and electrochemical oxidation (Bosio *et al.* 2020, Steter *et al.* 2014a, Steter *et al.* 2014b)

Among the AOPs used in pollutant degradation, some are employed in concert with synergistic effect yielding a higher removal efficiency than application of an individual AOP (Cuerda-Correa *et al.* 2016, Xiao *et al.* 2015). Therefore, some of these AOPs are discussed in the subsequent headings.

2.8.1 Ozonation

Ozone is a very strong oxidant (next only after fluorine and persulphate) with an oxidation potential ($E^{\circ} = 2.07$ eV) higher than that of hydrogen peroxide ($E^{\circ} = 1.78$ eV) (Oyama 2000). This thermodynamically unstable molecule undergoes exothermic decomposition releasing molecular oxygen. At 25 °C, it is more soluble in water than oxygen and capable of oxidizing a wide range of organic compounds. These properties of ozone have made it a candidate of choice for single use or in combination with other AOPs. Ozone, chlorine, and chlorine dioxide are the common oxidants for the treatment of organic compounds in water treatment plants (Tay *et al.* 2010).

The use of ozone in the oxidation of phenol in industrial wastewater was reported several decades ago (Niesgowski 1953) where initial pH adjustment to basic conditions, between pH 10 – 12, was ideal for highest phenol removal. Under acidic conditions, ozone oxidizes phenol producing an *ortho*-hydroxylated product, catechol, besides hydroquinone and resorcinol (Oputu *et al.* 2020, Oyama 2000). The fate of the initial intermediates is pH dependent. Under acidic conditions, the formation of three- and four-carbon chain length acids (acrylic, maleic, fumaric, tartaric, mesotartaric) is favored (Oyama 2000). However, at basic pH, oligomerization of phenol and catechol is favored, forming dimers, trimers and tetramers (Oputu *et al.* 2020, Chrostowski *et al.* 1983).

Ozone treatment is a preferred option especially where industrial wastewater cannot be treated biologically due to high concentrations of toxic substances which hamper microbial survival and growth (Forero *et al.* 2001).

According to Tay *et al.* (2010), ozone-Fenton based treatment of parabens produced at least twenty degradation by-products (DBPs) through two broad pathways: hydroxylation of the aromatic ring and/or ester chain, producing an array of hydroxylated derivatives of the corresponding paraben while the degradation pathway produced majorly PHBA and hydroquinone. The pH-dependent process, with optimal removal at pH 12 employed ozone bubbled into a stirring reaction matrix over an hour reaction course. The rich cocktail of products was not subjected to toxicity screening to ascertain the safety of the degradation by-products formed, thereby providing no information on the toxicity or otherwise of the products compared against the starting material, leaving an obvious knowledge gap.

The use of ozonation alone may not achieve the desired complete removal of the target pollutants. To make up for this lapse, larger doses of ozone may be required (Martins and Quinta-Ferreira, 2009) thereby increasing the cost of the process. To make up for this shortcoming, the combination of ozone and other substances, such as a heterogeneous catalyst that facilitates the production of large amounts of hydroxyl radical in a process called catalytic ozonation, creates a synergistic approach that enhances attack against aromatic pollutants (Gomes *et al.* 2018, Xiao *et al.* 2015) thereby improving overall pollutant removal. In a heterogeneous Fe-catalyst based ozonation process, 32% and 79% total organic carbon (TOC) removal was achieved with Fe-catalyst alone and Fe-catalyst combined with hydroxyl radical, respectively; an enhanced removal due to the formation of Fe-O-OH on the surface of the catalyst (Li *et al.* 2018b). In the use of ozonation alone and catalytic ozonation employing volcanic rocks, Gomes *et al.* (2018) reported the degradation of MP, EP, PP, and BP follow a similar pattern both in ozone requirement, time and product formation. With 123 mg/L and 55 mg/L for single- and catalytic-ozonation, respectively, complete removal of initial 9 mg/L MP was attained within two hours at 25°C. The major reaction products were hydroquinone and hydroxylated derivatives of benzoic acid (Gomes *et al.* 2019, Gomes *et al.* 2018). This implies a

complete removal of the parent parabens, but an accumulation of transformation products. Catalytic and photocatalytic ozonation also lowers the toxicity of the products formed by improving mineralization of parabens (Gmurek *et al.* 2019, Marquez *et al.* 2014) further underscoring its environmental importance. Different reaction times have been recorded for the highest attained pollutant removals recorded, ranging from 30 min to several hours (Gmurek *et al.* 2019, Zhao *et al.* 2019, Li *et al.* 2018b).

Failure to achieve complete mineralization, production of hydroxylated DBPs and other aromatic derivatives, and often lack of toxicity assay leaves the reader in doubt as to the safety of the effluent after treatment. Moreover, varying the catalyst combined with ozone also alters the transformation products formed and the degradation pathways on a similar paraben substrate (Gmurek *et al.* 2019). In addition, assessing the toxicity of the products formed depends on the species of the test organism since individual organisms have different tolerance or response to toxic agents (Gomes *et al.* 2019), hence the need to maintain uniform assays to provide easy comparison of results.

Comprehensive reviews of applications of heterogenous photocatalytic ozonation in wastewater treatment, reaction mechanisms, economics of the process and future perspectives on this growing technology have been provided elsewhere (Xiao *et al.* 2015, Nawrocki 2013)

2.8.2. Fenton and Electro-Fenton (EF) AOPs

Fenton processes are based on the use of hydrogen peroxide as the oxidant and soluble Fe^{2+} ions as the catalyst usually at low pH, between 3 and 4, to enhance iron solubility and consequently maximize yield of hydroxyl radicals (Roudi *et al.* 2018, Tony and Bedri 2014, Chang *et al.* 2008). The low-pH dependency of the Fenton-reagent makes it unfit for use in natural environments without pH adjustment, dividing the process into oxidation in acidic pH and coagulation in alkaline conditions (Cavillini *et al.* 2015). pH adjustment adds another dimension to the cost of treatment, further making the process less appealing for industrial applications. The Fenton reaction involving the formation of hydroxyl radical and other ions proceeds thus:

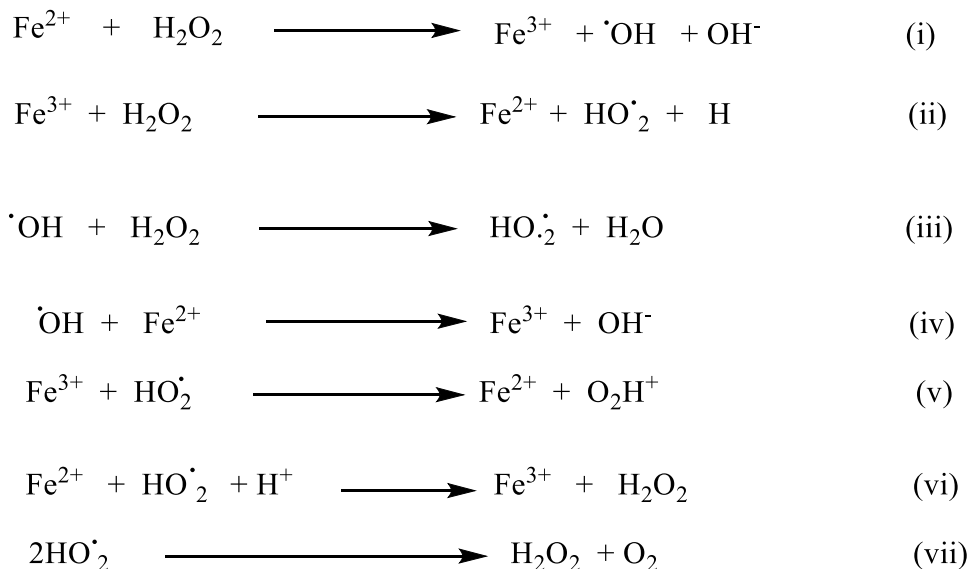


Fig. 2. 4: Fenton reaction scheme (Raoudi *et al.* 2018, Deng and Zhao 2015).

The decomposition of hydrogen peroxide facilitated by ferric ion produces hydroxyl radical (reaction I above). The Fenton reagent (ii and iii) scavenges the hydroxyl radical formed. Therefore, the molar ratio of the hydrogen peroxide and iron ion need be experimentally determined to provide the needed concentration that will effectively oxidize the target organic compounds and minimize undesired scavenging activities of the formed hydroxyl radical. The reduction of Fe^{3+} to Fe^{2+} in (ii) proceeds with a rate constant of $0.001\text{-}0.01 \text{ M}^{-1}\text{s}^{-1}$, several orders of magnitude less than (i) ($76.0 \text{ M}^{-1}\text{s}^{-1}$) (Nogueira *et al.* 2007), thereby imposing kinetic constraints for Fe^{2+} formed to take part in the Fenton process. The Fe^{3+} therefore constitutes a sludge under the conventional treatment conditions. The sludge must be removed and disposed of, increasing the cost of the treatment process and complexity.

According to the Fenton reaction scheme, modified systems can fit into and improve on the traditional process. These include photo-Fenton process, where applied UV irradiation improves on the reduction of Fe^{3+} to Fe^{2+} (Dominguez *et al.* 2019, Zuniga-Benitez *et al.* 2018, Lucas and Peres 2015). In the electro-Fenton process, an electrochemical approach is employed to generate either or both of the Fenton reagents (Rosales *et al.* 2018, Steter *et al.* 2018). In the Fenton-like process, the series of reactions begin with (ii), instead of starting with (i) (Deng and Zhao 2015) employing hydrogen peroxide and other cations

such as Co^{2+} , Mn^{2+} and Cu^{2+} (Pereira *et al.* 2012). Some of these applications are considered below in respect to the target CECs under study.

According to Steter *et al.* (2018), solar photoelectro-Fenton (SPEF) boron-doped diamond (BDD) produced a complete removal of MP, EP and PP in a real urban wastewater at 3 hours and attained 66% mineralization in 4 hours, with a great energy conservation efficiency. Formation of chlorinated DBPs was minimized since active chlorine use was minimal while DBPs at the end of the treatment were malic, formic and oxalic acids (Steter *et al.* 2018). The combined use of graphite and between 25-30% iron content in composing a cathode material for an electro-Fenton process produced between 95-100% removal of MP in 30 minutes and a 98.7% reduction in total organic carbon (TOC) content in 120 minutes (Rosales *et al.* 2018). The pseudo-first order process had optimal conditions at 100 mA and pH 3, and showed several hydroxylated intermediates were formed before eventual cleavage of the ring, yielding acids (Rosales *et al.* 2018).

In three hours of reaction time, parabens treatment by UV irradiation alone removed between 27 and 38% of initial parabens, while the combination of UV/ H_2O_2 improved removal efficiency to 62-92 %. The Fenton reagent alone was not an effective treatment option at the pH of PBs in aqueous solution wherein the experiment was conducted (Lucas and Peres 2015). Butyl paraben was most susceptible to degradation when UV/ H_2O_2 and UV/ $\text{H}_2\text{O}_2/\text{Fe}^{2+}$ were combined and PP was least susceptible under similar conditions (Lucas and Peres 2015).

Within the first hour of acetaminophen mineralization by EF, 1,4-benzoquinone, benzaldehyde and benzoic acid intermediates were produced and caused *V. fischerii* inhibition by 100% (Li *et al.* 2016). However prolonged reaction time of 8 hours enhanced mineralization of the toxic intermediates thereby reducing the toxicity of the reaction matrix, relative to the initial toxicity (Li *et al.* 2016). The production of such intermediates more toxic than the starting material shows the limitations of the EF process in treating acetaminophen. Although the aromatic intermediates are further mineralized to smaller organic acids, their risk in the process cannot be overlooked.

A combination of Fenton and other AOPs produces high pollutant removal efficiency, however the cost of the process, effects of the chemicals on the materials, ecotoxicity

implications of the DBPs formed, handling the sludge formed are some of the drawbacks of the process.

2.8.3 Electrochemical oxidation as an AOP

The application of electrochemistry in the treatment of contaminated water has taken either of two approaches, electric current based generation of reactive species and direct anodic oxidation. Among these, the latter yields very poor removal efficiency and is rarely chosen (Martinez-Huitle and Andrade 2011), hence the former will be considered. Mechanisms of the reactions, heterogenous applications, intermediates formed and feasibility of this AOP have been reviewed (Ganiyu *et al.* 2018, Martinez-Huitle and Andrade 2011).

The degradation of MP by electrochemical oxidation (ECO) and sonolysis, or both, showed the synergistic effect leads to higher removal and mineralization efficiency on MP (Steter *et al.* 2014b). Up to 60% of initial 100 mg/L MP was mineralized in 120 minutes at pH 5.7 using ultrasound at a frequency of 20 kHz and 523 W cm^{-2} , with highest synergistic effect observed at $35 \text{ }^\circ\text{C}$ and a current input of 10.8 mA cm^{-2} . In another study, 10 mg/L each of MP, EP, PP, BP and BzP were completely removed in 10 minutes under optimized conditions using a current density of 12.5 mA cm^{-2} , NaCl electrolyte at 3.0 g/L and the final effluent showed no neurotoxicity as when compared against untreated samples (Bosio *et al.* 2020), showing the ability of these conditions to treat PBs contamination.

In another development, stainless steel electrodes supplied direct current densities of 9.5 mA cm^{-2} and tested at pH 3, 5, 7 and 9 demonstrated optimal removal of 10 mg/L of acetaminophen at 540 minutes (Zavala and Estrada 2016). An array of oxidation products formed included hydroquinone, *p*-aminophenol, *p*-nitrophenol, 1,4-benzoquinone, and N-acetyl-benzoquinone imine (NABQI) (Bedner and Macchrehan 2006) which were not completely mineralized by the end of the treatment process (Zavala and Estrada 2016). As applicable to other AOPs, the heterogenous use of ECO with other AOPs is a common practice aimed at improving the removal efficiency. Electro-Fenton (Su *et al.* 2013), sono-electro-chemical (Frontistis 2020) and photo-electro-Fenton (De Luna *et al.* 2012) processes have been reported.

Although the processes are feasible and well demonstrated to achieve good pollutant removal efficiency, the cost implications in form of electricity consumption, maintenance of the materials such as electrodes due to wear down effect (Zavala and Estrada 2016), procurement of the electrolytes and other oxidizing reagents and diminishing removal efficiency with prolonged treatment cycles (Bosio *et al.* 2020) make them a challenge for effective implementation. The production of intermediates is also a major concern, since the ecotoxicological effects of such intermediates need be considered. For instance, the electro-oxidation of BP yields radicals identified by the chemical formulae ($C_4H_5O_4^-$, $C_{11}H_{13}O_5^-$, $C_{11}H_{11}O_5^-$) (Gomes *et al.* 2016). The key parameters that govern the process include current density, the linear velocity of the electrolyte, ratio between the anode surface and the solution volume, composition of the electrode and pH of the reaction medium (Polcaro *et al.* 2002).

2.8.4 Other AOPs

Other AOPs have also been employed in the treatment of parabens and acetaminophen. Some of these include UV irradiation processes (Dominguez *et al.* 2019, Gryglik and Gmurek 2018, Tan *et al.* 2014), sonochemical oxidation (Frontistis 2020), and hydrogen peroxide-based processes (Hansen and Anderson 2012). The above references have reported the reaction conditions, removal efficiencies and optimized parameters. Moreover, direct photochemical degradation of PP under aerobic conditions at 330 nm leads to complete mineralization of PP but produce intermediates more toxic than PP; while under anaerobic conditions, the substrate is efficiently eliminated as dead-end products (unidentified due to lack of standards), although not known to be toxic, are however recalcitrant to further UV light degradation (An *et al.* 2014).

General reviews of AOPs are available for further consideration of the reader (Cuerda-Correa *et al.* 2019, Miklos *et al.* 2018) while a comprehensive review of the formation of oxidation by-products by AOPs has been reported (Ike *et al.* 2019). Any of these AOPs may be accompanied by other non-radical oxidative mechanisms, whose contributions to the overall EC removal efficiency is determined by the AOP type and the reaction conditions. These processes have also been reported (Deng and Zhao 2015).

2.9. Oxidoreductases in wastewater treatment

The application of enzymes in the treatment of wastewater has always focused on the use of oxidoreductases, prominent of which are tyrosinases, laccases, and peroxidases. The first two shall be briefly considered, whereas the focus shall be on peroxidases.

2.9.1 Tyrosinases

Tyrosinases (*o*-diphenol:dioxygen oxidoreductase, EC 1.10.3.1) are widely distributed among different living organisms, prokaryotes, plants, fungi, arthropods and mammals, and are classified as type-3 copper-containing (metalloenzymes) proteins (Ullrich and Hofrichter 2007). The active site of the enzyme contains two copper atoms, coordinated by 3 histidine residues (Decker and Tucek 2000). The active site can exist in three different states, deoxy-, oxy- and met-tyrosinase, determined by oxidation state of the copper and its linking with the dioxygen (Ullrich and Hofrichter 2007, Sanchez-Ferrer *et al.* 1995). The enzyme catalyzes the formation of *o*-quinones in a two-step sequential process by hydroxylating monophenols to form *o*-diphenols which are oxidized to *o*-quinones (Varga *et al.* 2019, Duran *et al.* 2002) using molecular oxygen. The quinones can further polymerize spontaneously to form brown or black pigments (Wada *et al.* 1994). According to the mechanism of the reaction, only the oxy-tyrosinase form which is the oxidized form of the enzyme, is active in the conversion of monophenol to *o*-diphenol through an enzyme-substrate complex. The *o*-diphenol is either released from the active site or it is oxidized to the corresponding *o*-quinone (Rodriguez-Lopez *et al.* 2001). Tyrosinase have a wide range of substrate specificity (Varga *et al.* 2019), able to react with several phenolic compounds, leading to the formation of oligomers which may precipitate out of solution (Abdollahi *et al.* 2018, Lee *et al.* 1996, Wada *et al.* 1994) and can be separated. β -tyrosinase gene extracted from a thermophile *Symbiobacterium* sp. SMH-I and cloned in a mutant strain of *E. coli* secreted the enzyme with optimal pH between 6.5 and 9.0 and remains catalytically active at 65 °C and was shown to reduce 100 mM phenol to 8 mM in 24 h (Lee *et al.* 1996). Reviews of the mechanism of action, prospects and applications, kinetic properties and toxicity evaluation of tyrosinase-treated effluents have been made (Varga *et al.* 2019, Kanteev *et al.* 2015, Zaidi *et al.* 2014).

2.9.2. Laccases

Laccases (*p*-diphenol:dioxygen oxidoreductase, EC. 1.10.3.2) are grouped under the superfamily of multi-copper oxidases (MCOs) characterized by different substrate specificities and varying biological functions (Janusz *et al.* 2020) using oxygen as substrate to oxidize aromatic and non-aromatic compounds. Due to the unique spectral properties of copper involved with laccase active sites, they are categorized into three groups; type 1 (T1), type 2 (T2) and type 3 (T3) or blue copper, normal copper and coupled binuclear centres, respectively (Solomon *et al.* 1992). The three components work together and sequentially to attain catalytic activity. Type 1 accepts electron from reducing substrates and transfers it to a trinuclear copper cluster formed between T2 and T3, about 13 Å apart from T1, where molecular oxygen serving as the terminal electron acceptor is reduced to water (Skalova *et al.* 2011). Since T1 abstracts electrons from substrates to initiate the catalytic process, its oxidation potential determines the pace and substrate range of the reaction, such that mutant variants with increased redox potential of T1 can oxidize the high redox potential compound 1,2-dihydroxyanthraquinone-3-sulfonic acid, a compound natural laccases cannot oxidize (Gunne *et al.* 2014). This redox potential also forms the basis for classifying laccases into low and high redox potential groups (Janusz *et al.* 2020, de Salas *et al.* 2019, Klonowska *et al.* 2002). Bacteria, insects and plants generally produce the low-redox potential laccases while high-redox potential laccases predominate among fungi (Munk *et al.* 2015). Perhaps this partly accounts for the vast industrial applications of fungal laccases (Munk *et al.* 2015).

Laccases cannot directly add oxygen into phenolic rings, however through a cascade of reactions *p*-quinones and *p*-hydroquinones can be formed through the intermediates phenoxyl radicals, cyclodienone cations with the addition of water (Ullrich and Hofrichter 2007). Due to the presence of cupredoxin-like domains, MCOs can reduce dioxygen to water without production of toxic by-products (Janusz *et al.* 2020). These properties inform the choice of laccases in the treatment of phenolic and non-phenolic-contaminated waters (Becker *et al.* 2017, Viswanath *et al.* 2014). Becker *et al.* (2014) reported the treatment of EDCs: estrone (E1), 17β-estradiol (E2), estriol (E3), 17α-ethinyl estradiol

(EE2), bisphenol A (BPA), nonylphenol (NP), Propyl paraben and benzylbutylphthalate (BBP) as individual contaminants and in binary mixtures, using free and immobilized fungal laccases from *Trametes versicolor* and *Myceliophthora thermophila*. Reported removals varied between 82% in 6 h and up to 99% in 24 hours through surface adsorption onto the immobilization supports. A comprehensive review on the use of laccase in wastewater treatment is reported (Gasser *et al.* 2014, Viswanath *et al.* 2014).

2.9.3 Peroxidases

Peroxidases (EC.1.11.1.7) are a prominent member of the oxidoreductase enzyme class. These undergo oxidative reactions employing hydrogen peroxide as an electron acceptor. Horseradish peroxidase (HRP) is a heme-containing oxidoreductase, which has been widely employed in research, diagnostics, and several other applications. Of the different HRP isoenzymes, HRP isoenzyme C (HRP C), has been the most extensively studied and much of the insights into the structural features and characteristics of heme-peroxidases emanated from over a century of research with HRP (Veitch 2004). Structurally, the plant-based superfamily of peroxidases is classified under three classes according to derived amino acid sequence and crystal structure analysis (Smith and Veitch 1998). These are: mitochondrial yeast cytochrome c peroxidase (CCP), cytosol and chloroplast ascorbate peroxidases (APXs) forming class I; secretory fungal peroxidases constitute class II of which prominent examples are lignin peroxidase (LiP) and manganese peroxidase (MnP) from *Phanerochaete chrysosporium* while class III comprises the secretory plant peroxidases, such as the classical HRP and SBP (Smith and Veitch 1998, Welinder 1992). Class III peroxidases share a unique sequence of 34 amino acid residues between helices F and G, partly forming the substrate access channel which is not found in class I and II peroxidases (Gajhede *et al.* 1997). Since SBP is employed in this study, we shall focus on class III. Peroxidases are preferred for their multifunctional activities and broad substrate specificity. Specifically, SBP is a cheap source of peroxidase with abundance around the world and adds economic benefits to the soybean value chain.

2.9.3.1 Structural features and properties of HRP C and SBP

Mature plant SBP contains 306 amino acid residues having a pyrrolidone carboxylic acid in the N-terminus and a serine residue at the C-terminal (Welinder and Larsen 2004). The HRP C also consists of 306 amino acid residues (Smith *et al.* 1990). However, some have reported 308 amino acid residues (Veitch 2004, Welinder 1979). Although approximately 18% of the enzyme's molecular mass is contributed by glycosylated moieties (Gray *et al.* 1996), glycosylation is not required for the correct folding nor activity of the enzyme (Smith *et al.* 1990). However, Hummer and Spaduit (2019) reported loss of optimal catalytic activity and reduced thermostability in non-deglycosylated recombinant HRP C (rHRP C). A mature SBP would contain seven glycosylation sites on Asn 56, 130, 144, 185, 197, 211 and 216, some of which are as fully glycosylated as that on Asn 216 (Welinder and Larsen 2004). This contrasts with another report of only 4 glycosylation sites on Asn 185, 197, 211 and 216 (Gray and Montgomery 2006). The glycans are on average composed of 2 mols of N-acetylglucosamine (GlcNAc), 3.3 mol of mannose, 0.7 mol of xylose and 0.9 mol of fucose residues (Gray *et al.* 1996). Gray and Montgomery (2006) reported an asymmetrical distribution of glycans, predominantly on the substrate-channel face, as observed from the crystal structure of SBP, whereas glycans of HRP C are evenly distributed over the enzyme surface. HRP C has 9 possible glycosylation sites on Asn: 13, 57, 158, 186, 198, 214, 255, 268, and 316 (Ryan *et al.* 2006). The molecular mass of HRP C is 44100 Da, comprised of 7580 Da of carbohydrates, 550 Da heme group and 80 Da calcium (Veitch 2004, Welinder 1979). The SBP however has a total molecular mass of 40660 Da, comprised of 7400 Da carbohydrates, 550 Da of heme group and 80 Da of calcium (Henriksen *et al.* 2001). The similarity in calcium and heme content is important, considering the vital roles these play in enabling proper folding and catalysis, respectively in the enzyme (Smith *et al.* 1990). Although they have similar number of amino acid residues, the difference in molecular mass could be attributed to the differences in the composite amino acids, since the enzymes have about 70% residue homology between them (Welinder and Larsen 2004). Another possible reason is the variation in the kind of glycan found at the glycosylation sites and the extent of glycosylation, since glycan content varies with the source and "maturity" of the enzyme (Veitch 2004).

HRP C has four disulphide bridges between cysteine residues: 11-91, 44-49, 97-301 and 177-209 (Veitch 2004). Similarly, SBP has four such bridges between cysteine residues 11-91, 44-49, 97-299 and 176-208 (Welinder and Larsen 2004, Henriksen et al. 2001). Beside the number of bonds being similar, the participating cysteine residues are also similar in the first two instances, illustrating the close subfamily sequence homology, warranting the placement of both enzymes in class III. These polypeptides fold creating a secondary structure with 13 alpha-helices in both enzymes, but with 2 and 3 beta-sheets in SBP and HRP C, respectively (Henriksen *et al.* 2001, Gajhede *et al.* 1997). HRP C has two domains, proximal and distal, with the heme group situated in between them (Veitch 2004) (Figure 2.5). HRP C is found in the roots, cell wall and vacuoles of horseradish plant (*Armoracia rusticana*) (Veitch 2004). SBP is predominantly located in the seed coat, also found in leaf and stem of soybean (Schmitz *et al.* 1997).

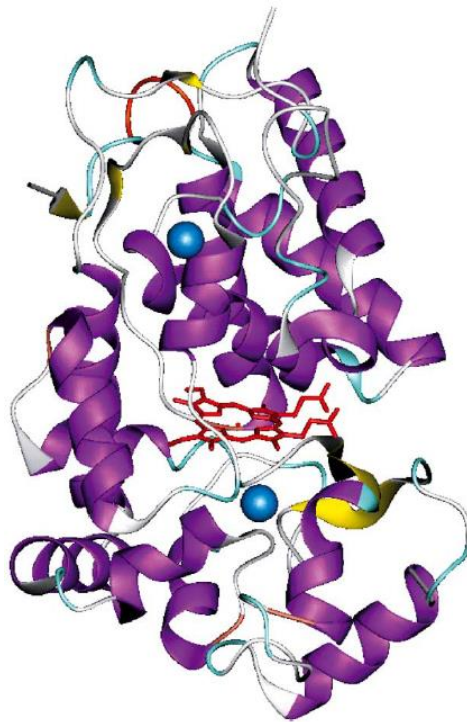


Fig. 2.5 Three-dimensional crystal structure of HRP C (Adapted from Veitch 2004, with permission). The red portion represents the heme group situated between the two domains; each domain contains one calcium atom in blue. Purple and yellow colors represent the alpha helices and beta sheets, respectively.

2.9.3.2. Amino acids involved in catalysis

The heme pocket contains distal Arg38 and His42, which are crucial to catalysis (Ryan *et al.* 2006). A mutation replacing His42 with Ala results in a decreased rate of compound I (Figure 2.6) formation by six-fold (Newmyer *et al.* 1996). These residues are engaged in acid-base catalysis, and the cleavage of O-O bond in hydrogen peroxide, thereby facilitating the formation of compound I (Smith and Veitch 1998, Rodriz-Lopez *et al.* 1996). Specifically, distal His42 is thought to enhance the formation of compound I by acting as a general acid-base catalyst, where it abstracts a proton from hydrogen peroxide, enabling the formation of a Fe.OOH (ferric peroxide) intermediate, and eventually transfers the proton to the distal oxygen of the ferric peroxide complex, during the cleavage of the dioxygen bond (Mukai *et al.* 1997, Newmyer *et al.* 1996). This is plausible considering the histidine imidazole side chain has a very low pK_a of *ca* 2.5 while the R group of Arg38 has a very high pK_a (Henriksen *et al.* 2001). The formation of compound I can still proceed without Arg38, at a lower rate, however its presence aids the efficiency of the reaction and provides the binding affinity for ligands such as hydrogen peroxide (Smith and Veitch 1998).

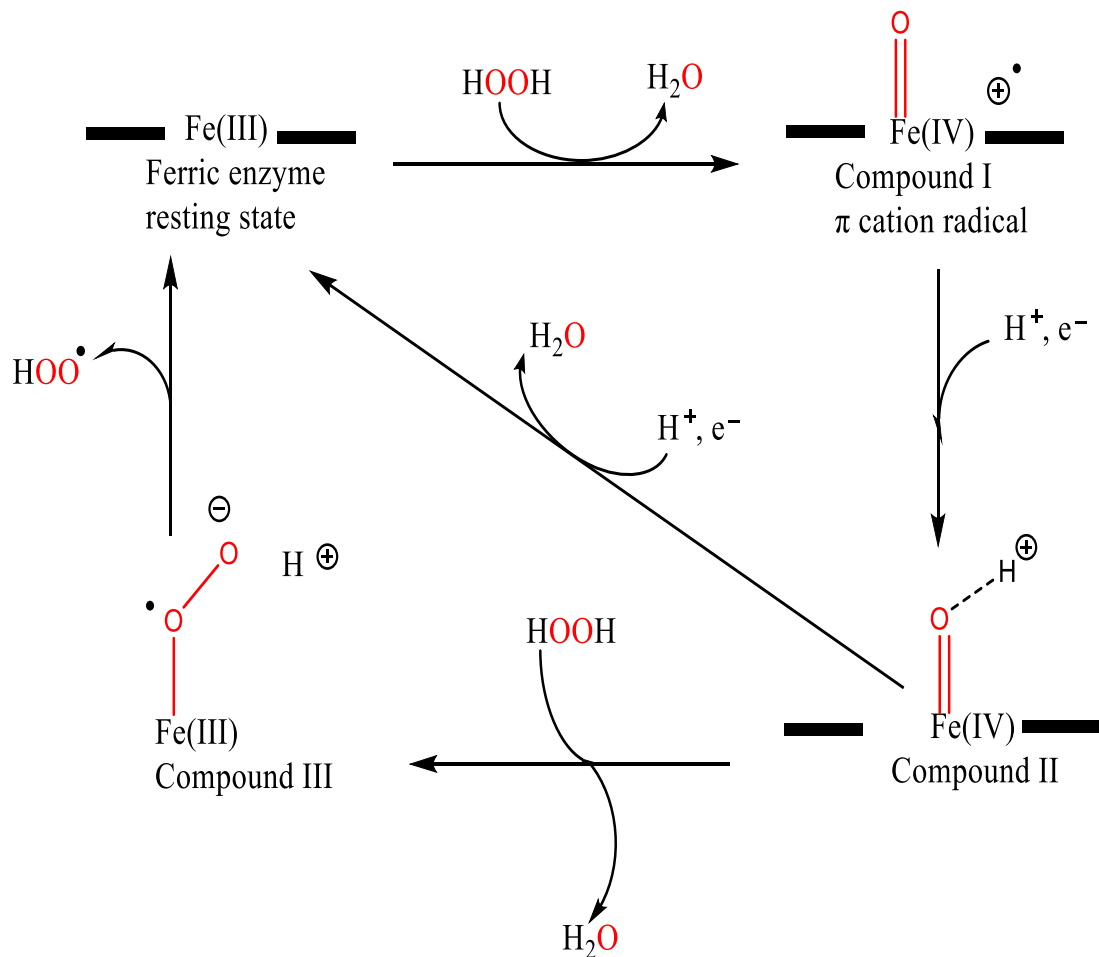


Fig.2.6 Peroxidase cycle. Atoms in red represents the mechanism of oxygen atoms taken from hydrogen peroxide (Modified from Dunford *et al.* 2016)

Phe142 acts indirectly to facilitate the binding of aromatic donor molecules to the active site and subsequent structural changes that enhances catalysis to occur (Veitch *et al.* 2004). Alanine replacement of Phe142 by site-directed mutagenesis showed a rHRP C 3-4 times weaker in its binding to its aromatic substrate than the wild type HRP C but demonstrated normal folding and heme pocket structure (Veitch *et al.* 2004).

Asn70 forms a hydrogen bond between the amide oxygen to the -NH group of imidazole on distal His42 in the active site (Veitch 2004). This bonding helps to maintain the basicity of the residue as a decrease in the basicity affects the ease of proton and electron transfers (Nagano *et al.* 1996). Proximal Asp247 complements by accepting a proton from His42

thereby enhancing the electron density on the imidazole ring and cleaves the O-O bond via a “push” effect (Nagano *et al.* 1996). Other amino acids directly or indirectly involved in peroxidase catalysis include Phe41, which blocks substrates from accessing the ferryl oxygen of compound I (Veitch 2004). His170 restrains the heme moiety in position and prevents distal coordination while ensuring the heme moiety maintains the 5-coordinated state which favours the catalytic process (Newmyer *et al.* 1996). Mutation of this amino acid leads to the accumulation of a 6-coordinate heme species which does not favour catalysis (Howes *et al.* 2001).

2.9.3.3. Catalysis in peroxidases

Substrate binding to HRP C is facilitated through hydrogen bonding and hydrophobic interactions between amino acid residues on the distal side of the heme and the substrate molecule (Howes *et al.* 2001). The peroxidase cycle begins with the resting enzyme state through compound I and compound II and eventually completing the cycle with a return to the resting state. The stages of the cycle are explained below.

2.9.3.3.1 Formation of compound I

To begin the peroxidase cycle, hydrogen peroxide binds to heme iron atom of peroxidase in its resting state, forming ferric-hydroperoxide complex (Fe(III).OOH) (Ortiz de Montellano 2010). This complex is described as Compound 0 and marks the initiation of the catalytic cycle (Veitch 2004). It has been described by kinetic analysis as a transient compound whose conversion to compound I defines the rate-limiting step in the peroxidase cycle (Baek and Van Wart 1989).

The critical roles of Arg38 and His42 as a proton acceptor from hydrogen peroxide and as charge stabilizer, respectively was reported by Poulos and Kraut (1980) and tagged Poulos-Kraut mechanism, based on cytochrome c peroxidase from yeast. This model is generally applicable to plant peroxidases as well (Dunford *et al.* 2016). The rate-determining step (Compound 0 or ground state to Compound I) entails breaking the bonds of the distal hydrogen atom in the ferric-hydroperoxide complex to form water and in the process oxidation state of iron changes from III to V. The distal His42 imidazole deprotonates the peroxide and delivers the proton to the ferryl complex, cleaving the O-O bond and forming water (Fig.2.6). Compound I is therefore two oxidizing equivalents above the resting state,

and a high oxidation state intermediate having an Fe(IV)=O center and a porphyrin-originating *pi*-cation radical (Ciric-Marjanovic *et al.* 2016).

2.9.3.3.2 Compound II

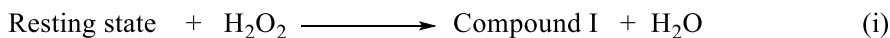
This is formed by one electron reduction of Compound I, while the [Fe(IV)] state is still present on the molecule but the porphyrin radical is quenched (Ortiz de Montellano 2010). X-ray crystallographic evidence shows compound II is bonded to a single protonated oxygen atom showing an iron-oxygen bond length of 1.86 Å-1.92 Å and could be represented as [Fe(IV)-OH (Hersleth *et al.* 2006). In HRP, the oxygen atom involved in this complex formation is hydrogen-bonded to Arg38 and to a water molecule which is linked to His42 and Arg38 via hydrogen bonding (Ortiz de Montellano 2010). Compound II, a strong oxidant oxidizes a phenolic (or anilino) group releasing an aryl radical and is itself reduced to the resting state via the abstraction of a hydrogen from yet another phenolic group (Figure 2.6).

2.9.3.3.3 Compound III

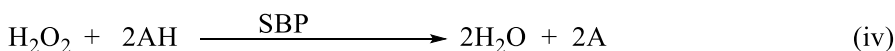
This is essentially a dead-end complex produced from compound II in the presence of excess hydrogen peroxide (and low/no [reducing substrate]). The iron is in oxy-ferryl state. It is thought the oxidation of high concentration of hydrogen peroxide yields superoxide, which combines with ferric enzyme to form this intermediate, Fe-O-O (Ortiz de Montellano 2010). In HRP, it is not a catalytically active form of peroxidase. HRP Compound III crystal structures shows iron bonded to oxygen atom at 1.8 Å and a Fe-O-O bond angle of 126° (Berglund *et al.* 2002). The farthest oxygen is linked to His42 and Arg38 and a water molecule via hydrogen bonds (Ortiz de Montellano 2010). This dead-end product slowly reverts to the resting state of the enzyme (Dunford 1999). Therefore, the entire cycle is completed either from compound II reverting to the resting state or as compound III reverts gradually to the resting state.

The overall reaction therefore oxidizes two phenolic molecules to phenolic radicals and consumes a molecule of hydrogen peroxide, converting it to two water molecules. Theoretically, there is 2:1 ratio established between the aromatic molecules and hydrogen

peroxide, for every complete round of the peroxidase cycle. These reactions are written in the form of chemical equations as shown below.



In Summary,



2.9.3.4 Applications of peroxidases in treatment of CECs

Peroxidases have been employed in the treatment of carbocyclic-aromatics like phenolics (Mashhadi *et al.* 2019a), heterocyclic-aromatics like quinolines (Mashhadi *et al.* 2019b), anilines (Ciric-Marjanovic *et al.* 2016) at experimentally determined optimal treatment conditions with varying removal efficiencies. Comprehensive reviews of peroxidase-based CECs treatment, treatment conditions, removal efficiency, prospects and challenges have been reported (Morsi *et al.* 2020, Alshabib and Onaizi *et al.* 2019, Bilal *et al.* 2019).

2.9.3.5 Apparent inactivation of HRP/SBP during catalysis

The formation of oligomerized phenolic precipitates provides a surface for the adsorption of the enzyme (Nakamoto and Machida 1992). Once adsorbed on the surface, the enzyme becomes apparently inactive in solution, leading to loss of or reduced catalysis evident in lower removal rates. Under this condition, prolonged incubation time will produce removal kinetics markedly different from the apparent pseudo-first order process usually observed for SBP-catalyzed phenolics removal (Goodwin *et al.* 1995). Adsorption immobilizes SBP unto the phenolic precipitate, causing a lowering of its specific activity (Feng *et al.* 2013) but does not create an irreversible inactivation, characteristic of hydrogen peroxide or cyanide. SBP remains catalytically active at elevated temperatures but is irreversibly inactivated at 90.5 °C while HRP C is inactivated at 81.5 °C (McEldoon and Dordick 1996). This irreversible inactivation of SBP is thought to proceed through loss of the haem group, in which case SBP has higher affinity for its haem group than HRP C (Henriksen *et al.* 2001). Within the conditions of wastewater treatment, however, this is not expected since

the temperatures of neither the wastewater treatment plants nor the effluents are ever as high as those reported for inactivating SBP.

2.9.3.6 SBP catalyzed phenolic oligomerization

The aryl radicals formed from the peroxidase cycle tend to react spontaneously and indiscriminately. These reactions produce oligomers which couple following the resonance delocalization pattern of the aryl molecule (Figure 2.7). Huxian and Taylor (1994) and Yu *et al.* (1994) reported oligomers with different orientation pattern from HRP-catalyzed treatment of phenol. These followed either of C-C coupling and/or O-C coupling. Another unstable bonding not observed was O-O bonding (not shown) which is highly unstable and breaks down to the monomeric radical products which enter back into the reaction matrix. These coupling orientations are shown in Figure 2.7.

According to this sequence, following the resonance stabilization pattern, any modified phenolic with a group at carbon atom 4, *para* to the hydroxyl group has only the carbon atom *ortho* to the phenolic group available for participation in any oligomerization reactions. Liang *et al.* (2016), Li *et al.* (2014) and Porter *et al.* (1985) all reported the formation of oligomers of acetaminophen following enzyme-mediated treatment, showing C-C and C-O bonding involving carbon atoms *ortho* to the hydroxyl group in phenol. When the dimers are formed, if they are soluble, they may remain in solution and undergo the peroxidase cycle oxidation reactions again, to form higher oligomers of the order of trimers, tetramers, and even more (Du *et al.* 2016, Potter *et al.* 1985). Depending on the reaction medium and type of phenol, the cycle can continue if the products are soluble in the reaction solution, producing very large polymers. Eker *et al.* (2009) reported polymers weighing up to 4100 Da were obtained from phenols using SBP.

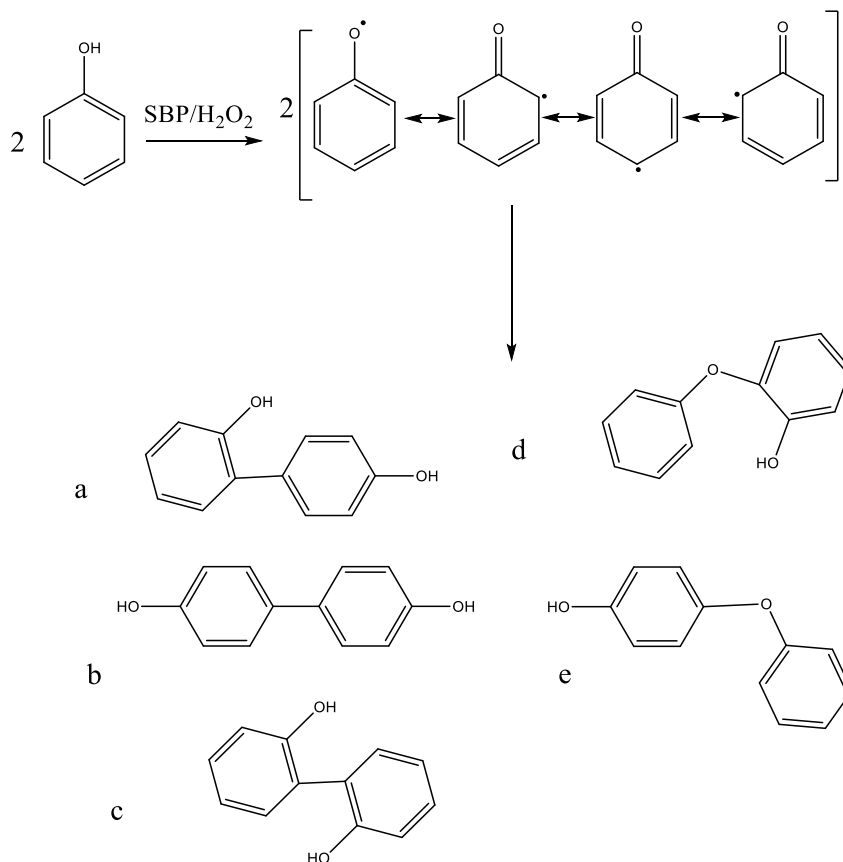


Fig.2.7 Resonance pattern of phenol and possible oxidative dimer coupling patterns between phenolic radicals following SBP-catalyzed treatment in the presence of hydrogen peroxide. The C-C oxidative coupling produces a) *ortho-ortho* dimer b) *ortho-para* dimer c) *para-para* dimer; and the C-O oxidative coupling d) *O-ortho* and e) *O-para*.

2.9.3.7 Selling points of SBP

HRP is sourced from the roots and other parts of horse radish plant (*Armoracia rusticana*), its seasonal availability and long cultivation duration before maturity coupled with low per plant yields poses great challenge to sustained industrial use. It is also a niche crop, low quantities, difficult to harvest; and extraction of enzymes leaves large quantities of biomass for disposal. Moreover, it has several isoenzymes making downstream processing a challenge (Humer and Spadiut 2019). Of the isoenzymes, HRP C has better catalytic efficiency for phenol oligomerization than SBP, but lower thermostability and greater susceptibility to hydrogen peroxide mediated suicide inactivation than SBP (Bodalo *et al.* 2004, Henriksen *et al.* 2001). These shortcomings have been improved on in SBP, making

it a preferred candidate for industrial and research use (Loughran *et al.* 2014). SBP has broad pH activity spectrum between 3.0 and 10.0 (Wright and Nicell 1999) while highest activity when tested with phenol is observed between pH 6.0 and 8.0 (Steevensz *et al.* 2009). Fernandes *et al.* (2020) reported that, at pH 6.5 and 71.6°C, SBP displayed optimal catalytic activity for the treatment of 2,4-dichlorophenol. Kamal and Behere (2003) used the standard assay substrate 2,2'-azino-bis-(3-ethylbenzthiazoline-6-sulphonate)] (ABTS) and reported the highest catalytic activity and conformational stability of SBP to be around pH 5.5, where the enzymes' secondary structure assumes the highest conformational flexibility and heme-exposure to solvent, hence aiding catalysis most efficiently. At all pH values, k_{cat} and k_{cat}/K_M values for SBP are higher than those for HRP C, making SBP a more potent peroxidase than HRP C using ABTS (Kamal and Behere 2003). Yang *et al.* (2019) studied the applications of SBP and HRP C and reported the superior activities of SBP, against HRP. Nicell and Wright (1997) compared the reaction rate constants of SBP and HRP (a mixture of the different isozymes) and reported SBP is about an order of magnitude slower than HRP. Further to this, Bodalo *et al.* (2006) suggest HRP would be the ideal industrial choice peroxidase on the lone count that it acts faster than SBP. Therefore, the choice of peroxidase for an industrial process may be determined by a critical examination of the interplaying factors of effluent characteristics, operational requirements and economic considerations (Bodalo *et al.* 2006). A comprehensive comparative review of HRP and SBP highlighting biotechnological applications, and prospects of SBP was reported by Ryan *et al.* (2006).

In several biotechnological processes, the availability and source/cost of the biotechnological resource poses major constraints to the process. However, SBP can be sourced at lower costs than the HRP (Wright and Nicell 1999). The catalytic efficiency of SBP varies per cultivar (Steevensz *et al.* 2013), post-harvest storage duration, storage temperature, and mechanical damage on the soybean seeds (Lentz and Akridge 1997). Since SBP is obtained from soybean seed hulls, the quantity of soybeans produced is a direct reflection on the amount of SBP that can be generated.

According to United States Department of Agriculture, (USDA), 2020 global soybean production is estimated at 363 million metric tonnes, an improvement in production from

the 336 million metric tonnes produced in 2019, a 7.9% production increase. Per country production shows the first three producers are Brazil, USA, and Argentina with 131.0, 112.3, and 53.5 million metric tonnes, respectively. The source ranked Canada in 7th position with 6.13 million metric tonnes production for 2020. In Ontario, soybean production is in millions of tonnes per annum, peaking at 4.2 million tonnes in 2018 and declining by about 0.5 million metric tonnes between 2018 and 2019 production year, while national production in recent years peaked during 2017 at 7.7 million metric tonnes and declined consistently by 0.3 and 1.3 million metric tonnes between 2017 and 2018, and 2018 and 2019 production years, respectively (Figure 2.8). This large production is substantial to provide the hulls required to produce SBP, to sustain this biotechnological process. The extraction process, and economics of SBP production from soybean hulls have been carefully articulated by Hailu *et al.* (2010).

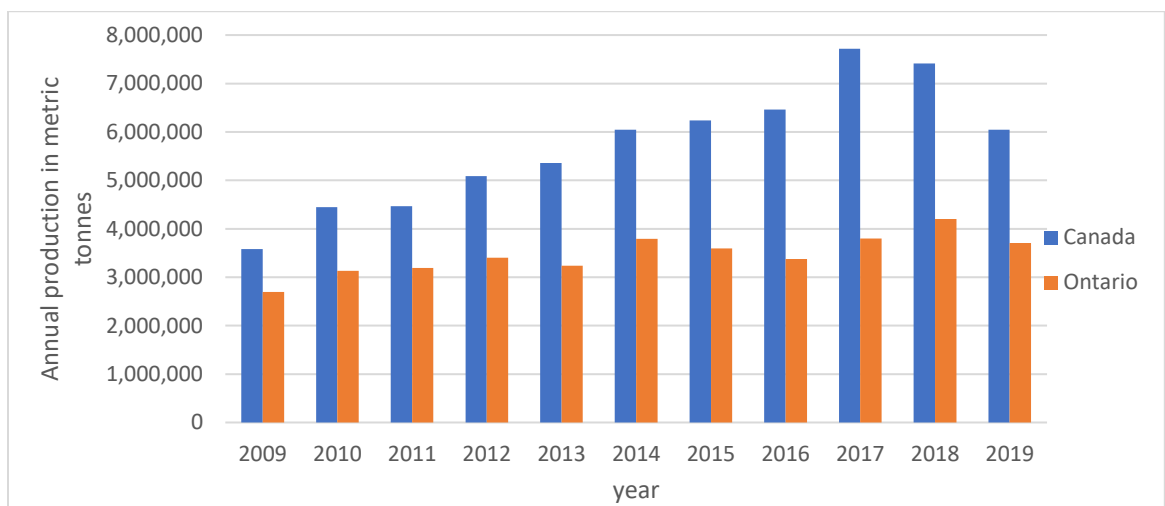


Fig. 2.8. Annual soybean production in Ontario and Canada (Modified from Statistics Canada, Table 001-0017 and <https://soycanada.ca/statistics/production>, assessed August 7th, 2020)

2.9.3.8 Effects of dissolved substances on peroxidase-catalyzed removal of phenolics

The effects of cations, anions, and organic compounds on HRP-catalyzed removal of phenol was reported (Wagner and Nicell 2002). Sulphate salts of zinc, nickel, manganese

and copper and nitrate salts of chromium, iron and cobalt were employed, since these metal salts are often detected in industrial wastewater (Roongtanakiat *et al.* 2007, Kadirvelu *et al.* 2001). Cations at 0.01 mM dm^{-3} does not affect phenol removal, but at 1.0 mM dm^{-3} , Cr^{3+} and Cu^{2+} in the presence of 1.3 mM dm^{-3} hydrogen peroxide could oxidize 30% and 50% initial phenol concentration, respectively, without HRP (Wagner and Nicell 2002). In the presence of HRP, these cations did not promote phenol removal, which could be attributed to the faster reaction rate of the enzyme-catalyzed removal process compared to the cation-based phenol removal in the presence of hydrogen peroxide alone (Wagner and Nicell 2002). At pH 5.0 and 1.0 mM dm^{-3} , Mn^{2+} and Zn^{2+} can cause a decline in phenol removal (Wagner and Nicell 2002). This decline in removal is thought to be due to interactions of manganese ions with carbonyl groups on HRP globular protein, thereby modifying its affinity for the substrates or increasing the vulnerability of the enzyme towards hydrogen peroxide inactivation (Brzyska *et al.* 1997).

The chloride salts of sodium, calcium, magnesium and ammonium plus ammonium sulphate were reported for their possible effects on HRP catalyzed removal of phenol (Wagner and Nicell 2002). Phenol removal declined in the presence of these salts at varied concentrations, between $0.01 - 0.05 \text{ mol dm}^{-3}$ (about 0.94-4.7 g/L), depending on the salt, and above the upper limit, no further increment produced any noticed removal effects. The monovalent cationic salts of sodium chloride and ammonium chloride had highest effect at 0.01 mol dm^{-3} , at which concentration also precipitation occurred in the experimental samples but not in the salt-free control; while the divalent cations containing salts reduced phenol removal at 0.05 mol dm^{-3} , accompanied with precipitates formation, which has the tendency to inactivate the enzyme and halt catalysis (Wagner and Nicell 2002). It is obvious an increase in the ionic strength of the solution could further enhance precipitation of the oligomerized phenolics, creating more surfaces for HRP adsorption and cause an apparent inactivation of the enzyme (Nakamoto and Machinda 1992) and consequently a decline or loss in its activity.

Reducing anions, of; thiosulphate, iodide, nitrite, sulphide (S^{2-}) sulphite (SO_3^{2-}) at 10 mg dm^{-3} did not have any negative effect on HRP-catalyzed removal of phenol (Wagner and Nicell 2002). However, at higher concentrations of thiosulphate, more hydrogen peroxide

was required to effect phenol removal to similar efficiencies. This is because, oxidized phenolic radicals oxidized thiosulphate, thereby requiring more hydrogen peroxide to produce more phenolic radicals in a manner to keep phenol removal sustained, hence a surge in hydrogen peroxide consumption (Wagner and Nicell 2002). It may also be due to direct reaction of peroxide with the reducing anions at the high concentrations which increases pathways of peroxide consumption. Cyanide is a competitive inhibitor of the classical peroxidase, HRP, and binds strongly to the native form heme, preventing the formation of the ferric peroxide complex which is instrumental to the formation of Compound I of the enzyme, thereby inhibiting catalysis from taking place (Wang and Hasabe 2011, Mukai *et al.* 2004). This effect however is reversible in the presence of increased concentration of hydrogen peroxide (Wagner and Nicell 2002).

HRP is largely tolerant to organic solvents like acetonitrile, methanol and dioxane up to 20%, 50% and 30% v/v, respectively (Ryu and Dordick 1992). Higher organic solvent concentrations than these cause a decline in HRP catalytic efficiency. This catalytic efficiency decline occurs when exposure of the active site to organic solvents reduces the local polarity which causes increase in hydrogen bonding of phenolic substrates (Ryu and Dordick 1992). This follows at higher acetonitrile concentrations than 20%, this phenomenon could set in thereby affecting phenolics removal. Other factors responsible for diminished catalytic efficiency in organic solvents may include conformational changes, suboptimal pH situation, transition state destabilization, active centre blockage and unfavourable energetics of substrate desolvation (Klibanov 1997).

2.10 Mass Spectrometry (MS) in environmental studies

Liquid chromatography coupled to mass spectrometry or tandem mass spectrometry (LC-MS and LC-MS/MS) have evolved as the gold standard for analytical precision and for dealing with mixtures without separation. They have both been employed in the determination of CEC concentrations in the environment (K'oreje *et al.* 2019, Bradley *et al.* 2020) and in the determination of oligomerization products of enzyme catalyzed CECs removal treatments (Liang *et al.* 2016, Li *et al.* 2014). Some of the predominantly used ionization techniques for environmental samples include electrospray ionization (ESI), atmospheric solids analysis probe (ASAP), both of which could be employed either in the

positive or negative ionization modes, depending on the chemical properties of the targeted CECs. MALDI-TOF, a soft ionization technique for large molecular weight polymers has also been employed in situations where such polymers have been suspected to constitute precipitate biomass (Eker *et al.* 2009).

2.11 Summary of literature as related to dissertation objectives

The presence of these CECs in the environment is well established, alongside their toxic effects on aquatic organisms and/or humans. Several treatment regimens, especially those employing strong oxidants targeting complete mineralization of the CECs to inorganic CO₂ have been experimented. However, the attendant side reactions often deter complete mineralization, beside the formation of degradation by-products which are suspected, or even established as being toxic. The application of laccases, tyrosinases and even HRP as alternative enzyme-based treatment regimen are important, however these enzymes are in relatively limited supply and may not be found in quantities enough to sustain an industrial scale treatment protocol at affordable sustainable costs. It is in the light of these, that SBP with its outstanding qualities and easier availability is being employed to treat these CECs. The assay of the reaction parameters, extent of removal and products formed will establish the success or otherwise, of the treatment regimen, hence the essence of this study.

CHAPTER 3

MATERIALS AND METHODS

3.0 Chemicals and enzymes

Para-hydroxybenzoic acid, PHBA (CAS # 99-96-7 $\geq 99.0\%$ pure) was sourced from BDH (Toronto, ON, CA), Methyl paraben (CAS # 99-76-3, $\geq 99\%$ pure, lot number SLBG8043V), propyl paraben (CAS 94-13-3, $\geq 99\%$ pure, lot number BCBW9224), butyl paraben (CAS 94-26-8, $\geq 99\%$ pure, lot number BCBR2196V) and acetaminophen (CAS 103-90-2, 98-102.0% pure, lot number MKBV3323V) were purchased from Sigma-Aldrich (Oakville, ON, CA).

Novo Arthromyces ramosus peroxidase (ARP) was a donation from Novozymes Inc., (Franklinton, NC, US). Soybean peroxidase (E.C. 1.11.7, Lot #18541NX) of industrial grade was obtained as a crude powdery extract from Organic Technologies, (Coshocton, OH, US). Catalase (lyophilized powder from bovine liver, (CAS 9001-05-2, lot number SLBR6403V), containing 3940 units/mg protein was purchased from Sigma-Aldrich.

Thirty-percent (30%) hydrogen peroxide solution (CAS 7722-84-1) was obtained from ACP Chemicals, (Montreal, QC, CA) and stored at 4°C from which dilutions were prepared as required. 4-Aminoantipyrine (4-AAP) was bought from BDH Inc. (Toronto, ON, CA), and Phenol (CAS 108-95-2, 99% pure) was procured from Aldrich Chemical Corporation (Milwaukee, WI, US).

3.1 Buffer salts and standard buffers

Sodium acetate (CAS 127-09-3), sodium bicarbonate, (CAS 144-55-8), sodium phosphate dibasic (CAS 7558-79-4), sodium phosphate monobasic (CAS 7558-80-7) were purchased from ACP Chemicals, glacial acetic acid (CAS 64-19-7, $\geq 99.5\%$ pure) was from Sigma-Aldrich, standard buffers pH 4.00 \pm 0.01, pH 7.00 \pm 0.01 and pH 10.00 \pm 0.01 were purchased from ACP Chemicals.

3.1.1 Buffers: choice and preparation

Choice of buffers was made depending on the pH-range of their buffering capacity and their respective UV-Vis cut-off compared against the analytical wavelengths chosen for the compounds, either individually or as a mixture, both for UV-Vis spectrophotometry analysis and in the UV-Vis detector of the HPLC system.

Buffers employed covered pH 3.6-10.0 and were prepared according to Gomori (1955). Acetate buffer was used for pH 3.6-5.5, phosphate buffer was employed between pH 6.0-8.5 while carbonate–bicarbonate buffer covered between pH 9.2–10.0. Stock buffers were 200 mM and were diluted to the required concentration in the batch reactor at the point of use. Water used was deionized and sourced from Culligan, (Windsor, ON).

3.1.2. Preparation of compound stock solutions

Acetaminophen and PHBA were readily soluble in water so stock solutions were 5.0 mM and 4 mM, respectively. MP was 4.0 mM stock solution, comprising 5% (v/v) acetonitrile while the batch reactors contained 1.25% (v/v) of acetonitrile. PP was prepared to 2.0 mM in 5% (v/v) acetonitrile, thus its batch reactors contained 2.5% (v/v) acetonitrile. BP was prepared to 2.0 mM in 10% (v/v), thus having 5% (v/v) acetonitrile in the batch reactors. For the mix-5 reactions, the batch reactors contained 0.2 mM each of the five compounds and the total concentration of acetonitrile in the batch reactors was 1.25% (v/v).

3.2 HPLC solvents and Accessories

Acetonitrile (CAS 75-05-08, 99.9% pure) was purchased from Thermo Fischer Scientific Company (Ottawa, ON, CA). Water of analytical grade, and formic acid (CAS 64-18-6, 95%) were procured from Sigma-Aldrich, Polyether sulfone (PES) syringe filters, 0.22 µm pore size and 25 mm in diameter were purchased from Sarstedt (Montreal, QC, CA). Waters C18 Symmetry columns (5 µm silica particle size, 100 Å pore size, 4.6 mm inner diameter and 150 mm long, with optimal operational pH range of 2.0-8.0) were purchased from Waters (Mississauga, ON, CA). Solvents and modifiers employed - acetonitrile and acetic acid - have UV-Vis cut-off of 190 nm and 230 nm, respectively. This choice rules

out any signal interferences which could mask the signal strength of the analytes leading to inaccurate analysis.

3.3 Instruments

3.3.1 UV-Vis spectrophotometer

An Agilent (Mississauga, ON, CA) UV-Vis spectrophotometer, model number 8453, connected to a Hewlett Packard Vectra ES/12 computer and able to cover a wavelength range of 190-1100 nm having 1 nm resolution, was employed for SBP activity and phenol concentration analyses as well as determining the λ_{\max} of the compounds which informed the adopted analytical wavelength both in the UV-Vis spectrophotometer and in the HPLC. Quartz cuvettes with 1 cm pathlength were procured from Hellma Limited (Concord, ON, CA) and employed for absorbance analysis within the UV-Vis range. One cuvette was used both for the blank and sample analysis, to minimize errors.

A Corning (NY, US) LSE compact centrifuge, S/N 74115013 was used to meet centrifugation need, used either at 3000 rpm (gravity = 1910) or at 3500 rpm (gravity = 2228). An Oakton (Montreal, QC) PC 700 pH meter (pH range: 0.00-14.00, accuracy: 0.01 pH, resolution ± 0.01 pH) was used with a double junction micro pH probe from Thermo Fischer Scientific were employed for pH measurements. pH electrode storage solution was sourced from Thermo Fischer Scientific, (Chemsford, MA, USA). Magnetic stirrers (Micro V magnetic stirrers, 0-1100 rpm, model 4805 and Magstirrers, 100-1500 rpm, model 82026-764) were procured from VWR International Inc. (Mississauga, ON, CA) were used for stirring. Various sizes of Teflon-coated magnetic stir bars were procured from Cole-Parmer Canada Inc. (Montreal, QC, CA).

3.3. HPLC and HPLC protocols

A Waters High performance liquid chromatography (HPLC) system was procured from Waters, (Mississauga, ON, CA) having a binary pump model 1525 and an autosampler model 717, a UV-Vis dual wavelength detector model 2487, fitted with a column earlier described and operated at ambient temperatures, typically $22^{\circ}\text{C} \pm 2^{\circ}\text{C}$. Breeze version 2.0 software was used for data collation and analysis. The latter parts of the experiments were employed on another Waters HPLC system sourced from the same vendor operating with

an autosampler model 2707, binary pumps model 1525 and a dual wavelength absorbance detector model 2489. Breeze software version 3.3 was used on this system unit for the data acquisition and analysis.

HPLC protocols (Table 3.1) were employed to acquire the calibration curves against which

Table 3.1: HPLC analytical conditions for the analysis of the CECs (flow rate 1.0 mL/min)

Substrate	Aqueous* solvent (%)	Acetonitrile (%)	Time (min)	Analytical Wavelength
Acetaminophen	90.0	10.0	0.00	247 nm
	90.0	10.0	5.01	
	70.0	30.0	10.00	
	10.0	90.0	10.01	
	90.0	10.0	15.00	
	90.0	10.0	17.00	
Butyl and propyl paraben	40.0	60.0	0.00	270 nm
	40.0	60.0	5.00	
	20.0	80.0	5.01	
	40.0	60.0	8.01	
	40.0	60.0	11.00	
Methyl paraben	60.0	40.0	0.00	270 nm
	60.0	40.0	1.00	
	20.0	80.0	5.00	
	60.0	40.0	8.00	
	60.0	40.0	11.00	
Mix 5	80.0	20.0	0.00	247 nm and 270 nm
	40.0	60.0	7.00	
	20.0	80.0	15.00	
	80.0	20.0	20.00	
	80.0	20.0	25.00	
PHBA	20.0	80.0	10.00	255 nm

* comprised of 0.1% formic acid

each sample concentrations were read. Briefly, three stock solutions were prepared, and the required dilutions were made from these stocks, between 0.5 μ M and either 400 μ M, 500 μ M or 1000 μ M depending on the compound. The acquired data was represented as mean \pm STD for triplicate injections and they were used in plotting the calibration curves, which are provided under Appendices C and D, for single compound studies and mix-5, respectively.

To ensure analytical reliability, the HPLC protocols were validated using linear regression analysis from which parameters to determine the limit of detection (LOD) and limit of

quantitation (LOQ) for each of the protocols, following standard analytical procedures. Briefly, LOD was determined using the formula:

$$LOD = 3.3\left(\frac{\sigma}{s}\right)$$

While LOQ was determined by:

$$LOQ = 10\left(\frac{\sigma}{s}\right)$$

Where σ is the standard error of the intercept,
 s is the slope of the curve.

The values obtained are presented in Appendix Tables C-1 and D-1 for single compound and mix-5 protocols, respectively.

3.4 SBP Activity assay: stock solution, reagents formulation and activity assay

3.4.1 SBP extraction

Dry powdered SBP crude extract kept at -15°C was removed to room temperature for about 10 minutes and 1.4 g was weighed out into 100 mL of distilled water. This was kept stirring at ambient temperature at 200 rpm for 24 hours to allow for dissolution of the enzyme. The turbid suspension was centrifuged at 3500 rpm (gravity = 2228) for 20 minutes. The supernatant was then carefully transferred into a labelled dry glass bottle and stored in the fridge at 4°C .

3.4.2 Preparation of 10x Phenol reagent

This reagent was prepared in 0.50 M phosphate buffer, pH 7.4, to which was added 0.941 g of phenol (to give 100 mM) and made up to a total of 100 mL with distilled water.

3.4.3 SBP activity assay

To determine the activity of the crude SBP stock solution, a colorimetric method to assay the formation of a pink chromophore with absorption maxima at 510 nm formed from the oxidative coupling of phenol and 4-AAP in the presence of hydrogen peroxide and SBP was employed, following an established method (Ibrahim *et al.* 1997). Working reagent was freshly prepared, comprised of 5.0 mL of 10x phenol reagent, 100 μL of 100 mM hydrogen peroxide solution, giving a resultant 0.2 mM hydrogen peroxide in the

working reagent, and 25 mg of 4-AAP (to give 2.4 mM) made up to 50 mL of water. Three SBP dilutions were prepared, having dilution factors (DF) of 30, 40 and 50.

To ensure no time was lost between dispensing and start of the assay, a quartz cuvette was inserted in the cuvette holder and 50 μ L of diluted SBP sample added, to which 950 μ L of freshly prepared reagent was rapidly dispensed to provide thorough mixing and start the reaction which was allowed to run for 30 seconds. The absorbance change corresponding to the formation of the chromophore was monitored at 510 nm at 5 s intervals. Since the three reactants of 4-AAP, hydrogen peroxide and phenol were present in non-limiting concentrations but SBP was limiting, the initial rate of the reaction is in direct proportion with the concentration of SBP. One unit of SBP activity was defined as the amount of enzyme catalyzing the conversion of 1.0 μ mol of hydrogen peroxide per minute under the assay conditions (typically pH 7.4 and 22 \pm 2 $^{\circ}$ C). SBP concentrations are presented as U/mL. Appendix A provides further details.

Whenever there was need to assay SBP activity at the end of an oligomerization reaction, a residual SBP assay was performed. Even though the principle is similar, since the residual SBP must be smaller than the initial activity determined at the start of the reaction, the mixture proportion of the supernatant, serving as the SBP sample, was increased to either 100 μ L or 200 μ L, and complemented with 800 μ L or 900 μ L, respectively, of freshly prepared assay reagent, to a total of 1000 μ L. For the residual SBP, the reagent was reformulated to ensure the final concentration of each reactant in the cuvette reaction mixture was maintained to enable a common basis for results comparison.

3.5 Hydrogen peroxide assay

Hydrogen peroxide as a reactant in the peroxidase cycles is very important, as it may be the limiting factor. Therefore, to determine its effect on the 3-hour oligomerization reaction, the residual hydrogen peroxide was analyzed by a colorimetric end-point method, according to Wu *et al.* (1997). The ARP in the reagent in the presence of hydrogen peroxide, catalyzes the oxidation of phenol producing phenolic radicals which couple with 4-AAP non-enzymatically, forming a quinoneimine chromophore, with a λ_{max} at 510 nm. The mixture stood at room temperature for 18 minutes to allow the pink color to develop.

The absorbance readings were taken at 510 nm against an appropriate blank. The details of the procedure are given in Appendix B.

3.5.1 Effects of incremental addition of hydrogen peroxide on substrate removal

For reactions that did not attain the target 95% substrate conversion after optimization, incremental additions of hydrogen peroxide was performed. A quarter of the total hydrogen peroxide was added at intervals and the substrate conversion was monitored as usual and where necessary, residual hydrogen peroxide was also determined.

3.6 Batch reactor protocol

Key reaction parameters were chosen for optimization, based on previous studies. These are pH, SBP activity, and concentration of hydrogen peroxide for a 1 mM solution. Since this was a study to establish the feasibility of the treatment process and explore comparative removal of the phenolic compounds, this common concentration was chosen. The extent of removal of the substrate, starting at 1.0 mM was determined at 3 h in a buffered (40 mM, unless stated otherwise) magnetically stirred batch reactor solution. The 1.0 mM starting concentration and 3 h course of the reaction are laboratory set standards by which comparison with previous studies within the group can be made. Stability of the compounds in aqueous solutions and buffered solutions was checked by measuring the absorbance at the maximum wavelength over 48 hours. Sets of reactions were accompanied by no-enzyme and no-peroxide blanks, in order to check for enzyme induced or hydrogen peroxide mediated oxidation of the compounds. Range-finding experiments were conducted with single batch reactors, while narrow range experiments were conducted in triplicates.

At 3.0 h (except where otherwise stated), the samples were quenched with 100 μ L of catalase stock solution prepared and stored at 4°C (19700 U/ml, to give 98.5 U/mL in batch reactor). This was followed by stirring at about 400 revolutions per minute (rpm) for a minute to ensure a homogenous mixture of the catalase with the solution. For time-sensitive experiments, such as during the first five time points in time-course studies, samples were

removed from batch reactors and immediately injected into test tubes containing 50 μ L of catalase stock solution and vortexed at 500 rpm to ensure rapid and thorough mixture in order to decompose the hydrogen peroxide and thereby stop the reaction immediately. The batch reactors were then filtered through 0.2 μ m pore size PES filters and the midstream filtrate was collected into a clean borosilicate 2 mL vial for analysis by HPLC. Filters were rinsed after similar batch reactors and used for the next sample until they were too clogged with the hydrophobic precipitates to be used.

pH optimization began with range finding experiments between pH 3.6 and 10.0, at 1.0 pH unit increments, using the trio of acetate, phosphate and carbonate-bicarbonate buffer systems. This optimization was done at stringent enzyme conditions, targeting not less than 20% of the initial compound remaining, but in the presence of non-limiting peroxide, (typically 1.5-2.0 fold of substrate concentration). This was achieved by providing a limited supply of enzyme activity, in order to make obvious the best pH point which provides the highest removal of the compound. When the wide-range plot showed the optimal removal range, a narrow pH range study followed typically employing 5-7 assay pH point at 0.5 pH unit intervals to determine the exact optimal pH point.

SBP optimization was carried out at the determined optimal pH in the presence of a non-limiting peroxide. As in pH optimization, range-finding experiments were carried out while varying SBP activity, until an acceptable range was found, following which narrow range experiments were performed until the SBP activity units corresponding to $\geq 95\%$ removal of the initial compound was determined. Where this extent of removal was not achieved, residual SBP and hydrogen peroxide assay was carried out to ascertain the limiting reactant and appropriate adjustments were made and the experiment was repeated.

Hydrogen peroxide optimization was performed through range-finding followed by a narrow range of typically 5-7 assay points at appropriate intervals until the concentration yielding the highest removal was found. If the target removal was not achieved, residual SBP and hydrogen peroxide were checked, and the experiments were redesigned. Following hydrogen peroxide optimization, where the target 95% removal was not achieved, SBP optimization was repeated to ensure the optimum SBP activity units were employed for the studies.

Using the three optimized parameters, the time-dependence of substrate conversion was determined over 3 h in a 200 mL batch reactor. Five – ten-mL samples of the reaction mixture were drawn from the same batch, immediately quenched in pre-aliquoted catalase tubes and vortexed. Samples were filtered and midstream volumes were taken for residual compound analysis by HPLC. These experiments were also performed in triplicate.

SBP activity testing was carried out daily. Batch reactions were designed with a total volume of 20 mL in 30 mL glass batch reactors. Water, buffer and compound from a freshly prepared stock solution (except where otherwise stated) were combined and allowed to stir for 5-10 minutes (especially for new compounds) to check for precipitation. Thereafter the required SBP was added and finally hydrogen peroxide was added to start the reaction which was magnetically stirred at 200 rpm for 3 h. The buffer used was 40 mM and 5 mM for compound removal studies and oligomers analysis by mass spectrometry, respectively. Compound concentration was 1.0 mM, except for the mix-5 reactions, which had 0.2 mM each of the five compounds. Since the solutions of the compounds were stable, mix-5 working solutions were prepared from stock solutions up to 48 hours old.

All the compounds except PHBA were analyzed by gradient protocol employing similar mobile solvents of 100% acetonitrile and water acidified with formic acid at 0.1% (v/v), as given (Table 3.1).

3.7 Mass spectrometry analysis

After enzymatic treatment, reaction solutions were centrifuged at 3500 rpm (gravity = 2228) for 20 min. The supernatant was then filtered through a 0.2 μ m PES filter and collected in a glass vial for MS analysis. The precipitate was further washed with analytical grade water by adding 15 mL in a precipitate containing centrifuge tube and centrifuged at similar conditions. This was done twice for each precipitate sample, to ensure the removal of phosphate buffer from the precipitate to minimize background interferences arising from the buffer in the mass spectra of the analytes. The washed precipitate was collected in a glass vial and dissolved in 100% analytical grade acetonitrile for MS analysis. Solutions meant for ESI analysis were prepared using water and acetonitrile at 1:1 where the water was acidified with formic acid at 0.1%. MS analysis was carried out by injecting 5 μ L of solution in the sample loop of a Waters Xevo®-G2-XS ToF mass spectrometer. For ESI

analysis, the sample loop was provided with a constant flow of an equal volume (50:50) of 0.1% aqueous formic acid and acetonitrile. Where ASAP ionization source was used, desolvation gas temperatures (DGT) was varied between 300 °C and 500 °C. Corona current was 1.0 μ A. Data acquisition was performed either in the positive- or negative-ion mode. The acquired mass spectra were subjected to qualitative analysis for molecular formulae targeting possibly formed oligomers and oligomer derivatives as determined by phenol oligomerization reaction scheme (Fig. 2.7) was analyzed using MassLynx software Version 4.1.

3.8 Sources of error

No experimental study is error proof. These may arise from the instruments used (random errors) or errors that occur over time with repetition, with precision. These could however be minimized. In these studies, random errors were minimized by ensuring all analytical instruments were calibrated and used within the manufacturer's specifications. Samples run in HPLC had standards at intervals along to run to check for consistency of the results of standards. Freshly prepared HPLC solvents were also adopted to check for deviations. UV-Vis spectrophotometers analysis employed appropriate blanks. Besides, to handle systematic errors, analyses were done in triplicate, and results presented as mean \pm STD. Moreover, volumetric and gravimetric instruments of analysis were often calibrated to ensure they are all working properly.

CHAPTER 4

RESULTS and DISCUSSION

4.0 SBP reaction parameter optimization – an overview

Optimization of enzymatic reaction conditions required preliminary range-finding experiments necessarily starting with pH to ascertain the narrow range of pH within which analysis could be focused. Secondly, when high enzyme activity is employed, the removal process is less sensitive to pH changes (Caza *et al.* 1999), apparently broadening the optimum activity pH range. Therefore, to avoid this false optimum pH phenomenon, pH optimization must be done at limiting SBP amounts, creating stringent conditions, which is consistent with previous reports (Steevensz *et al.* 2009, Wu *et al.* 1997). With limiting SBP, the pH at which highest compound removal is achieved determines the optimum pH. Compound removal under stringent conditions targets a remaining percentage of not less than about 20% of initial concentration, creating an obvious space between the curve and the independent variable's baseline (x-axis).

The minimum effective enzyme activity (referred to below as 'optimum') needed to achieve 95% conversion of substrate at optimal pH in the presence of sufficient peroxide was determined next. For 1 mM starting concentration of various phenolics, Caza *et al.* (1999) reported that the SBP requirements varied widely: phenol, 2-chlorophenol, *o*-cresol and 2,4-dichlorophenol required 0.90 U/mL, 0.23 U/mL, 0.60 U/mL and 0.08 U/mL to achieve 95% removal, respectively. Similarly, the [H₂O₂]/[substrate] ratios at optimal pH and minimum effective SBP activity were 1.2, 0.8, 0.9 and 0.7 for phenol, 2-chlorophenol, *o*-cresol and 2,4-dichlorophenol, respectively (Caza *et al.* 1999). Therefore, with structural modification on the phenolic ring, the susceptibility of the compound to SBP removal could be greatly altered, leading to a sharp change in the amounts of SBP required to achieve optimal removal of the compound, as seen in the cases of phenol and 2,4-dichlorophenol.

4.1 pH optimization

4.1.1 Range-finding experiments

The pH optimization for acetaminophen conversion was conducted between pH 3.6 and 10.0, beginning with 1.0 U/mL of SBP (results not shown) and the remaining substrate was below protocol's LOQ (Table C-1). Thus, the SBP activity was reduced until the range of 0.002 to 0.03 U/mL was adopted for the optimization as shown in Figure 4.1. It was observed with reducing SBP activity, the curve kept rising above the baseline, indicating increasingly limiting SBP activity, until at 0.002 U/mL, stringent conditions were established resulting in a tentative optimal pH range around pH 7.0. This shows for a 'good' substrate, small increments in SBP activity may result in large improvements in removal efficiency. Under the extreme limiting SBP activity of 0.002 U/mL, pH 7.0 may be a good point for acetaminophen treatment, however this effect diminishes with further SBP increment, as seen from 0.003 U/mL curve. At 0.003 U/mL, 0.004 U/mL and 0.005 U/mL, the curves show flattened minima range between pH 7 and 8, indicating the likelihood of a broad optimal pH range and not just a one-point pH optimum. The relatively high SBP activity of 0.03 U/mL creates a broad pseudo optimum pH range across pH points 4.0 to 8.0, which agrees with the report of Caza *et al* (1999) that with large SBP activity, high compound removal occurs thereby nullifying the effect of pH. In industrial processes where cost is a determining factor, high SBP does entails a directly proportional increment to process cost. Hence the need to find the minimum effective enzyme activity. The sharp decline in compound removal efficiency above pH 8.0 is thought to be as a result of change due to ionization of acetaminophen at the respective pH points. With a pK_a value of 9.38 (Table 2.2), approaching this pH point entails the basic form of the compound is building up in solution, depleting the acidic forms which have the capacity to donate a proton and facilitate the peroxidase cycle for the conversion of compound I to compound II and the return of compound II to the resting state. In consideration of acid-base behavior of the compound, it is thought the dominance of the protonated species will favor substrate turnover leading to oxidative oligomerization.

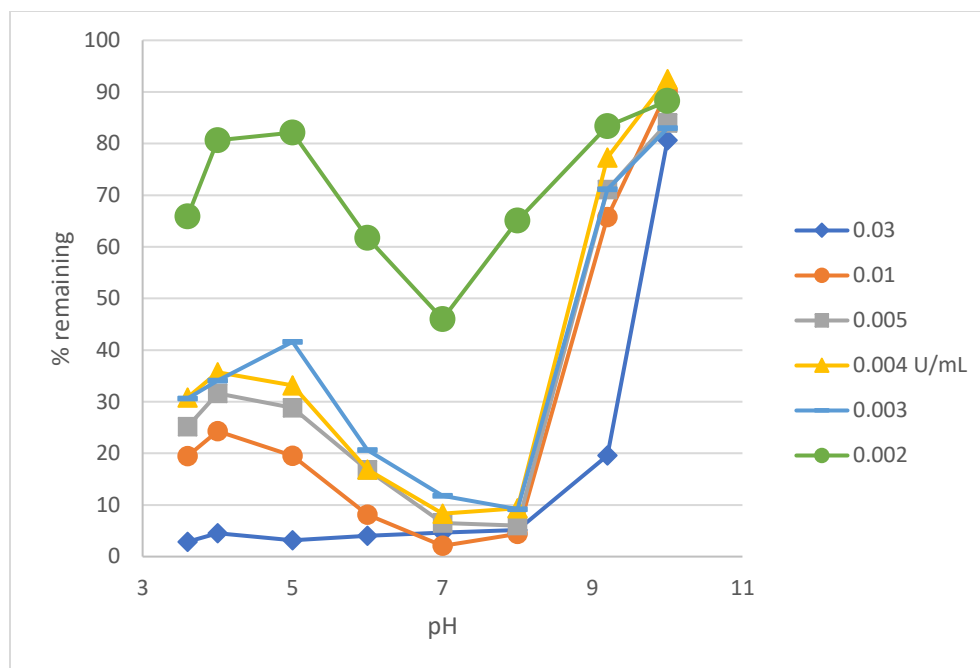


Fig. 4-1: pH optimization of acetaminophen – range finding using varying amounts of SBP. Reaction conditions: 1.2 mM hydrogen peroxide, 1.0 mM acetaminophen and 40 mM buffers for 3 h

Figure 4.2 shows range-finding experiments for pH optimization of PHBA. At 0.5 U/mL SBP was limiting enough to create a good curve for further studies. At 2.0 U/mL, the pH was broadened unlike at the limiting enzyme amounts. PHBA has two pK_a values, 4.54 and 9.37 (FooDB) corresponding to the carboxyl and the phenolic groups, respectively. It is uncertain if the carboxylate ion affects binding interactions with the enzyme leading to slow removal efficiency observed over the wide acidic pH range. All the SBP activities used showed steep slopes indicating improvement and decline in removal efficiency between pH 4.0 and 6.0, and between pH 8.0 and 9.2, respectively. A flattened base observed between pH 6 and 8 indicates a range of optimal activity. The effect observed especially between pH 9.2 and 10.0 could be due to non-enzymatic reaction of PHBA under the high basic conditions, especially of the carboxylate group on the ring. This is thought so even as all the other compounds which have a modified carboxylate group have not exhibited the effect (Figures 4-1, 4-3/4-5). Based on the highest removals observed, the pH range 5.0 - 8.0, was used for the narrow-range optimization experiments.

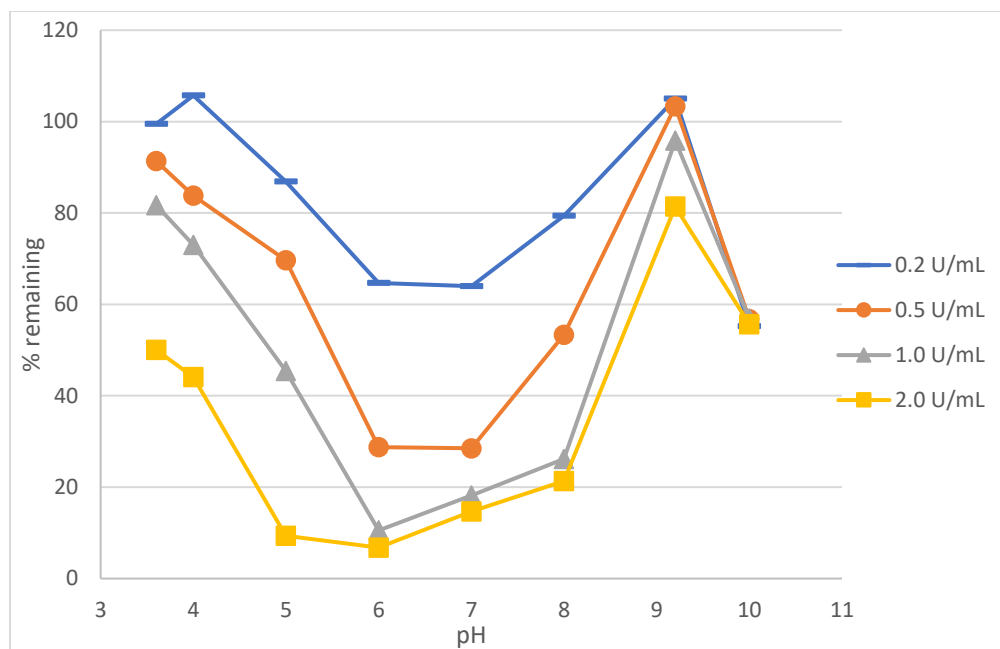


Fig. 4-2. pH optimization of PHBA – range finding, using varying amounts of SBP. Reaction conditions: 1.5 mM H₂O₂ and 40 mM buffers for 3 h

Figure 4-3 shows range-finding experiments for MP conversion. In contrast with PHBA, the pH change from 4.0 - 6.0 did not produce a sharp increase in removal efficiency, but a sharp decline was observed between pH 8.0 and 9.2, as for PHBA. This feature is replicated among all the parabens studied (Figures 4.3 – 4.5). In hindsight, it is inferred that the steep acidic limb in the pH curve for PHBA, Figure 4-2, must be due to change in ionization of its carboxyl group, the carboxylate form being the better substrate.

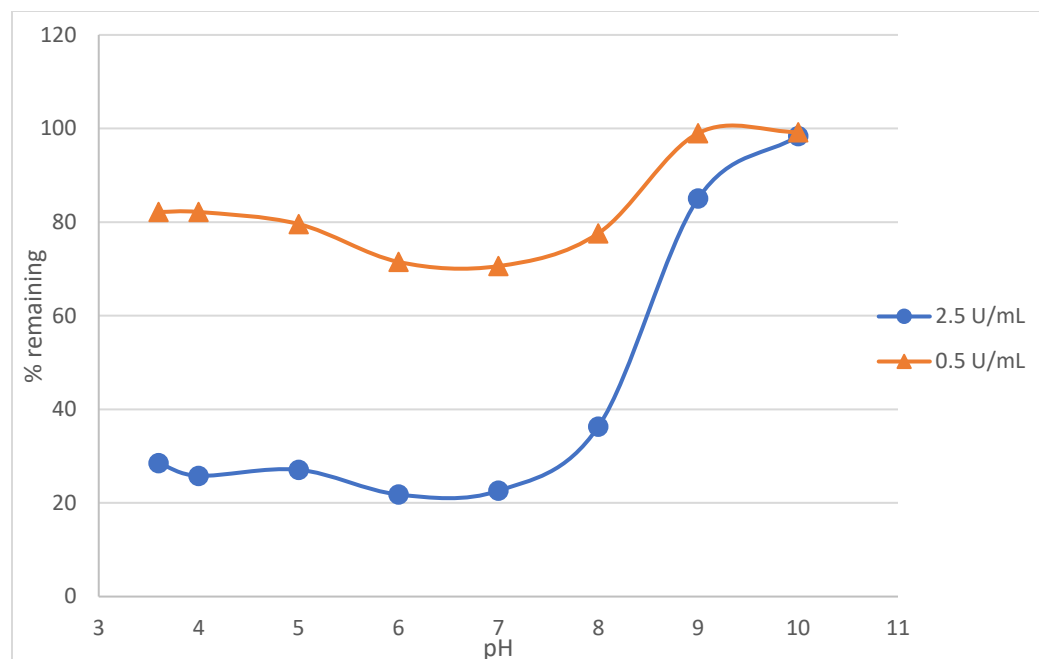


Fig. 4-3. pH optimization of MP – range finding, using varying amounts of SBP. Reaction conditions: 1.0 mM substrate in 1.25% (v/v) acetonitrile 1.5 mM H₂O₂ and 40 mM buffers for 3 h

Range-finding experiments for pH optimization of PP and BP were conducted as shown in Figures 4-4 and 4-5, respectively. For BP, although the amount of enzyme used was not stringent as in other cases, since the curve showed a similar pattern with the other parabens, it was obvious that the expected optimal pH range would be between pH 5.0 and 8.0. The initial experiments were conducted with 0.5 mM BP, to avoid precipitation, since there was uncertainty to the solubility of the compound under experimental conditions. However, with the experiences gathered from these results, subsequent experiments were conducted using 1.0 mM but with a slight increase in organic solvent component, acetonitrile, to increase solubility of the compounds.

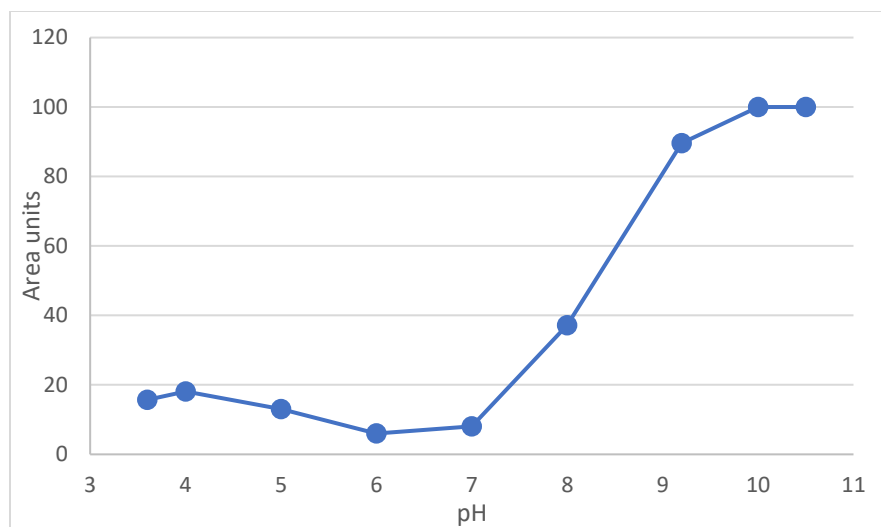


Fig. 4-4. pH optimization of PP – range finding. Reaction conditions: 1.0 mM substrate in 2.5% (v/v) 1.5 mM H₂O₂, 1.5 U/mL SBP and 40 mM buffers for 3 h

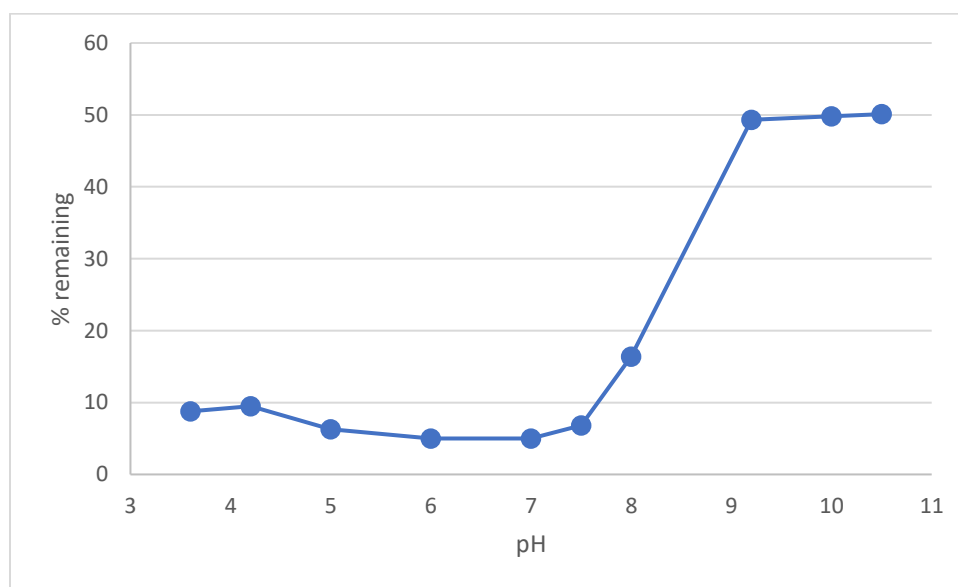


Fig. 4-5. pH optimization of BP – range finding. Reaction conditions: 0.5 mM substrate in 2.5% (v/v) acetonitrile, 0.6 mM H₂O₂, 0.75 U/mL SBP and 40 mM buffers for 3 h and 0.5 mM BP.

A similar trend is observed between all the five compounds. An increase in the pH produces an increasing substrate removal until a pH is reached where removal is stable over about 2 units of pH range and thereafter substrate removal decreases sharply until the last pH point. This agrees with previous reports (Steevensz *et al.* 2009, Wright and Nicell 1999). These compounds all being phenolics, have their phenolic hydroxyl group pK_a in the alkaline

region (Table 2.2). This is the proton donor group in the molecule that facilitates the conversion of compound I to compound II and the eventual return of compound II to the resting state in peroxidase cycle (Dunford *et al.* 2016 as shown in Figure 2.7). As the necessarily protonated form of the phenolic group is progressively diminished as the pH nears and then surpasses the pK_a , hence a sharp decline in removal between pH 8.0 and 10.0.

4.1.2 pH optimization – narrow-range experiments

Following the determination of the appropriate pH range and amount of SBP to be used for the detailed pH optimization, narrow-range pH optimizations were conducted for the respective compounds at 0.5 pH unit intervals in triplicate. Control reactions were conducted at pH 7.0, since all study ranges included it. No-enzyme and no-peroxide controls were provided to determine if either of these alone have any oxidative effect on the substrates. In all cases, these controls showed $\leq 5\%$ substrate conversion. Therefore, any compound removal observed could be attributed to the catalytic effects of SBP and hydrogen peroxide.

Under stringent conditions, acetaminophen showed highest removal over a relatively broad pH range (Figure 4-6). This optimal pH range of 6.5-8.0 agrees with previous reports. Lu

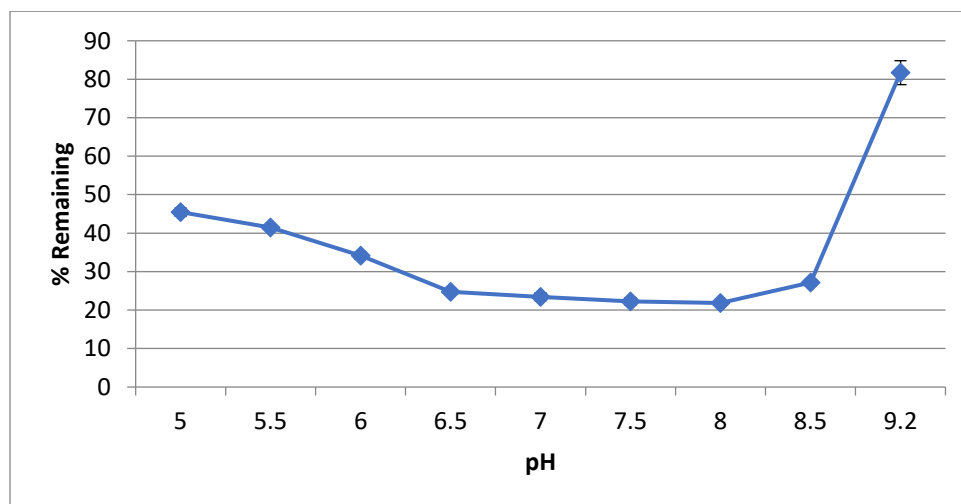


Fig. 4-6. pH optimization for acetaminophen – narrow-range. Reaction conditions: 0.0025 U/mL of enzyme, 1.2 mM hydrogen peroxide in 40 mM buffer for 3 h. Results presented as mean \pm SD where error bars represent the SD of triplicate determinations

et al. (2017) and Potter *et al.* (1985) had reported the oligomerization of acetaminophen at pH 7.0 and 7.4, respectively using HRP. It is also seen that increasing the amount of SBP tend to reduce the pH effect, giving rise to an optimal range rather than an optimal point, when 0.002 U/mL in Figure 4-1 is compared with the range observed from the curve of 0.0025 U/mL in Figure 4-6. This agrees with the report on effect of enzyme concentration on pH optimal range by Caza *et al.* (1999).

In slight contrast to acetaminophen, PHBA (Figure 4-7) and the parabens (Figures 4-8/4-10) showed optimal oligomerization at pH 6.5, with only minor variations between pH

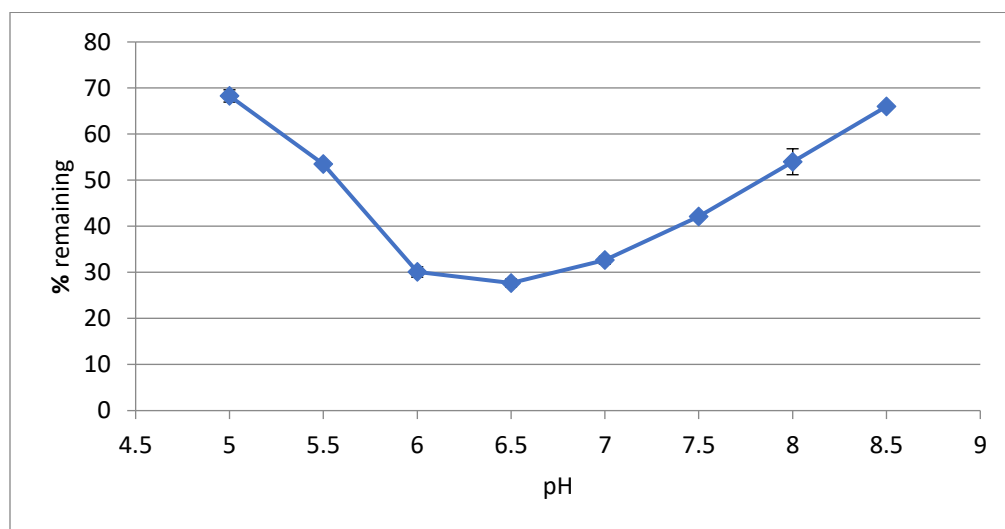


Fig. 4-7. pH optimization for PHBA – narrow-range. Reaction conditions: 1.5 mM H₂O₂, and 0.5 U/mL enzyme in 40 mM buffer for 3 h. Results presented as mean±SD where error bars represent the SD of triplicate determinations

6.0 and 7.0. It has been established SBP has a wide optimal pH range between 5.5 and 8.0 (Fernandes *et al.* 2020, Steevensz *et al.* 2009). The pH optima determined here agree with these previous reports. Since SBP is catalytically active over a wide range of pH, the optimization can be envisaged as the pH at which the protonated species of the compounds are most susceptible to deprotonation to provide protons to facilitate the peroxidase cycle. This is plausible since pH change towards the pK_a point of the phenolic hydroxyl group in all five cases witnessed a sharp decline in removal efficiency. In all the cases, when SBP

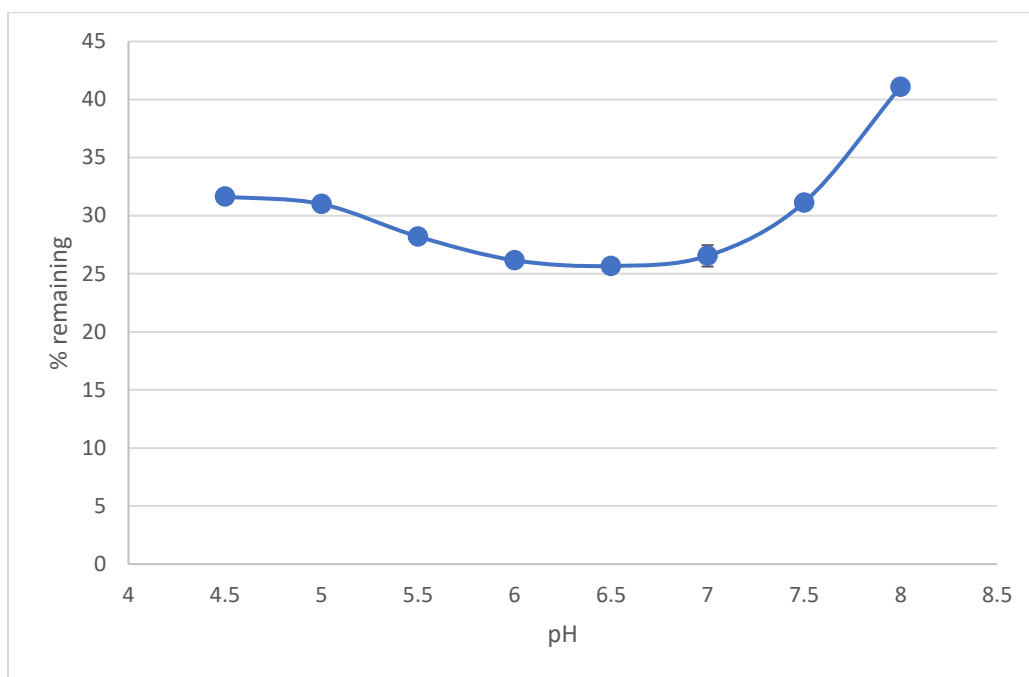


Fig. 4-8. pH optimization for MP narrow-range. Reaction conditions: 1.5 mM H₂O₂, in 40 mM buffer for 3 h. Results presented as mean±SD where error bars represent the SD of triplicate determinations

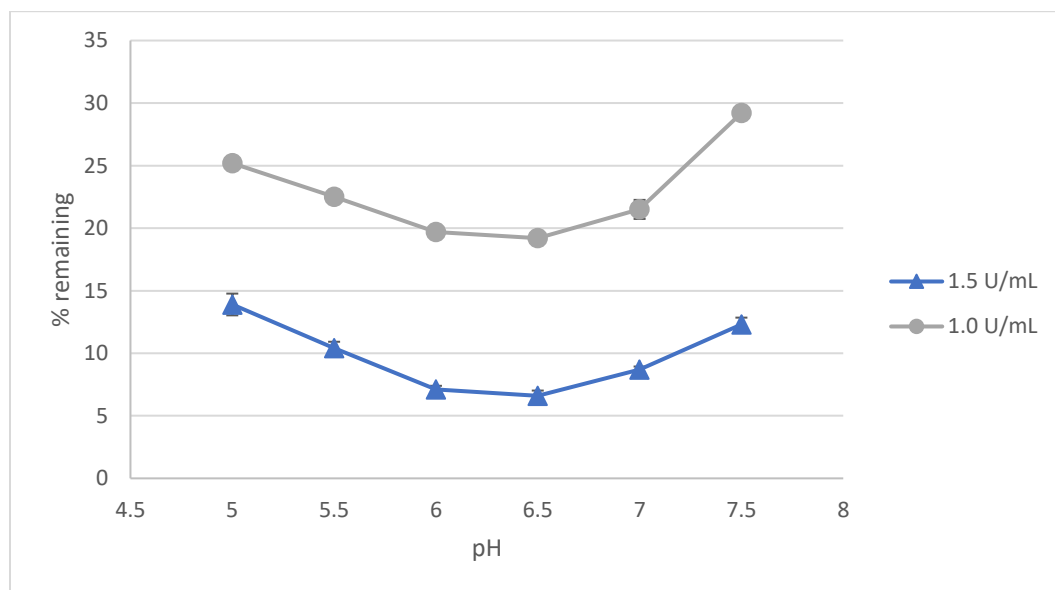


Fig. 4-9. pH optimization for PP – narrow-range. Reaction conditions: 1.2 mM H₂O₂, 40 mM buffer, PP for 3 h using varied amounts of SBP activity. Results presented as mean±SD where error bars represent the SD of triplicate determinations.

was not in limiting concentrations, the optimum pH was broadened over a range of pH points, further underscoring the importance of pH optimization under stringent SBP conditions.

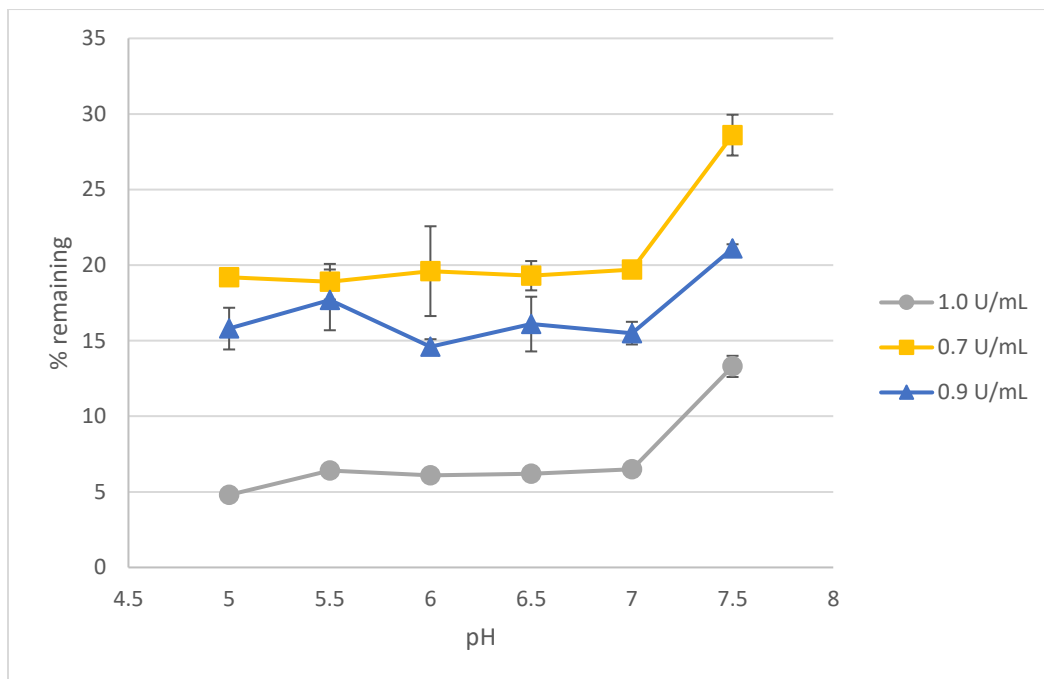


Fig. 4-10. pH optimization for BP – narrow-range. Reaction conditions: 1.0 mM H₂O₂, for 3 h in 40 mM buffers using varied amounts of SBP activity. Results presented as mean±SD where error bars represent the SD of triplicate determinations.

Other phenolics have been shown to have optimal removal pH in agreement with the present study. Ely *et al.* (2017), studied the removal of phenol from biorefinery wastewater using HRP and reported optimal removal at pH 6.32. In another development, the oligomerization of phenol, 2-, 3-, 4-chlorophenols and *p*-cresol was achieved with SBP in synthetic wastewater at pH 6.0, 7.5, 5.0, 8.0 and 7.0, respectively (Caza *et al.* 1999). Chagas *et al.* (2015) reported optimal pH of 6.0 for the removal of phenolics from synthetic wastewater and coffee processing wastewater using SBP. All values are within the optimal catalytic pH range of SBP found here. Since the structural modifications on the aromatic ring may affect the acid-base properties of the compound, it is thought this may be responsible for the shift in optimal pH of these phenolics as reported (Caza *et al.* 1999). In

the current study, the structural differences of the compounds, aside from PHBA, are in the carboxyl derivative groups which do not contribute any acid-base properties to the compound, hence the similar optimum oligomerization pH obtained for the four compounds.

The best observed oligomerization pH for all the compounds were chosen for optimizations of other parameters, namely SBP and hydrogen peroxide concentration.

4.2 SBP optimization for the oligomerization of CECs

4.2.1 Range finding

The results of SBP range finding studies for acetaminophen are shown in Figure 4-11. About 95% of initial 1 mM acetaminophen was removed from solution with 0.006 U/mL of SBP activity. No further removal was observed with increasing amounts of SBP after

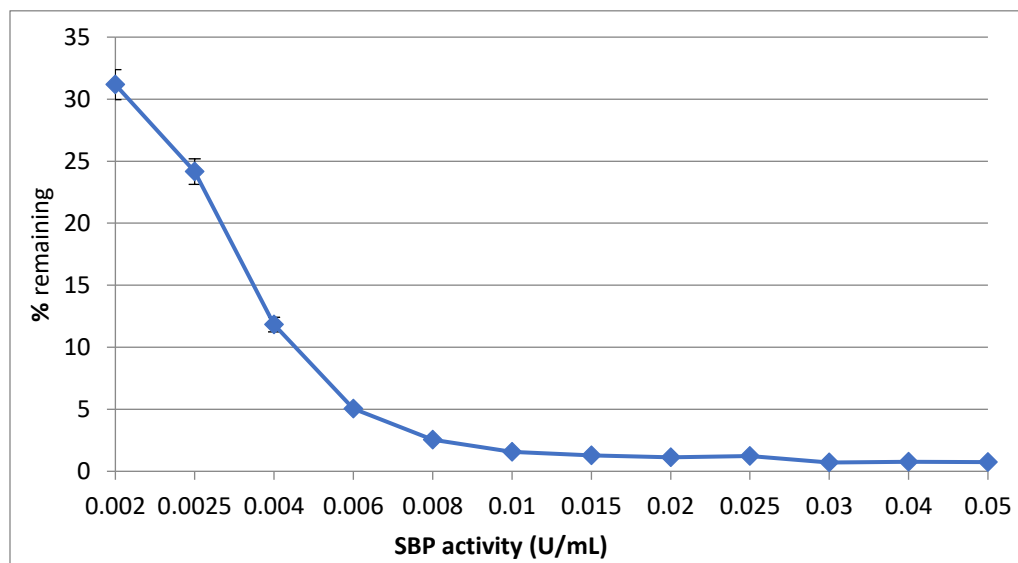


Fig. 4-11. SBP optimization of acetaminophen – range finding. Reaction conditions: 1.0 mM substrate, 40 mM phosphate buffer pH 8.0, 1.3 mM hydrogen peroxide for 3 h.

0.01 U/mL, indicating near-complete substrate removal. Lack of substrate removal with increasing amounts of SBP could be either because the substrate is removed completely with lesser amounts of SBP, and the abundance of SBP in the reaction in turn hampers hydrogen peroxide, a co-substrate of the enzyme from participating in the reaction. Heme peroxidases such SBP are known to demonstrate catalase-like activity (Dunford *et al.* 2016, Battistuzzi *et al.* 2010, Vlasits *et al.* 2010). Vlasits *et al.* (2010) reported in the absence of

external electron donor sources, heme peroxidases tend to break down hydrogen peroxide through a mechanism other than obtainable in monofunctional catalases, that uses redox intermediates such as compounds I, II and III, hydrogen peroxide reduction and oxidation yielding both dioxygen and superoxide. This superoxide could in turn undergo other reactions producing hydroxyl radicals which may alter the conformational stability of the enzyme, by distorting the enzyme backbone and side chain groups. Any SBP increase after 0.01 U/mL in this study, makes the SBP present in relatively large amounts more than required to utilize the aromatic substrates as electron donors. Thus, the enzyme tends to oxidize hydrogen peroxide producing a steady curve that shows no increase in acetaminophen removal as observed between 0.015 U/mL to 0.05 U/mL. This approach is thought to be more plausible considering the small amount of precipitate formed (evidenced by ease of reaction matrix filtration) to form an adsorbent surface upon which SBP would be immobilized. In industrial applications, any further addition of SBP beyond the minimum effective point will only amount to incurring process cost without treatment efficiency. The range of 0.002 U/mL and 0.05 U/mL was chosen for subsequent narrow-range SBP optimization.

The wide-range SBP optimization for PHBA is shown in Figure 4-12. Doubling the amount

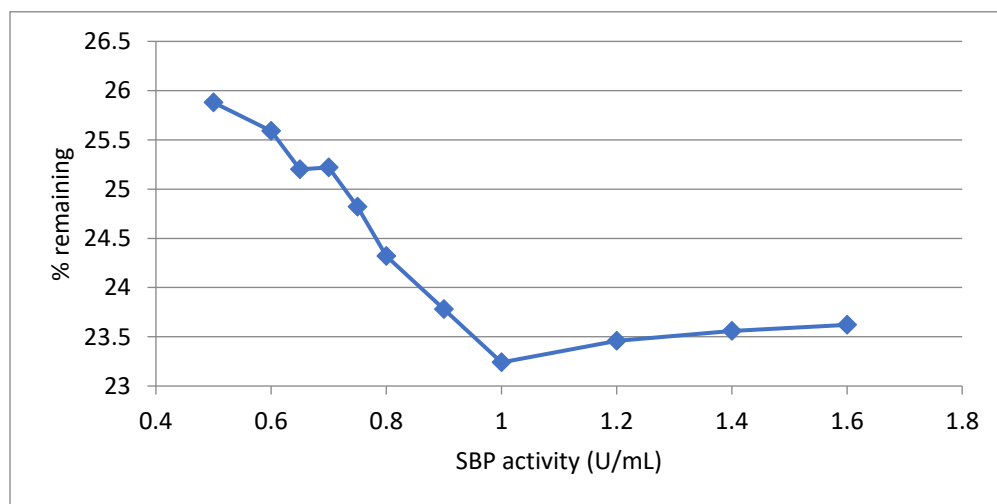


Fig. 4-12. SBP optimization of PHBA – range finding. Reaction conditions: 1.0 mM substrate 40 mM phosphate buffer pH 6.5, 1.5 mM H_2O_2 for 3 h

of SBP from 0.5 to 1.0 U/mL produced a mere increment of 2.65% substrate removal thus, compared with acetaminophen, PHBA is a poor substrate for SBP treatment, relative to acetaminophen. The apparent decline in removal after 1.0 U/mL is due to the blown-up scale on the y-axis, since the increase of 0.6 U/mL SBP only produced a corresponding 0.38% removal of PHBA. The possibility of limiting peroxide at such high SBP activities will be investigated later (Figure 4-22).

Range finding studies for the oligomerization of MP are presented in Figure 4-13. At 2.3 U/mL the highest oligomerization of MP is observed, which may be the highest amount of SBP required at these conditions to achieve substrate removal. Further increases of SBP above 2.5 U/mL did not produce any commensurate substrate removal. Oligomerized MP accumulated as precipitates in the reaction matrix (considering the difficulty to filter the reaction matrix, and the profuse precipitates that accumulated following overnight settling or centrifugation, pictures of which are not shown). Nakamoto and Machida (1992) reported an apparent inactivation of peroxidases following adsorption unto oligomerized insoluble phenolic precipitates which encapsulate the enzyme thereby causing a loss of activity. This effect, however, could be resolved in the presence of additives such as polyethylene glycol and gelatin (confirmed by Wu *et al.* 1997) which act by suppressing the adsorption. In another development, Eker *et al.* (2009) reported SBP catalyzed polymerization of phenolics could yield polymers having molecular mass of up to 4000, depending on the chemical properties of the reaction medium and the phenolic monomer. Reaction medium employing organic solvents such as dioxane, methyl formate, acetone and dimethylformamide mixed with water up to 95% v/v solvents were used for HRP catalyzed polymerization of phenolics and polymers with molecular mass averaging between 400 and 26000 were reported (Dordick *et al.* 1987). The extent of polymerization was found to be dependent on similar factors as outlined later by Eker *et al.* (2009). Phenolic precipitates create favorable surfaces for the adsorption of the free enzyme in solution. This immobilizes the enzyme and diminishes its specific catalytic activity by altering the K_m and/or V_{max} (Feng *et al.* 2013).

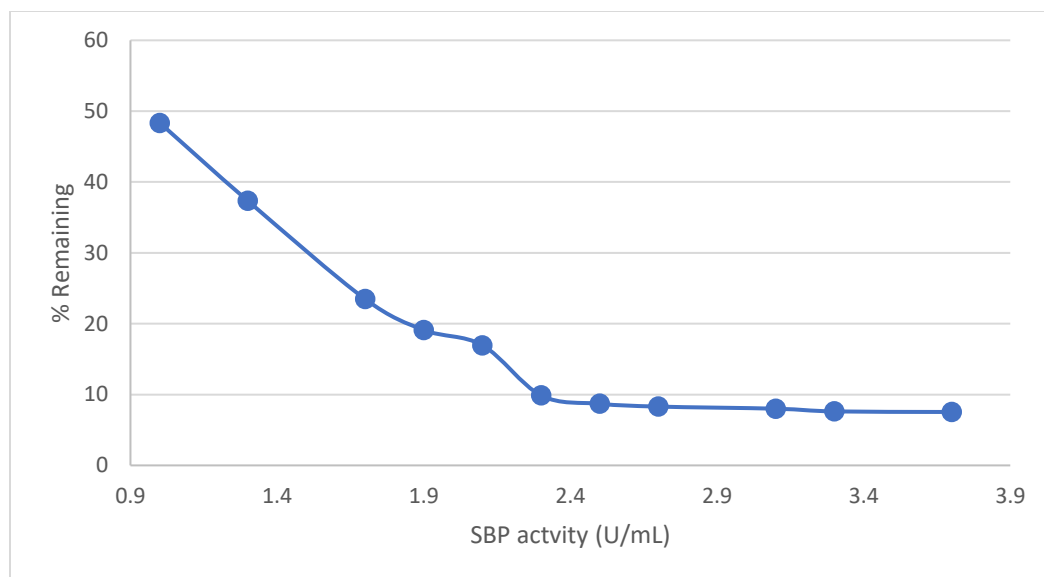


Fig. 4-13. SBP optimization for MP – range finding. Reaction conditions: 1.0 mM substrate, 40 mM phosphate buffer pH 6.5, 1.4 mM hydrogen peroxide for 3 h.

Oligomerization of PP was conducted at the optimal pH as shown in Figure 4-14. SBP activities above 1.1 U/mL produced no corresponding substrate removal.

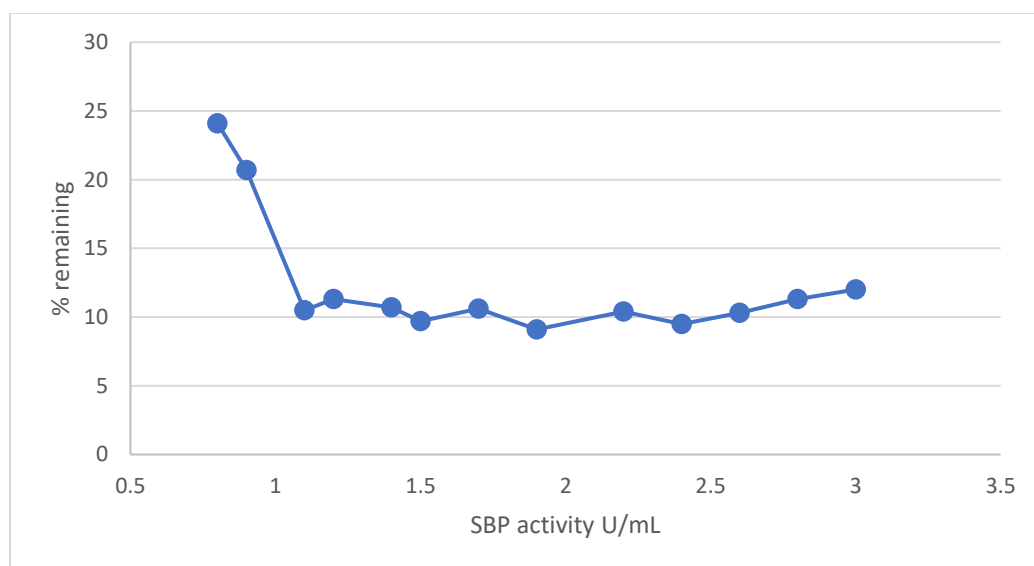


Fig. 4-14. SBP optimization for PP – range finding. Reaction conditions: 1.0 mM substrate, 40 mM phosphate buffer pH 6.5, 1 mM H₂O₂ for 3 h

Oligomerization of BP is shown in Figure 4-15. Removal was stable between 1.0 U/mL and 2.2 U/mL with slight decline, supposedly artifactual, considering these are single-point determinations.

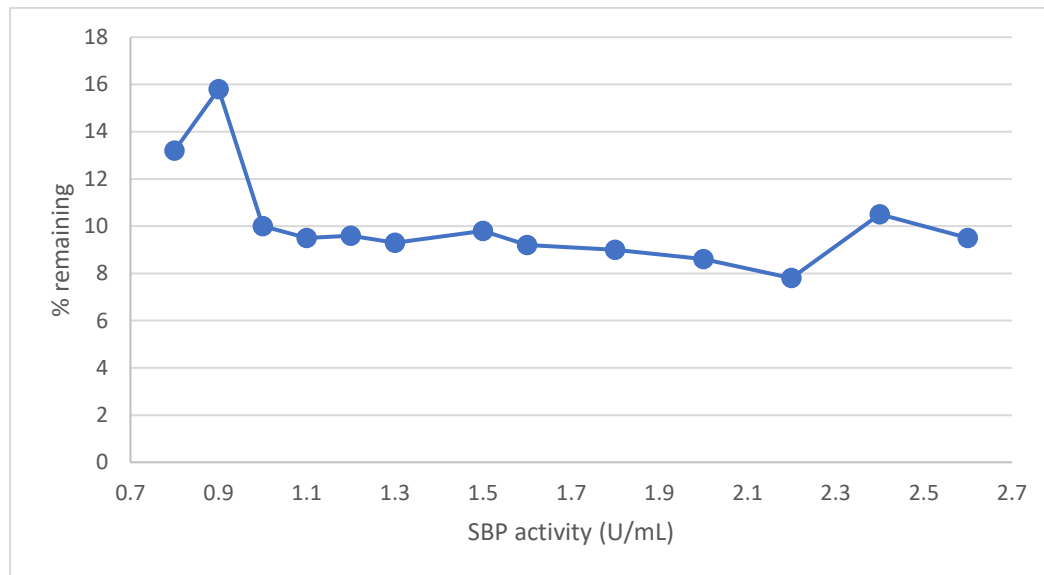


Fig. 4-15. SBP optimization of BP –range finding. Reaction conditions: 1.0 mM substrate, 40 mM phosphate buffer pH 6.5, 1 mM H₂O₂ for 3 h

4.2.2 SBP optimization for the oligomerization of CECs – narrow range

Having established the approximate ranges of SBP which can be used to achieve substantial removal, these ranges were adopted in the five instances to optimize SBP requirement within a narrow range, as shown in Figures 4-16 to 4-20 below.

SBP requirement for oligomerization of acetaminophen was optimized between 0.002 U/mL and 0.05 U/mL (Figure 4-16). Increase of SBP beyond 0.02 U/mL did not produce any increase in substrate removal. Therefore, optimal enzyme requirement for oligomerization of SBP was chosen as 0.006 U/mL, yielding the target removal of 95%.

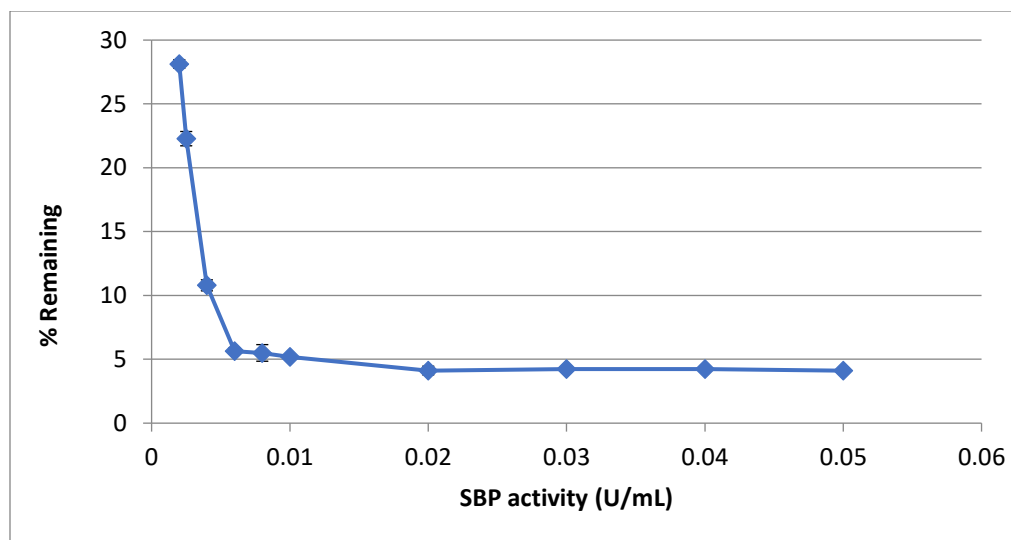


Fig. 4-16. SBP optimization of acetaminophen – narrow range. Reaction conditions: 1.0 mM substrate, pH 8.0 using 40 mM phosphate buffer, 1.3 mM hydrogen peroxide for 3 h. Results presented as mean±SD where error bars represent the SD of triplicate determinations.

In Figure 4-17, the oligomerization of PHBA was optimized between 1.2 and 1.9 U/mL.

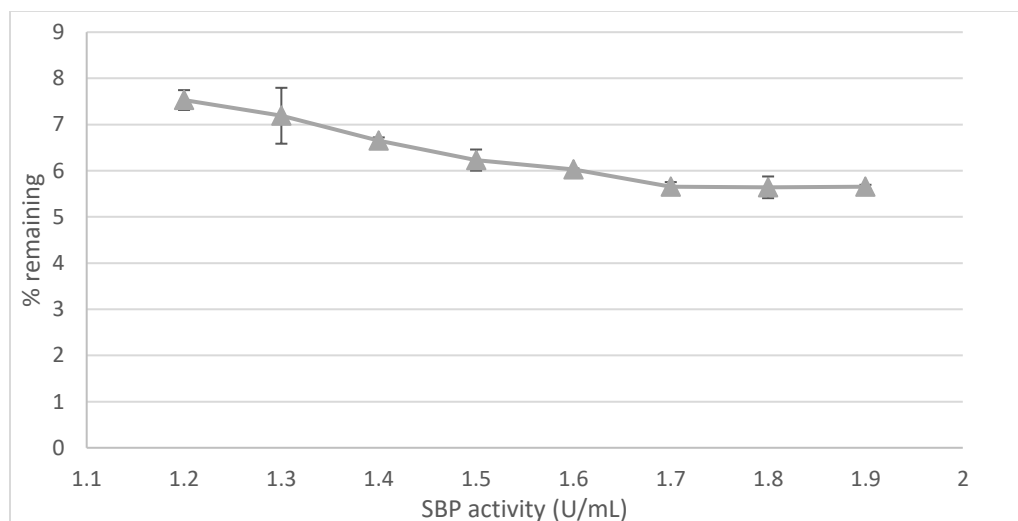


Fig. 4-17. SBP optimization for PHBA – narrow range. Reaction conditions: 1.0 mM substrate, 2.0 mM H₂O₂, 40 mM phosphate buffer pH 6.5, 3 h incubation. Results presented as mean±SD where error bars represent the SD of triplicate determinations.

The flat baseline at the last two points of the curve shows additional SBP did not produce any further substrate removal. The reaction did not have visibly settling oligomers after standing overnight, ruling out the possibility of SBP adsorption unto oligomeric precipitate. This is in contrast with observations with MP (Figure 4-18). This might also be due to limiting presence of hydrogen peroxide as a result of SBP-catalyzed degradation of H₂O₂, which limits the available co-substrate. Considering the carboxylate moiety in PHBA is an electron-withdrawing group from the aromatic ring, this may also hamper complete oligomerization, since it is reported (Xu *et al.* 1995) electron-withdrawing groups on a benzene ring are shown to hinder substrate oligomerization. Therefore, it was predicted the oligomers formed may be of low molecular weight. This was later confirmed with MS product analysis, as shown later. Since PHBA is a highly soluble compound, the formed dimers may remain soluble in solution thereby not precipitating, unlike the experience with the parabens. Moreover, the carboxyl group with a *pKa* of 4.54 as in carboxylate form which could facilitate strong ionic interaction with the aqueous environment, keeping the dimer soluble. Thus, beside alum coagulation, it is thought lowering the pH to below the *pKa* of the carboxyl group may cause the formed dimer to precipitate.

Figure 4-18 shows the conversion of MP following incubation with a narrow range of SBP activities. MP showed a lot of precipitate formed and this decline in removal with increased SBP has been earlier explained, based on Figure 4-13.

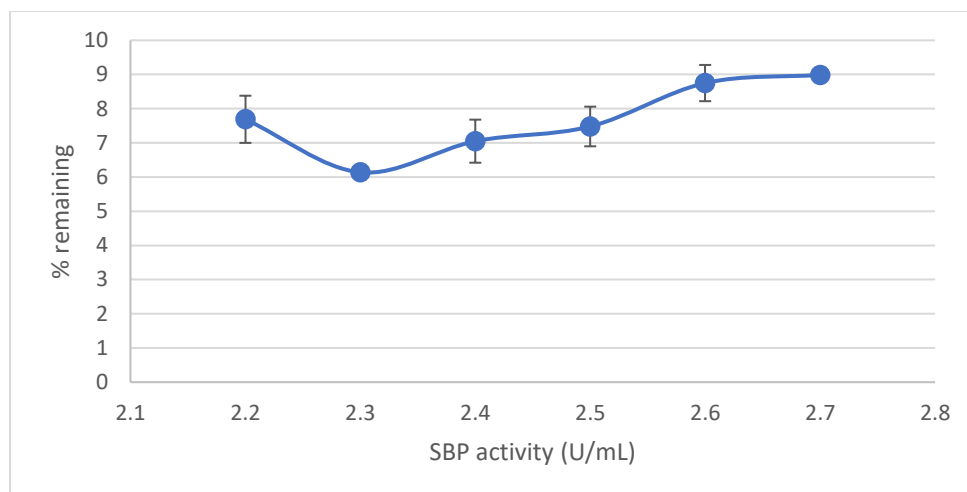


Fig. 4-18. SBP optimization for MP – narrow range. Reaction conditions: 1.4 mM hydrogen peroxide, 40 mM phosphate buffer pH 6.5, incubated for 3 h. Results presented as mean±SD where error bars represent the SD of triplicate determinations.

The optimization of SBP requirement for PP and BP removal are shown in Figures 4-19 and 4-20, respectively. About 94% removal was achieved with 1.1 and 1.2 U/mL SBP, respectively, and these removals could not be significantly improved with additional SBP.

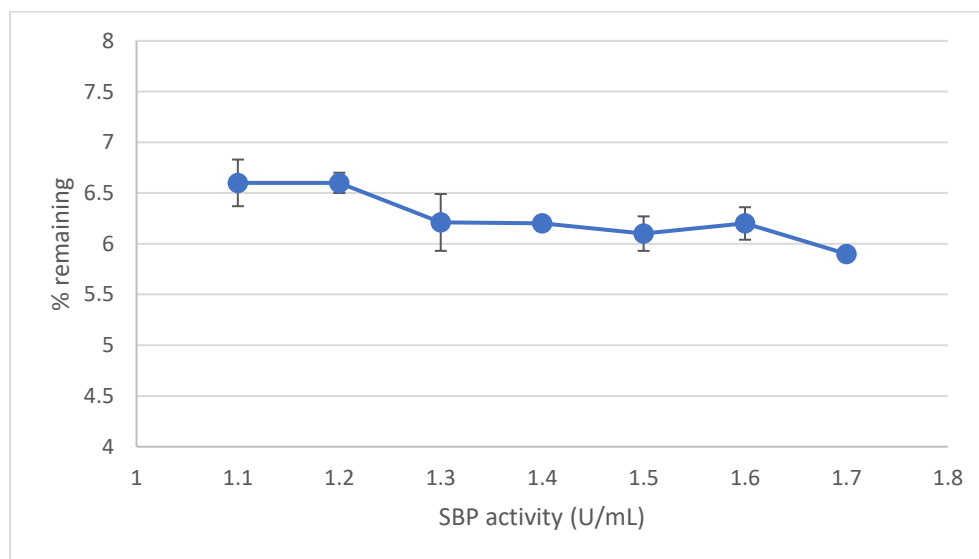


Fig. 4-19. SBP optimization for PP – narrow range. Reaction conditions: 1.0 mM substrate, 40 mM Phosphate buffer pH 6.5, 1.0 mM H₂O₂ for 3 h. Results presented as mean±SD where error bars represent the SD of triplicate determinations.

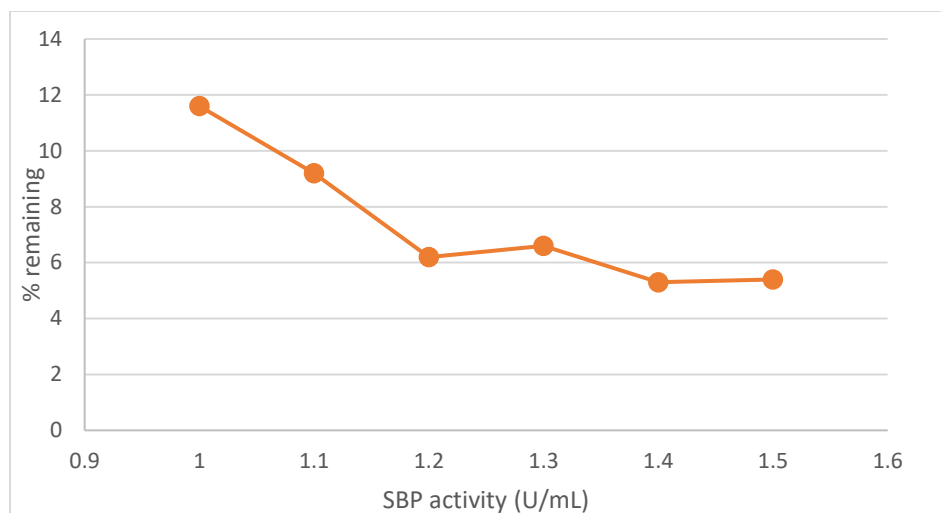


Fig. 4-20. SBP optimization for BP –narrow range. Reaction conditions: 40 mM phosphate buffer pH 6.5, 1.15 mM H₂O₂, for 3 h. Results presented as mean±SD where error bars represent the SD of triplicate determinations.

The five compounds have different SBP requirement to achieve the highest observed removal (Figures 4-16 to 4-20). Since all compounds were initially 1.0 mM, it gives common basis for comparison. Acetaminophen required 0.006 U/mL to achieve about ≥95% removal while 1.7 U/mL SBP was required to achieve similar removal efficiency for PHBA. This SBP requirement is 283 times more for PHBA than it was for acetaminophen. None of the three parabens at the SBP optimization conditions could achieve ≥95% removal. The SBP required for the highest attained oligomerization of about 94% in MP, PP and BP was 2.3 U/mL, 1.5 U/mL and 1.2 U/mL, respectively. Therefore, the SBP requirement is in the order MP>PP>PHBA>BP>>Acet.

From a previous report, SBP catalyzed oligomerization of an initial 1 mM solution achieved ≥95% removal of phenol, 2-chlorophenol, *o*-cresol and 2,4-dichlorophenol using 0.90 U/mL, 0.23 U/mL, 0.60 U/mL and 0.08 U/mL, respectively (Caza *et al.* 1999). However, Stevensz *et al.* (2009) reported 1.5 U/mL was required to achieve 95% removal of 1.0 mM phenol in synthetic wastewater using SBP. The SBP requirement for acetaminophen is 1-2 orders of magnitude lower than all these reports, while MP is >2-fold higher than all the reports. This more efficient removal of acetaminophen is thought to be due to the substitutions on the aromatic ring and the regioselectivity of the substituted

group. Xu *et al.* (1995) reported in the presence of amines/amides, or electron donating groups, peroxidase catalyzed oligomerization is enhanced, and the reaction rate is faster. This is thought to be the case for acetaminophen.

It is also worth the mention, with increasing alkyl chain length, the SBP requirement decreases. To overcome solubility challenge and obtain 1 mM batch reactor concentration, the parabens were dissolved in solvents having acetonitrile. BP, PP and MP had acetonitrile batch reactor content (v/v) of 5, 2.5 and 1.25%, respectively. According to Ryu and Dordick (1992), acetonitrile does not affect peroxidase activity up to 20% v/v. Therefore, this concentration is within safe operational corridors, and should not affect the catalytic efficiency of the enzyme. Considering the nature of the organic solvent, it is thought its presence created the environment for keeping hydrophobic oligomers from precipitating in BP, an effect which was minimal in MP, since acetonitrile was four times less in MP reaction mixtures than BP. This facilitated more precipitate accumulation in MP than in BP, hence the more enzyme adsorption effect in MP batch reactors than BP samples, warranting more SBP consumption in MP oligomerization reactions than BP.

Considering the trend among the parabens, the SBP requirement for MP was higher and called for further investigations. Reaction conditions were further varied to ascertain the SBP optimal requirement. At the end of the 3 h reaction time, residual supernatant SBP activity determined for initial SBP activities of 2.3 U/mL, 2.4 U/mL, 2.5 U/mL and 2.6 U/mL were 0.5%, 0.4%, 0.5% and 0.4%, respectively. Peroxide at 1.5 mM was used in all four cases above. Residual peroxide for above corresponding SBP amounts were 6.4, 3.1, 2.3 and 3.5% of starting concentrations at the end of the reaction. The last readings thought to be artifactual variations since it does not follow the decreasing peroxide pattern established for the first three samples. From these results, it is obvious the polyphenolic precipitates formed had adsorbed the enzyme from reaction matrix leaving no SBP available for substrate conversion. This could account for the poor removal efficiency with increased enzyme concentration. The declining content of residual H₂O₂ is thought to arise from SBP facilitated degradation. Under these conditions, more addition of SBP cannot produce a corresponding removal efficiency but rather increase the process costs. Incremental addition of H₂O₂ was done at four 30-minute intervals from the start of the

reaction. It was found MP removal increased by about 5% while residual H₂O₂ and SBP were 9.1% and 0.3% respectively (results not shown). The increment in residual H₂O₂ is thought to be due to failure of the adsorbed SBP to degrade it. To further investigate this, incremental addition to a total batch reactor amounts of 2.3 U/mL SBP in 4 rounds at 30 minutes interval, beginning from the start of the reaction was conducted. Residual H₂O₂ was determined to be 0.8%, 8 times less than when both components were fully present at the start of the reaction. Residual supernatant SBP was 0.3%, which shows it might have been adsorbed on the polyphenolic precipitate. These reports agree with Nakamoto and Machida (1992) and Feng *et al.* (2013) that reduction in catalytic efficiency (apparent inactivation) is due to adsorption of the enzyme on the surface of oligomerized phenolic precipitate. Therefore, to save operational costs, the first point on the SBP optimization curve (Figure 4-18) with highest substrate removal is considered the optimal SBP activity.

PHBA had finer precipitates which did not settle even after standing overnight yet used more SBP than previously reported for phenolics (Steevensz *et al.* 2009). Besides the earlier advanced reasons, another mechanism hampering the completion of the reaction in PHBA is thought to be due to the scavenging effect of the recalcitrant electron-withdrawing phenoxy-carboxylate ions in solution. Pylypchuk *et al.* (2018) also reported the presence of radical scavengers in reaction medium can obstruct the oxidative coupling of aryl radicals thereby retarding the rate of substrate removal. This they reported is pronounced when a susceptible compound is in a reaction matrix with a recalcitrant compound, citing the examples of a binary mixture of acetaminophen and diclofenac (DCF), respectively.

4.3 Hydrogen peroxide optimization

The stoichiometry of the peroxidase-catalyzed reaction between peroxide and phenolic (or anilino) compound follows a molar ratio of 1:2. However, experimental evidence has shown this is seldom the case, necessitating experimental determinations to determine the required H₂O₂ to achieve optimal substrate removal conditions. With SBP, the molar ratios for 1.0 mM phenol, 2-chlorophenol, *o*-cresol, and 2,4-dichlorophenol have been reported as [H₂O₂]/[substrate] ratios of 1.2, 0.8, 0.9 and 0.7, respectively (Caza *et al.* 1999). Ibrahim *et al.* (2001) reported the ratio of 1.1 from studies with real wastewater samples. In another study, SBP catalyzed removal of aniline and *o*-anisidine in synthetic wastewater yielded

the molar ratio of 1.5 and 1.25, respectively (Mazloun *et al.* 2016). From studies with HRP, Lu *et al.* (2017) reported the molar ratios for phenol, acetaminophen, 2,4-dichlorophenol to be 2.0, 2.0 and 1.0, respectively. This molar ratio defines the optimal required hydrogen peroxide concentration, below which H₂O₂ concentration becomes limiting thereby halting the removal of the substrate. Concentrations of H₂O₂ in excess of this tend to inactivate SBP by either of several established pathways (Dunford *et al.* 2016, Steevensz *et al.* 2009, Ibrahim *et al.* 2001). Excess H₂O₂ concentrations or limited substrate concentrations tend to favor the production of compound III, a catalytically reversibly inactive form of the enzyme, which can only slowly be converted to the resting state of the enzyme, as illustrated in Figure 2.7 above and in Dunford *et al.* (2016). Since the optimal ratio is defined and the above reported results gives a guide to peroxide requirement, a range was developed based on these guides and the narrow range optimizations were done as shown in Figures 4-21/4-25.

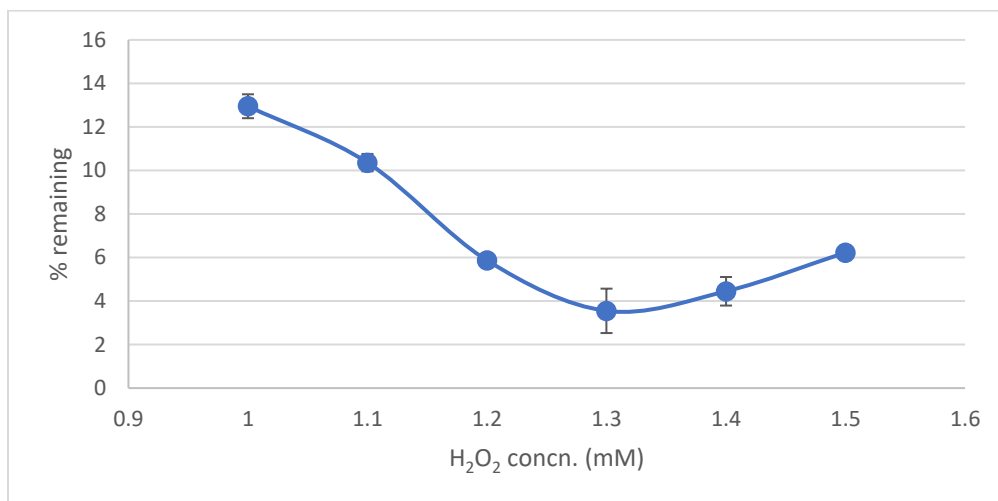


Fig. 4-21. Hydrogen peroxide optimization of acetaminophen. Reaction conditions: 40 mM Phosphate buffer pH 8.0, 0.006 U/mL of SBP for 3 h. Results presented as mean±SD where error bars represent the SD of triplicate determinations.

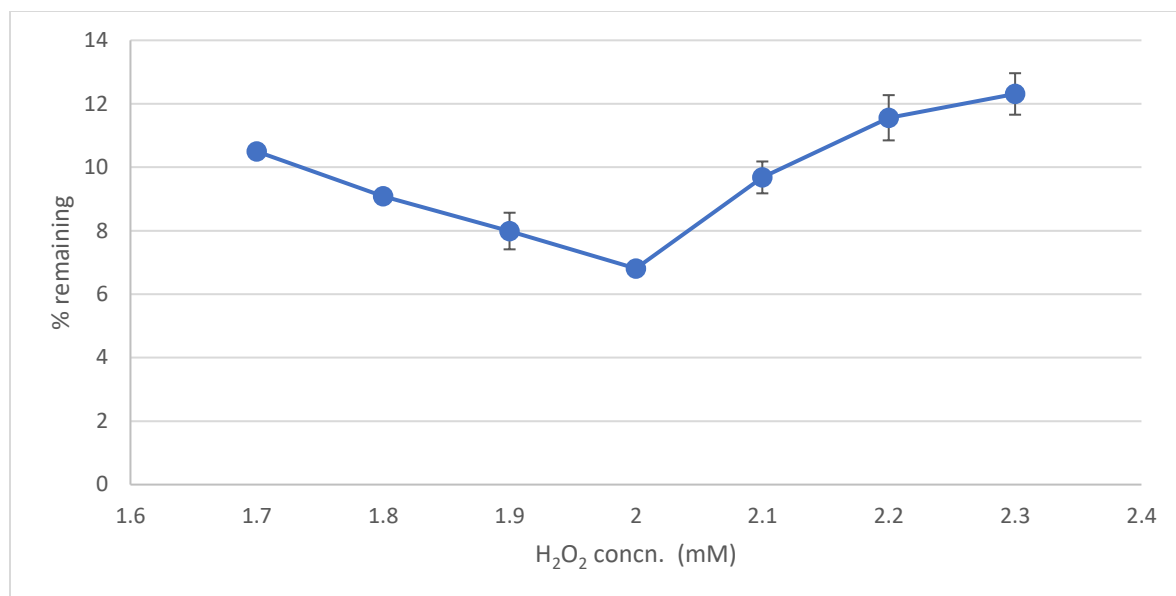


Fig. 4-22. Hydrogen peroxide optimization for PHBA. Reaction conditions: 40 mM Phosphate buffer pH 6.5, 1.2 U/mL SBP for 3 h. Results presented as mean±SD where error bars represent the SD of triplicate determinations.

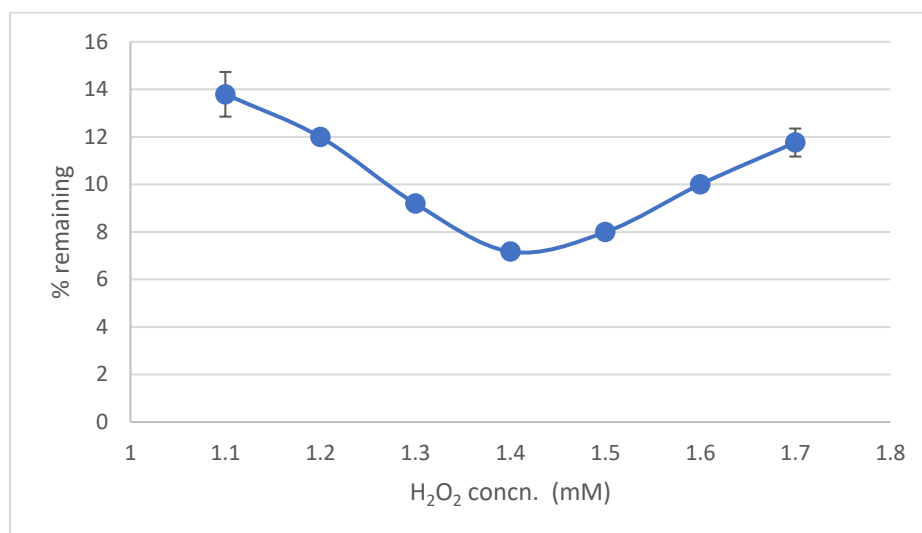


Fig. 4-23. Hydrogen peroxide optimization for MP. Reaction conditions: 40 mM phosphate buffer pH 6.5, 2.3 U/mL SBP for 3 h. Results presented as mean±SD where error bars represent the SD of triplicate determinations.

Hydrogen peroxide optimization of PP and BP are shown in Figures 4-24 and 4-25. These

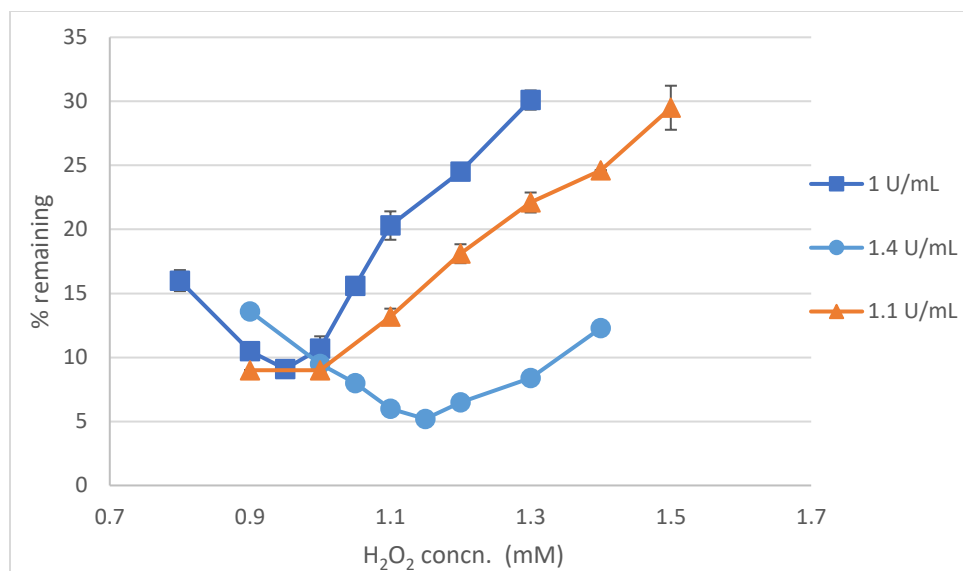


Fig. 4-24. Hydrogen peroxide optimization for PP. Reaction conditions: 40 mM Phosphate buffer pH 6.5, varied amounts of SBP for 3 h. Results presented as mean±SD where error bars represent the SD of triplicate determinations.

Figures show multiple curves indicating a repeat of SBP optimization after H₂O₂ optimization was done, to obtain best activities of SBP required to achieve highest removals. Due to the large error margin on the 1.3 U/mL curve of Figure 4-25, 1.4 U/mL was preferred as being more reliable and hence chosen as the optimal amount of SBP required. It is for a similar reason that 1.15 mM peroxide is considered better than 1.10 mM for BP removal.

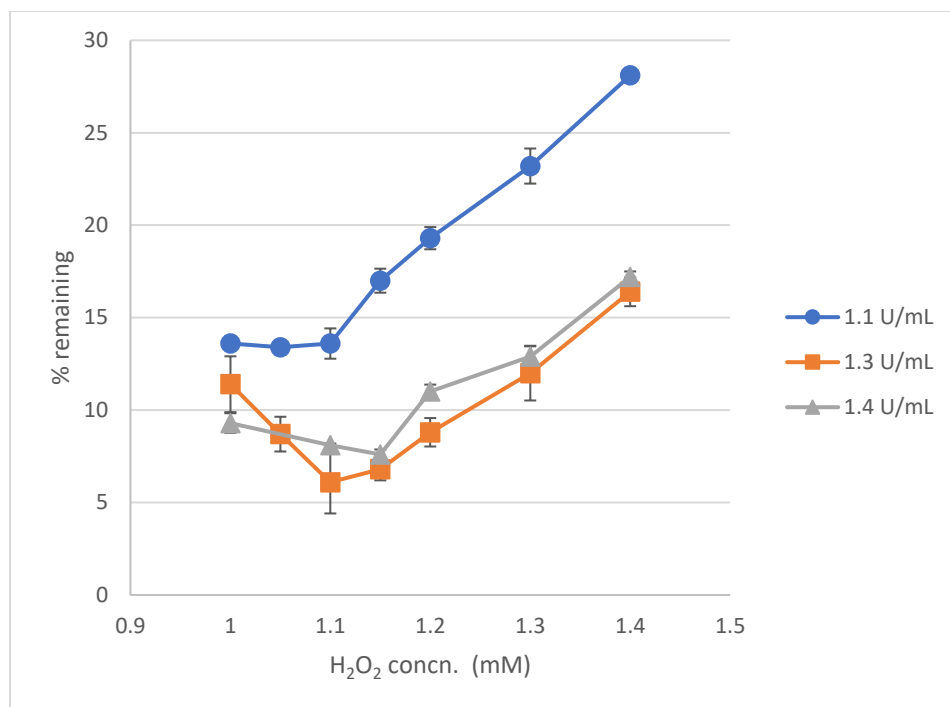


Fig. 4.25. Hydrogen peroxide optimization for BP. Reaction conditions: 40 mM Phosphate buffer pH 6.5, varied SBP for 3 h. Results presented as mean \pm SD where error bars represent the SD of triplicate determinations.

Optimized peroxide was divided into four aliquots and added incrementally at 30-minute intervals from the start of the reaction for PHBA, PP and BP. The results (figures not shown) showed increments in removal of the residual compounds were $3.7\pm 0.0\%$, $1.9\pm 0.2\%$ and $2.2\pm 0.2\%$ for PHBA, PP and BP, respectively. This was above the target removal of 95%. This agrees with Mashhadi (2019) who reported increment of 5% for incremental addition of optimized peroxide dose over single dose additions.

Optimized parameters for the CECs studied are summarized in Table 4.1. The optimized H₂O₂ concentration for 1.0 mM substrate is in descending order of PHBA>MP>Acet>PP=BP. Below this concentration, compound removal is limited due to insufficient H₂O₂. The conversion of the resting state enzyme to the catalytically active compound I and thence compound II is dependent upon H₂O₂, and in the event of limiting concentrations of H₂O₂, this important step is halted. Supporting this thought is the report of Cheng and Harper Jr (2012), which affirmed the rate of compound removal is dependent

upon the enzyme substrate interaction and not on the frequency of collision between the radicals. More so that the aryl radical formation and release step is secondary and maybe slower than compound I formation step in the peroxidase catalytic cycle and entirely dependent upon initial step of enzyme-H₂O₂ interaction which facilitates the conversion of resting state enzyme to compound I.

With excess H₂O₂ concentrations, there is enhanced conversion of the resting state enzyme to the other forms, Compounds I and II and then Compound III. However, Nicell and Wright (1997) from modelling studies stated that compound III predominates over the other forms of the enzyme. Since compound III is a catalytically inactive form of peroxidase, the entire reaction rate drops making removal efficiency decline, thus the foregoing curves tip upwards above the optimum peroxide concentrations. This is thought to be the case between the H₂O₂ concentrations points at: 1.4 -1.5 mM in Figure 4-21; 2.1-2.3 mM in Figure 4-22; 1.5-1.7 mM in Figure 4-23; 1.2-1.4 mM in Figure 4-24; and 1.2-1.4 mM in Figure 4-25 above.

Once formed, compound III may undergo decomposition through any of three alternate pathways. The very reactive bound peroxy radical which binds very close to the tetrapyrrole structure may oxidize the porphyrin moiety (Valderrma *et al.* 2002) by eliminating the carbon bridges connecting the pyrrole rings resulting in the cleavage of the porphyrin macrocycle thereby forming an open-chain tetra-pyrrole structure (Nakajima and Yamazaki, 1980). In other words, the ring is opened, irreversibly inactivating the enzyme. Compound III may also catalyze the oxidation of the surrounding protein producing an oxidized group of amino acid side chain moiety or it may oxidize a substrate molecule thereby repairing the porphyrin moiety and returning to the ground state (Valderrma *et al.* 2002, Dordick *et al.* 1986). Lastly it may undergo irreversible decay releasing free radical superoxide and dioxygen which undergo rapid rearrangement upon release and decompose to form hydroxyl free radicals in solution which are reported to oxidize amino acid side chains. The formed free radicals may undergo several molecular interactions between the protein backbone and amino acid side chains until they find the lowest reduction potential, which in proteins is cysteine residues (Davis and Dean, 1987). Since cysteine residues are also involved in the disulphide bridge formation, it is thought

these may interfere with the integrity of the four disulphide bridges in SBP (Henriksen *et al.* 2001), consequently affecting the structural integrity of the protein and hence its catalytic activity. This may explain the decline in SBP activity between start of the reaction and the end of the 3-h reaction course (results not shown).

Table 4.1: Summary of parameter optimization and removals of studied CECs.

Compound (1.0 mM)	Optimization parameter			[H ₂ O ₂]/ [Substrate]	% removal*
	pH	SBP (U/mL)	H ₂ O ₂ (mM)		
Acet	8.0	0.006	1.3	1.3	96.5
PHBA	6.5	1.5	2.0	2.0	93.2
MP	6.5	2.3	1.4	1.4	92.8
PP	6.5	1.4	1.15	1.15	94.8
BP	6.5	1.4	1.15	1.15	93.2

*% removals are taken from the least remaining substrate concentration points on hydrogen peroxide optimization plots (Figures 4-21 to 4-25).

4.4 Mixed existence demands mixed treatment – exploring possibilities

Real wastewater samples, originating from manufacturing facilities (Kleywegt *et al.* 2019), effluents from municipal wastewater treatment plants (Ghoshdastidar *et al.* 2015), receiving and surface waters (Ebele *et al.* 2020, Blair *et al.* 2013, Kolpin *et al.* 2002) contain a matrix of CECs. Recently, Bradley *et al.* (2020) surveyed surface water across the US and reported a median of 4 out of 120 target pharmaceuticals were detected at each sampled location. Therefore, any study to treat wastewater effluents that focuses on only one contaminant might be a great laboratory-scale experiment but devoid of the capability to extrapolate the findings to real wastewater situations where many other contaminants may be present. These experimental results may be limited by the matrix effects. Unfortunately, Zheng and Colosi (2011) observed there has been little attention given to

studies focusing on simultaneous treatment of CECs. Recently, Liu *et al.* (2019b) broke the fallow ground and reported simultaneous aqueous chlorination of sulfamethoxazole, diclofenac and acetaminophen. The study demonstrated the production of hetero-dimer pairs of sulfamethoxazole-acetaminophen and diclofenac-sulfamethoxazole, in a pH-dependent process facilitated by oxidative coupling through the amine-nitrogen of sulfamethoxazole. Xiang *et al.* (2020) reported success in the removal of 4-chlorophenol, BPA and NP by chlorination of aqueous mixtures.

Part of the challenges hampering simultaneous studies of CECs is analytical. In the event a set of CECs does not have a common absorbance wavelength for analysis, it becomes a challenge to simultaneously monitor the compounds present. Liu *et al.* (2019b) used HPLC fitted with a diode array detector (DAD) to analyze the mixture of SMX, DCF and Acet at 210 nm. This is a seemingly common wavelength where many aromatic rings show appreciable absorbance.

Considering an obvious research gap and the need to scale up laboratory experimental design to bear the semblance of environmental reality, the five ECs studied here were mixed (mix-5) to study SBP-catalyzed removal of these contaminants. To overcome the analytical wavelength challenge, a common wavelength was used, which was different from the isosbestic point. The parabens had their acid band absorption maxima at 256 nm, PHBA at 255 nm and Acet at 247 nm. Although about 8 nm apart, it was observed the signal strength for parabens and PHBA was stronger at 247 nm, compared to that of Acet at 255 nm, thus the analysis for the mixture in the acidic conditions was conducted at 247 nm. Checks were done with analysis at the dual wavelengths, namely 247 nm and 270 nm, being the isosbestic point of the parabens, where measurements were to be carried out inclusive of both acidic and basic pH during pH optimization. There was no difference in observed compound removal when checked for parabens at both analytical wavelengths, hence 247 nm was safely used.

Enzyme-catalyzed reactions for the simultaneous oligomerization of CECs are rarely reported in the literature. Dordick *et al.* (1987) reported copolymerization of different phenols in 85% v/v dioxane. Another study (Hachi *et al.* 2017) employed laccase from

Trametes versicolor for the removal of acetaminophen and diclofenac in synthetic wastewater. The process was largely successful with enhanced removal of both compounds in binary mixture than in single compound studies. Similarly Pylypchuk *et al.* (2018) used immobilized laccase from *Trametes versicolor* with and without Cd(II) to treat a binary mixture of acetaminophen and diclofenac and reported 99% and 95% removal of acetaminophen and diclofenac, respectively, in the presence of Cd(II) ions.

The calibration curves of the compounds in mix-5 are attached in Appendix D Figures A1-6 to A1-10. A summary of the retention times and characteristics of the calibration curves for individual CECs are also included in the Appendices as Table D-1. Compared with the summary of the calibration curves observed in the single compound studies, these clearly have higher extinction coefficients. These can be accounted for by the wavelengths employed. The isosbestic wavelengths are often not the maximal wavelength of analysis. These compounds demonstrated higher absorbance of the acid band than at the isosbestic point, consequently the higher extinction coefficient at the 247 nm, in keeping with Beer-Lambert's law.

4.4.1 Optimizations for mix-5 treatment

For the mixture study, pH optimization was done, range-finding experiments in non-replicate points followed by narrow-range experiments with triplicate points. The choice of the initial SBP units was based on an average of the optimized SBP units from the individual treatments (Table 4-1), each pro-rated to the ten-times lower concentration employed and in mix-5. The results are shown from Figure 4-26. The range finding experiments showed removal of acetaminophen at all the pH points below protocols' LOQ. This indicates high SBP activity can undo pH limitations for acetaminophen oligomerization. Since substrate removal is dependent upon enzyme-substrate interaction (Cheng and Harper Jr 2012), it is thought the high SBP activity used provided ample enzyme available for substrate interaction, hence the exhaustive conversion of acetaminophen.

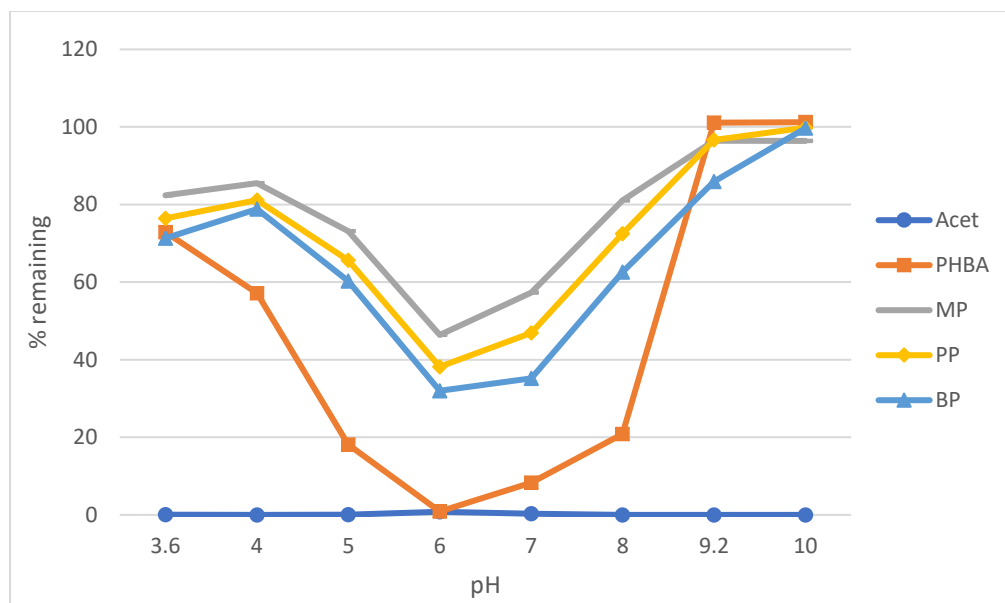


Fig. 4-26. pH optimization for removal of mix-5 – range finding. Reaction conditions: 0.1 mM each of the 5 compounds, 40 mM buffer pH 3.6 - 10, 0.9 U/mL SBP and 1.0 mM H₂O₂ for 3 h.

Considering the amount of SBP in mix-5 is 150 times more than was used to attain $\geq 95\%$ removal (Fig.4-16) in single-compound studies, the complete removal of acetaminophen is expected. There is sharp increase in removal efficiency between pH 4.0 and 6.0 for four of the compounds and a steep decline in removal efficiency for the same compounds after pH 7.0. A similar pattern was observed for the single compounds. The difference between the least and highest removals for the five compounds at pH 6 and 7 was 46% and 57%, respectively. Therefore, for subsequent studies in a narrow range, pH 5.5 – 7.5 was chosen. Since 0.9 U/mL SBP could not establish stringent conditions for PHBA and Acet, subsequent studies were carried out with reduced amounts of SBP to observe for stringency.

The removal of mix-5 was studied at reduced SBP dose of 0.6 U/mL (Figure 4-27). With the inclusion of pH 6.5, the removal was observed to be highest at pH 6.0 and 6.5. These two pH points are prospective optima points for mix-5 treatment. The three parabens clustered far above the baseline indicating increasing difficulty to treat these compounds in the presence of limiting SBP. Since 0.6 U/mL was not stringent for PHBA and

acetaminophen, a further reduction in SBP activity to observe enzyme stringency was done at 0.3 U/mL and 0.1 U/mL, as shown in Figure 4-28 and 4-29, respectively.

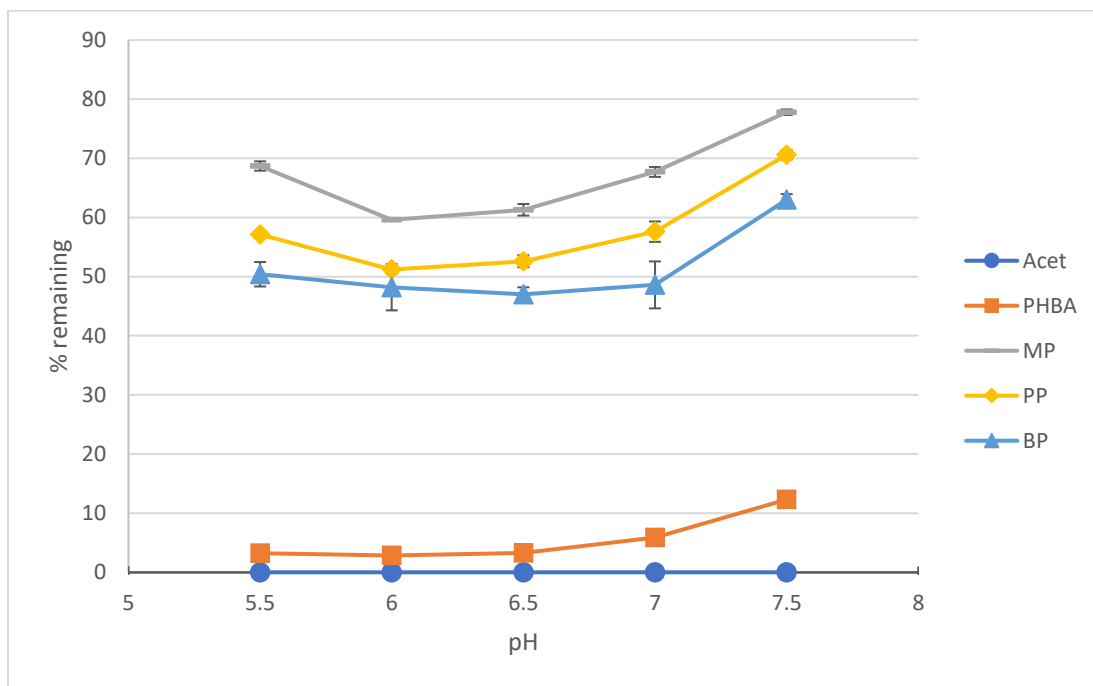


Fig.4-27 pH optimization of mix-5 – narrow range. Reaction conditions: 0.1 mM each of the compounds, 0.6 U/mL SBP, 1.0 mM H₂O₂, 40 mM phosphate buffer for 3 h. Results presented as mean±SD where error bars represent the SD of triplicate determinations.

At 0.3 U/mL, (Figure 4-28) this SBP activity was stringent for all compounds except acetaminophen, which is expected, being 50 times more than the activity used to obtain $\geq 95\%$ removal of the single compound at 1.0 mM. The differences between the highest removed and least removed compounds, being acetaminophen and MP at pH 6.0 and 6.5 were 82.5% and 83.7%, respectively. There was a relatively steep gradient between pH 6.0 and pH 6.5 for PHBA, while other compounds maintained a similar removal level. This removal difference was 3.5%. This small difference may imply the process can proceed at either of these two pH points. Although the acceptable pH range for discharge of treated

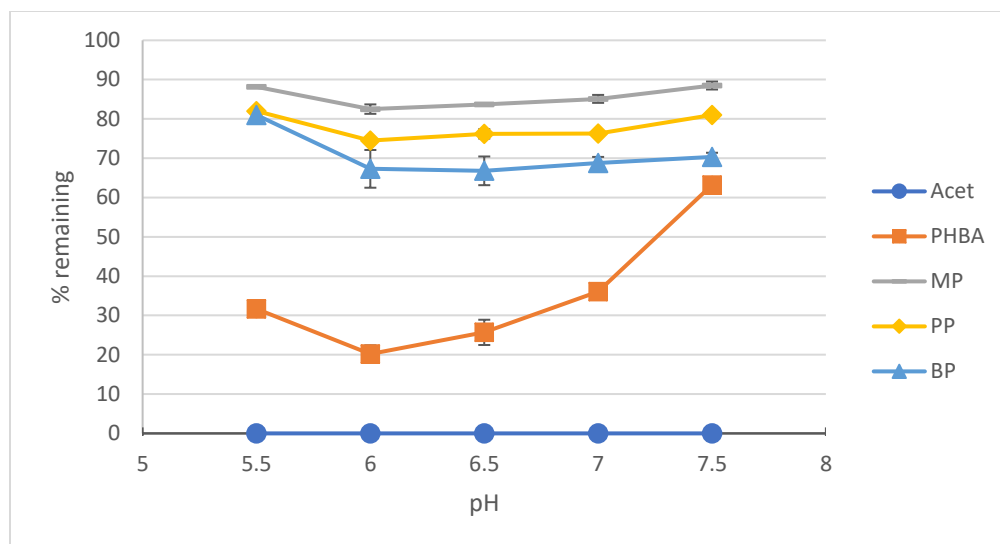


Fig.4-28 pH optimization of mix-5: Narrow range with reduced amount of SBP. Reaction conditions: 0.3 U/mL SBP, 0.1 mM of each compound, 1.0 mM H₂O₂, 40 mM phosphate buffer for 3 h. Results presented as mean±SD where error bars represent the SD of triplicate determinations.

wastewater effluents is pegged between 6 and 8.0 (Metcalf and Eddy 2014), the closer the effluents are to the neutral pH, the better for the receiving water bodies. The previous studies (except for acetaminophen) were carried out at pH 6.5, therefore, to have basis for comparison, mix-5 is better studied at similar pH with the majority of the compounds (Table 4-2). Pylypchuk *et al.* (2018) reported the laccase-catalyzed binary treatment of acetaminophen and diclofenac was successfully done at pH 7.0. From another report, Hachi *et al.* (2017) studied immobilized laccase mediated simultaneous treatment of acetaminophen and carbamazepine (CBZ) at pH 4, 7 and 10 and reported highest removal was achieved at pH 7.0. These results agree with the present study.

Further reduction in SBP amount to 0.1 U/mL showed decline in removal of all compounds except acetaminophen (Figure 4-29). At both pH 6.0 and 6.5, PHBA became the second least removed compound, taking the place of PP in previous instances (Figures 4-26 to 4-28). It has been reported the removal of recalcitrant substrates is enhanced in the presence of susceptible substrates (Hachi *et al.* 2017). The rate of oligomers formation is dependent upon the radical formation step and not on the frequency of radicals' collision (Wang *et al.* 2018, Cheng and Harper Jr 2012). Thus, it is thought with very little activity of enzyme

present, the competition for the enzyme is heightened against PHBA. Although this is a complex process, Xiang *et al.* (2020) studied 4-chlorophenol, BPA and nonylphenol (NP) and reported mixed radicals from these compounds preferentially cross-coupled rather than self-coupling, a process which improves the overall removal of the individual compounds.

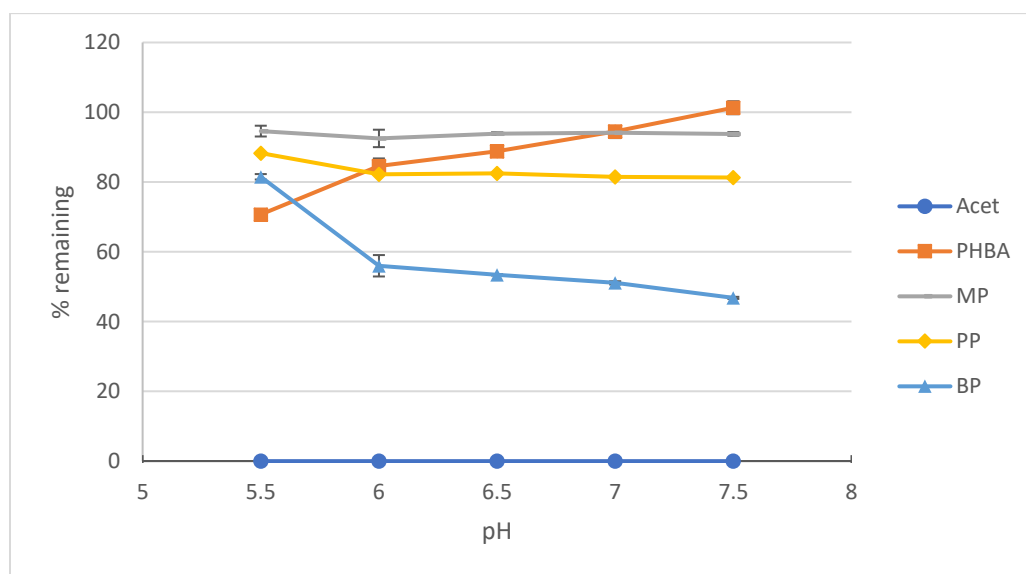


Fig. 4-29 pH optimization of mix-5 – narrow range with further reduced amount of SBP. Reaction conditions: 0.1 U/mL SBP, 0.1 mM each of the compounds, 1.0 mM H₂O₂, 40 mM phosphate buffer for 3 h. Results presented as mean±SD where error bars represent the SD of triplicate determinations.

Since less of the other compounds were oxidized here than at 0.3 U/mL (Fig. 4-28), cross-coupling may have been reduced for PHBA, owing to decline of radicals of the other compounds. Since PHBA is very poor at self-coupling because of the carboxylate group on the benzene ring (Xu *et al.* 1995), this lower removal could be expected. Under very stringent SBP conditions, the rate of acetaminophen reaction was faster than the rest of the compounds since the enzyme available was still 17 times more than required to achieve ≥95% removal of 1.0 mM acetaminophen as observed in single compound treatment. This could be a disadvantage, if the other compounds have an incomparably slower rate of reaction, which is thought to be the case. This may not have influenced the removal of the other compounds as it was observed when 0.3 U/mL SBP was used (Figure 4-28), thereby heightening the competition between the remaining four compounds.

At approximately pH 5.5, Kamal and Behere (2003) reported two occurrences aiding maxima catalytic ability of SBP against ABTS. Firstly, solvent exposure to *delta-meso* heme edge is more than at any other pH. Secondly, the reduction of *beta*-strands and *beta*-turns in the secondary structure of SBP is maximal, making the heme more exposed to reaction solvent and increasing the overall conformational flexibility of the protein. The one logarithmic unit above the reported pH 5.5 observed in this study may be attributed to the acid-base chemistry properties of the phenolics studied. In another study, SBP-based oligomerization of phenolics was shown to be highest at pH 6.4 and more than 90% activity was recorded between pH 5.7 and 7.0 (Wright and Nicell 1999), which agrees with the present study. However, Geng *et al.* (2001) used guaiacol to assay for SBP activity and reported optimal catalytic activity at pH 6.0. Considering these different reports, it is plausible to state there is a pH range within which SBP catalysis is highest, not at a single pH for all substrates.

The optimal pH of 6.5 was used for subsequent experiments. To attain similar total substrate concentration in solution as in the single-compound studies, the individual substrate concentrations were increased to 0.2 mM, for a total of 1.0 mM. Having the pH optimum of mix-5 at pH 6.5, it was hypothesized peroxide and enzyme requirements may also follow a similar manner. Thus, the optimal requirements for the individual treatment of the compounds were pro-rated and used for further studies, with adjustments to accommodate above and below this pro-rated value. Based on this, peroxide requirement was set for 1.46 mM, pending the experimental optimization. Wide-range SBP optimization (Figure 4-30), was done between 0.98 U/mL to 2.18 U/mL. Acetaminophen was removed below LOQ, while PHBA was less than 5% of initial 0.2 mM for most of the SBP activities used. This indicates susceptibility of these two compounds to

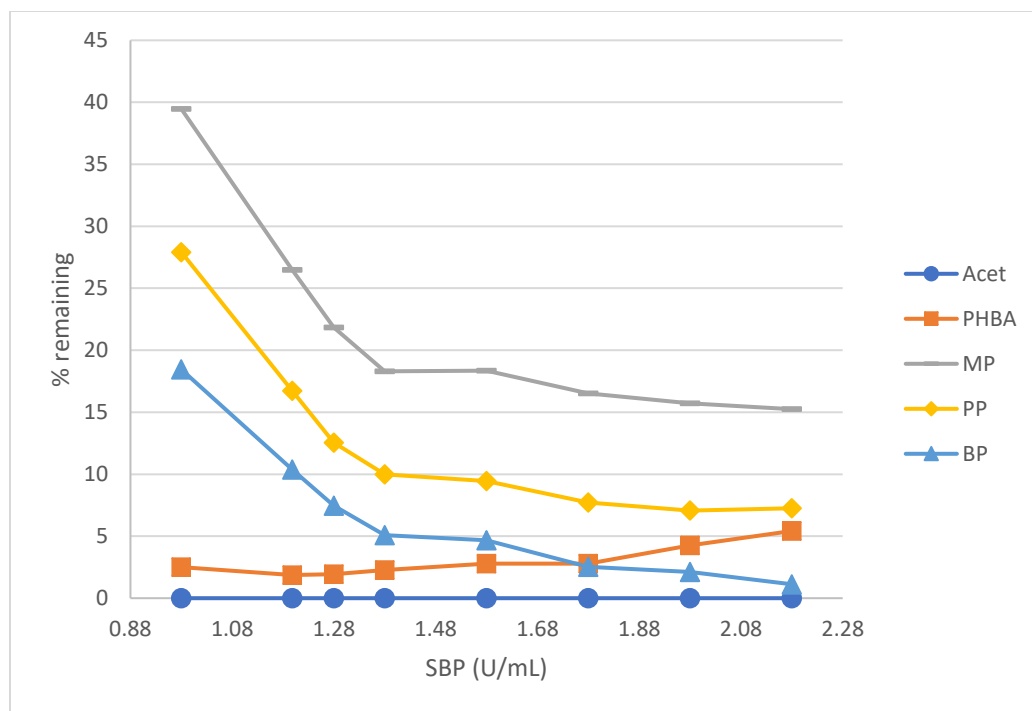


Fig. 4-30 SBP optimization of mix-5 – range finding. Reaction conditions: 0.2 mM of each component of mix-5, 1.46 mM hydrogen peroxide, 40 mM phosphate buffer at pH 6.5 for 3 h.

oligomerization at the experimental conditions. Based upon these findings, a narrow range of 1.18 U/mL and 1.58 U/mL was used for further studies, as shown in Figure 4-31.

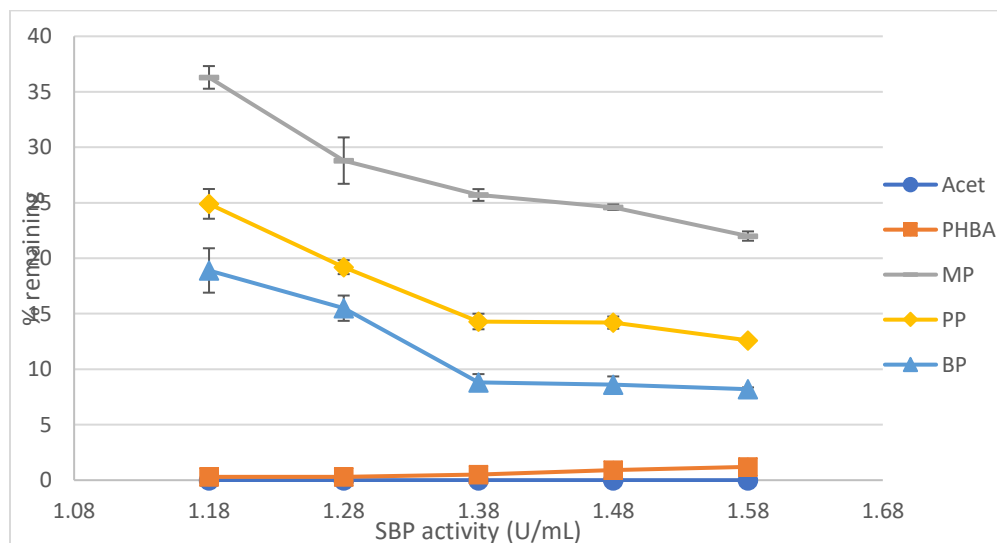


Fig. 4-31 SBP optimization of mix-5 – narrow range. Reaction conditions: 0.2 mM of each component of mix-5; 1.46 mM hydrogen peroxide, 40 mM phosphate buffer at pH 6.5 for 3 h. Results presented as mean±SD where error bars represent the SD of triplicate determinations

Diminishing increases in removal efficiency with increasing SBP are thought to be due to accumulation of polyphenolic precipitates which were formed. All the parabens show poorer removal than when they were treated singly. This could be due to decrease in the organic solvent which was only about 1.75% v/v of the solvent composition. Although this is higher than the 1.25 % v/v used for MP single treatment, the presence of the PP and BP caused more precipitates to accumulate since these are less soluble than MP. Since the removal plot flattened between 1.38 U/mL and 1.48 U/mL and considering the minimum amount of SBP is desired for use to save process cost, 1.38 U/mL was chosen for further studies.

Wide-range peroxide optimization was done between 1.06 mM and 1.76 mM (Figure 4-32). The removal pattern was like previous mix-5 optimizations, following from most

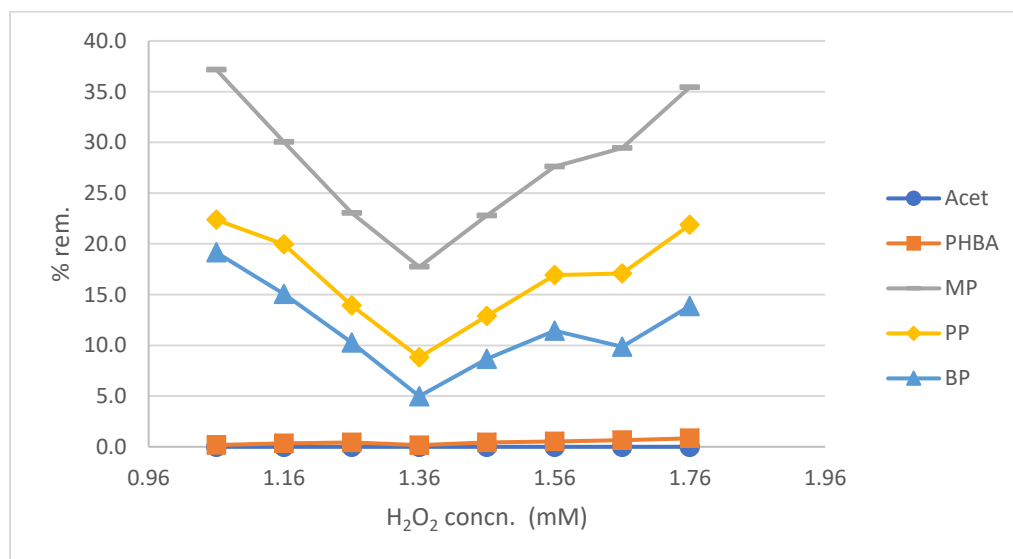


Fig. 4-32 Hydrogen peroxide optimization of mix-5 – range finding. Reaction conditions: 1.38 U/mL SBP, 0.2 mM of each component of mix-5, 40 mM phosphate buffer pH 6.5 for 3 h.

removed to least removed as Acet>PHBA>BP>PP>MP. Highest removal was observed at 1.36 U/mL. Based on this, an array between 1.16 mM and 1.56 mM was chosen for narrow range optimization, Figure 4-33. The removal process stabilized between 1.36 mM and 1.46 mM, expected to the optimal range. The decline in removal efficiency between the last two points of the paraben curves may be due to excess peroxide. Since the substrates

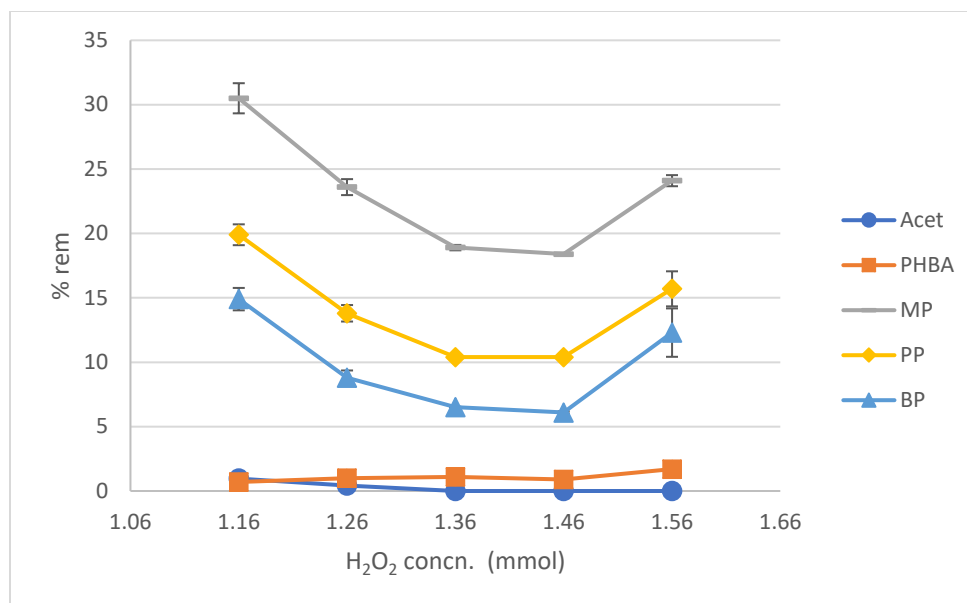


Fig. 4-33 Hydrogen optimization of mix-5 – narrow range. Reaction conditions: 1.38 U/mL of SBP, 0.2 mM of each component of mix-5, and 40 mM phosphate buffer pH 6.5 for 3 h. Results presented as mean±SD where error bars represent the SD of triplicate determinations

are still plentiful, it may not be due to lack of substrate which, Valderrama *et al* (2002) reported may trigger inactivation of SBP. Although PHBA appears to have a removal decline, this is less than 2% and may be considered insignificant.

Reduced solubility of polyphenolic precipitates owing to reduced organic solvent composition for PP and BP may be responsible for their decreased removal, compared to the single treatments. In a mixed system, competition is created and since removal rate depends on enzyme-substrate interaction (Xiang *et al.* 2020), poorly interacting substrates may suffer reduced access to the enzyme thereby halting their removal rates.

Residual analysis (results not shown) showed about 10% of supernatant SBP and less than 5% peroxide thus warranting an increase from the pair of 1.46 mM and 1.38 U/mL, in Figure 4-33. Since peroxide and SBP can limit the oligomerization process, a need to ensure more of supernatant residual SBP and peroxide is justified. Among several pairs tested, that of 1.56 mM and 1.43 U/mL gave supernatant residual SBP of 16.6±2.6% and peroxide at 5.1±0.1%. Triplicate removal studies were conducted at 3 hours and 5

hours (Appendices E-1 and E-2). This increase did not cause the anticipated improvement in removal efficiency for MP and PP. This implies the polyphenolic precipitate formed may be the major source impeding further removal of MP and PP. This underscores mixed effect where cross-coupling was favored over self-coupling may enhance the removal of recalcitrant compounds over single treatment process, to the extent they are able to access the enzyme. This agrees with Xiang *et al.* (2020) and Pylypchuk *et al.* (2018) who also reported enhanced substrate removal in mixed systems than in single systems.

Another option was to double the reaction time and monitor the removal efficiency (Figure 4-34). While the curves for MP and PP flattened out over the additional three hours, BP gained a further removal of 9.27% between the 3rd and 5th hours and

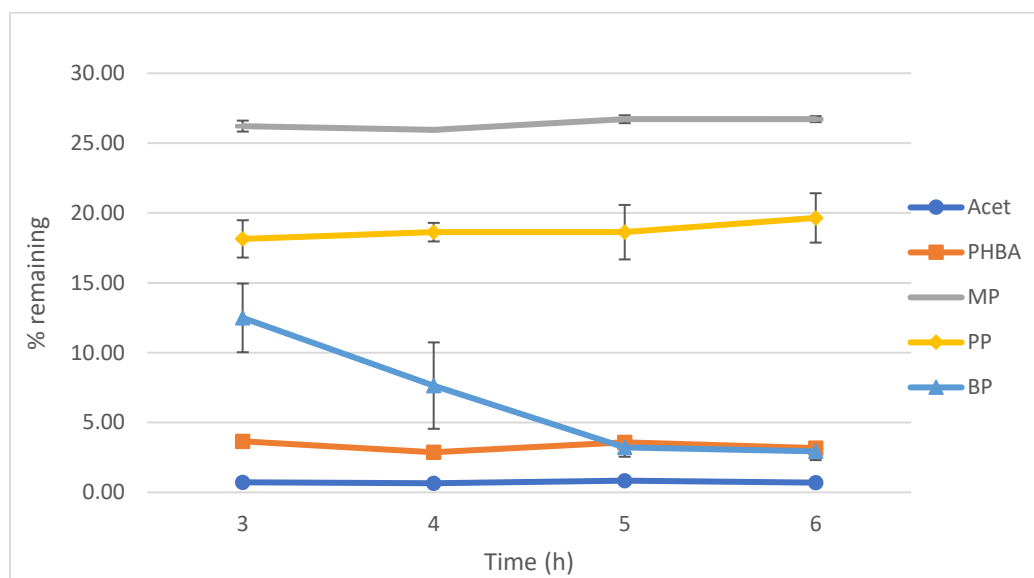


Fig.4-34 Effects of extended incubation time on mix-5 removal. Reaction conditions: 0.2 mM each of the constituent compounds, 1.43 U/mL of SBP, 1.56 mM hydrogen peroxide, and 40 mM phosphate buffer pH 6.5 for 3 h. Results presented as mean±SD where error bars represent the SD of triplicate determinations

thereafter flattened out. Under stringent conditions, BP may be more susceptible for SBP than MP and PP hence its increased removal over time.

Since the removal rate attained is less than target 95% for the MP and BP, further investigations were needed to achieve the target. Residual studies for SBP and peroxide

from varying the amounts of SBP and peroxide were carried out along with incremental additions of peroxide, and centrifugation.

In conventional treatment, coagulation/clarification maybe employed to separate sediments or dissolved substances from water and further clarify it for treatment. Therefore, centrifugation was adopted to speed up the process over natural settling under gravity. The supernatant was collected and following from predetermined residuals of the compounds, SBP and peroxide, additional SBP activity and aliquot of peroxide were provided, in a similar ratio as at the beginning. This was incubated for another three hours and the removal was monitored. This technique was able to drive the removal of PP and BP to $\geq 95\%$ while MP was at about 94% (Figure 4-35). This shows the role of polyphenolic

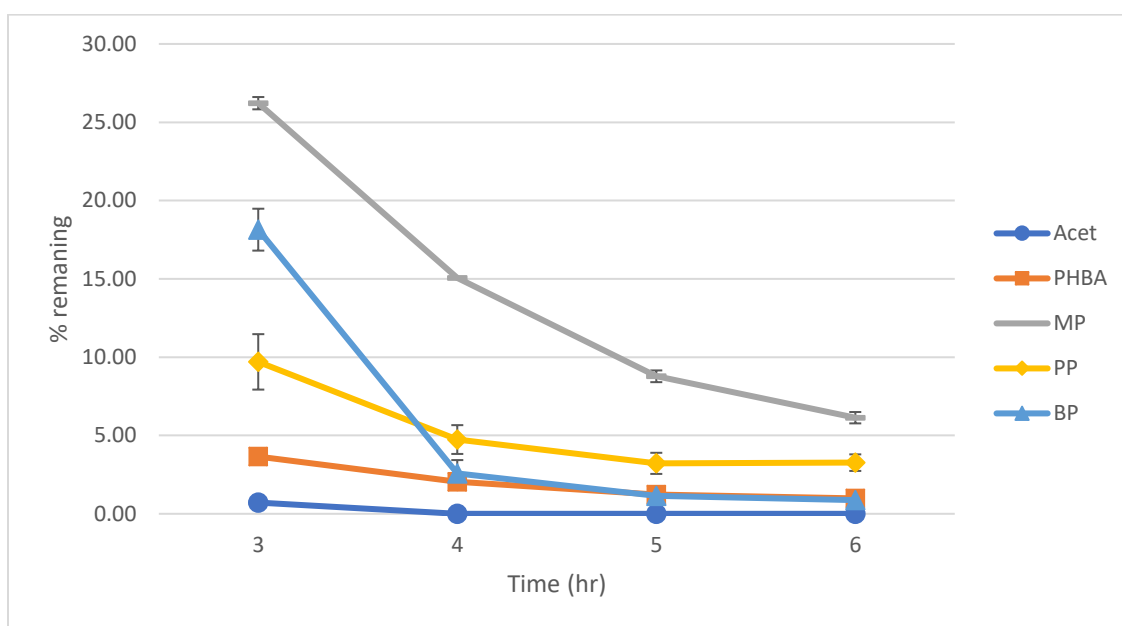


Fig.4-35 Effect of centrifugation, extended incubation time, and additional SBP and H₂O₂ on removal of mix-5. Reaction conditions: 0.2 mM each of the constituent compounds, 1.43 U/mL of SBP, 1.56 mM hydrogen peroxide added at pre-determined 4 points intervals. Reaction mixture was taken at respective time points and quenched with catalase and analyzed. Results presented as mean \pm SD where error bars represent the SD of triplicate determinations

precipitates as enzyme immobilizers which arrest further catalysis leading to reduced compound removal efficiency. Since peroxide is the major driver of the peroxidase cycle via conversion of resting state SBP to compound I, it may control the rate of the reaction. Moreover, Silva *et al.* (2013) reported improved removal of SBP catalyzed treatment of

CECs following incremental additions of peroxide. This is thought to control the rate of polyphenolic precipitates formation and may improve the removal efficiency. Therefore, two incremental peroxide-addition approaches were adopted, by adding a quarter aliquot of the optimized peroxide dose at 22-min (Figure 4-36) and at 44-min (Figure 4-37) intervals. The longest unnormalized half-life in single-compound study was 17.0 ± 1.5 min, (Table 4-4), so this time was chosen to ensure each of the compound would have, in principle attained its half-life before receiving a new dose of the peroxide.

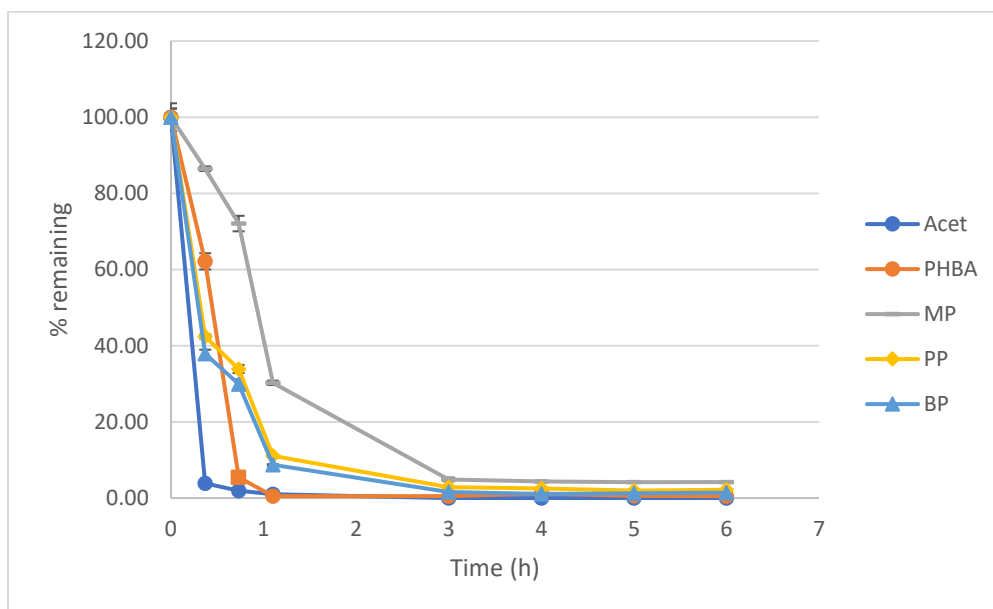


Fig.4-36 Effect of incremental addition of hydrogen peroxide after at the longest half of the individual mix-5 component – reaction conditions: 0.2 mM each of the constituent compounds, total peroxide concentration was 1.56 mM and 1.43 U/mL, 40 mM phosphate buffer pH 6.5. Results presented as mean \pm SD where error bars represent the SD of triplicate determinations

Controlled addition of peroxide improved the removal efficiency of the recalcitrant compounds. A comparison of the remaining compounds following different treatment

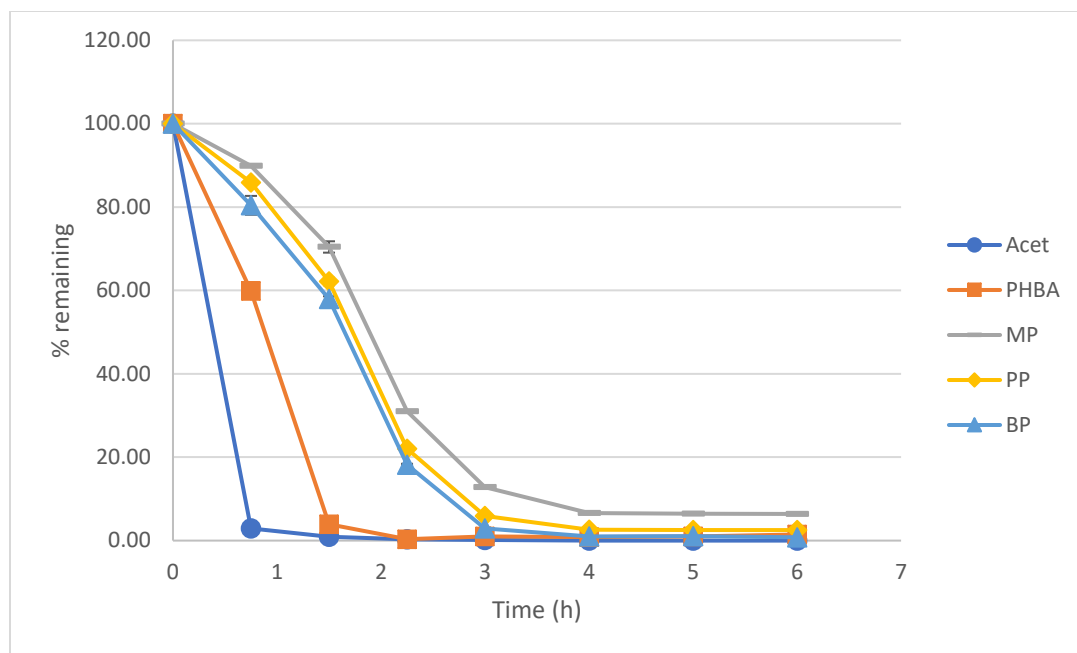


Fig. 4-37 Effect of incremental addition of hydrogen peroxide at twice the longest half of the individual mix-5 component– reaction conditions: 0.2 mM each of the constituent compounds, total peroxide concentration was 1.56 mM and 1.43 U/mL, 40 mM phosphate buffer pH 6.5. Results presented as mean±SD where error bars represent the SD of triplicate determinations

protocols are illustrated in Table 4-2. In the twice-longest half-life, 87%, 94% and 97%

Table 4-2: Summary of % remaining of MP, PP and BP under three different treatment conditions

Time(h)/ treatment	Straight reaction course			Incremental H ₂ O ₂ at longest half-life			Incremental H ₂ O ₂ at twice longest half-life		
	MP	PP	BP	MP	PP	BP	MP	PP	BP
3	26.2	12.5	18.1	4.90	2.90	1.60	12.8	5.89	2.90
4	26.0	7.64	18.6	4.86	2.50	1.08	6.57	2.58	1.00
5	26.7	3.22	18.6	4.17	1.97	1.30	6.43	2.57	1.04
6	26.7	2.93	19.7	4.25	2.15	1.42	6.39	2.52	0.79

Reaction conditions: 0.2 mM of each component of mix-5, 1.43 U/mL SBP, total of 1.56 mM H₂O₂ in 40 mM phosphate buffer pH 6.5.

removal were achieved at 3 h for MP, PP and BP, respectively, compared to 74%, 88%, and 82%, respectively when the reaction was run with single peroxide addition at time zero. Incremental addition of peroxide is thought to improve compounds removal by limiting profuse polyphenolic precipitates formation at the start of the reaction but allowing it to accumulate gradually over time. This helps by enhancing the amount of free enzyme available that continues to undertake catalysis and does not become entrapped by the precipitate solid matrix. According to Nicell (1991) the protective effect of borate on HRP is its ability to prevent the precipitation of its polymeric reaction products. Alternatively, it may be that excess amount of peroxide at the start of the reaction may rather lead to inactivation of the enzyme either through formation of the catalytically inactive compound III or by facilitating enzyme suicide inactivation of SBP.

To illustrate the gain in compound removal in different treatment protocols, the traditional single addition of reactants was compared against the incremental addition of peroxide, either at longest half-life or at twice of longest half-life (Table 4.3). The results show enhanced removal efficiency by incremental addition of peroxide.

Table 4-3: Summary of % improvements in parabens removal efficiency between different treatment processes.

Time(h)/ treatment	Incremental H ₂ O ₂ at longest half-life			Incremental H ₂ O ₂ at twice longest half-life		
	MP	PP	BP	MP	PP	BP
3	21.3	9.6	16.5	13.4	6.60	15.4
4	21.6	5.14	17.5	19.4	5.10	17.6
5	22.5	1.25	17.3	20.3	0.70	17.6
6	22.2	0.780	18.2	20.3	0.40	18.9

Reaction conditions: 0.2 mM of each component of mix-5, 1.43 U/mL SBP, total of 1.56 mM H₂O₂ in 40 mM phosphate buffer pH 6.5.

Mashhadi (2019) reported 5% increase in removal efficiency when peroxide was added incrementally compared with single-dose addition at time zero for treatment of 1.0 mM

2-aminothiazole. This approach also reduced optimal peroxide requirement from for the compound from 2.0 mM in single addition to 1.5 mM in incremental addition. This improved removal with reduced peroxide input could be of great economic gain in industrial processes where unit cost could be enhanced by lower materials consumption. However, the same author reported for similar concentrations of 3-aminopyrazole and 3-aminoquinoline, incremental addition of peroxide did not reduce peroxide requirement but improved compound removal efficiency by 5% and 4%, respectively. The requirements must be experimentally determined since chemical properties of compounds may determine their enzyme-substrate interactions and consequently their removal efficiencies. Generally, between 5 and 10% increased removal efficiency can be achieved from incremental addition of peroxide over single addition (Mashhaddi 2019). However, in this study removal efficiencies were observed between 0.4% to 23% owing to incremental peroxide addition over single addition. This difference could be due to the peculiar chemical properties of the compounds studied, the extent and nature of precipitates formed, and the timing of the incremental peroxide addition.

The effect of incremental addition of peroxide on the removal pattern of compounds can be compared between Figure 4-36 and Figure 4-37. In both cases, acetaminophen and MP are the most and least removed compounds, respectively. However, with limiting concentration of peroxide, BP and PP appear to be easier removed than PHBA. This was noticed earlier when limiting SBP was used at 0.1 U/mL (Figure 4-29) and possible explanations were provided which are also applicable in this situation. It is plausible to reason, the enhanced removal of PHBA is dependent upon the removal of PP and BP. This is because at 22 minutes, PHBA is about 60% remaining while BP is about 38% remaining. At 44 minutes, less than 6% of PHBA is remaining while there is only a slight increase in removal efficiency between 22 and 44 minutes for PP and BP, a sharp contrast to what is observed in the first 22 minutes of the reaction (Figure 4-36). This removal pattern at 44 minutes agrees with the observation in Figure 4-37. For a poorly removed compound such as PHBA, the presence of other aryl radicals other than its kind in solution is thought to have increased the oligomerization of PHBA via cross-coupling thereby increasing its removal efficiency sharply between 22 and 44 minutes. Alternatively, it may be that PHBA oligomerization is enhanced only when there is reduced competition for the enzyme from

these competing substrates. This is reasonable considering at 22 minutes, 84%, 72% and 58% of acetaminophen, BP and PP had been removed (Figure 4-36) which would reduce the competition for the substrate thereby increasing the chances of PHBA-enzyme interaction, a critical step in catalysis.

Single peroxide addition has proved less effective in treating the mix-5 compounds than the incremental dose even over increased reaction time (Table 4-3). Between the two incremental routes, addition of peroxide at about half-life time of the longest compounds showed greater removal efficiency at 3 hours, 4 hours and at 6 hours than incremental dosing at about twice the longest half-life. The set target was to achieve $\geq 95\%$ removal at 3 h for all compounds. This may have been achieved with incremental peroxide addition at 22-minutes, but not at 44-minutes. At 6 hours, the average remaining of the recalcitrant compounds was 2.61% and 3.23% for incremental peroxide addition at about half-life and at about twice half-life, respectively. Although the latter fails to meet the set removal standard, the difference in the average total compounds remaining is minimal, and maybe considered negligible.

For treatment of the mix-5, it may be concluded the incremental addition of peroxide is better than single dosage. These incremental additions may be better done based on the individual compounds' reaction rates, which gives an informed decision of how spacing the incremental peroxide dosage could be achieved. For the incremental peroxide addition, removal efficiency is of the decreasing order of Acet >> PHBA > BP > PP > MP which may be attained at the above 95% removal target for each compound at 3 h.

4.5 Time Course Studies – Single-Compound and mix-5

The removal reactions were studied over a 3-h time course. The choice of this time is a set laboratory standard which enables comparison with previously studied compounds within the group, rather than any particular industrial practice. In conventional wastewater treatment, holding time determines the size of treatment reactors, to cater for prolonged storage thereby influencing overall cost, and *vice-versa* for short treatment times. Therefore, short holding time is desirable if complete treatment could be achieved within

such a time. Targeting 95% removal within 3-h is also a deliberate research goal to improve on cost-efficiency of industrial wastewater treatment processes.

Removal rates can be understood in the context of reaction kinetics, especially for comparison sake, since different reaction conditions are obtainable for the single-compound treatments. Typically, the initial removal of substrates follows pseudo-first-order kinetics, assuming the concentrations of the enzyme and peroxide are constant through some period of the observation. However, for a complete time course under optimized conditions, it is expected that first-order behavior would be lost due to depletion of enzyme and/or peroxide concentration (Feng 2013 and Dunford 1999). Depletion of enzyme activity may be attributed to the production of polyphenolic precipitates that trap the SBP leading to its loss of specific activity and/or making it unavailable for further catalysis (Feng *et al.* 2013), while peroxide is consumed during the reaction (Wagner and Nicell 2002, Nakamoto and Machida, 1992).

First-order law is defined by the differential rate law as

$$\text{Rate} = -\frac{d[S]}{dt} = k[S] \quad (\text{i})$$

Where:

k = rate constant of first-order chemical reaction

$[S]$ is the concentration of the reactant or substrate

$\frac{d[S]}{dt}$ represents the change in the concentration of the substrate over time

By rearranging and integrating (i) above,

$$\ln[S] = \ln[S]_0 - kt \quad (\text{ii})$$

$[S]_0$ is the initial substrate concentration and

$[S]$ is substrate concentration at time, t , along the time course of the reaction

By this, the rate constant of the reaction is the slope of the plot of $\ln[S]$ against time,

At $t = t_{\frac{1}{2}}$,

Equation (iv) in terms of the half-life can be expressed as

$$t_{\frac{1}{2}} = \frac{0.693}{k} \quad (\text{iii})$$

Therefore, the time required for half the initial concentration of the reactant to be degraded can be calculated from (iii), provided k is known. These equations were employed to determine initial rate constant, k , and half-lives from the time-course plots.

Time course plots for the respective compounds are shown in Figures 4-38 to 4-42. Except for BP, all other compounds observed initial reaction rates comparable with traditional first-order chemical reaction model. For BP, about 20% of the compound was removed in the first minute of the reaction. All compounds could not be fit through the whole time-course into a first-order model, for reasons earlier advanced.

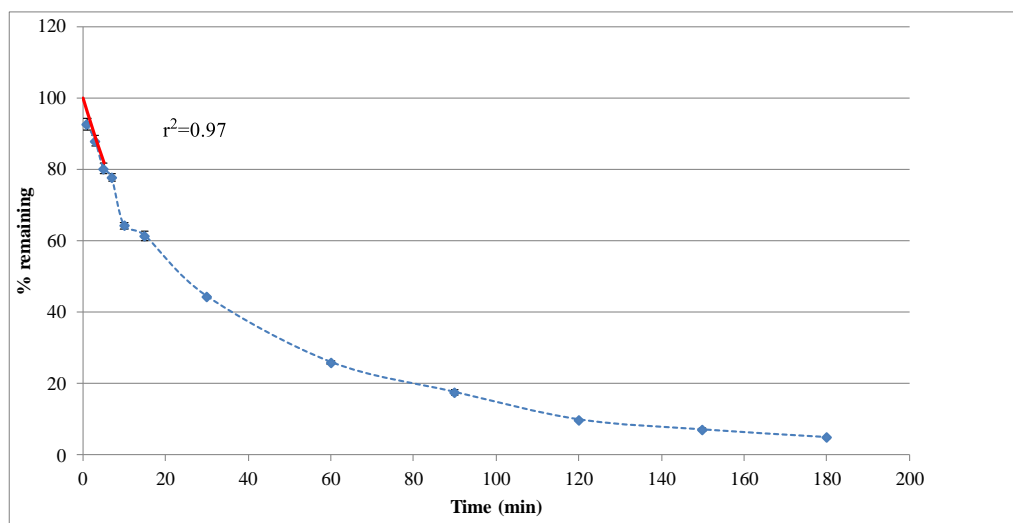


Fig. 4-38 Time course for 1.0 mM acetaminophen under optimized conditions of pH 8.0, 0.006 U/mL SBP, 1.3 mM peroxide. Solid line represents exponential function fitting by linear regression analysis to the semi-ln version using the initial reaction time points corresponding to first-order behavior. Parameters thus are plotted for the exponential function (r^2 noted). Dotted line represents smooth joining of experimental data points. Data presented as mean \pm SD of triplicate determinations.

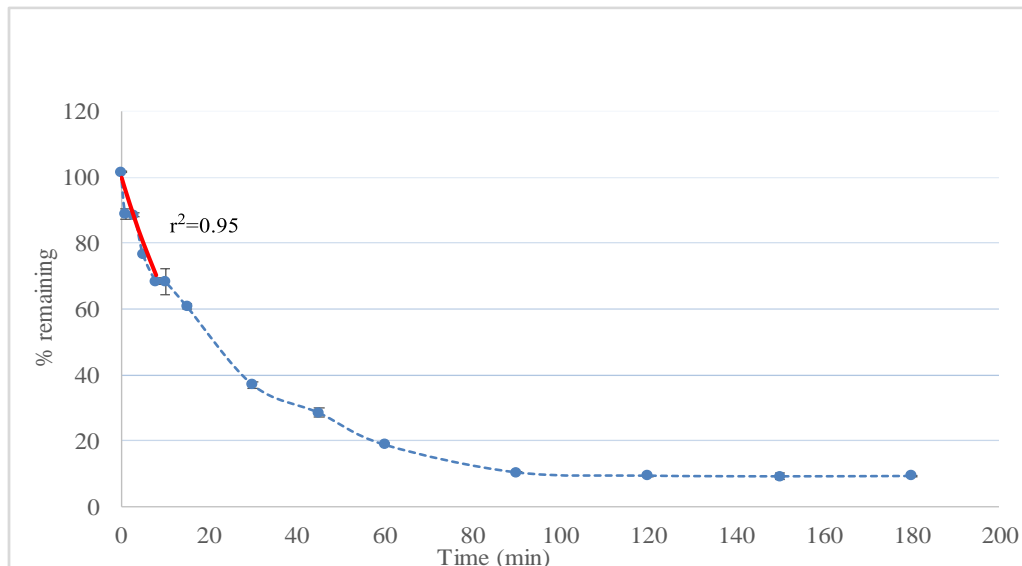


Fig. 4-39 Time course for 1.0 mM PHBA under optimized conditions of pH 6.5, 1.5 U/mL SBP, 2.0 mM peroxide. Solid line represents exponential function fitting by linear regression analysis to the semi-ln version using the initial reaction time points corresponding to first-order behavior. Parameters thus are plotted for the exponential function (r^2 noted). Dotted line represents smooth joining of experimental data points. Data presented as mean \pm SD of triplicate determinations.

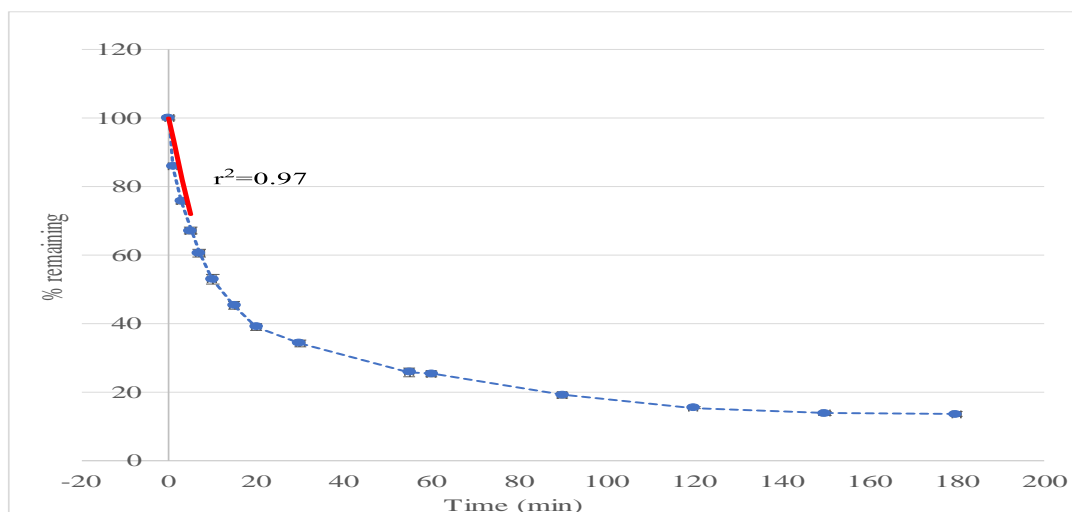


Fig. 4-40 Time course for 1.0 mM MP under optimized conditions of pH 6.5, 2.3 U/mL SBP, 1.4 mM peroxide. Solid line represents exponential function fitting by linear regression analysis to the semi-ln version using the initial reaction time points corresponding to first-order behavior. Parameters thus are plotted for the exponential function (r^2 noted). Dotted line represents smooth joining of experimental data points. Data presented as mean \pm SD of triplicate determinations.

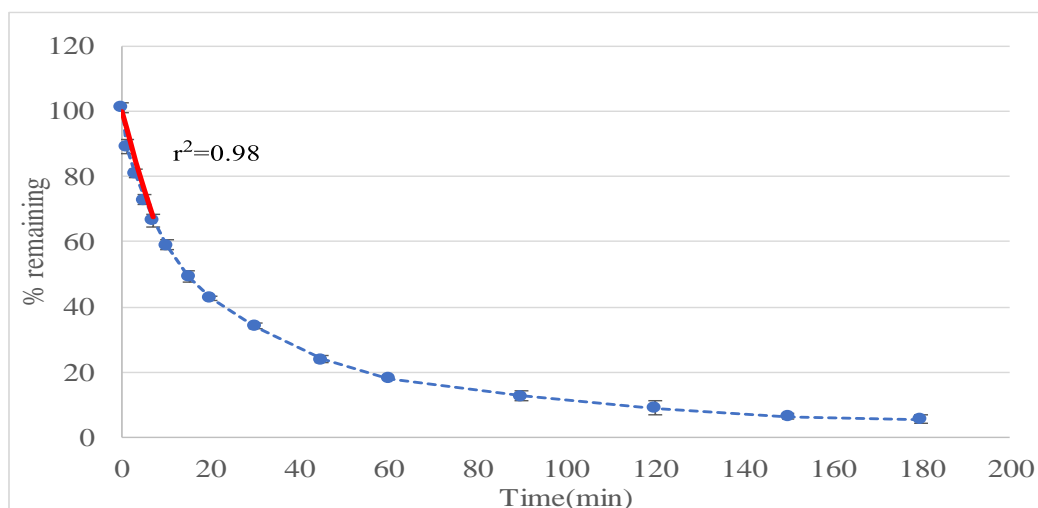


Fig.4-41 Time course for 1.0 mM PP under optimized conditions of pH 6.5, 1.4 U/mL SBP, 1.15 mM peroxide. Solid line represents exponential function fitting by linear regression analysis to the semi-ln version using the initial reaction time points corresponding to first-order behavior. Parameters thus are plotted for the exponential function (r^2 noted). Dotted line represents smooth joining of experimental data points. Data presented as mean \pm SD of triplicate determinations.

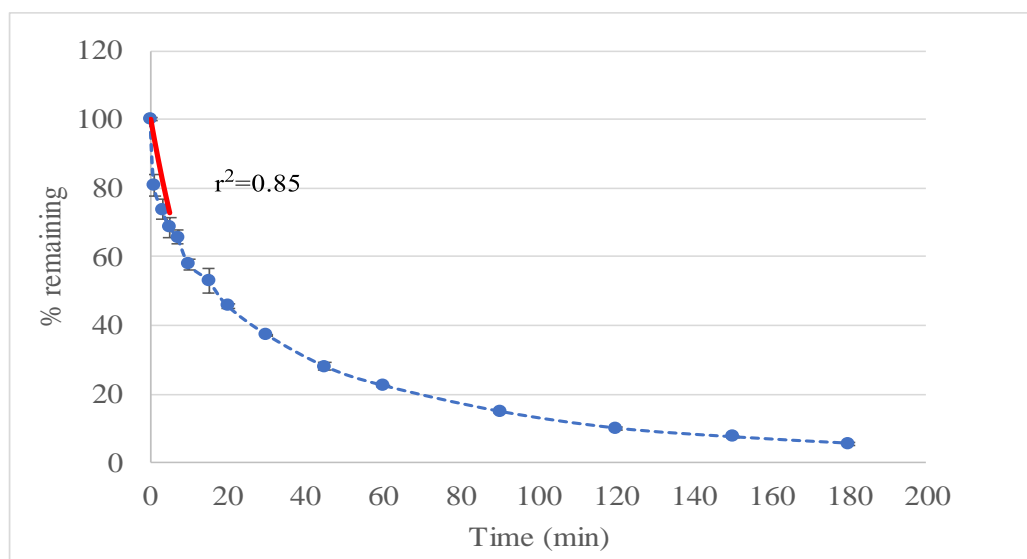


Fig.4-42 Time course for 1.0 mM BP under optimized conditions of pH 6.5, 1.4 U/mL SBP, 1.15 mM peroxide. Solid line represents exponential function fitting by linear regression analysis to the semi-ln version using the initial reaction time points corresponding to first-order behavior. Parameters thus are plotted for the exponential function (r^2 noted). Dotted line represents smooth joining of experimental data points. Data presented as mean \pm SD of triplicate determinations.

To facilitate comparison among the compounds and with previously published works, rate constants were normalized by dividing each individual compounds' rate constant by the dimensionless value of the activity of SBP (in U/mL) used for its optimization (Table 4-1). Half-lives were normalized by multiplying the determined compound's half-life by the amount of enzyme used for the reaction. The calculated parameters for single-compound treatments are summarized in Table 4-4.

Table 4-4 Summary of chemical reaction kinetics for single-compound studies

Compound	k (min ⁻¹)	$t_{\frac{1}{2}}$ (min)	Normalized k (min ⁻¹)	Normalized $t_{\frac{1}{2}}$ (min)
Acet	0.0408±0.0035	17.0±1.5	6.80±0.58	0.100±0.009
PHBA	0.0444±0.006	15.6±2.1	0.030±0.004	23.4±3.2
MP	0.0660±0.007	10.5±1.1	0.029±0.003	24.2±2.6.
PP	0.0558±0.0046	12.4±1.0	0.040±0.003	17.4±1.4
BP	0.0636±0.0174	10.9±3.0	0.045±0.012	15.2±4.2

Normalized k in the single-compound studies is in the order of Acet>>BP≈PP>PHBA≈MP while normalized half-lives are in the increasing order of Acet<<PP≈BP<PHBA≈MP. The normalized rate constant for acetaminophen was 150 times higher than the next compound, BP, and at least 230 times faster than the last compound, MP, highlighting the fast removal of the compound. Mashhadi (2019) reported normalized half-lives (min) for the same SBP preparation of 1.19, 5.0, 6.06, 7.7, 11.3, 108, and 3240 for 3-hydroxyquinoline, hydroxybenzotriazole, 4-AAP, 2-aminoimidazole, indole, 2-aminobenziimidazole and 2-aminobenzothiazole, respectively. Kaur *et al.* (2020) reported normalized half-lives for the same SBP preparation of 0.048 and 0.0097 min for CI Methyl Orange and *p*-anisidine, respectively. Although most of these compounds are mainly anilino aromatic heterocyclics (except 3-hydroxyquinonoline), their single functional groups make them merit a

comparison. Normalized rate constants and half-lives for the parabens and PHBA are similar, suggesting a similar treatment regimen can be employed for these structurally related compounds. The relative ease of acetaminophen treatment points to its ease of removal, in relation to the parabens. The derived rate constants are reasonably precise ($r^2=0.85$ for BP, others above 0.90; values $\pm(8 - 15\%)$ for the individual compounds).

The time course plot for the removal of mix-5 within the first two minutes of the reaction is presented in Figure 4-43. A separate time course study within this initial time was

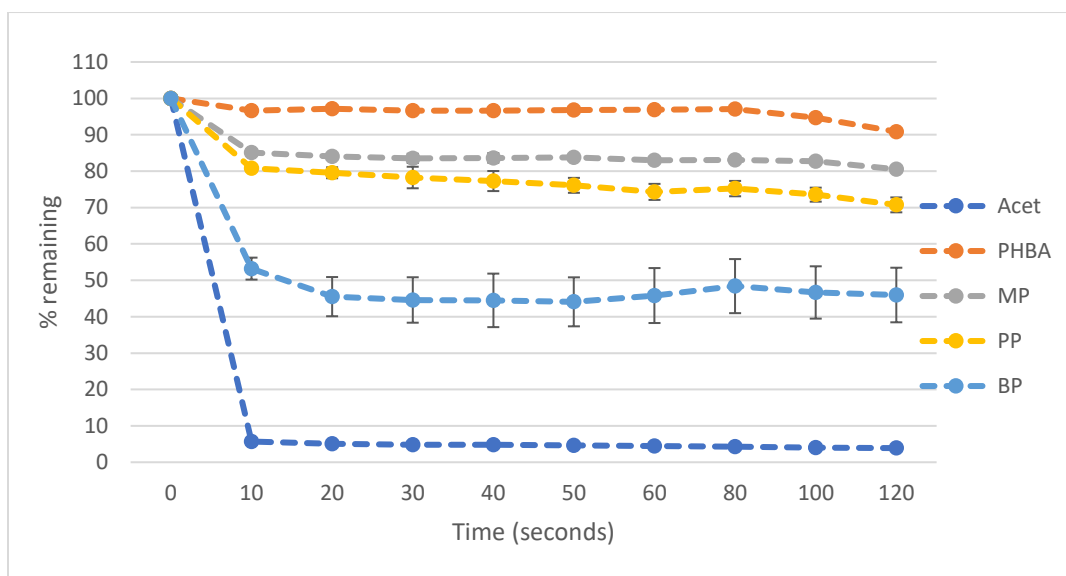


Fig.4-43 Time course for mix-5 (0.20 mM each) for first 2 minutes under optimized conditions of pH 6.5, 1.43 U/mL SBP, 1.56 mM peroxide. Dotted line represents smooth joining of experimental data points. Data presented as mean \pm SD of triplicate determinations.

necessary to elucidate the rate at which acetaminophen and BP were oligomerized, in respect to the other compounds. The amount of SBP used in this study is at least 4-fold over that employed for single treatment, which could account for the fast removal rate observed. *Gomes et al.* (2018b) studied the photolysis of PP and BP using mercury lamps and reported PP was more susceptible to degradation than BP, the reverse of what is observed in this study. This could be due to the different treatment approach employed for the studies.

A 3-hour time course plot for mix-5 is presented in Figure 4-44. Considering the two figures, produced under the mix-5 optimized conditions developed in Section 4.5 above, two distinct phases of the reaction may be observed, which may be classified as fast phase and slow phase. Acetaminophen and BP showed the greatest fast phase, where 95% and about 55% of the compounds were removed during the first 10 and 20 seconds, respectively of the reaction (Figure 4-43). Other compounds, PP and MP also had significant removal within this phase, accounting for 21% and 16% removal, respectively at 20 seconds. PHBA removal fitted better into the first-order reaction model for the initial reaction course than MP and PP (Figure 4-44) and its kinetic parameters were calculated within this time, unlike

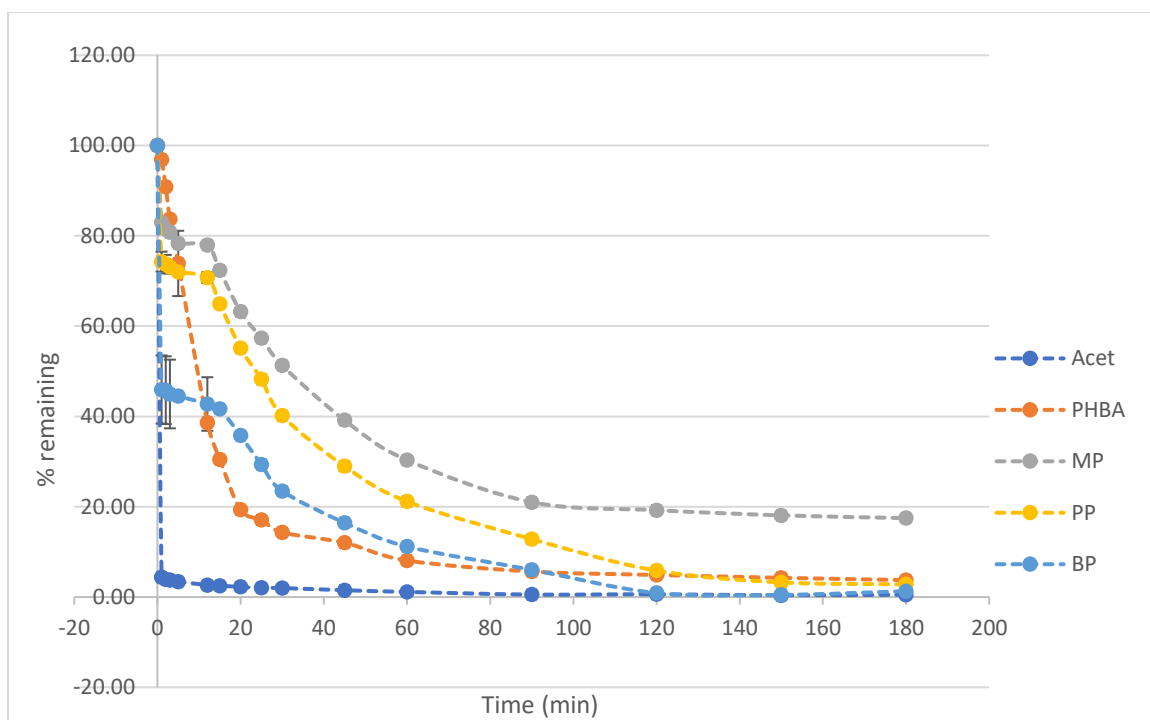


Fig.4-44 Time course for mix-5 (0.20 mM each) under optimized conditions of pH 6.5, 1.43 U/mL SBP, 1.56 mM peroxide. Dotted line represents smooth joining of experimental data points. Data presented as mean \pm SD of triplicate determinations

acet and BP, whose half-lives were determined by extrapolating onto the x-axis (time axis) of Figure 4-43 (not shown) corresponding to 50% removal from the curve. Therefore, these values are without uncertainties (Table 4-5). The fast reaction phase is thought to be due to the mixture effect, where the production of acetaminophen radicals might have triggered

a surge of reaction by indiscriminately attacking other non-oxidized compounds through radical transfer, leading to the formation of radicals from the less enzymatically reactive substrates and consequent oligomerization. Wang *et al.* (2020) reported the role of phenoxy radicals in enhancing removal of other phenolics under mixture conditions. The decline in removal, the slow phase, obviously noticeable for the parabens between 10 seconds (Figure 4-43) and up to 12 minutes (Figure 4-44) is thought to correspond to course with diminishing radical production from acetaminophen, which could limit radical transfer and hence removal of these parabens. The kinetic parameters for mix-5 reactions are summarized in Table 4-5. The normalized rate constant for Acet has apparently reduced between the single-compound treatment and in mix-5. Acet appears to have lost

Table 4-5 Summary of reaction kinetics for mix-5 under optimized conditions

Compound	k (min ⁻¹)	t _{1/2} (min)	Normalized k (min ⁻¹)	Normalized t _{1/2} (min)
Acet	≥8.32	≤0.0833	≥5.82	≤0.119
PHBA	0.063±0.004	11.0±0.7	0.045±0.003	16.0±1.0
MP	0.0398±0.0179	17.4±7.8	0.0279±0.0125	24.9±11.2
PP	0.0508±0.0298	13.6±7.98	0.0355±0.0208	19.5±11.5
BP	≥2.97	≤0.233	≥2.08	≤0.333

about 15% and has also apparently become slower by 9% when compared between single treatment and mix-5. Since the uncertainties are not known, this value cannot be wholly relied upon. This may be due to the different amount of SBP activity units used for the different treatment conditions. The normalized rate constants for MP and PP are 2-fold lower in mix-5 than in single treatment, while the normalized rate constant for PHBA has about 50% gain in the mix-5 over single compound treatment. The normalized half-lives for MP and PP are apparently very high. This is expected since the r² value for the fitting into the integrated rate law was less than 50%, owing to the fast removal in the first 20 seconds followed by the slow removal phase. This entails a reasonable deviation from first-order behavior within the initial duration of the reaction. BP has a notable increase in

normalized rate constant of about 47-fold in mix-5 compared to single compound treatment. Zhang and Colosi (2011) reported similar rate constants between equimolar phenolics in single-compounds and in mixture treatments. The altered reaction mixture compositions owing to the optimized parameters under these conditions is thought to be responsible for the markedly different chemical reaction kinetic parameters observed in this study.

4.6 Mass spectral evidence for formation of oligomers following SBP treatment

Theoretical prediction of the peroxidase reaction is that the aryl radicals formed diffuse from the active site of the enzyme into the reaction matrix and couple to form dimers. If the dimers formed are soluble, they may be substrates for the enzyme and undergo another catalytic cycle, this time producing a dimer radical which can undergo similar non-enzymatic oxidative coupling until the oligomeric products are insoluble and precipitate out of solution. This is the selling point of biocatalytic treatment over other AOPs. For instance, mineralization techniques are associated with formation of DBPs, incomplete oxidation may lead to more toxic intermediates and even when it is complete, CO₂ is formed increasing the carbon footprint of the WWTP (Hu *et al.* 2019, Talib and Randhir 2017, Strutt *et al.* 2009). Conversely, the formation of insoluble oligomers which may be separated by sedimentation is applauded, as it overrides the downfalls of mineralization techniques.

Several studies have reported oligomerization of phenolics with varying chain length both in laboratory based studies using peroxidases (Wang *et al.* 2020, Lu *et al.* 2009, Potter *et al.* 1985), microbial consortia in natural habitats such as soil (Zhou *et al.* 2019, Liang *et al.* 2016), in the presence of DOM (Li *et al.* 2017) and from natural samples such as surface water (Li *et al.* 2017) and different soil types (Li *et al.* 2014). Chlorination of synthetic wastewater containing a mixture of CECs has also been shown to produce oxidatively coupled oligomers (dimers) of the constituent compounds (Xiang *et al.* 2020, Liu *et al.* 2019). Thus, oligomerization and polymerization are not only limited to enzyme-(peroxidase, hydrolases and transferases) based treatment techniques (Kobayashi *et al.*

2005), but also other processes employing only chemical treatment (Xiang *et al.* 2020, Liu *et al.* 2019).

Different oxidative coupling patterns have been reported between the participating atoms (Yu *et al.* 1994). In a monophenoxyl radical, high unpaired electron densities are associated with oxygen, *ortho* and *para* C-atoms (Ye and Schuler 1989). Therefore, are most favored for oxidative coupling with similar carbons atoms of the other molecules.

In this study, since *o*-, *o*- coupling is the major route (the *p*-position is blocked) and C-C coupling predominates over to *O*-C coupling in peroxidase catalyzed reactions involving acetaminophen (Lu and Huang 2009), the M/S resolved and identified phenolic oligomers are presented with C-C oxidative coupling orientation, showing bonding between the two C atoms *ortho* to the hydroxyl group between participating molecules. Assignment of molecular formulae was done after cross matching the experimental *m/z* peaks to the theoretical ones within a deviation of 10 ppm, consideration of ¹³C isotopes *m/z* peak presence and relative ratio to the supposed molecular *m/z* peak and the use of isotopic modelling tools. Where published literature is available, the results are also compared to ensure the highest accuracy is achieved. De Laurentiis *et al.* (2014) reported acceptable transformation products following acetaminophen treatment and matched them with the error limits of between 13 and 20 ppm.

Unlike degradation, these oligomerizations tend to mimic the humification process observed in natural environments where monomers are oligomerized and the oligomers can easily bind to DOM or earth surfaces, thereby making it easy for removal or remaining biologically inactive (Lu and Huang 2009). Contrary to mineralization, this approach helps to reduce the amount of carbon dioxide that would have been generated (carbon footprint) from a conventional treatment process, (Strutt *et al.* 2008) thereby minimizing greenhouse gas (GHG) effects on the atmosphere.

4.6.1 Acetaminophen

Positive-ion electrospray ionization (ESI+) was employed due to its soft nature on acetaminophen molecules. Hawavitharana *et al.* (2008) reported that positive-ion MS for acetaminophen was successfully implemented and produced a strong signal owing to protonation of nitrogen of the N-acetyl group. Several authors who employed LC-MS (Liu

et al. 2019, Wang *et al.* 2018, De Laurentiis *et al.* 2014) have reported an analysis for acetaminophen using this ionization technique. All m/z peaks identified in acetaminophen mass spectra are in the positive ionization mode and hence protonated. The MS scan of acetaminophen standard between 50 and 1200 m/z is shown in Figure 4-45. The strong peak at m/z 179.0936 has been consistent even with blank samples (data not shown), raising the concerns it may arise from artifacts associated with the preparation process.

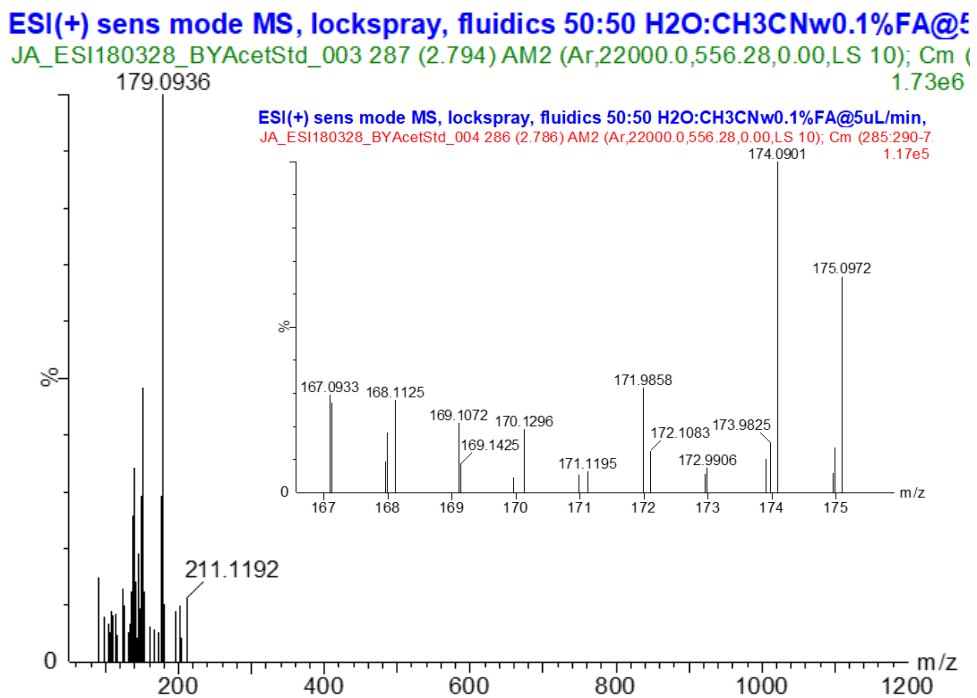


Fig.4-45 ESI(+)-mass spectrum of acetaminophen

Oligomerization of acetaminophen at the optimized conditions produced evidence of dimers, trimers, tetramers, both in the reaction precipitate and the supernatant, and a pentamer in the precipitate. Since the objective of this study was not a quantitative assessment of the respective oligomers produced, the subject is left beyond the scope of this work. The products formed are depicted in Figures 4-46 and 4-47, in the full-scan mass spectra of supernatant and precipitate, respectively. Numbers represent possible m/z peak for monomer and oligomers.

ESI(+) sens mode MS, lockspray, fluidics 50:50 H₂O:CH₃CNw0.1%FA @ 5uL/mi
JA_ESI180328_BYAcetpH8sol_002 243 (2.378) AM2 (Ar,22000.0,556.28,0.00,LS 10); Cm (240:2
3.02e6

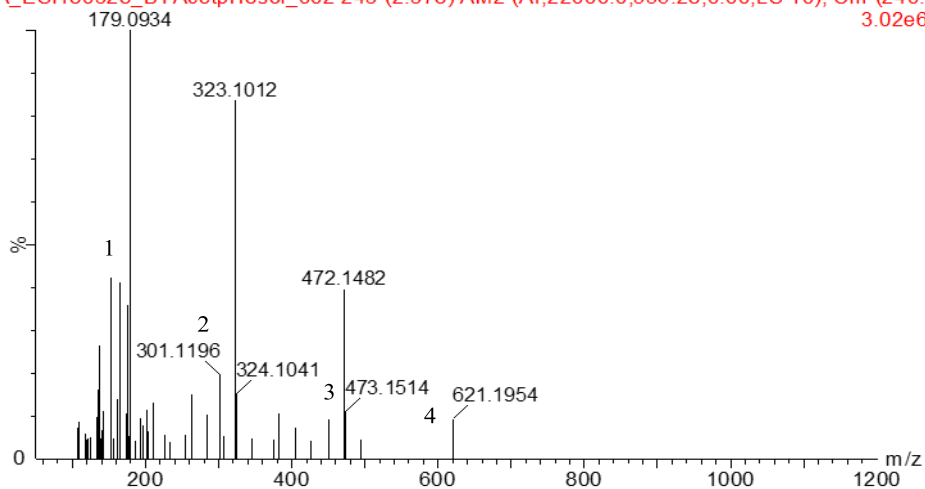


Fig. 4-46 ESI(+)-mass spectrum of acetaminophen supernatant under optimized conditions

ESI(+) sens mode MS, lockspray, fluidics 50:50 H₂O:CH₃CNw0.1%FA @ 5uL/mi
JA_ESI180328_BYAcetpH8ppt_001 240 (2.352) AM2 (Ar,22000.0,556.28,0.00,LS 10); Cm (235:2
3.05e6

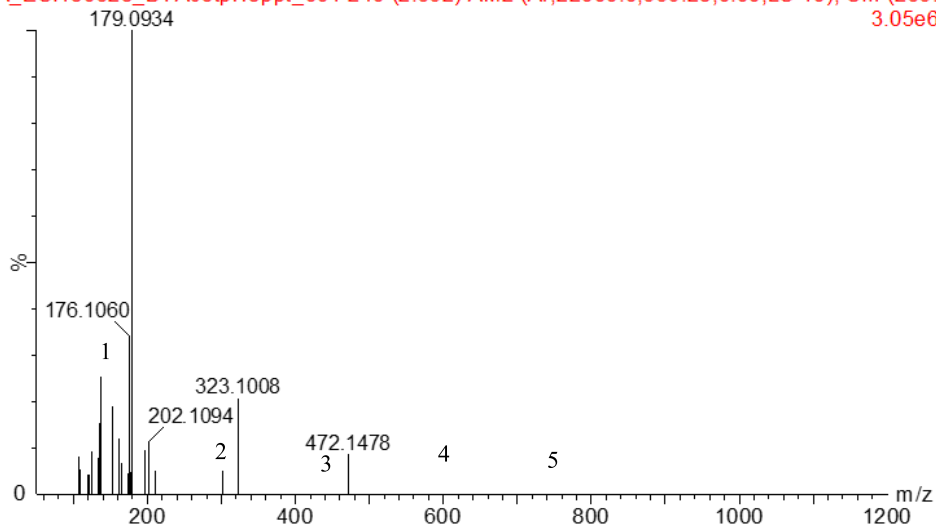


Fig. 4-47 ESI(+)-mass spectrum of acetaminophen precipitate under optimized conditions

The oligomers from acetaminophen highlighted in Figures 4-46 and 4-47 are summarized in Table 4-6. The following pages will highlight the detailed mass spectral results from Figures 4-48 to 4-55, plausible structures Figure 4-56.

Table 4-6 Acetaminophen monomer and oligomers following SBP treatment as observed from precipitate and supernatant

Molecular formula	M^{+}_{theo}	M^{+}_{expt}	ppm
Precipitate			
$C_8H_9NO_2$	152.0712	152.0725	8.5
$C_8H_8NO_2Na$	174.0531	174.0531	0.6
$C_{16}H_{16}N_2O_4$	301.1188	301.1190	0.7
$C_{16}H_{15}N_2O_4Na$	323.1008	323.1008	0.0
$C_{24}H_{23}N_3O_6$	450.1665	450.1669	0.9
$C_{24}H_{22}N_3O_6Na$	472.1485	472.1478	-1.5
$C_{32}H_{30}N_4O_8$	599.2142	599.2141	-0.2
$C_{32}H_{29}N_4O_8Na$	621.1961	621.1951	-1.6
$C_{40}H_{37}N_5O_{10}$	748.2619	748.2563	-7.5
$C_{40}H_{36}N_5O_{10}Na$	770.2448	770.2390	-7.5
Supernatant			
$C_8H_9NO_2$	152.0712	152.0721	5.9
$C_8H_8NO_2Na$	174.0531	174.0532	0.6
$C_{16}H_{16}N_2O_4$	301.1188	301.1196	2.7
$C_{16}H_{15}N_2O_4Na$	323.1008	323.1012	1.2
$C_{24}H_{23}N_3O_6$	450.1665	450.1652	-2.9
$C_{24}H_{22}N_3O_6Na$	472.1485	472.1482	-0.6
$C_{32}H_{30}N_4O_8$	599.2142	599.2128	-2.3
$C_{32}H_{29}N_4O_8Na$	621.1961	621.1947	-2.3

The focus of the study was to convert monomers to oligomers therefore, the presence of monomers will be deliberately overlooked, except to note this was also detected in the mass spectra, indicating a trace residual of the compound in solution. This is justifiable considering the instrument is sensitive to minute concentrations of ng/L, such signals may be detected. An exception is where there is a modification of the monomer, in a manner that differs from what is observed from mass spectrum for the standard samples.

The mass spectrum between m/z 138 and 176 is shown in Figure 4-48, covering the monomer and a sodium salt of the monomer, represented by peaks 1 and 2, respectively. The protonated monomer appears at m/z 152.0734 with its ^{13}C peak adjacent to it. Since the m/z peak at 174.0533 was not observed in the standards' mass spectrum prepared with deionized water only (Fig.4-45 insert), it is thought to be a modification of the monomer owing to the presence of Na^+ in solution, arising from the use of sodium phosphate buffer. This peak is assigned the molecular formula $\text{C}_8\text{H}_9\text{NO}_2\text{Na}$ and is correct to an error of 1.1 ppm for the molecular ion (unlike the insert peak at m/z 174.0901 which has an error of 211 ppm). Its proposed structure is presented in Figure 4-56 (a). The presence of a sodium-oligomer salt ion, all resolved within less than 5 ppm error margin is observed for all the identified oligomers, except pentamer where the corresponding m/z peak displayed poor signal strength. The presence of this group is thought to contribute to the solubility of the oligomers at pH 8, considering the pK_a of these compounds is between 8.4 and 9.4, even the tetramers of acetaminophen were found present in the supernatant, with appreciably high ion intensity. Perhaps the use of an alternate buffering system within this pH range that does not have a sodium cation, such as Tris buffer may prove if the supernatant may still contain oligomers up to tetramers, to account for the effect of the phosphate buffer on the solubility of the oligomers.

ESI(+) sens mode MS, lockspray, fluidics 50:50 H2O:CH3CNw0.1%FA @ 5uL/min, BYA
JA_ESI180328_BYAcetpH8ppt_001 240 (2.352) AM2 (Ar,22000.0,556.28,0.00,LS 10); Cm (235:240-72:7:
5.81e5

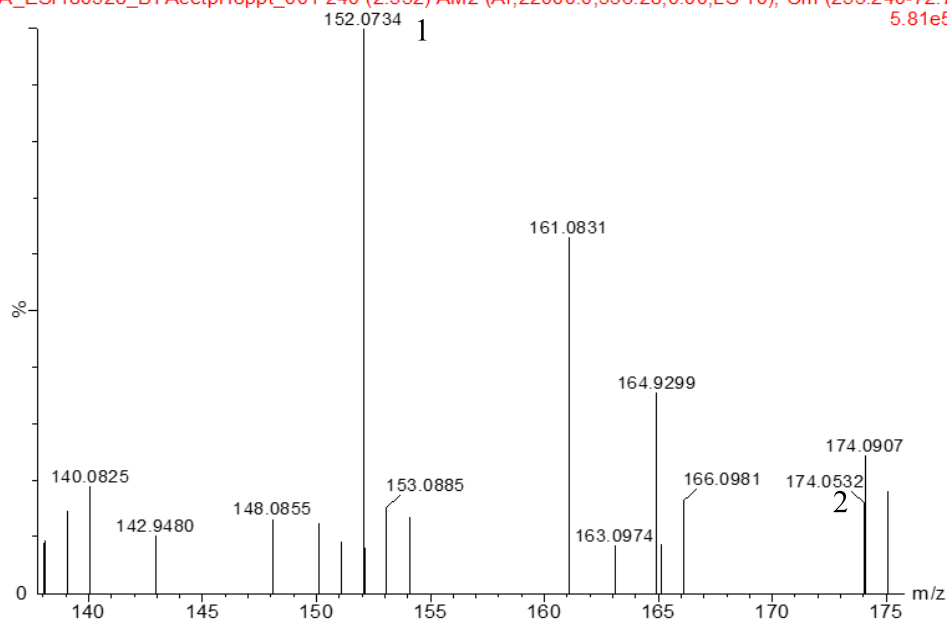


Fig. 4-48 ESI(+) mass spectrum of acetaminophen supernatant under optimized conditions showing monomer and its sodium salt

In Figures 4-49 and 4-50, the m/z peaks designated 1 both correspond to acetaminophen dimer, obtained from the precipitate and supernatant, respectively and assigned the molecular formula $C_{16}H_{16}N_2O_4$. The m/z peaks tagged 2 are assigned the molecular formula $C_{16}H_{15}N_2O_4Na$ representing the sodium salt of the dimer. The proposed molecular structures are shown in Figures 4-56 (b) and (c), respectively.

ESI(+) sens mode MS, lockspray, fluidics 50:50 H2O:CH3CNw0.1%FA @ 5uL/min, BYAcetpH8sol, C8H

JA_ESI180328_BYAcetpH8ppt_001 240 (2.352) AM2 (Ar,22000.0,556.28,0.00,LS 10); Cm (235:240-72.77)

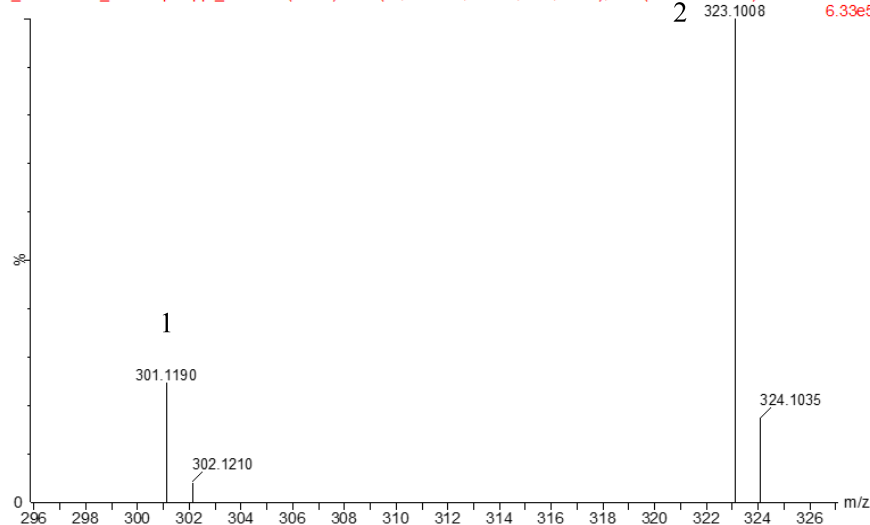


Fig. 4-49 ESI(+) mass spectrum of acetaminophen precipitate under optimized conditions showing dimer and its sodium salt

ESI(+) sens mode MS, lockspray, fluidics 50:50 H2O:CH3CNw0.1%FA @ 5uL/min, BYAcetpH8sol

JA_ESI180328_BYAcetpH8sol_002 243 (2.378) AM2 (Ar,22000.0,556.28,0.00,LS 10); Cm (240:245-69.74)

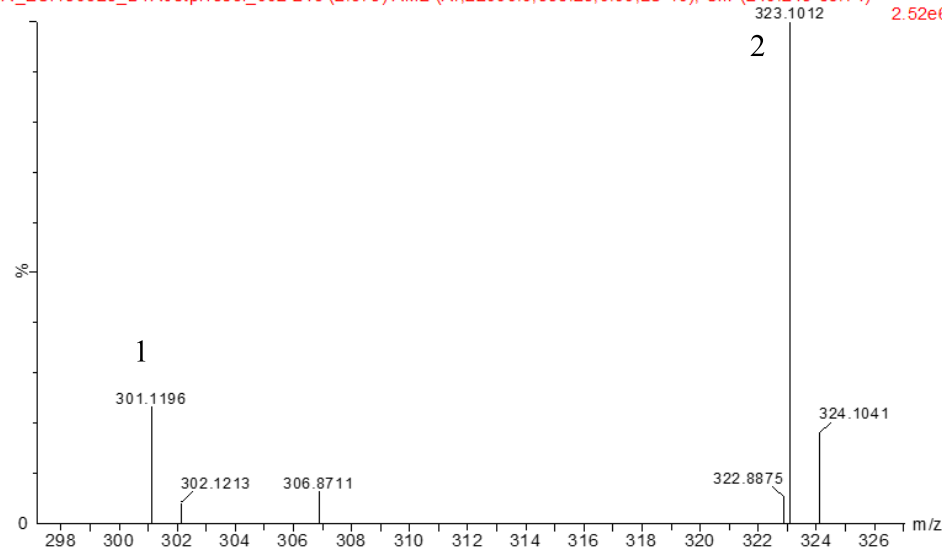


Fig. 4-50 ESI(+) mass spectrum of acetaminophen supernatant under optimized conditions showing dimer and its sodium salt

Figures 4-51 and 4-52 represent the mass spectra in the trimer range for the enzymatic precipitate and supernatant, respectively. The m/z peaks assigned 1 in both figures represent the protonated trimer, which is assigned the molecular formula $C_{24}H_{24}N_3O_6$ while the ^{13}C isotope peaks are designated 2. The peaks designated 3 appear to be the

unprotonated m/z peak for the trimer sodium salt ions, with the molecular formula $C_{24}H_{23}N_3O_6Na$ and showing a deviation of -0.6 ppm and 1.5 ppm, for Fig.4-56 and 4.57, respectively, further rationalizing these formula assignments. The m/z peak marked 4 is thought to be a protonated trimer sodium salt ion and while m/z peak 5 may be the ^{13}C isotopic peaks of the trimer sodium salt ions. The proposed molecular structures for the

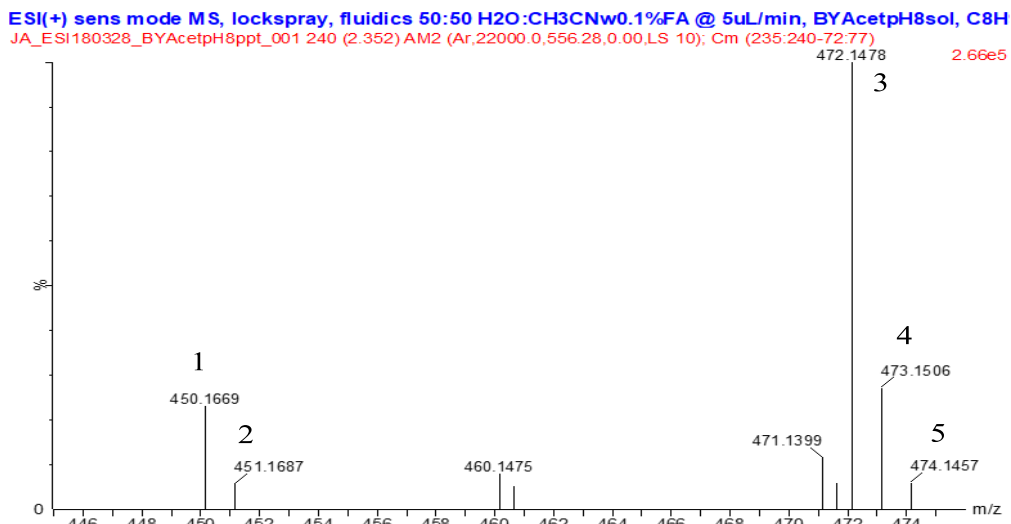


Fig. 4-51 ESI(+ mass spectrum of acetaminophen precipitate under optimized conditions showing trimer and its sodium salt

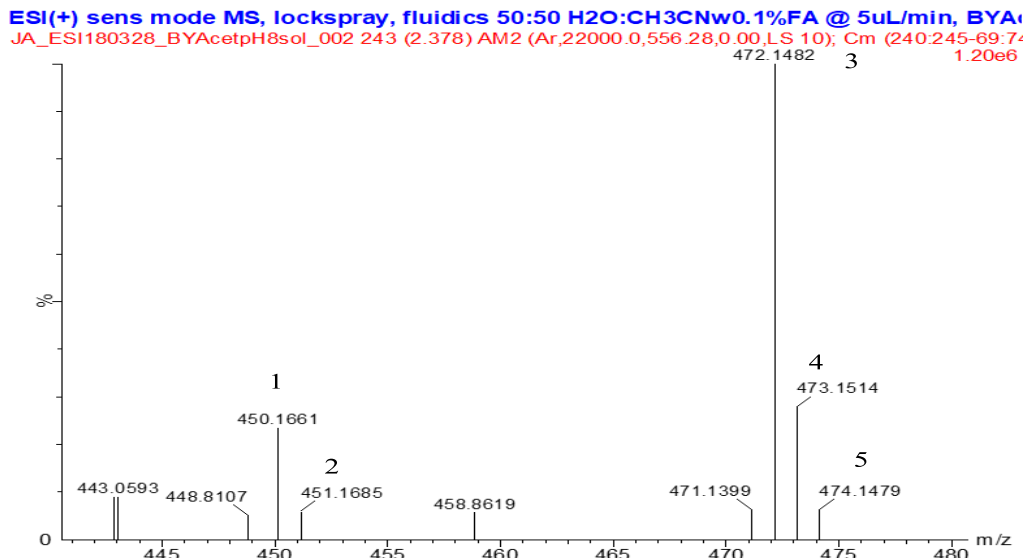


Fig. 4-52 ESI(+ mass spectrum of acetaminophen supernatant under optimized conditions showing trimer

trimer and its sodium salt ion are presented in Figures 4-56 (d) and (e), respectively. The protonation of molecular ions is not complete, leading to the appearance of unprotonated molecular ion peaks observed here.

The tetramers formed are shown in Figures 4-53 and 4-54, for precipitate and supernatant,

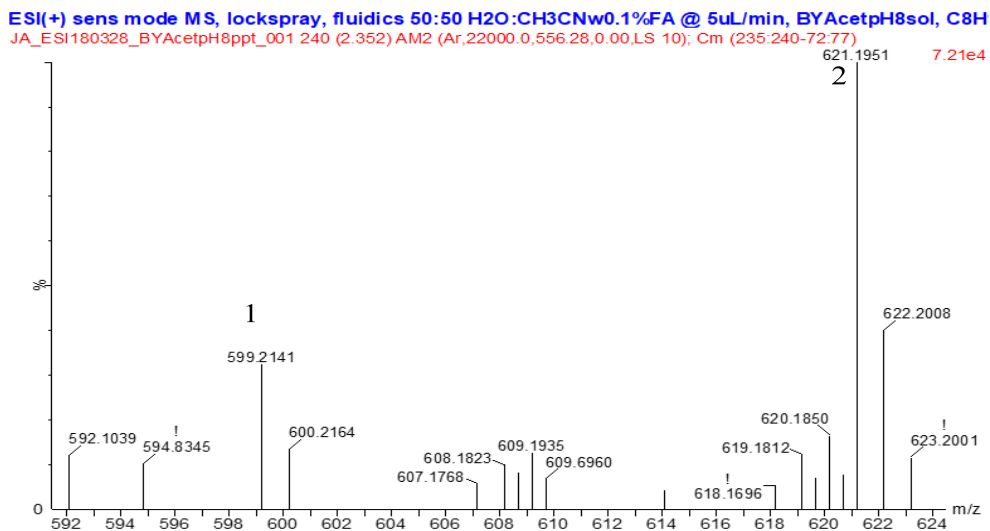


Fig. 4-53 ESI(+ mass spectrum of acetaminophen precipitate under optimized conditions showing tetramer and its sodium salt

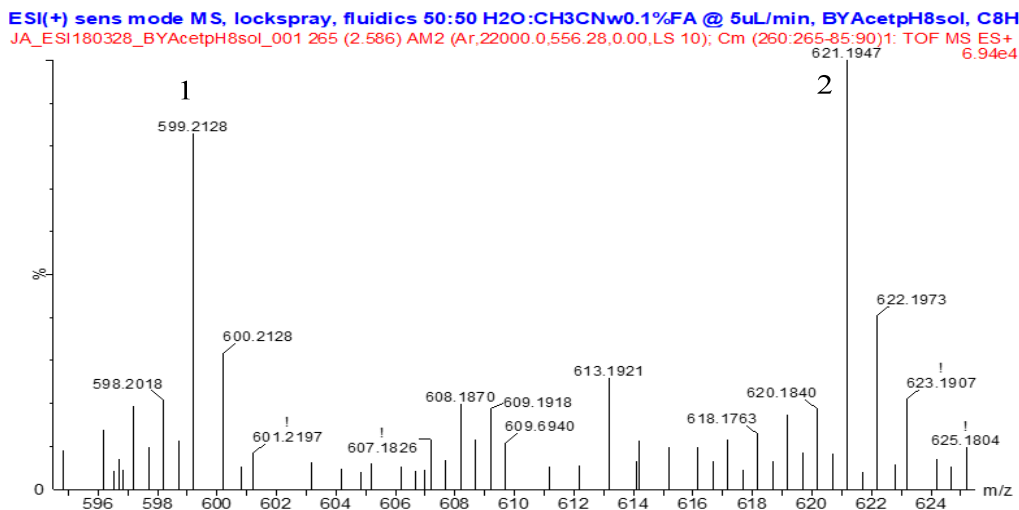


Fig. 4-54 ESI(+ mass spectrum of acetaminophen supernatant under optimized conditions showing tetramer and its sodium salt

respectively. The peaks numbered 1 in both figures represent the protonated tetramer

molecule, assigned the molecular formula $C_{32}H_{30}N_4O_8$, while the adjacent peaks numbered 2 both correspond to tetramer sodium salt ion, assigned the molecular formula $C_{32}H_{29}N_4O_8Na$. The corresponding proposed structures are presented in Figures 4-56 (f) and (g), respectively.

In Figure 4-55, peak 1 represents the protonated pentamer, and is assigned the

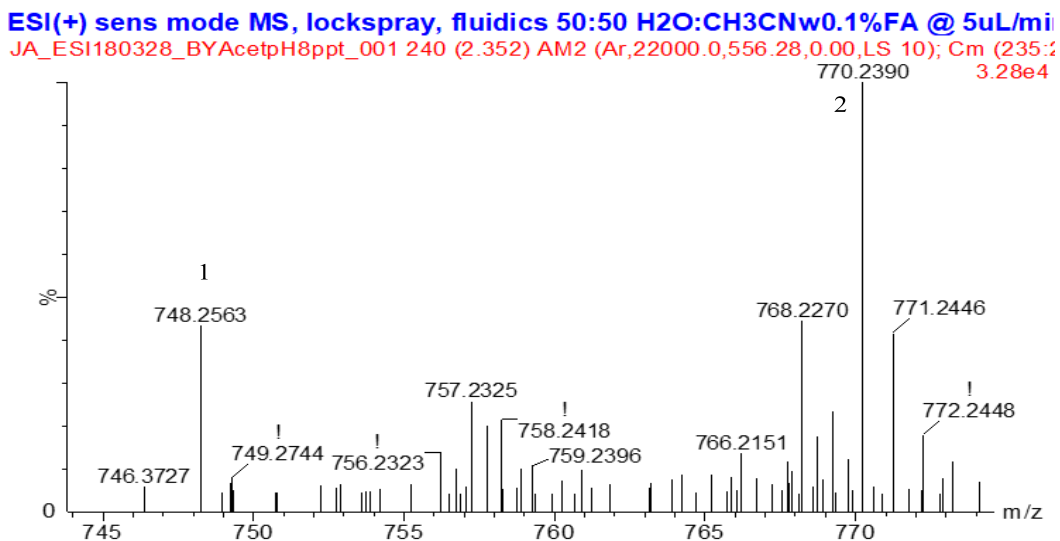


Fig. 4-55 ESI(+)-mass spectrum of acetaminophen precipitate under optimized conditions showing pentamer and its sodium salt

molecular formula $C_{40}H_{37}N_5O_{10}$. The peak labelled 2 corresponds to the protonated sodium-pentamer salt ion and is assigned the molecular formula $C_{40}H_{36}N_5O_{10}Na$. The proposed molecular structures for these peaks are shown in Figure 4-56 (h) and (i), respectively.

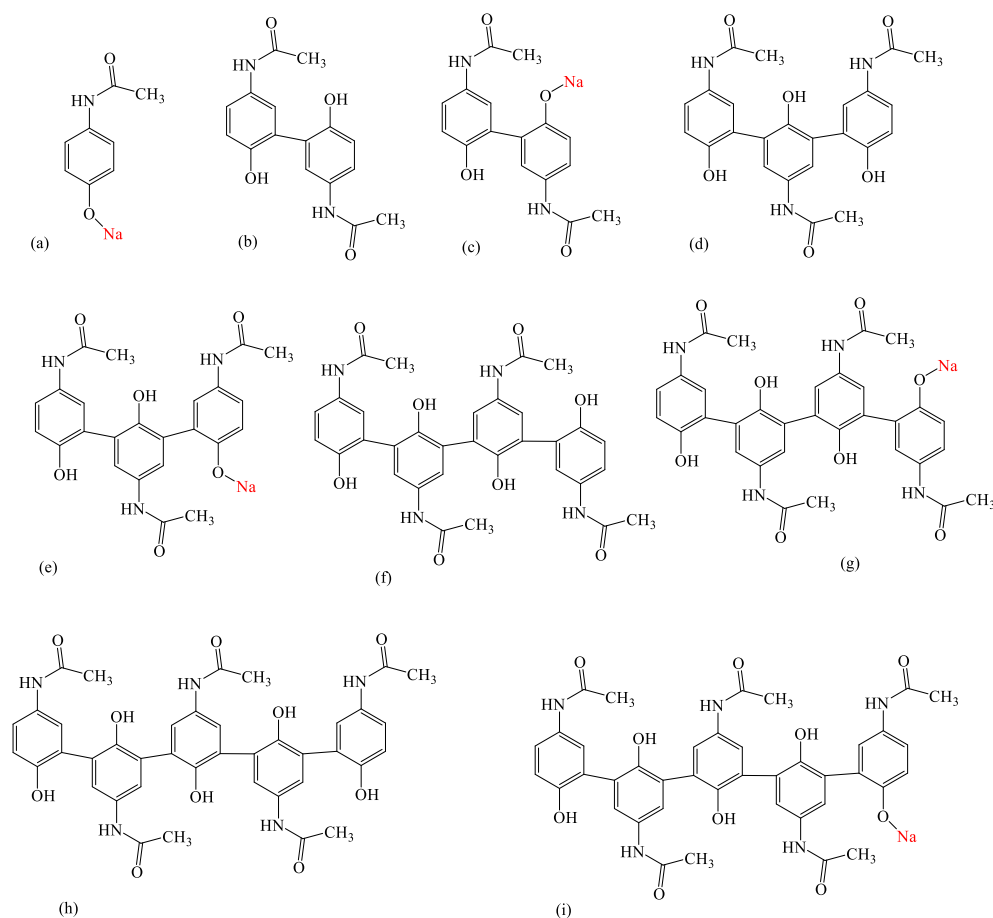


Fig.4-56 Proposed structures of acetaminophen modified monomer and oligomers formed following SBP treatment under optimized conditions.

4.6.2 Structural isomerism in acetaminophen oligomerization

The phenol oxidative coupling pattern advanced by Yu *et al.* (1994) supports the basic understanding of how an unpaired electron would resonate around the ring, as also supported by Ye & Schuler (1989). Thus, in terms of regiochemistry, the coupling products shown conform to the *ortho*-carbons as being the most likely points of connection (due to radical spin density delocalization), but the ring connections could also have been drawn as O-C couplings (indistinguishable by MS). However, the structural formulae of enzyme-generated acetaminophen oligomers as reported by others (Pylypchuk *et al.* 2018, Lu *et al.* 2009, Potter *et al.* 1985) have suggested (evidence discussed below) the involvement of other atoms in the ring, Figure 4-57, structure (a) is conventional, structure (c) is

unconventional in its involvement of amide-nitrogen, where an amide itself has nitrogen lone-pair electron density delocalized away from the ring and onto the carboxyl oxygen..

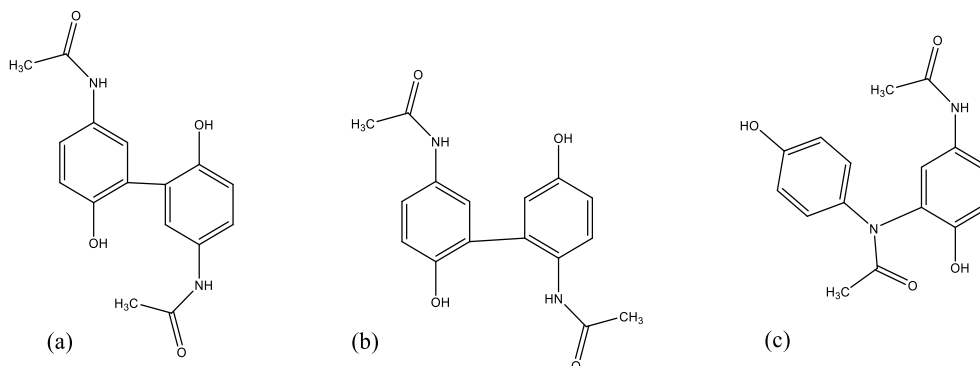


Fig.4-57 Oxidative coupling pattern of acetaminophen molecules under enzyme catalyzed reactions. (a) *o-o'* - diacetaminophen, (b) *o-m'* diacetaminophen and (c) *o-N* diacetaminophen

Porter *et al.* (1985) extensively reported on the methodologies employed in elucidating the structural formulae of these isomers. In their report, Lu *et al.* (2009) employed semiempirical calculations to determine the spin density ($e/\text{\AA}^3$) and charge density ($e/\text{\AA}^3$) to illustrate the tentative coupling pattern an acetaminophen radical would undertake, as reproduced in (Figure 4-58).

Figure 4-58 shows the chemical structure of an acetaminophen radical with atom numbering. The benzene ring carbons are numbered 1 to 6, the nitrogen is 7, the carbonyl carbon is 8, and the hydroxyl oxygen is labeled 'Hydroxyl O'. The carbonyl oxygen is labeled 'Carbonyl O'.

element	charge density ($e/\text{\AA}^3$)	Spin density ($e/\text{\AA}^3$)
N	-0.205	0.340
C1	0.139	0.051
C2	-0.128	0.230
C3	-0.080	-0.193
C4	0.135	0.398
C5	-0.149	-0.201
C6	-0.104	0.278
C7	0.300	0.058
C8	-0.246	0.001
Hydroxyl O	-0.163	0.199
Carbonyl O	-0.207	0.066

Fig.4-58 Semiempirical calculations of the distribution of spin and charge densities in an acetaminophen radical. Minor differences between values of C3 and C5, C2 and C6 are due to asymmetry of this particular molecular configuration. These pairs of carbon atoms are equivalent microscopically with mixtures of configurations (Source: Lu *et al.* 2009)

Based on these results, Lu *et al.* (2009) concluded:

- the single electron is most likely to be distributed on the carbon atoms of the benzene ring, the hydroxyl oxygen and the nitrogen atoms.

- b. Considering both charge and spin, the unsubstituted C-atoms (at 2,3,5,6) hold greater prospects for coupling, while the oxygen of OH and N of amido group may also be able to partake in coupling, according to radical coupling mechanism,
- c. All the possible coupling sites are partially negatively charged with O and N having the highest, and high charge density makes it kinetically less favorable for an incoming atom,
- d. Since C3 possess the lowest charge, it may be the most probable site for two acetaminophen radicals to couple forming a 3-3' coupling species. However, this does not exclude the possibility of bond formation at other potential sites.

These arguments account for the most often oxidative coupling observed between *o,o'*-coupling observed in acetaminophen oligomers. Being oxidative coupling, two hydrogen atoms are lost one from each of the participating monomers. Mass spectroscopy cannot distinguish among isomers. Lu *et al.* (2009) used HPLC/MS to separate the *o-*, *m'* dimers from the *o-*, *o'* ones, coupled ones, due to their differential retention times in a reverse-phase column. From chromatogram analysis based on peak height, the former may constitute about 5% of the total dimers formed in the reaction mixture. This illustrates kinetically favorable condition(s) towards *o-o'*-coupling over the *o-m'*. The *o-N'* coupling product was estimated at 1% of total products formed (Pylypchuk *et al.* 2018, Lu *et al.* 2009).

Since most of the oxidative coupling is *o-o'*-, this report has adopted it as the conventional coupling pattern and all proposed structural formulae of oligomers are represented in this manner. The reader is however informed that other coupling patterns for oligomers of the treated CECs are possible. Determining the exact molecular formula was not an objective in this study, hence the proposed structures may not be exact if subsequent structural formula analysis (by NMR, for example) showing regioselectivity of the coupling groups are conducted on the molecules.

Based on the oligomers observed in the MS analysis, a mechanism for SBP-catalyzed oligomerization for the formation of each identified oligomer has been proposed (Figure 6-59).

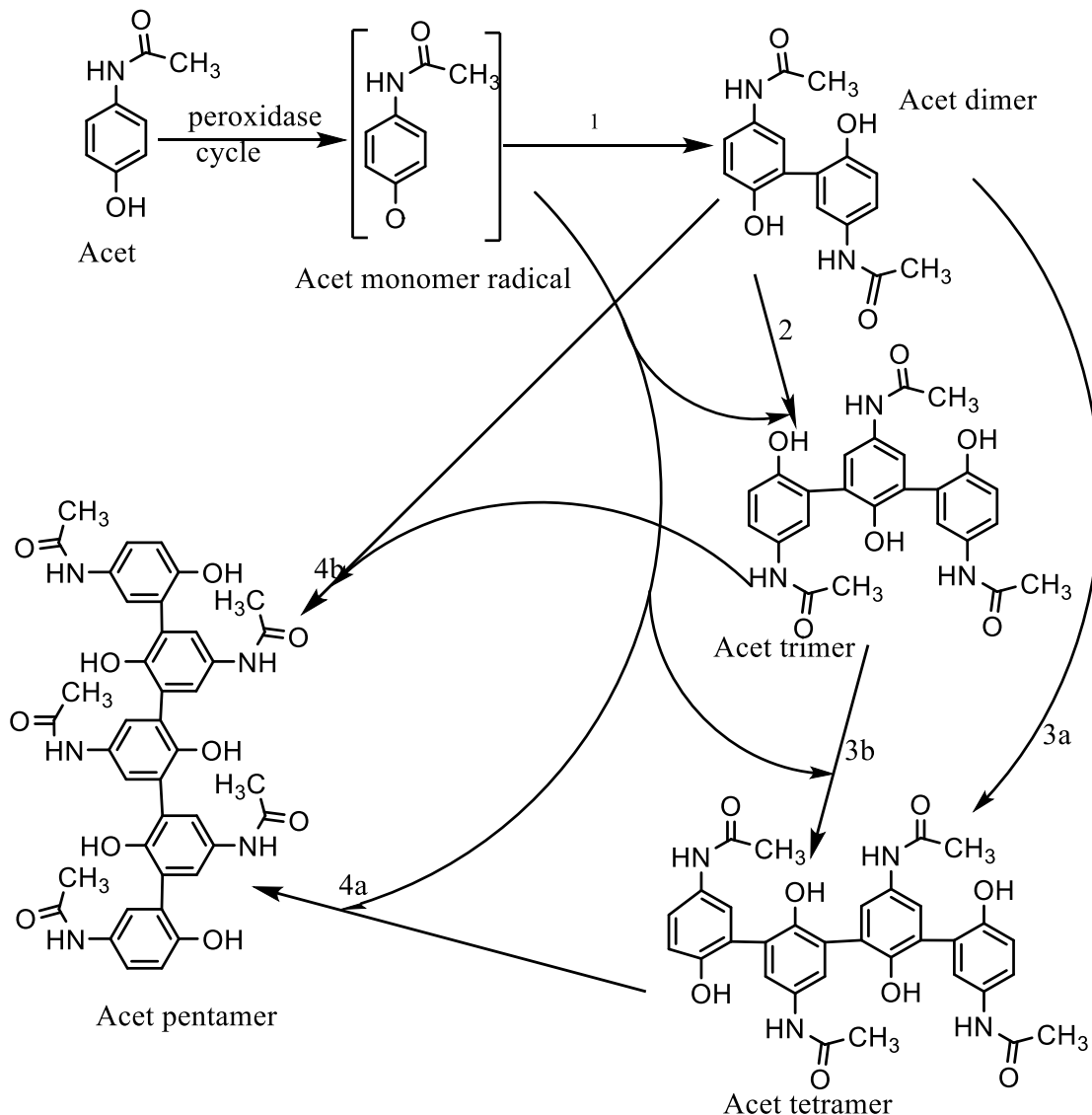


Fig. 4-59 Proposed mechanism of SBP-catalyzed oligomerization of acetaminophen. Numbers indicate the oxidative coupling route for the formation of the oligomers.

Above mass spectral analysis illustrated the oligomers formed both in precipitate and supernatant. As seen, there were not large differences, thus, following from here, and unless otherwise stated, either of these phases' products will be shown, depending on which phase exhibited the highest degree of oligomerization, or which oligomer formed showed the least deviation from the theoretically derived m/z peak value. In anticipation of the mixture studies and the need to minimize sample preparation yet obtain good analytical mass spectra and more hydrophobic oligomers due to the higher K_{ow} of the parabens

relative to acetaminophen, there was a switch in ionization source from ESI to ASAP, beginning with PHBA.

4.6.3 Mass spectral analysis of PHBA

Mass spectra of PHBA in the enzymatic reaction supernatant are shown in Figures 4-64 and 4-65. No oligomer was observed in the fine precipitate collected following centrifugation. The residual monomer peak is labelled 1 in Figure 4-60. The

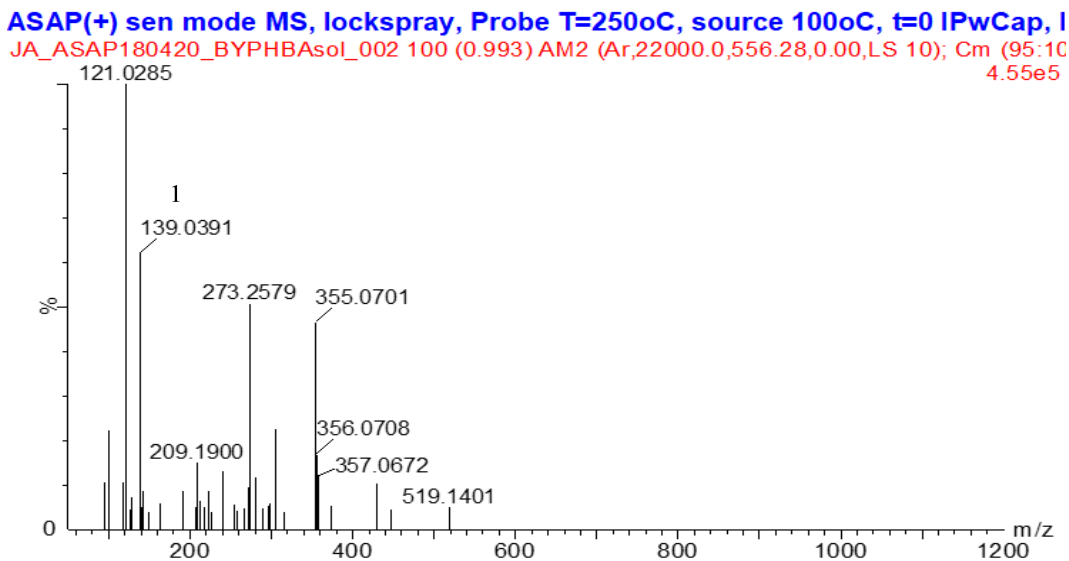


Fig. 4-60 ASAP(+)

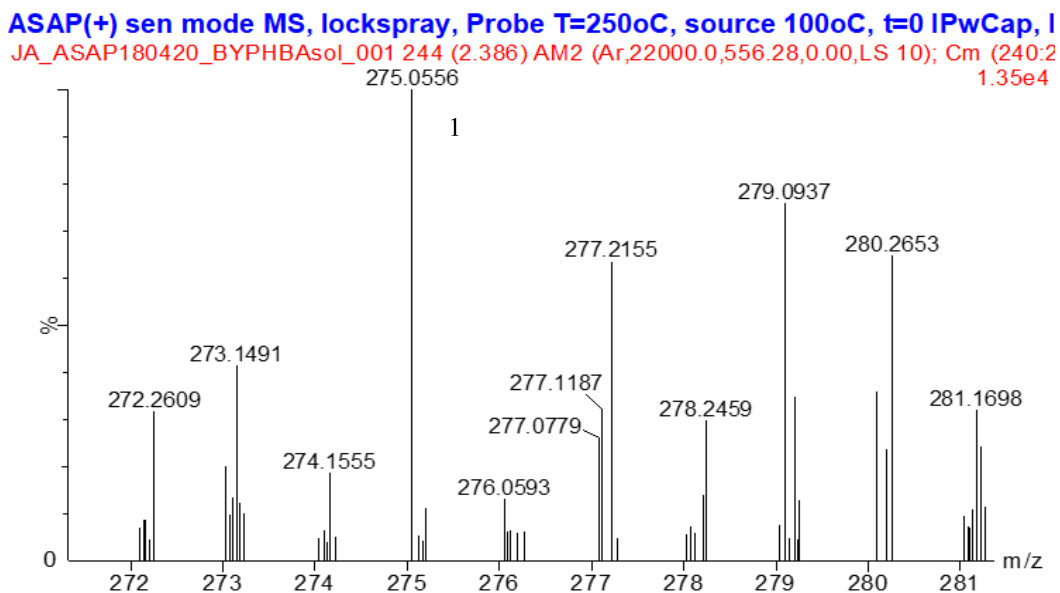


Fig. 4-61 ASAP(+)

protonated dimer is shown labelled 1 (Figure 4-61) and assigned the molecular formula $C_{14}H_{10}O_6$. A summary of the oligomer formed is presented in Table 4-7.

Table 4-7 PHBA and dimer following SBP treatment as observed from supernatant using ASAP(+)

Molecular formula	M⁺_{theo}	M⁺_{expt}	Ppm
$C_7H_6O_3$	139.0395	139.0391	-2.9
$C_{14}H_{10}O_6$	275.0556	275.0556	0.0

The proposed molecular structure is presented in Fig.4-62. Computational studies on the nature of PHBA shows the carboxylate moiety on the benzene ring exerts an electron withdrawing effect on the ring thereby reducing the spin densities on the prospective bonding carbon atoms (Xu *et al.* 1995). This may relate to the poor oligomerization capacity of PHBA, as observed from the mass spectra analysis.

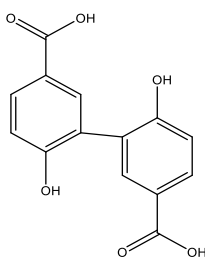


Fig. 4-62 proposed structure of PHBA dimer formed under optimized conditions

4.6.4 Mass spectral analysis of parabens – methyl paraben

Mass spectrometry analysis of parabens was done using the atmospheric solids analysis probe (ASAP) in the negative ionization mode, ASAP(-). Since much polyphenolic precipitates were formed, it was reasoned the use of ASAP may be advantageous in examining the precipitates. MS data acquisition in this technique presents all m/z peaks as

deprotonated peaks. Golmes *et al.* (2018b) also used negative ionization mode to acquire mass spectral data for parabens. The mass spectrum of the standard is shown in Figure 4-63 where the m/z peak at 151.0394 corresponds to the monomer. The mass spectrum is devoid of other background peaks, which was not the case with acetaminophen. This could be due to the level of purity of the standard used (section 3.0).

ASAP(-) sen mode MS, lockspray, Probe T=300oC, source 100oC, t=
JA_ASAPneg190911_BYMPstd_002 98 (0.976) AM2 (Ar,22000.0,554.26,0.00,LS 1
3.21e4

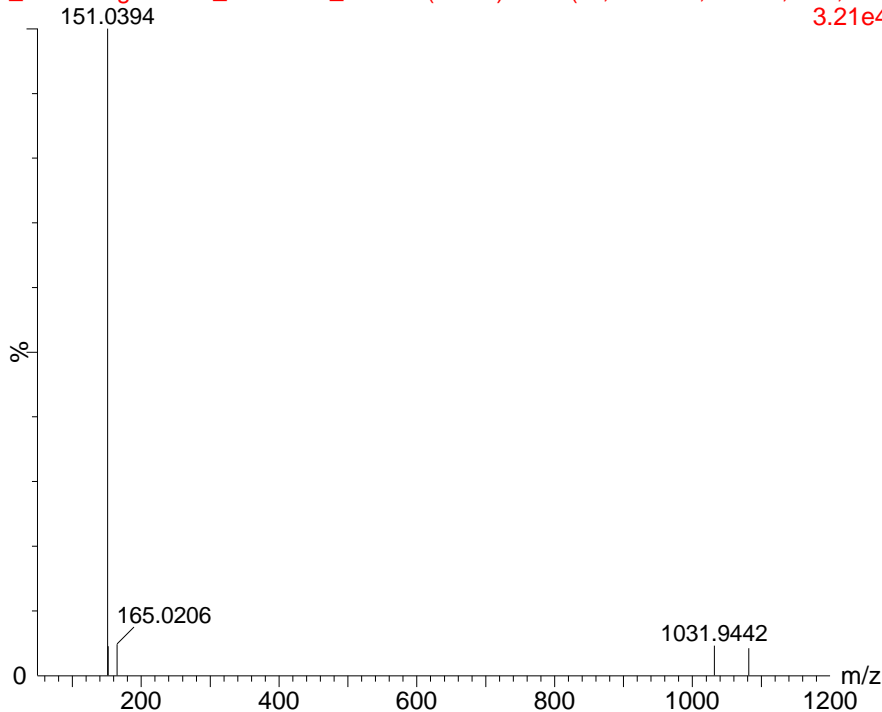


Fig. 4-63 ASAP(-) full scan mass spectrum of MP

The spectrum shown in Figure 4-64 represents the oligomerized products formed following MP treatment. The Arabic numerals denote the presence of possible oligomer m/z peaks. Peaks 5-7 are visible only at expanded scale. The monomer and oligomers of MP as detected from the precipitate are presented in Table 4-8. Detailed mass spectral results are highlighted in Figures 4-65 to 4-71. Oligomers observed in supernatant were dimers, trimers, tetramers and pentamers and their mass spectra are presented in Appendix F. The proposed structural formulae are similar to those shown for products found in precipitates as illustrated in Figure 4-72.

Table 4-8 MP and oligomers following SBP treatment as observed from precipitate using ASAP(-)

Molecular formula	M^r_{theo}	M^r_{expt}	ppm
C ₈ H ₈ O ₃	151.0395	151.0394	-0.7
C ₈ H ₈ O ₃	151.0395	151.0392	-2.0
C ₁₆ H ₁₄ O ₆	301.0712	301.0714	0.7
C ₁₆ H ₁₃ O ₇	316.0583	316.059	2.2
C ₂₄ H ₂₀ O ₉	451.1029	451.1002	-6.0
C ₂₄ H ₁₉ O ₁₀	466.09	466.0887	-2.8
C ₃₂ H ₂₆ O ₁₂	601.1346	601.1312	-5.7
C ₃₂ H ₂₅ O ₁₃	616.1217	616.1217	0.0
C ₄₀ H ₃₂ O ₁₅	751.1663	751.1622	-5.5
C ₄₀ H ₃₁ O ₁₆	766.1534	766.1534	0.0
C ₄₈ H ₃₈ O ₁₈	901.1980	901.1924	-6.2
C ₄₈ H ₃₇ O ₁₉	916.1851	916.1862	1.2
C ₅₆ H ₄₆ O ₂₁	1051.2297	1051.2286	-1.3
C ₅₆ H ₄₅ O ₂₂	1068.2324	1068.2369	4.2

The monomer peak numbered 1 in Figure 4-64 appears at m/z 151.0392. There is no evidence of a modification of the monomer. This contrasts with acetaminophen where a sodium salt of the monomer was observed in the supernatant, however it agrees with PHBA where no modification of the monomer was observed. A possible modification could have been oxygenation, which is observed in the oligomers of all the parabens. An oxidized oxygenated monomer would have a theoretical m/z value of 168.0423. The m/z peak observed at 168.0343 (too short to relative peaks to be seen in the mass spectrum) shows a deviation of 47.6 ppm, which is out of accuracy limits.

ASAP(-) sen mode MS, lockspray, Probe T=300oC, source 100oC, t=0 IPw
 JA_ASAPneg190911_BYMPppt_001 168 (1.655) AM2 (Ar,22000.0,554.26,0.00,LS 10);
 2.00e6

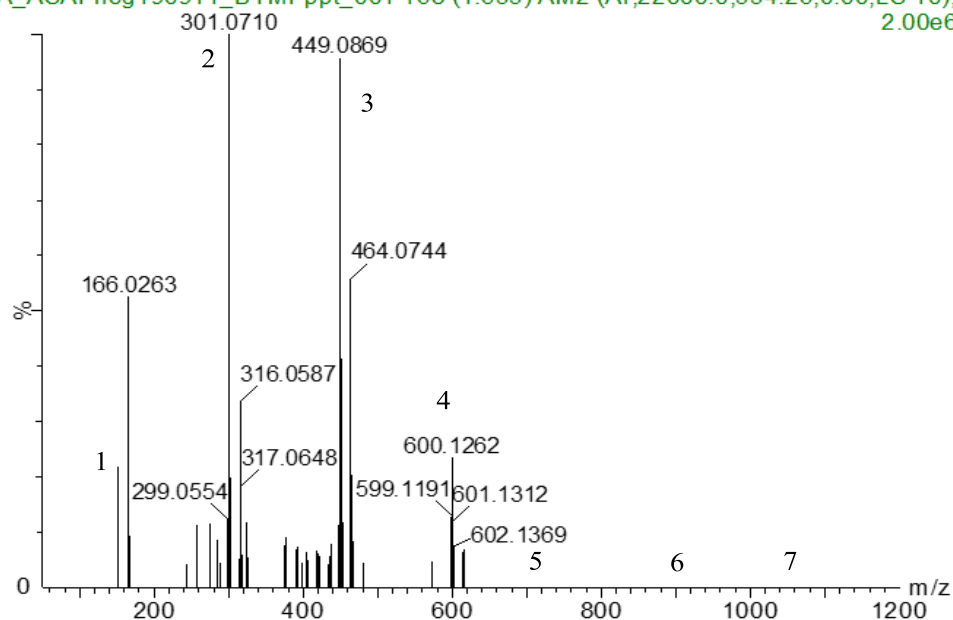


Fig. 4-64 ASAP(-) full scan mass spectrum of MP precipitate at the optimized conditions. Numbers indicate possible oligomer peaks, shown in expanded view between Fig.4-65 and 4-71

ASAP(-) sen mode MS, lockspray, Probe T=300oC, source 100oC, t=0 IPwCap, E
 JA_ASAPneg190911_BYMPppt_001 253 (2.483) AM2 (Ar,22000.0,554.26,0.00,LS 10); Cm (253:
 166.0265 2.06e6

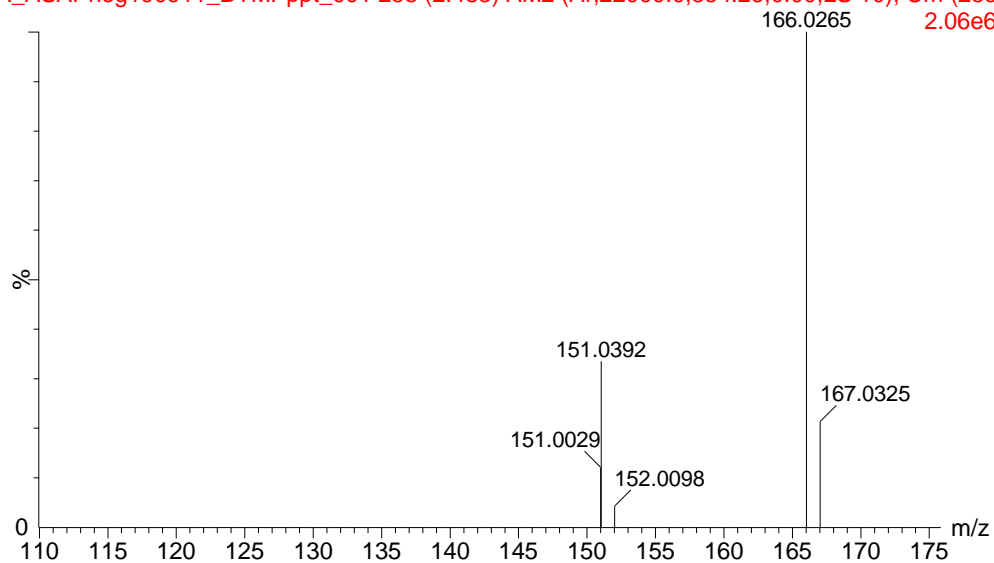


Fig. 4-65 ASAP(-) mass spectrum of MP precipitate between 110 and 175 m/z

The dimer of MP as found in the precipitate is shown in Figure 4-66. The peak at m/z 301.0714 corresponds to a deprotonated dimer and was assigned a molecular formula $C_{16}H_{14}O_6$. A peak was observed at m/z 316.0590 and close analysis suggests it may be an oxygenated product of the dimer. This was assigned a molecular formula of $C_{16}H_{13}O_7$. The tentative structural formulae of these dimers are shown in Figure 4-72 (a) and (b), respectively.

ASAP(-) sen mode MS, lockspray, Probe T=300oC, source 100oC, t=0 IPwCap, E
JA_ASAPneg190911_BYMPppt_001 253 (2.483) AM2 (Ar,22000.0,554.26,0.00,LS 10); Cm (253:

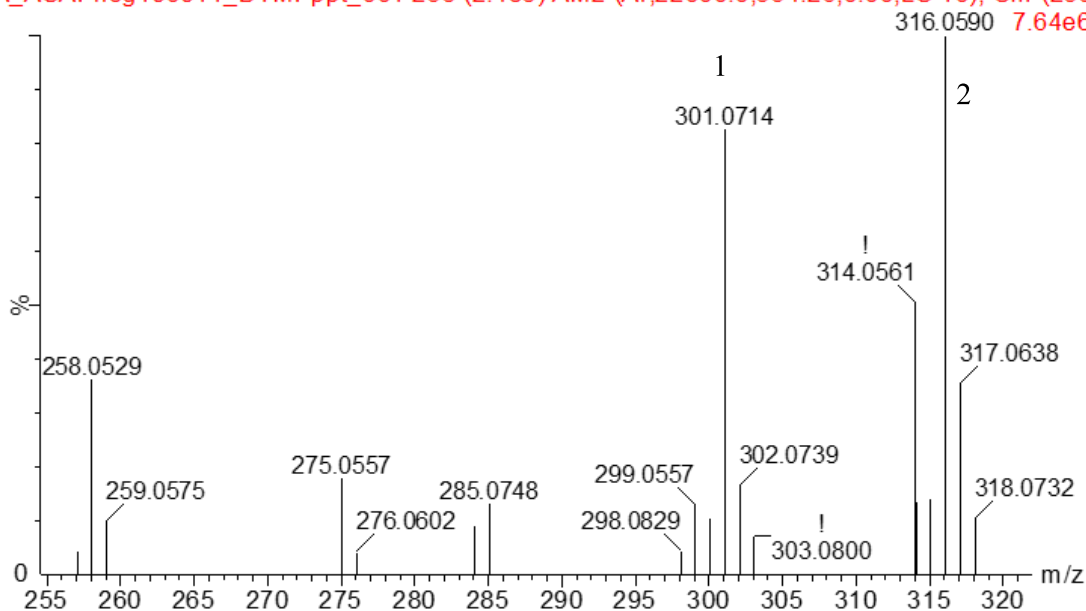


Fig. 4-66 ASAP(-) mass spectrum of MP precipitate at the optimized conditions showing dimer and oxygenated dimer

The peak at m/z 451.1002 (Figure 4-67) corresponds to a trimer and was assigned the molecular formula $C_{24}H_{20}O_9$. The m/z peak at 466.0887 is thought to be an oxygenated trimer product and was assigned a molecular formula of $C_{24}H_{19}O_{10}$. The suggested structural formulae for these trimers are illustrated in Figure 4-72 (c) and (d). Peaks with very strong ionization intensity appear at m/z 450.0916 and 449.0894, 1 and 2 amu just before the oligomer peak. Peaks of strong intensity preceding the oligomer peaks have been observed also from subsequent mass spectra. These are thought to be oxidized oxidative oligomers. Mashhadi (2019) also reported on the presence of oxidized oxidative oligomers from analysis of aryl compounds using ASAP. The occurrence of oxidative reactions in

techniques such as electrospray ionization or direct analysis in real time are common but have also been reported from the use of ASAP analysis (Madarshahian *et al.* 2017).

ASAP(-) sen mode MS, lockspray, Probe T=300oC, source 100oC, t=0 IPwCap, E
 JA_ASAPneg190911_BYMPppt_001 253 (2.483) AM2 (Ar,22000.0,554.26,0.00,LS 10); Cm (253:
 2.30e7

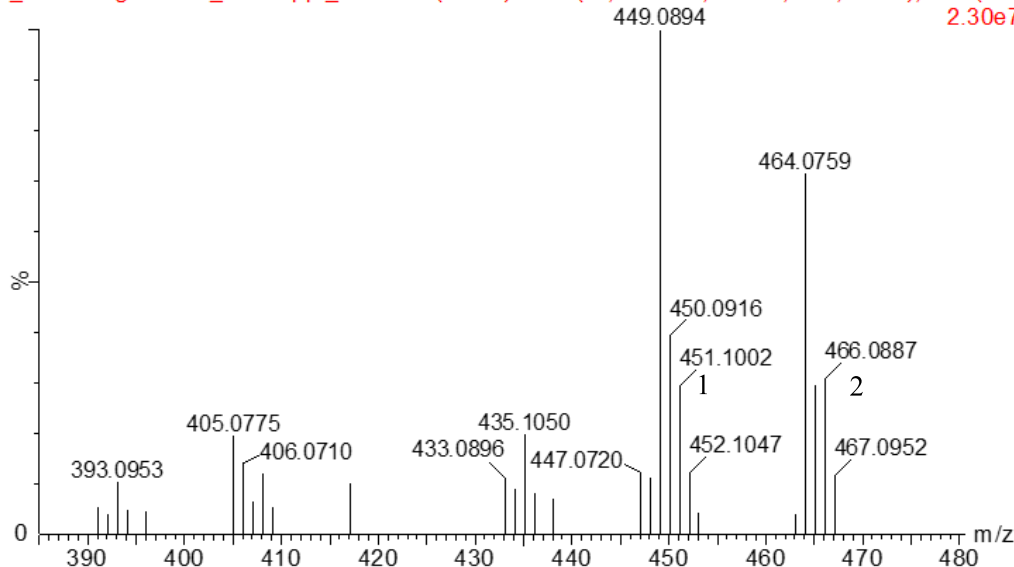


Fig. 4-67 ASAP(-) mass spectrum of MP precipitate under the optimized conditions showing trimer and oxygenated trimer

Figure 4-68 shows a deprotonated m/z peak at 601.1312 which corresponds to a tetramer and was assigned the molecular formula $C_{32}H_{26}O_{12}$. Another m/z peak observed at 616.1217 corresponds to an oxygenated tetramer product, whose molecular formula was assigned to be $C_{32}H_{25}O_{13}$. The tentative structural formulae for these tetramers are illustrated in Figure 4-72 (e) and (f), respectively. Further analysis of the mass spectrum showed evidence for a pentamer at m/z 751.1622 (Figure 4-69) and was assigned the molecular formula $C_{40}H_{32}O_{15}$. Another m/z peak thought to be an oxygenated derivative of the pentamer was observed

ASAP(-) sen mode MS, lockspray, Probe T=300oC, source 100oC, t=0 IPwC

JA_ASAPneg190911_BYMPppt_001 253 (2.483) AM2 (Ar,22000.0,554.26,0.00,LS 10); Cn 1.31e7

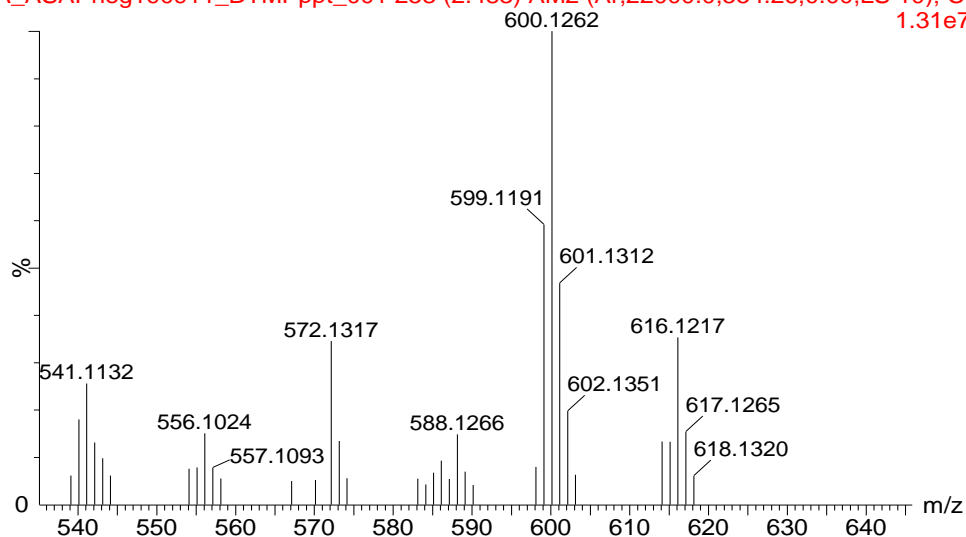


Fig. 4-68 ASAP(-) mass spectrum of MP precipitate at the optimized conditions showing tetramer and oxygenated tetramer

at m/z 766.1534 and was assigned the molecular formula $C_{40}H_{31}O_{16}$. Proposed structural formulae for these oligomers are as presented in Figure 4-72 (g) and (h),

ASAP(-) sen mode MS, lockspray, Probe T=300oC, source 100oC, t=0 IPwC

JA_ASAPneg190911_BYMPppt_001 253 (2.483) AM2 (Ar,22000.0,554.26,0.00,LS 10); Cn 1.53e6

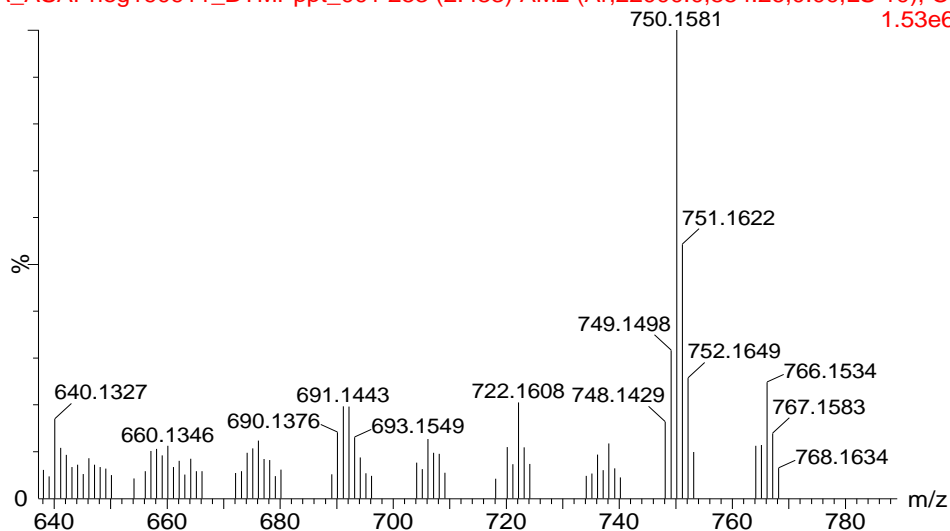


Fig. 4-69 ASAP(-) mass spectrum of MP precipitate at the optimized conditions showing pentamer and oxygenated pentamer

respectively. In Figure 4-70, m/z peak was observed at 901.1924. This is consistent with a MP hexamer and was assigned the molecular formula $C_{48}H_{38}O_{18}$. Its oxygenated derivative was observed to present m/z peak at 916.1862 and was allotted a molecular formula of $C_{48}H_{37}O_{19}$. These products are proposed to take the structural formulae represented in Figure 4-72 (i) and (j), respectively. The

ASAP(-) sen mode MS, lockspray, Probe T=300oC, source 100oC, t=0 IPwC
 JA_ASAPneg190911_BYMPppt_001 253 (2.483) AM2 (Ar,22000.0,554.26,0.00,LS 10); Cr
 8.18e4

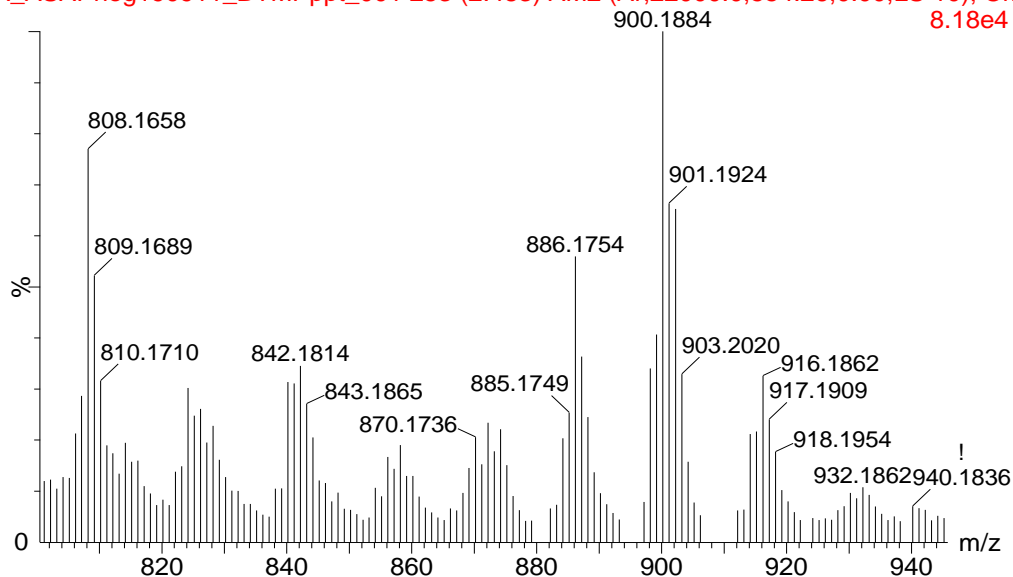


Fig. 4-70 ASAP(-) mass spectrum of MP precipitate under optimized conditions showing hexamer and a oxygenated hexamer

largest molecular weight oligomer observed in MP precipitate was a heptamer having m/z peak 1051.2286 (Figure 4-71). A supposed oxygenated derivative of the heptamer appeared at m/z peak 1068.2339 (arrow in insert). These products respectively agree to the molecular formulae $C_{56}H_{46}O_{21}$ and $C_{56}H_{45}O_{22}$, respectively. Their proposed structures are presented in Figure 4-72 (k) and (l), respectively.

ASAP(-) sen mode MS, lockspray, Probe T=300oC, source 100oC
 JA_ASAPneg190911_BYMPppt_001 253 (2.483) AM2 (Ar,22000.0,554.26,0.00,LS 10); Cn
 2.47e4

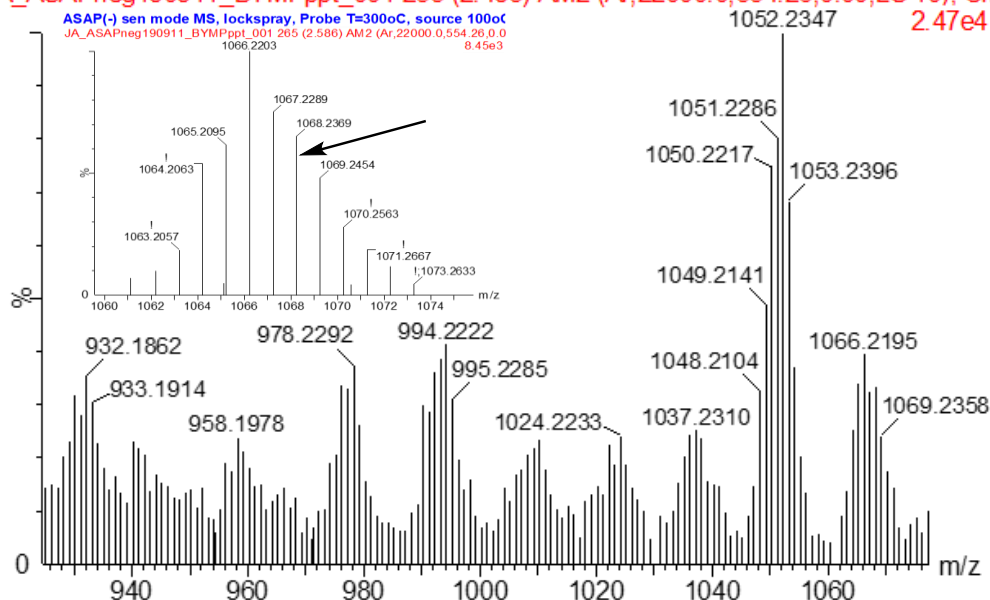


Fig. 4-71 ASAP(-) mass spectrum of MP precipitate under optimized conditions showing heptamer and oxygenated heptamer. Insert: oxygenated derivative of the heptamer.

Considering the octanol-water partition coefficient (Table 2.2), MP has lower aqueous solubility than acetaminophen and PHBA and an organic solvent composition of 1.25% was used in the reaction mixtures (section 3.1.2), the presence of which is thought to have facilitated the polyphenolic products to remain soluble enough to be accessed by the enzyme, hence the higher molecular weight oligomers obtained. Peroxidase-catalyzed oligomerization of aromatic substrates has been reported to produce oxygenated (Mashhadi 2019) and hydroxylated products (Ullrich and Hofrichter 2007). Verloop *et al.* (2016) reported hydroxylation of tea catechins is catalyzed by peroxidases, when HRP was used as a model peroxidase. Different carbon atoms in the molecules could be oxygenated in a manner dependent upon the concentration of peroxide in the reaction mixture. The exact mechanism of peroxidase catalyzed hydroxylation of phenolics is unclear. However, it is thought to share a similar mechanism with peroxygenases, since both employ heme group and peroxide as the oxidant (Verloop *et al.* 2016). Peroxygenases hydroxylate by transferring oxygen from peroxide onto the aromatic ring, following which an epoxide

intermediate is formed that spontaneously rearranges into a hydroxyl, doubling the functions of peroxide also as an oxygen donor (Klunge *et al.* 2009).

Although Verloop *et al.* (2016) demonstrated peroxidase-catalyzed hydroxylation of phenolics, Courteix and Bergel (1995) reported there is no experimental nor thermodynamic evidence linking the hydroxylation of phenolics with HRP. They suggested the production of hydroxyl radical may be associated with the peroxidase catalytic cycle, the radicals' attack on phenolics is entirely non-enzymatic. Evidence for the non-enzymatic hydroxylation is the lack of selectivity of the hydroxyl radical (Durliat *et al.* 1992). The mechanism of spontaneous parabens hydroxylation in the presence of hydroxyl radicals was proposed by Tay *et al.* (2010). The three-step process involves a hydroxyl radical attack on the paraben ring, which eventually displaces a hydrogen atom through an intermediate and then replaces it with hydroxyl group.

Gomes *et al.* (2018b) reported oxygenated derivatives of propyl- and butyl- parabens had lower retention times than the parent compounds on a C18 Symmetry column in LC-MS analysis, owing to the relatively decreased hydrophobicity of the oxygenated derivatives, although this was not investigated in the present study.

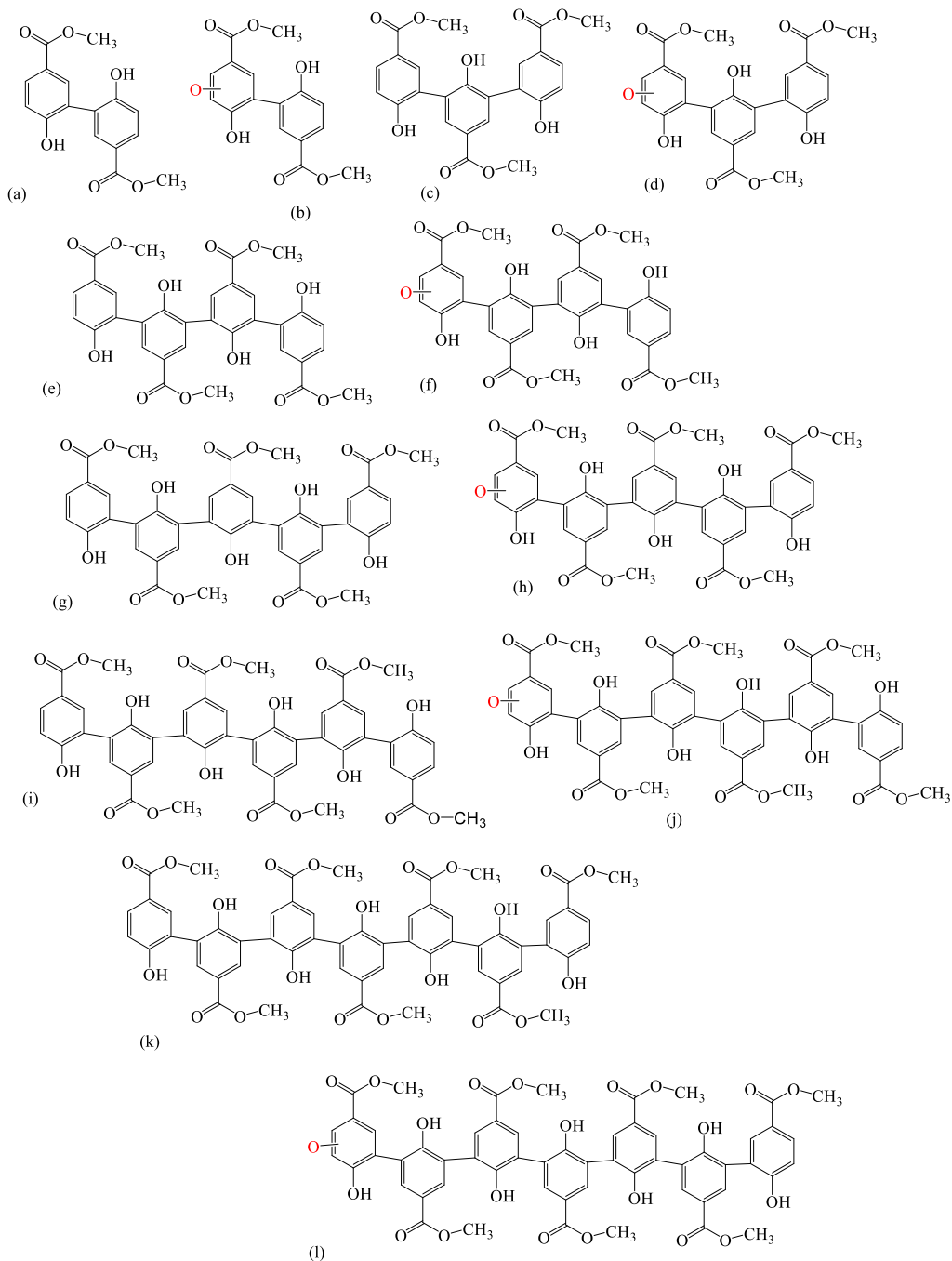


Fig. 4-72 proposed structures for the oligomers of MP found in precipitate under optimized conditions

4.6.5 Mass spectral analysis of PP

The full scan propyl paraben mass spectrum is presented in Figure 4-73. The deprotonated compound peak appears at m/z 179.0707. There is no evidence for a modified monomer, such as oxygenation. This is similar to the observations with MP and PHBA, but unlike

ASAP(-) sen mode MS, lockspray, Probe T=300oC, source 100oC, t=(
JA_ASAPneg190910_BYPPstd_001 102 (1.010) AM2 (Ar,22000.0,554.26,0.00,LS
3.26e4

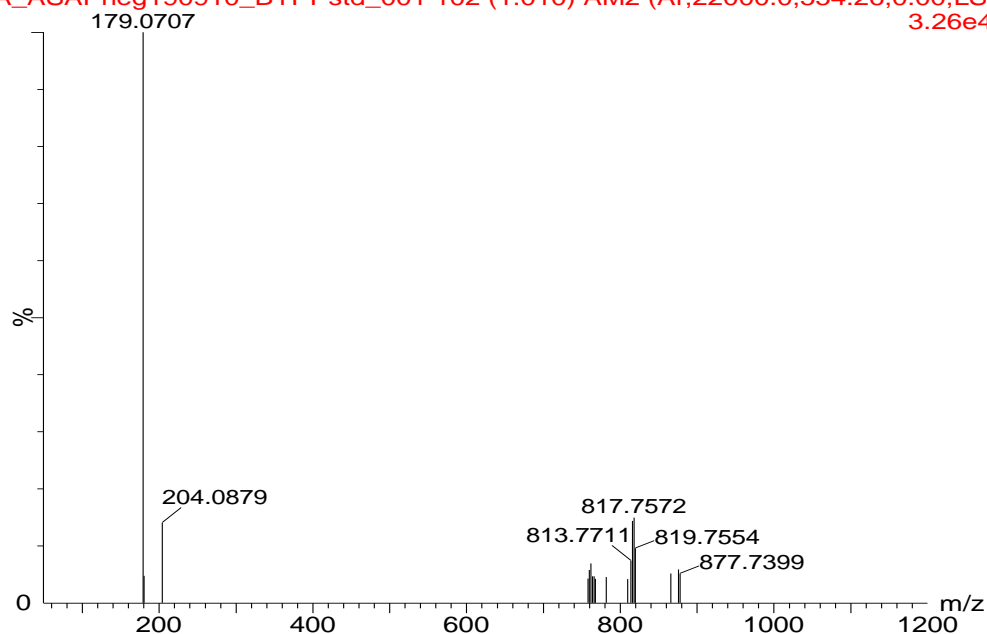


Fig. 4-73 ASAP(-) mass spectrum showing PP standard between 50 and 1200 m/z

acetaminophen. Considering the structural similarities between these compounds, this similar mass spectrum trend is expected. The mass spectra for the supernatant are placed in Appendix F and show oligomers of dimer, trimer and tetramer. There were oligomers in MP supernatant up to hexamers unlike in PP. The lower solubility of PP compared to MP may be responsible for greater hydrophobicity of PP oligomers, which makes oligomers to precipitate out of solutions, at the tetramer stage. Figure 4-74 shows the wide range mass spectrum of the precipitates. The m/z peaks for monomer and oligomers are numbered 1-7 (peaks 5-7 only seen on scale expansion). The exact m/z peaks as calculated are shown below (Figures 4-75 to 4-79). Residual monomer was also detected (not shown).

ASAP(-) sen mode MS, lockspray, Probe T=300oC, source 100oC, t=0 IPwCap, E
 JA_ASAPneg190911_BYPPppt_001 200 (1.969) AM2 (Ar,22000.0,554.26,0.00,LS 10); Cm (195:
 5.17e6

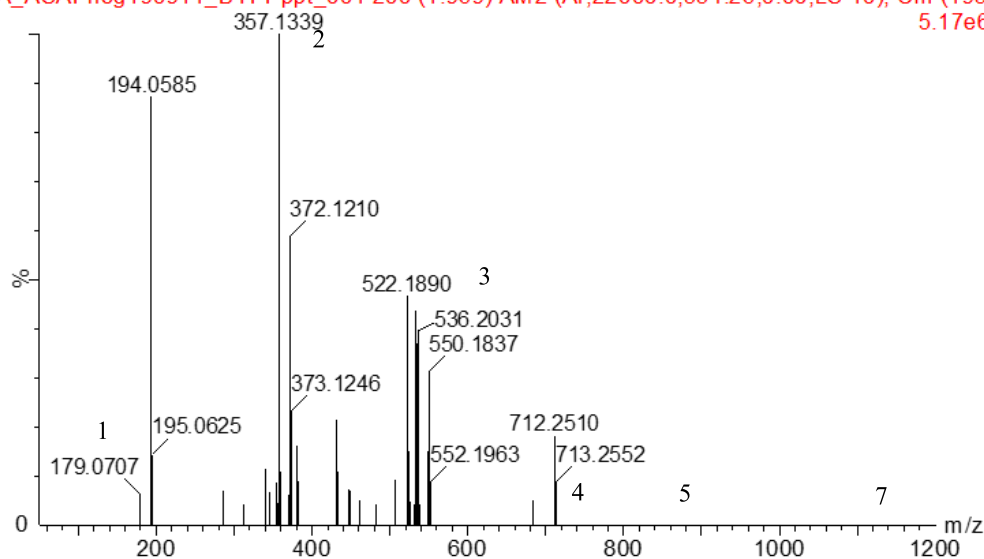


Fig.4-74 ASAP(-) mass spectrum showing PP precipitate

Detected oligomers labelled 1-7 (Figure 4-74) are summarized in Table 4-9.

Table 4-9 Showing PP and oligomers following SBP treatment as observed from precipitate and supernatant

Molecular formula	M_{theo}	M_{expt}	ppm
C ₁₀ H ₁₂ O ₃	179.0708	179.0707	-0.6
C ₁₀ H ₁₂ O ₃	179.0708	179.0707	-0.6
C ₂₀ H ₂₂ O ₆	357.1338	357.1339	0.3
C ₂₀ H ₂₁ O ₇	372.1209	372.121	0.3
C ₃₀ H ₃₂ O ₉	535.1968	535.1942	-4.9
C ₃₀ H ₃₁ O ₁₀	550.1839	550.1837	-0.4
C ₄₀ H ₄₂ O ₁₂	713.2598	713.2552	-6.4
C ₄₀ H ₄₁ O ₁₃	728.2469	728.2454	-2.1
C ₅₀ H ₅₂ O ₁₅	891.3228	891.3174	-6.1
C ₅₀ H ₅₁ O ₁₆	906.3099	906.3073	-2.9
C ₆₀ H ₆₂ O ₁₈	1069.3858	1069.3828	-2.8
C ₆₀ H ₆₁ O ₁₉	1084.3729	1084.38	6.5

The spectrum between 320 and 378 m/z is shown for the dimer of PP (Figure 4-75). The m/z peaks at 357.1339 and 372.1210 correspond to the deprotonated forms of the dimer and oxygenated dimer formulae $C_{20}H_{22}O_6$ and $C_{20}H_{21}O_7$, structures

ASAP(-) sen mode MS, lockspray, Probe T=300oC, source 100oC, t=0 IP

JA_ASAPneg190911_BYPPppt_001 200 (1.969) AM2 (Ar,22000.0,554.26,0.00,LS 10);
5.17e6

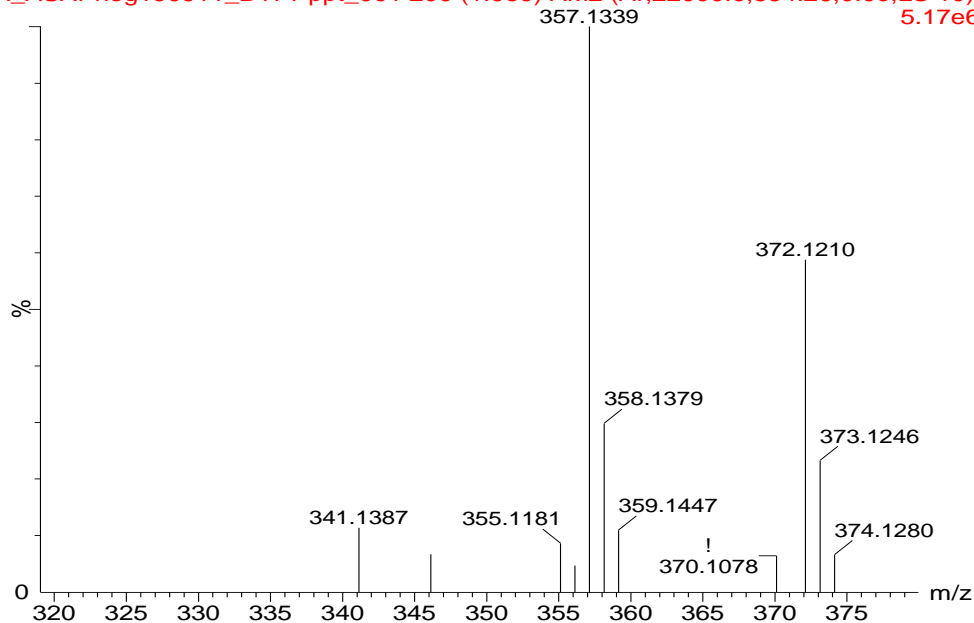


Fig.4-75 ASAP(-) mass spectrum of PP under optimized conditions showing dimer and oxygenated dimer

Figures 4-80 (a) and (b), respectively. Likewise, Figure 4-76 shows m/z peaks at 535.1942 and 550.1837, corresponding to deprotonated forms of trimer and oxygenated trimer of PP, formulae which $C_{30}H_{32}O_9$ and $C_{30}H_{31}O_{10}$, structures Figures 4-80 (c) and (d). Similarly, Figure 4-77 shows m/z peaks 713.2552 and 728.2454 evidence of the tetramer and oxygenated tetramer, formulae $C_{40}H_{42}O_{12}$ $C_{40}H_{41}O_{13}$, structures Figures 4-80 (e) and (f), respectively.

ASAP(-) sen mode MS, lockspray, Probe T=300oC, source 100oC, t=0 IP
JA_ASAPneg190911_BYPPppt_001 200 (1.969) AM2 (Ar,22000.0,554.26,0.00,LS 10);
2.42e6

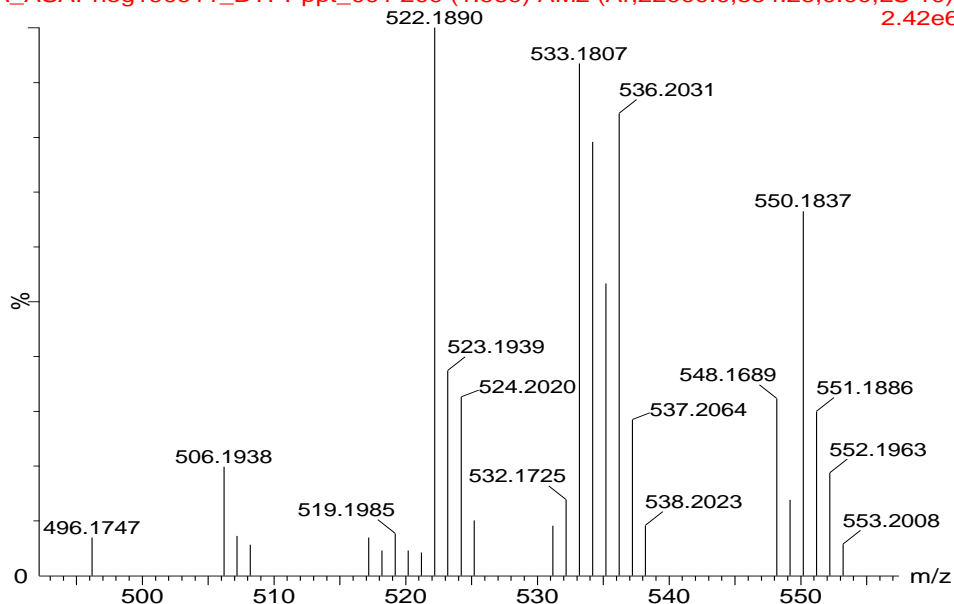


Fig. 4-76 ASAP(-) mass spectrum of PP precipitate under optimized conditions showing trimer and oxygenated trimer

ASAP(-) sen mode MS, lockspray, Probe T=300oC, source 100oC, t=0 IP
JA_ASAPneg190911_BYPPppt_001 200 (1.969) AM2 (Ar,22000.0,554.26,0.00,LS 10);
9.42e5

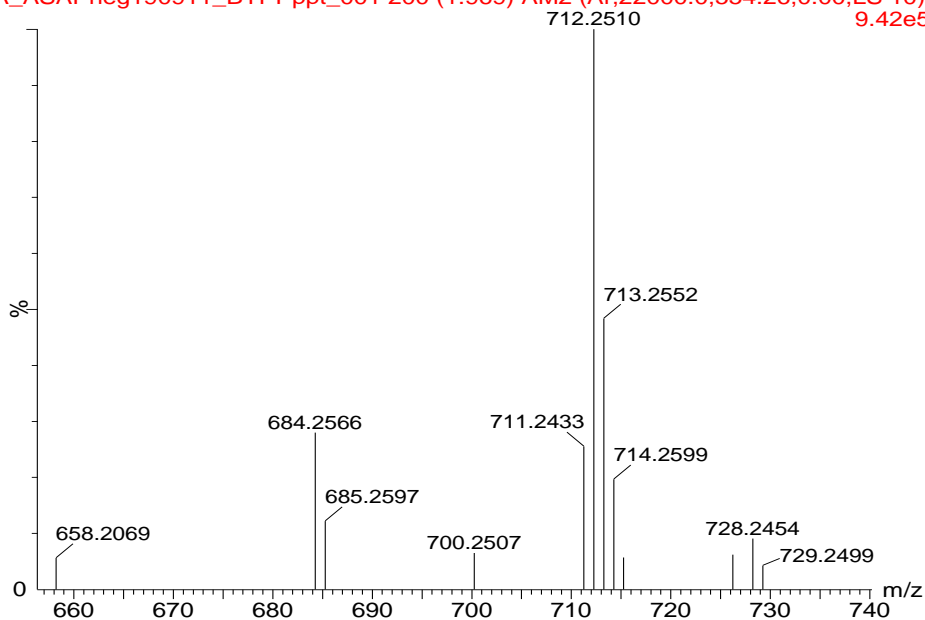


Fig. 4-77 ASAP(-) mass spectrum of PP precipitate under optimized conditions showing tetramer and oxygenated tetramer

Figure 4-78 show m/z peaks at 891.3174 and 906.3073 which corresponds PP pentamer and oxygenated pentamer $C_{50}H_{52}O_{15}$ and $C_{50}H_{51}O_{16}$, respectively with proposed structural formulae Figures 4-80 (g) and (h) respectively.

ASAP(-) sen mode MS, lockspray, Probe T=300oC, source 100oC, t=
JA_ASAPneg190911_BYPPppt_002 255 (2.500) AM2 (Ar,22000.0,554.26,0.00,LS
1.56e5

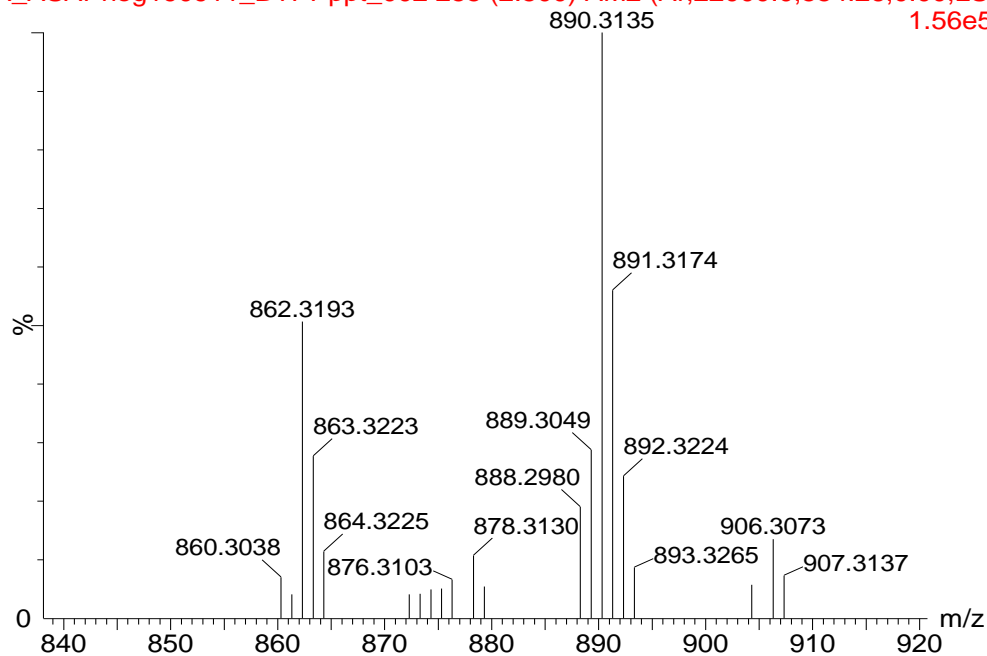


Fig. 4-78 ASAP(-) mass spectrum of PP precipitate under optimized conditions showing pentamer and oxygenated pentamer

Figure 4-79 show m/z peaks at 1069.3838 and 1084.3800 corresponding to the hexamer for PP with formulae $C_{60}H_{62}O_{16}$ and $C_{60}H_{61}O_{19}$, structures Figures 4-80 (i) and (j), respectively.

ASAP(-) sen mode MS, lockspray, Probe T=300oC, source 100oC, t=(
JA_ASAPneg190911_BYPPpt_001 223 (2.186) AM2 (Ar,22000.0,554.26,0.00,LS
5.84e3

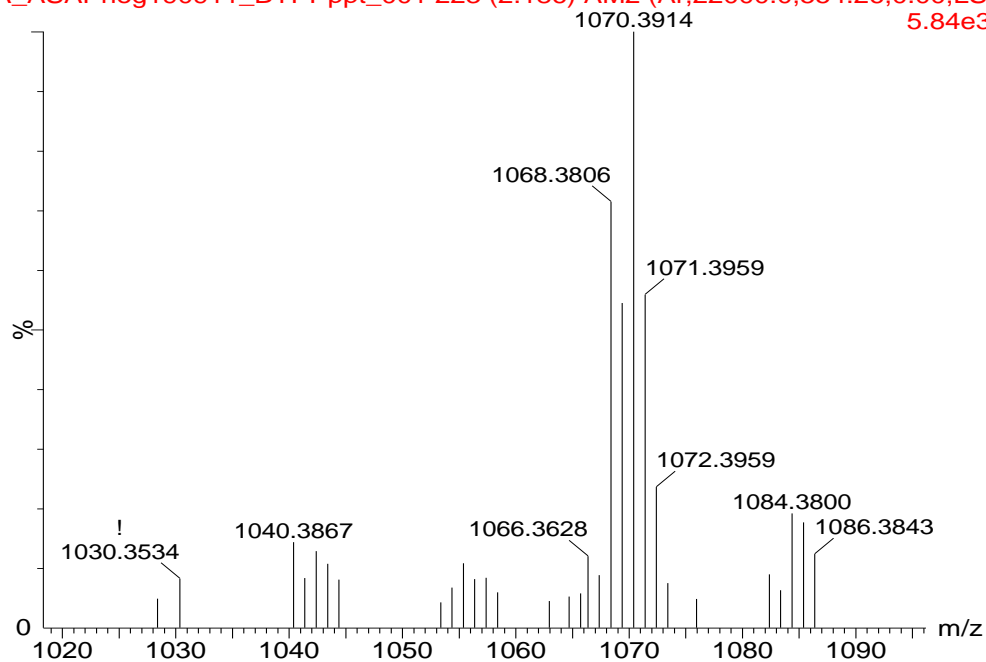


Fig. 4-79 ASAP(-) mass spectrum of PP precipitate under optimized conditions showing hexamer and oxygenated hexamer

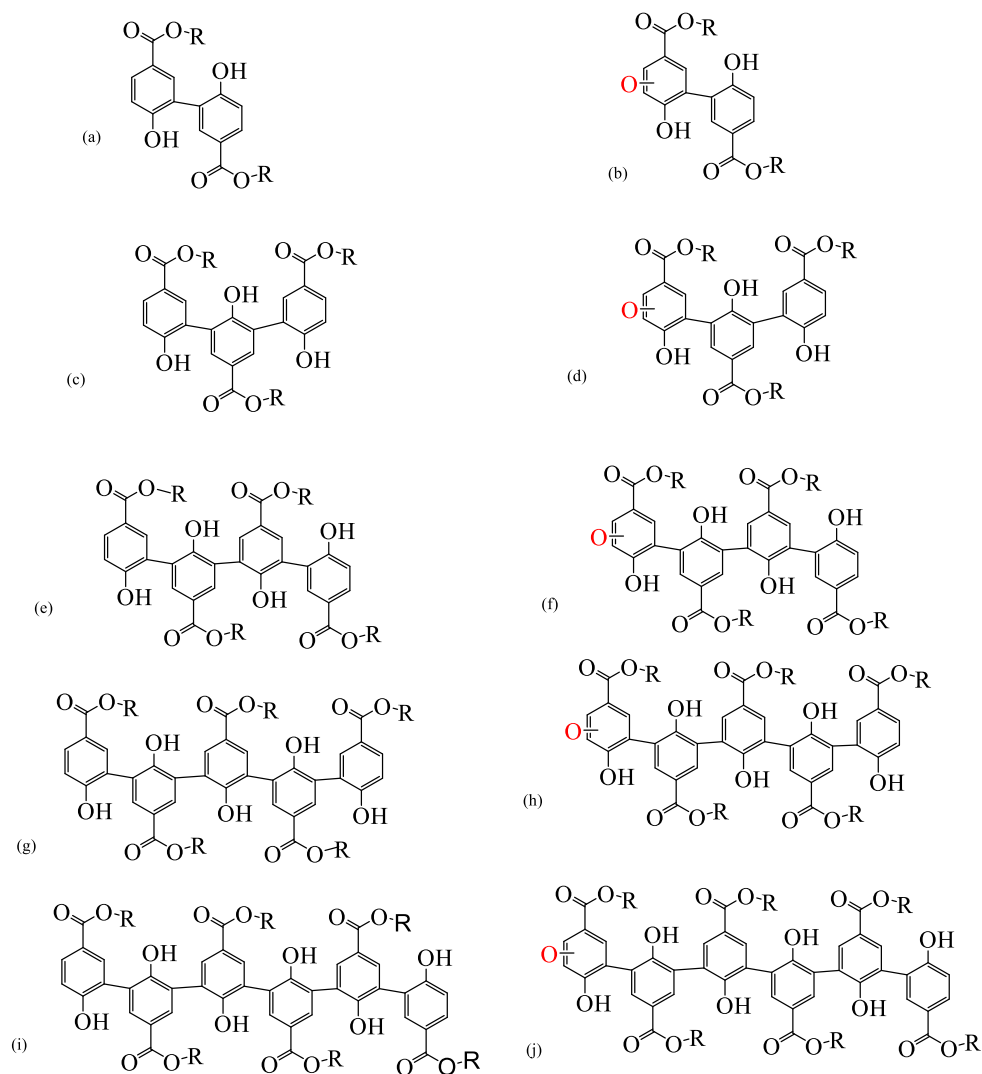


Fig.4-80 Proposed structures for oligomers of PP ($R = C_3H_7$)

4.6.6 Mass spectral analysis of butyl paraben

Butyl paraben was studied in ASAP(-) like the other parabens. Tay *et al.* (2018) also studied BP in negative ionization mode but employed a different ionization technique. Considering its high octanol-water partition coefficient ($\text{Log}K_{ow}$), and to maintain uniform initial concentration in the batch reactors to facilitate comparison of results between BP and previously reported parabens, BP batch reactors contained 5% (v/v) acetonitrile which does not pose any threat on enzyme activity, at this low concentration. This increased the solubility of the products formed. Mass spectral analysis conducted between 50 and 1500 m/z showed the supernatant contained oligomers up to heptamer (results for supernatant

are shown in Appendix F), similar to what was observed in the precipitate. The increase in acquisition m/z range in experimental samples over the standard was to cover the detected large oligomer molecular ions.

The full-scan mass spectrum for BP is shown in Figure 4-81. The monomer peak appears at m/z 193.0866. The spectrum of BP reaction precipitate under optimized

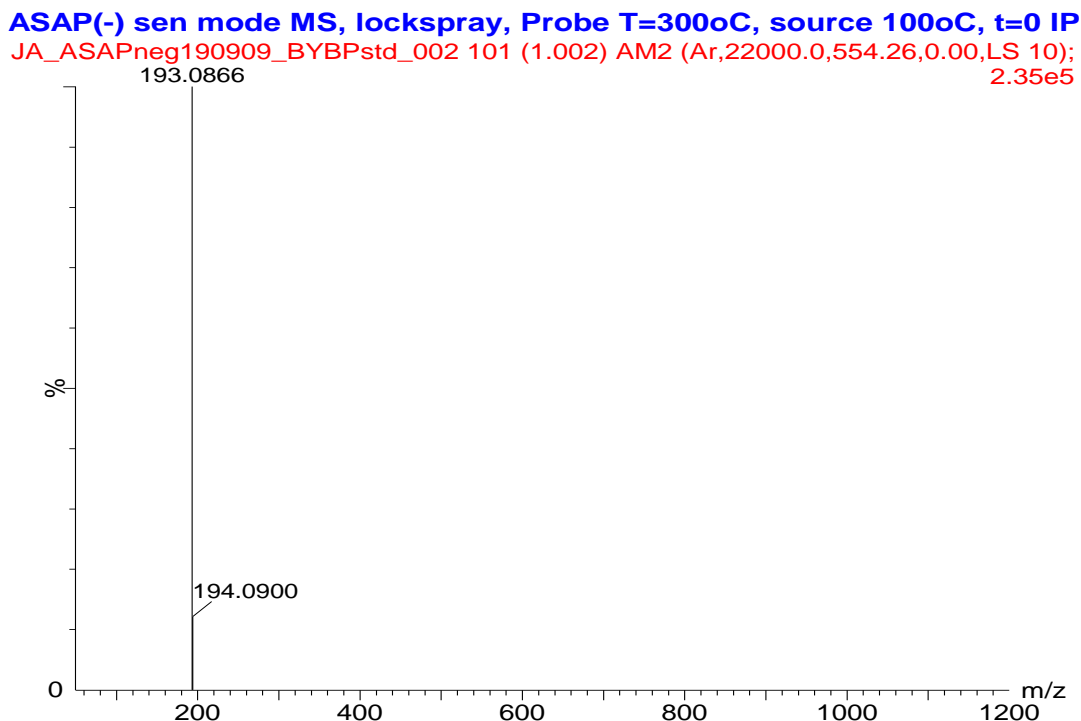


Fig. 4-81 ASAP(-) mass spectrum of BP

conditions are shown in Figure 4- 82. The numbered peaks represent possible m/z peaks of either monomer (1) or oligomerized products following SBP-catalyzed treatment. The detailed mass spectra for these products are shown in Figure 4-83/4-88. The identified peaks labelled 1-7 (Figure 4-82) are summarized in Table 4-10.

ASAP(-) sen mode MS, lockspray, Probe T=300oC, source 100oC, t=0 IPwCap, BY
 JA_ASAPneg190910_BYBPppt_004 272 (2.666) AM2 (Ar,22000.0,554.26,0.00,LS 10); ABS; Cm (2
 5.65e6

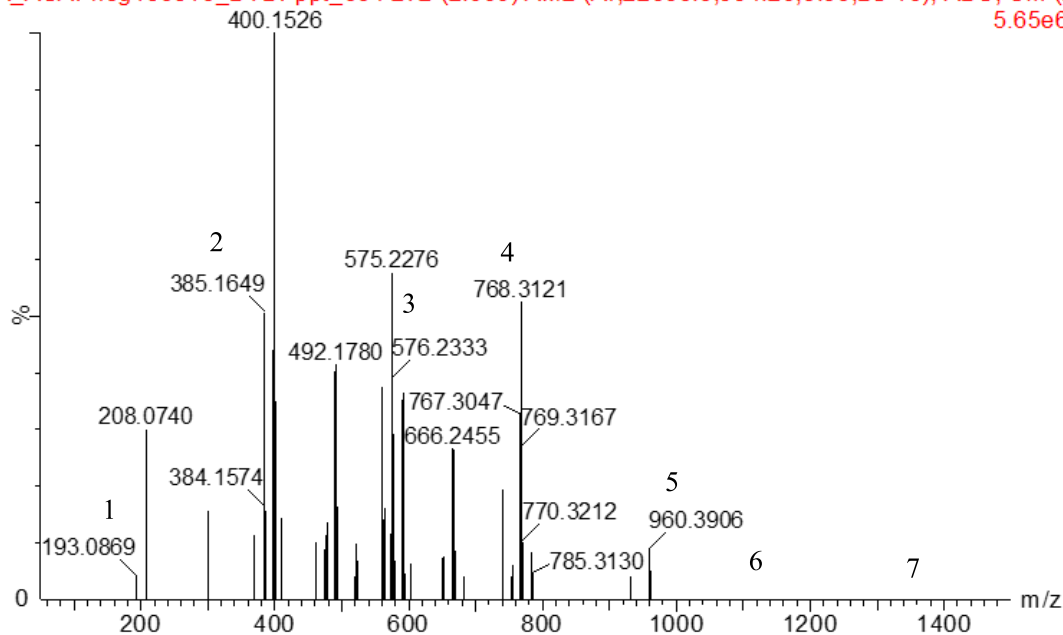


Fig.4-82 ASAP(-) mass spectrum of BP precipitate showing entire pane

Table 4-10 Showing BP and oligomers following SBP treatment as observed from precipitate and supernatant

Molecular formula	M_{theo}	M_{expt}	ppm
C ₁₁ H ₁₄ O ₃	193.0865	193.0866	0.5
C ₁₁ H ₁₄ O ₃	193.0865	193.0866	0.5
C ₂₂ H ₂₆ O ₆	385.1651	385.1654	0.8
C ₂₂ H ₂₅ O ₇	400.1522	400.1541	4.7
C ₃₃ H ₃₈ O ₉	577.2438	577.2410	-4.9
C ₃₃ H ₃₇ O ₁₀	592.2308	592.231	0.3
C ₄₄ H ₅₀ O ₁₂	769.3224	769.3174	-6.5
C ₄₄ H ₄₉ O ₁₃	784.3095	784.3105	1.3
C ₅₅ H ₆₂ O ₁₅	961.4010	961.3954	-5.8
C ₅₅ H ₆₁ O ₁₆	976.3881	976.3871	-1.0
C ₆₆ H ₇₄ O ₁₈	1153.4797	1153.4771	-2.3
C ₆₆ H ₇₃ O ₁₉	1168.4668	1168.4707	3.3
C ₇₇ H ₈₆ O ₂₁	1345.5568	1345.5581	-1.0
C ₇₇ H ₈₅ O ₂₂	1360.5454	1360.5443	-0.8

In Figure 4-83, m/z peaks at 385.1654 and 400.1541 correspond to a deprotonated dimer and oxygenated dimer of BP, consistent with the formulae $C_{22}H_{26}O_6$ and $C_{22}H_{25}O_7$,

ASAP(-) sen mode MS, lockspray, Probe T=300oC, source 100oC, t=0 IPwCap, B)
JA_ASAPneg190910_BYBPppt_002 294 (2.874) AM2 (Ar,22000.0,554.26,0.00,LS 10); Cm (291:2'
2.29e6

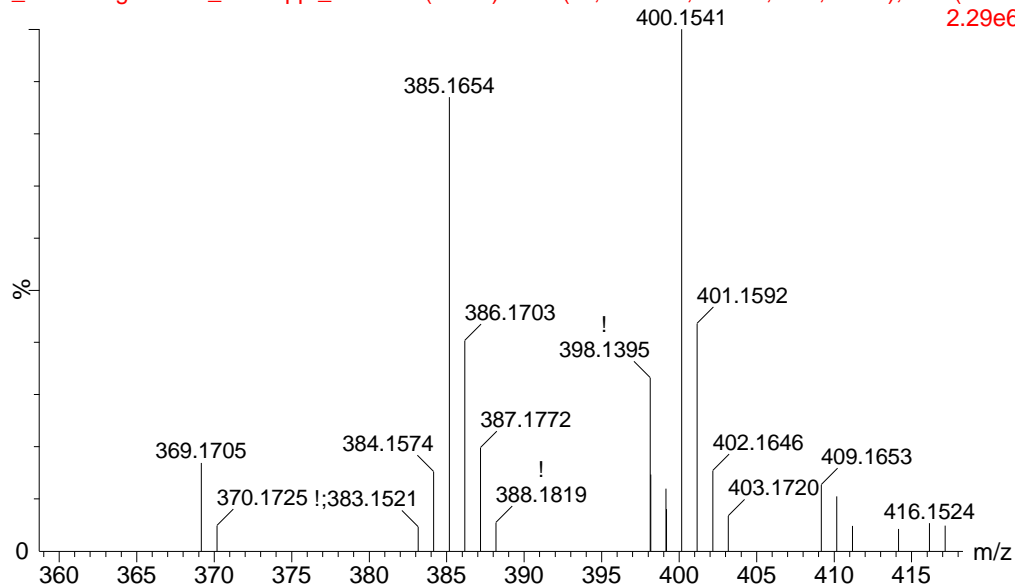


Fig.4-83 ASAP(-) mass spectrum of BP precipitate showing dimer and oxygenated dimer

structural formulae Figures 4-89 (a) and (b), respectively. Similarly, Figure 4-84 (presented on a narrow x-axis range to show the m/z peaks of interest) show m/z peaks at 577.2410 and 592.2310 corresponding to BP trimer and oxygenated trimer respectively with molecular formulae $C_{33}H_{38}O_9$ and $C_{33}H_{37}O_9$. structural formulae Figures 4-89 (c) and (d), respectively. Likewise, in Figure 4-85, m/z peaks at 769.3201 and 784.3105 correspond to a tetramer and oxygenated tetramer of BP, assigned molecular formulae $C_{44}H_{50}O_{12}$ and $C_{44}H_{49}O_{13}$, respectively, structures Figures 4-89 (e) and (f), respectively.

ASAP(-) sen mode MS, lockspray, Probe T=300oC, source 100oC

JA_ASAPneg190910_BYBPppt_002 294 (2.874) AM2 (Ar,22000.0,554.26,0.0) 1.60e6

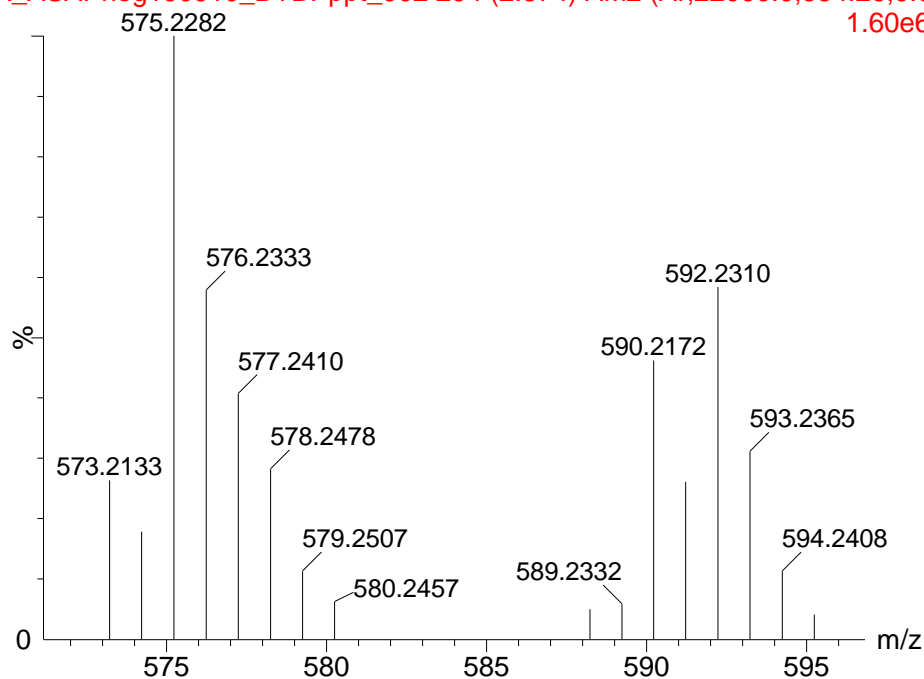


Fig.4-84 ASAP(-) mass spectrum of BP precipitate showing trimer and oxygenated trimer

ASAP(-) sen mode MS, lockspray, Probe T=300oC, source 100oC, t=0 IPwCap, B)

JA_ASAPneg190910_BYBPppt_002 294 (2.874) AM2 (Ar,22000.0,554.26,0.00,LS 10); Cm (291:2) 1.56e6

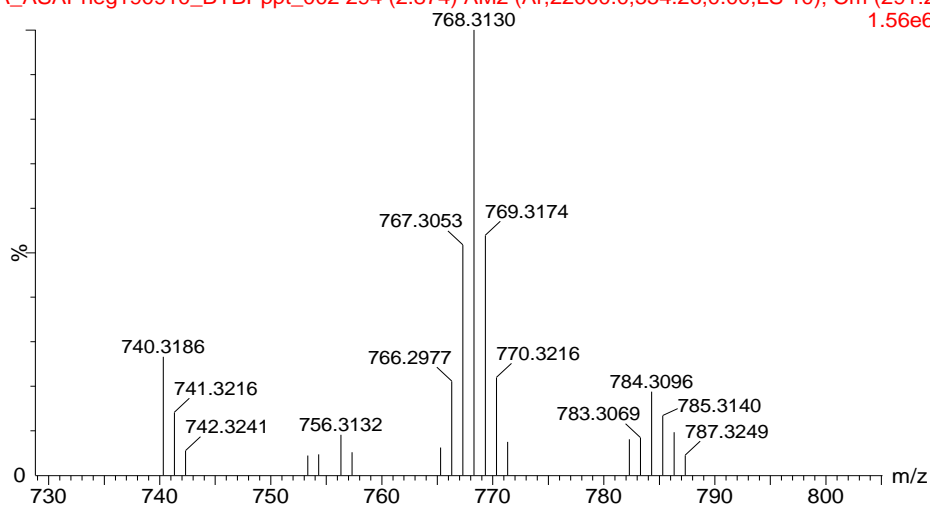


Fig. 4-85 ASAP(-) mass spectrum of BP precipitate showing tetramer and oxygenated tetramer

In Figure 4-86, m/z peaks at 961.3954 and 976.3871 represent pentamer and oxygenated pentamer of BP, assigned the formulae $C_{55}H_{62}O_{15}$ and $C_{55}H_{61}O_{15}$, respectively, structures

Figures 4-89 (g) and (h), respectively. Similarly, in Figure 4-87, hexamer and oxygenated hexamer of BP were identified at m/z peaks

ASAP(-) sen mode MS, lockspray, Probe T=300oC, source 100oC, t=0 IP
 JA_ASAPneg190910_BYBPppt_003 253 (2.483) AM2 (Ar,22000.0,554.26,0.00,LS 10);
 6.11e4

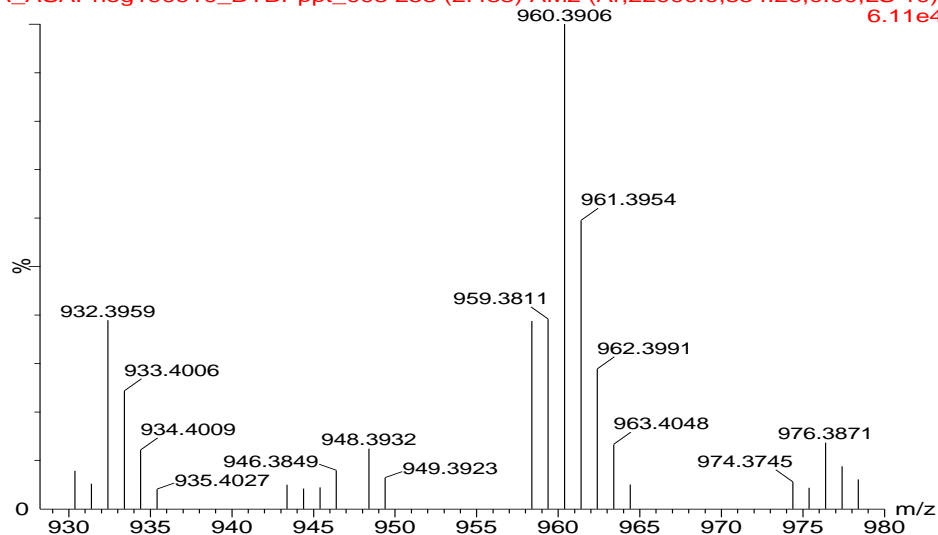


Fig.4-86 ASAP(-) mass spectrum of BP precipitate showing pentamer and oxygenated pentamer

ASAP(-) sen mode MS, lockspray, Probe T=300oC, source 100oC, t=0 IP
 JA_ASAPneg190910_BYBPppt_004 272 (2.666) AM2 (Ar,22000.0,554.26,0.00,LS 10);
 3.18e4

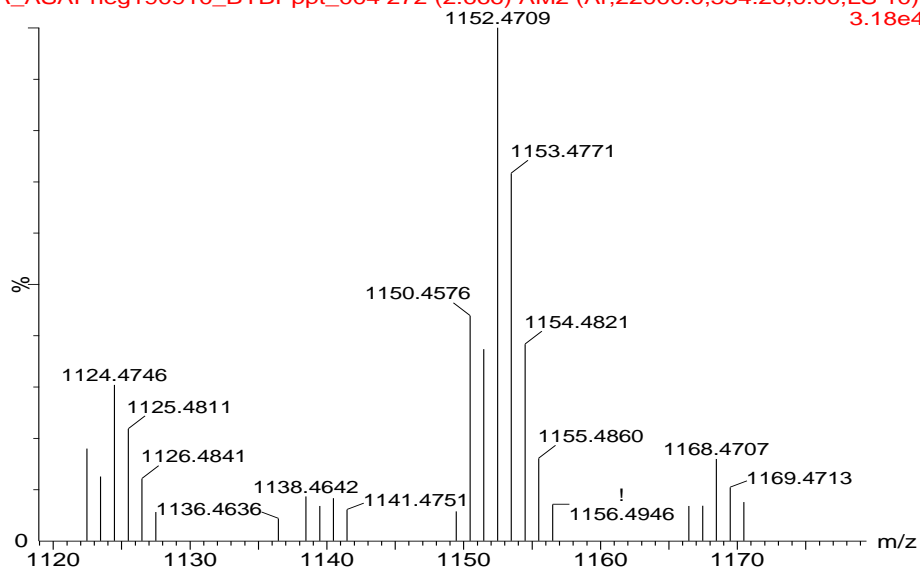


Fig. 4-87 ASAP(-) mass spectrum of BP precipitate showing hexamer and oxygenated hexamer

1153.4771 and 1168.4707 assigned formulae $C_{66}H_{74}O_{18}$ and $C_{66}H_{73}O_{19}$, structures Figures 4-89 (i) and (j), respectively. The highest observed oligomer of BP was heptamer and

oxygenated heptamer having m/z 1345.5568 and 1360.5443, assigned molecular formulae $C_{77}H_{86}O_{21}$ and $C_{77}H_{85}O_{22}$, structures Figures 4-89 (k) and (l), respectively.

ASAP(-) sen mode MS, lockspray, Probe T=300oC, source 100oC, t=0 IPwCap, B1
JA_ASAPneg190910_BYBPpt_004 272 (2.666) AM2 (Ar,22000.0,554.26,0.00,LS 10); ABS; Cm (2.34e3)

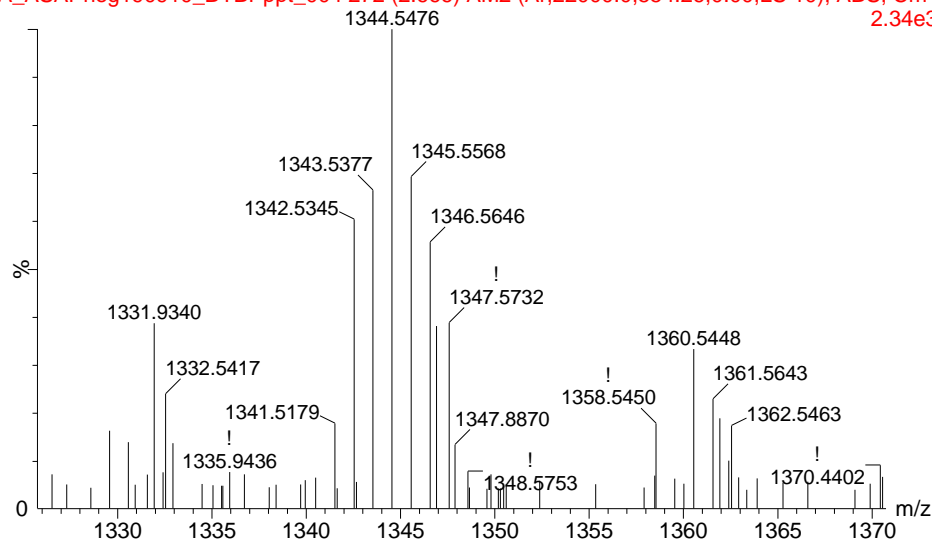


Fig. 4-88 ASAP(-) mass spectrum of BP precipitate showing heptamer and oxygenated heptamers

The tentative structures presented for the studied parabens (Figures 4-72, 4-80 and 4-89) are proposed based on the most likely oxidative coupling pattern, considering the *para*-position has been substituted and among the 4 unsubstituted carbon atoms, the *ortho*-position to the hydroxyl group is the most likely site for oxidative coupling of two aryl radicals (Lu *et al.* 2009). These structures do not take into account regioselectivity or any possible isomeric patterns.

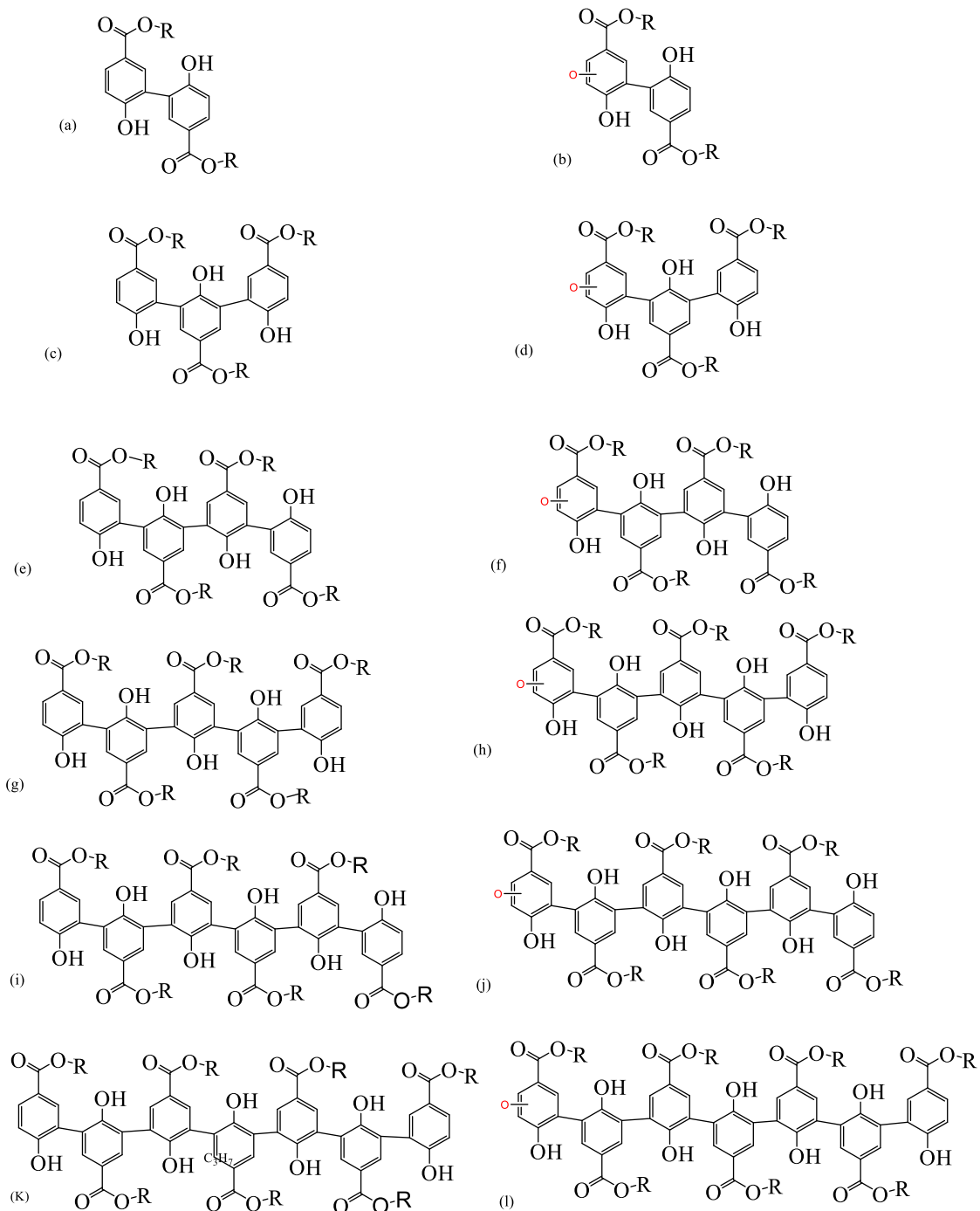


Fig. 4-89 Proposed structural formula for the oligomers of BP ($R=C_4H_9$)

Based on the oligomers observed, a pathway for the oligomerization of parabens is proposed (Figure 4-90). The diagram, to avoid becoming too clumsy, does not include radicals except for the monomer. It is important to bear in mind each product acting as a

substrate for another oligomer must have first undergone oxidation through the peroxidase cycle, becoming a radical,

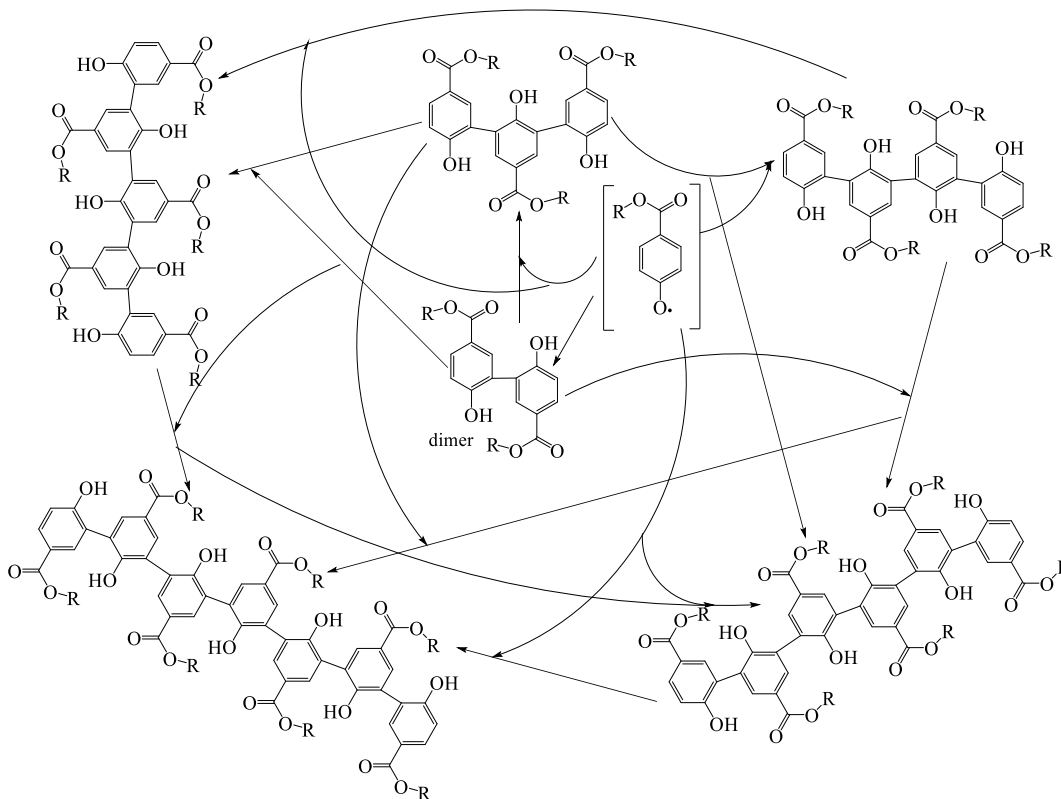


Fig.4-90 Proposed reaction pathway for oligomerization of parabens following SBP treatment. (R = CH₃, C₃H₇, C₄H₉)

as a pre-condition for non-enzymatic oxidative coupling to produce an oligomer. This is applicable to all the parabens mentioned above. The oxygenation and/or hydroxylation process and oligomers are also not shown in this proposed pathway but is already covered elsewhere (Tay *et al.* 2010). It is not certain if the modification occurs before or after the substrates' passage through the peroxidase cycle. However, going by the pathway proposed by Tay *et al.* (2010), it is thought the oligomers undergo the substitution after they have been oligomerized, due to radical attack. This agrees with previous reports (Carteix and Bergel 1995, Durlait *et al.* 1992) which maintained that hydroxylation is not an enzymatic process. Moreover, Verloop *et al.* (2016) also reported hydroxylation occurs after the oligomerization of tea phenolics.

4.7 Effect of desolvation gas temperature on molecular ions

Some of the crucial parameters in the application of ASAP ion source are desolvation gas temperature (DGT), corona current, cone voltage and collision energy (Du *et al.* 2014). Smith *et al.* (2012) compared the effects of cone voltage and DGT on the intensity and ionization efficiency of m/z peaks and observed the DGT is the most important factor in producing clear and distinctive mass spectra of polystyrene oligomers in ASAP. They reported that high cone voltage produced the undesirable effect of in-source fragmentation, and changing it amounted to only about 2% improvement in ionization intensity. This agrees with Du *et al.* (2014) who opined that DGT and corona current are most crucial in determining ionization efficiency. For instance, medium size plasticizers (an example of which is Di-n-butyl phthalate, $mwt = 278.38$ g/mol) may ionize well with a $0.1 \mu\text{A}$ corona current while higher molecular weight ones may require between 1.0 and $5.0 \mu\text{A}$ for efficient ionization (Du *et al.* 2014). Therefore, the use of $1.0 \mu\text{A}$ as the corona current in this study was adequate to provide effective ionization.

However, since the appropriate DGT for the analysis of these treated compounds was not determined, sample ionization was carried out at three temperatures by varying the DGT for each sample run between 300 and 500 °C for the single parabens and mix-5. The mass spectra scan at the three temperature points were collected and processed in a similar fashion to ensure similar scans are averaged and combined in a common manner. The resultant mass spectra for such scans between m/z 50 and 1200 for MP reaction mixture are shown (Figure 4-91). The other two parabens presented a similar pattern and are omitted. At 300 °C, a strong peak was observed at m/z 166.0262, which diminishes drastically with increasing temperature, between 400 °C and 500 °C (Figure 4-91 a, b, and c, respectively). Similarly, the peak at m/z 600.1259 could barely be noticed at 300 °C but increases in intensity with increasing temperature. This increased intensity is thought to be due to improved ionization efficiency owing to increases in the DGT. The last panel (Figure 4-91 (c)) shows a peak at m/z 750.1575, which is not visible in the mass spectra, produced at lower DGT. Moreover, the intensity of the base peaks in the panels increases from 4.47×10^5 to 4.50×10^6 to 1.88×10^7 at 300 °C, 400 °C and 500 °C, respectively. This

clearly shows increasing the DGT is very important in producing more efficient ionizations.

To further understand the ionization efficiency, the mass deviations at the respective temperatures were computed (Table 4-11). It be seen that at 500 °C, all the oligomer peaks are detected and within acceptable limits ppm, while at 300 °C, only some oligomers are detected. The ionization intensities of the respective m/z peaks whose ppm values were computed (data not shown) tend to display a bell-shaped pattern, characteristic of a normal distribution curve at 500 °C, unlike at the lower temperatures where the bell shape was truncated abruptly, possibly due to loss of ionization sensitivity.

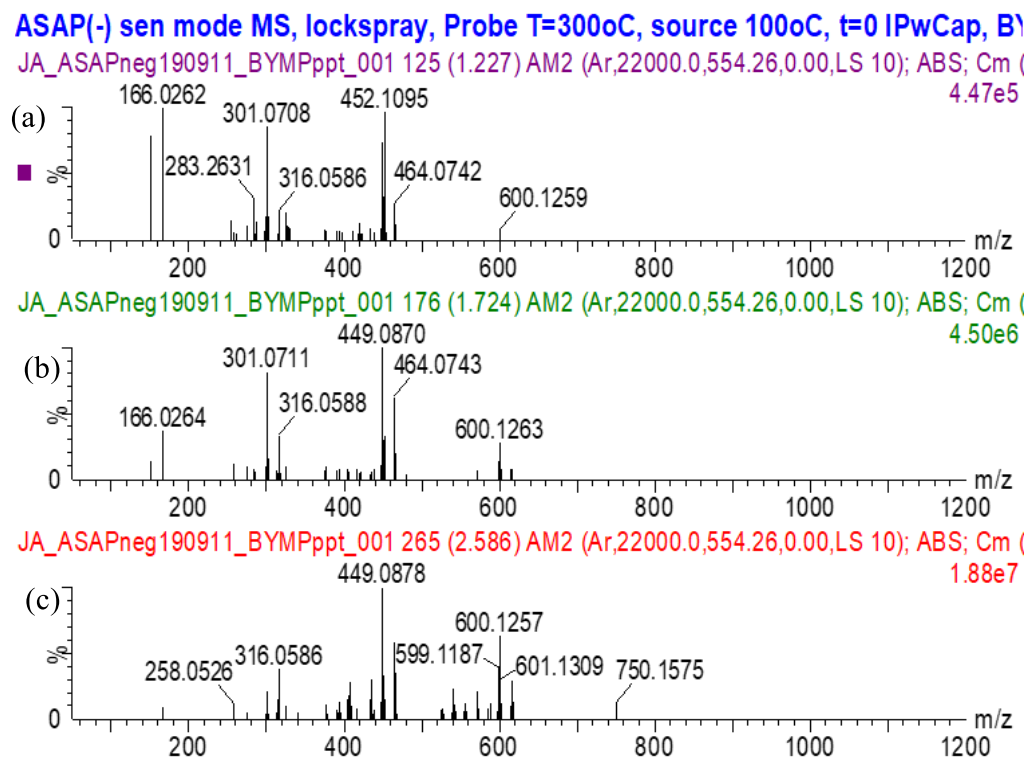


Fig. 4-91 ASAP(-) mass spectra of MP at three different desolvation gas temperatures (a) 300°C (b) 400 °C and (c) 500 °C.

The detection of molecular ions is worse with the high molecular mass BP than with MP (Table 4-11). This is thought to be because, with increasing molecular mass, higher temperature is necessary to move the molecules into the vapor phase where ionization will

occur consistent with the hypothesis of Smith *et al.* (2012). They reported 600 °C to be ideal for polystyrene. In this study, it is shown that 500 °C is necessary to put the oligomers of PP and BP in the gas-phase, while 400 °C would be ideal for MP.

Table 4-11 Effect of ionization temperature on detection of molecular ions in ASAP(-). Numbers represent mass deviation from the theoretical value in ppm

Temp (°C)/ Oligomer	1	2	3	4	5	6	7
MP							
300	-2.7	-1.3	-8.0	-6.0	-5.2	NS	NS
400	-2.7	-0.3	6.4	5.5	-6.4	-4.8	-2.5
500	-2.7	-1.0	-5.8	-6.2	-6.3	-5.7	-4.2
PP							
300	-1.1	-0.3	-7.1	-2.4	NS	NS	NS
400	-1.1	-0.3	-6.7	-7.0	-6.2	NS	NA
500	-0.6	-2.0	-4.1	7.6	-6.1	-5.4	NA
BP							
300	1.0	-0.8	-8.8	NS	NS	NS	NS
400	2.1	0.5	-5.4	-8.7	0.6	NS	NS
500	2.1	1.82	-6.4	-7.7	-6.6	-6.9	-8.0

1 = monomer, 2=dimer, 3=trimer, 4=tetramer, 5=pentamer, 6=hexamer, 7=heptamer. NS = Not seen; NA = Not available

4.8 Mass spectral analysis of mix-5 precipitates

The mix-5 was studied for oligomer formation using ASAP(+). The presence of Acet made it necessary to use the positive ionization mode, since the molecule can be easily protonated at the amido nitrogen which enables it and its oligomers to be detected in the mass spectrum (Hawavitharana *et al.* 2008). However, since there were five compounds, the combinational pattern at the respective level of oligomerization needs to be derived. For

example, AB and BA are permutations, and only one form was chosen. This is more so as the order of bonding was not important, as any such combination order will yield the same m/z peak value. For trimers although the pattern of bonding may be interesting to consider as in which monomer may be in the middle of the other two monomers, this was not part of the study objectives and so was not considered.

Sorting out the dimer combinations was manually done. However, the trimers were more difficult to sort and a program was designed to compute the possible combinations. From running the program, 125 permutations were obtained of which 35 combinations were derived. These combinations were used to determine the theoretical m/z values based upon which search for the oligomers was made in the mass spectrum. The program was also implemented for tetramers and pentamers which were detected. Although single-compound studies showed homo-hexamers of all three parabens, and heptamers of MP and BP, these levels of oligomerization were not detected in the mix-5 mass spectrum. This is plausible considering the reduced organic solvent content in this reaction mixture which was about 1.75 % (v/v), being less than the 2.5% and 5% that were used in the single-compound treatments of PP and BP, respectively but more than the 1.25% that was used in the single-compound treatment of MP. The hydrophobic nature of some of the monomers was a sufficient factor to cause the oligomers to easily precipitate out of solution, in the presence of limiting organic solvent to aid their solubility. This may have had the effect of limiting the degree of oligomerization.

The mass spectra for untreated monomers and residual monomers at the end of the reaction are not presented here. The mass spectra shown below cover dimers, trimers, tetramers and pentamers detected from the precipitates. Since those detected from the supernatant comprised of lower oligomers, they are not reported but the oligomers from precipitate are presented to show the largest molecular weight oligomers detected from mix-5. Besides, since the products are similar for the lower oligomers, reporting from both supernatant and precipitate may only be a futile attempt to duplicate the results. Presentations of oligomers arising from narrow m/z ranges taken out of the full-scan mass spectrum and are presented in Figures 4-93 to 4-143. Since these were studied in the positive-ion mode, all m/z peaks presented are protonated derivatives. The structural formulae are however presented as

dictated by the contributing monomers' molecular formulae. Fragmentation patterns, where shown, are also considered in the positive-ion mode. All identified oligomers were resolved within ≤ 10 ppm mass deviation. Du *et al.* (2014) also reported in a specialized mass spectrometry journal on resolving myriad of polymer additives from a reaction within a similar error margin.

4.8.1 Dimers from mix-5 precipitate

The dimers detected from mix-5 precipitate are presented in Table 4-12. Mass spectral data are shown in Figure 4-92 to 4-103, with plausible structures shown in Figure 4-104.

In addition to regioisomeric and permutational variations for plausible oligomer structures alluded to hereafter, the combination of different monomers could

Table 4-12 Dimers detected from mix-5 precipitate under optimized conditions using ASAP(+) ionization mode

Combination	Molecular formula	M^+_{theo}	M^+_{expt}	ppm
PHBA-PHBA	$C_{14}H_{10}O_6$	275.0556	275.0562	2.2
PHBA-MP	$C_{15}H_{12}O_6$	289.0712	289.0713	0.3
Acet-Acet	$C_{16}H_{16}N_2O_4$	301.1188	301.1188	0.0
MP-MP	$C_{16}H_{14}O_6$	303.0869	303.0859	-3.3
PHBA-PP	$C_{17}H_{16}O_6$	317.1025	317.1022	-0.9
PHBA-BP	$C_{18}H_{18}O_6$	331.1182	331.1176	-1.8
MP-PP	$C_{18}H_{18}O_6$	331.1182	331.1176	-1.8
MP-BP	$C_{19}H_{20}O_6$	345.1338	345.1328	-2.9
PP-PP	$C_{20}H_{22}O_6$	359.1495	359.1480	-4.2
PP-BP	$C_{21}H_{24}O_6$	373.1651	373.1647	-1.1
BP-BP	$C_{22}H_{26}O_6$	387.1808	387.1796	-3.1

produce additional constitutional isomers not discernable by MS analysis. It is possible to distinguish these structurally unique products with LC-MS owing to differential retention times based on distinct interactions with the silanol-C18 stationary phase of the column. Such characterization of the array of products formed is beyond the scope of this dissertation. Moreover, the use of an off-line chromatographic system in this work would not provide for such determinations without fraction collection.

The full-scan mass spectrum of mix-5 precipitate is shown in Figure 4-92. Cross-coupled products involving acetaminophen were not noticed, even though a homo-

ASAP(+) sen mode MS, lockspray, Probe T=300oC, source 100oC, t=0 IPwCap, B
JA_ASAP190912_BYMix5ppt_002 287 (2.661) AM2 (Ar,15000.0,556.28,0.00,LS 10); ABS; Cm (2f
4.42e5

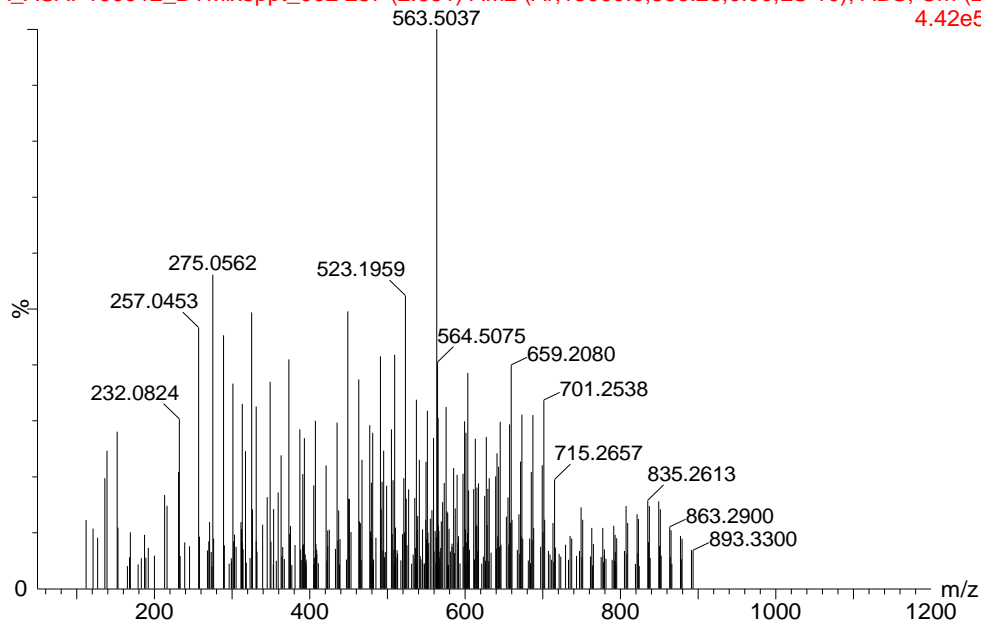


Fig. 4-92 Full scan ASAP(+) mass spectrum of mix-5 precipitate under optimized conditions

dimer of acetaminophen was observed Figure 4-93 (m/z 301.1188 with a molecular formula $C_{16}H_{16}N_2O_4$ and structural formula Figure 4-104(a)). Since the protocol employed could assay for all monomers in a standard sample and also a homo-dimer of acetaminophen was detected, it is obvious the protocol has the analytical competence to assay for all the CECs. It is thought the inability to detect cross-coupled oligomers involving acetaminophen may be due to the very fast consumption of Acet in the reaction under the experimental conditions. From the time course of mix-5 (Figure 4-43), it is seen that acetaminophen was almost entirely consumed within the first 3 minutes of the reaction, unlike the other CECs. Since the dominant radicals in solution within this time would be those of acetaminophen, self-coupling route would have been favored over the cross-coupling route, consistent with the detection of a homo-dimer of acetaminophen. Porter *et al.* (1985) reported that in the presence of a high concentration of peroxidase, the concentration of acetaminophen radical increases in a direct proportion. This surge in

acetaminophen radical production may be responsible for a drive towards self-coupling than cross-coupling. However, an analysis of the products formed within the first three minutes of the mix-5 reaction may be necessary to provide better insight into the coupling pattern of the CECs within this initial 3-minute reaction time.

ASAP(+) sen mode MS, lockspray, Probe T=300oC, source 100oC, t=0 IPwCap, BYMi
 JA_ASAP190912_BYMix5ppt_002 287 (2.661) AM2 (Ar,15000.0,556.28,0.00,LS 10); ABS; Cm (282:28
 1.62e5

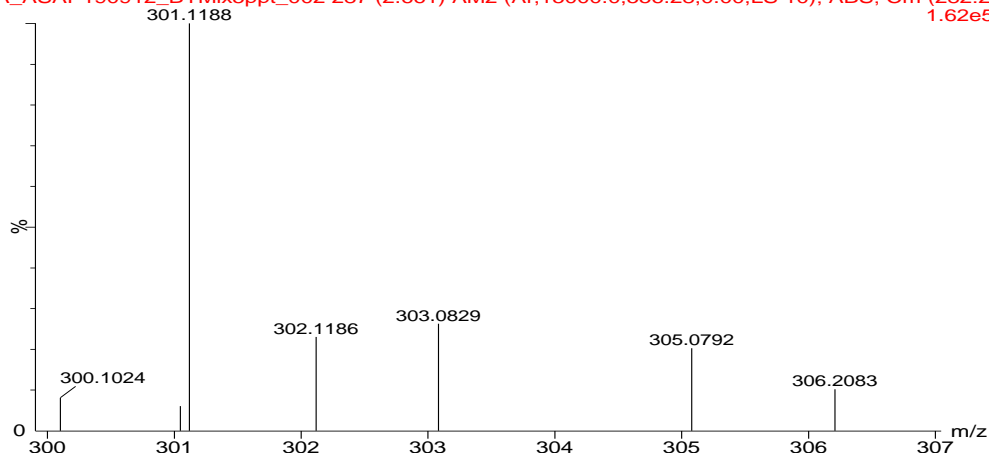


Fig. 4-93 ASAP(+) mass spectrum of mix-5 precipitate under optimized conditions showing a homo-dimer of Acet

A protonated dimer of PHBA-PHBA in Figure 4-94 has m/z peak at 275.0562 and

ASAP(+) sen mode MS, lockspray, Probe T=300oC, source 100oC, t=0 IPwCap, B
 JA_ASAP190912_BYMix5ppt_002 287 (2.661) AM2 (Ar,15000.0,556.28,0.00,LS 10); ABS; Cm (27
 2.48e5

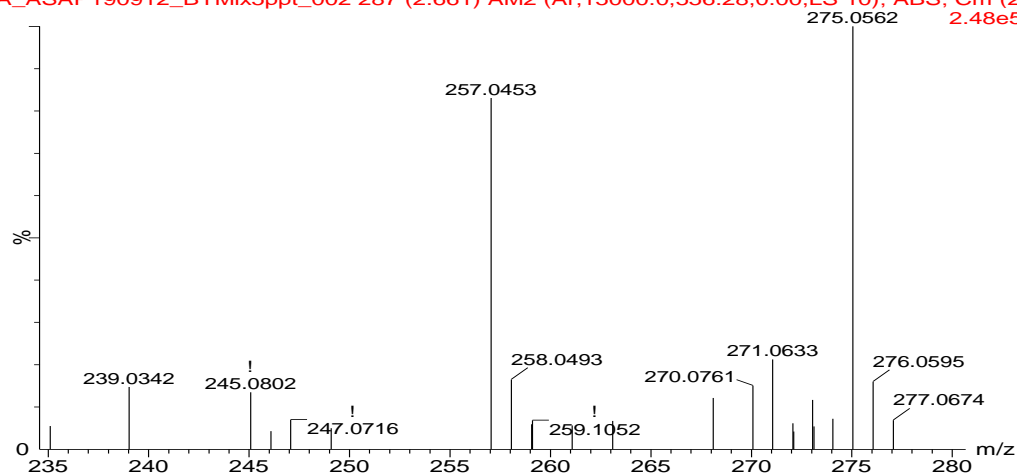


Fig. 4-94 ASAP(+) mass spectrum of mix-5 precipitate under optimized conditions showing a dimer of PHBA-PHBA

correspond to the formula $C_{14}H_{10}O_6$ with structural formula at Figure 4-104 (b). The m/z peaks at 257.0453 and 239.0342 corresponds to loss of -OH and -OH, in succession.

Figure 4-95 shows a protonated dimer of PHBA-MP at m/z 289.0713 which correspond to the molecular formula $C_{15}H_{12}O_6$ with a structural formula in Figure 4-128 (c). The fragmentation of parabens is known to occur at the ester bond, releasing the -OR group from the rest of the carbonyl group on the carbon ring (Nicolescu 2017). This will produce different fragments depending on the order of removal. Since fragmentation under the analytical conditions may be a random process, both are bound to occur simultaneously in the system. The removal of $-OCH_3$ may produce the m/z peak at 257.0453 and subsequent fragmentation may produce m/z peak at 239.0342. Alternatively, first fragmentation of -OH may produce m/z peak 271.0633 and subsequent removal of $-OCH_3$ may produce that at 239.0342. The presence of several high intensity peaks within a mass spectrum of

ASAP(+) sen mode MS, lockspray, Probe T=300oC, source 100oC, t=0 IPwCap, B
 JA_ASAP190912_BYMix5ppt_002 287 (2.661) AM2 (Ar,15000.0,556.28,0.00,LS 10); ABS; Cm (2?
 2.48e5

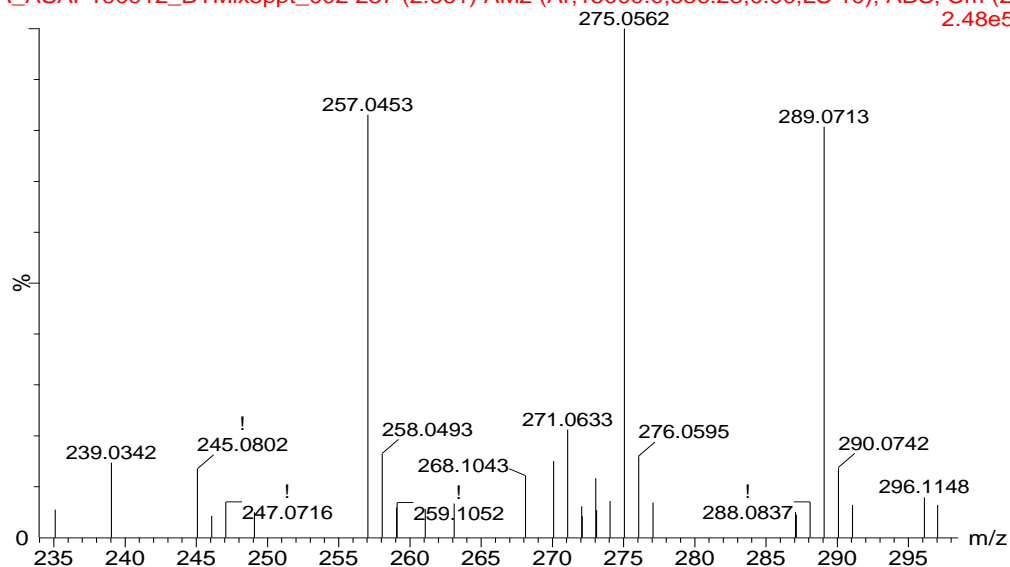


Fig. 4-95 ASAP(+) mass spectrum of mix-5 precipitate under optimized conditions showing a dimer of PHBA-MP.

interest may be seen in subsequent figures, which may be arising from fragments with strong signal intensity. For example, the difference between 289.0713 and 275.0562 corresponds to the loss of a methylene group, thought to be from the former. Similarly, the m/z peak at 257.0453 has been shown to be a fragment signal following the splinter of a methoxy group, from the 289.0713 m/z peak. Considering the matrix nature of the samples and the myriad of oligomers formed, this is expected.

A dimer of PHBA-PP is presented at m/z 317.1022 (Figure 4-96) and corresponds to a formula $C_{17}H_{16}O_6$ and structural formula Figure 4-104 (d). The m/z peaks observed at 257.0453 and 239.0342 are thought to be fragments following the fragmentation of $-OC_3H_7$ and $-OH$ from the PP and PHBA residues, respectively.

ASAP(+) sen mode MS, lockspray, Probe T=300oC, source 100oC, t=0 IPwCap, B
 JA_ASAP190912_BYMix5ppt_002 287 (2.661) AM2 (Ar,15000.0,556.28,0.00,LS 10); ABS; Cm (2
 2.48e5

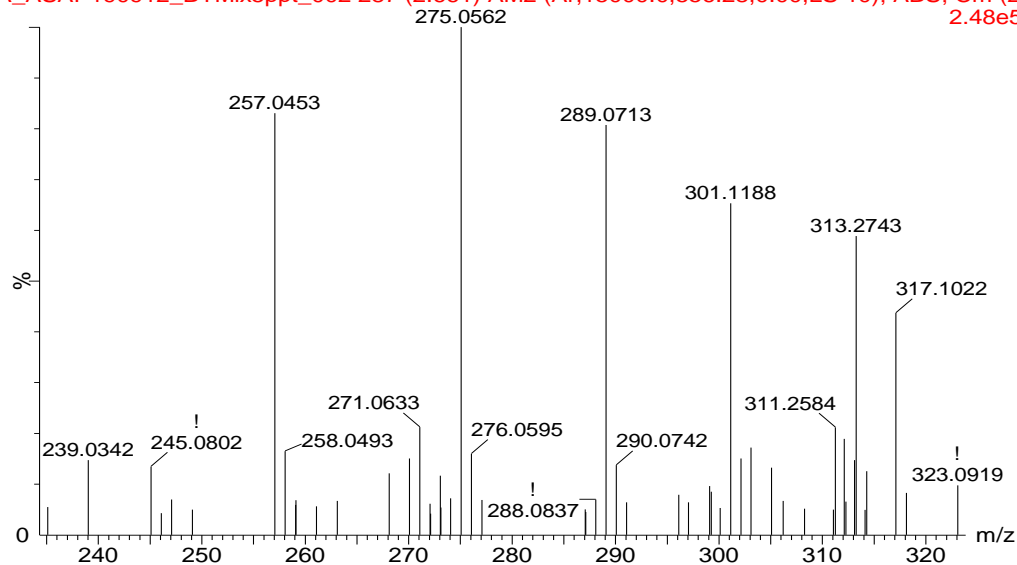


Fig. 4-96 ASAP(+) mass spectrum of mix-5 precipitate under optimized conditions showing a dimer of PHBA-PP

Similarly, a m/z peak 331.1176 in Figure 4-97 corresponds to a dimer of PHBA-BP, with a molecular formula $C_{18}H_{18}O_6$ and a structural formula Figure 4-104 (e). Fragmentation of $-OC_4H_9$ from BP may produce the m/z peak at 257.0453. Following here, the fragmentations are not highlighted. These were shown to illustrate this occurrence as observed in the mass spectra, more so that the alkoxy groups are similar for all the oligomers, these illustrations suffice to create an understanding of the fragmentation pattern in subsequent presented mass spectra.

ASAP(+) sen mode MS, lockspray, Probe T=300oC, source 100oC, t=0 IPwCap, B
 JA_ASAP190912_BYMix5ppt_002 287 (2.661) AM2 (Ar,15000.0,556.28,0.00,LS 10); ABS; Cm (28
 2.48e5

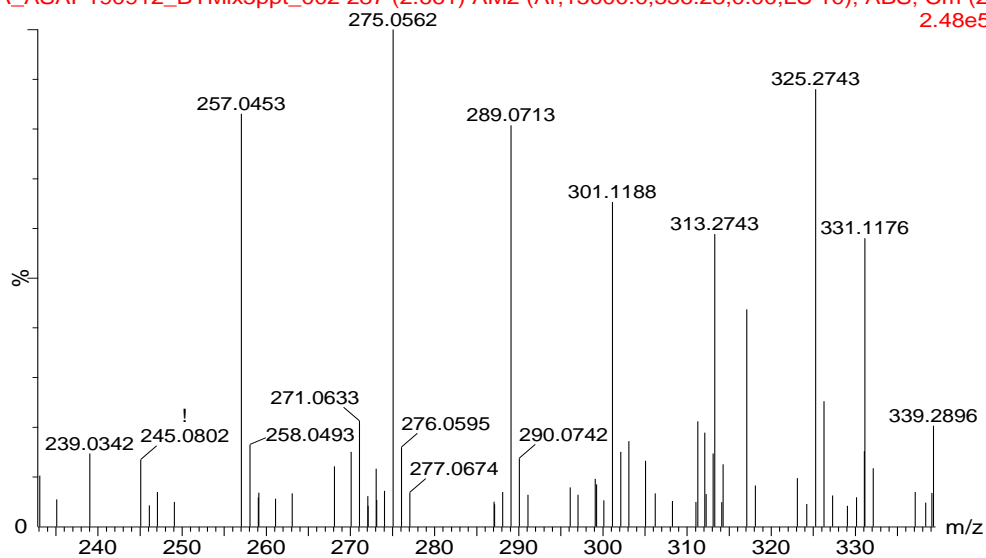


Fig.4-97 ASAP(+) mass spectrum of mix-5 precipitate under optimized conditions showing a dimer of PHBA-BP

Figure 4-98 shows a m/z peak for MP-MP dimer at 303.0859, corresponding to the molecular formula C₁₆H₁₄O₆ with structural formula Figure 4-104 (f). Likewise,

ASAP(+) sen mode MS, lockspray, Probe T=300oC, source 100oC, t=0 IPwCap, BYMix5ppt,
 JA_ASAP190912_BYMix5ppt_002 247 (2.295) AM2 (Ar,22000.0,556.28,0.00,LS 10); Cm (243:248-49:54)
 1.73e5

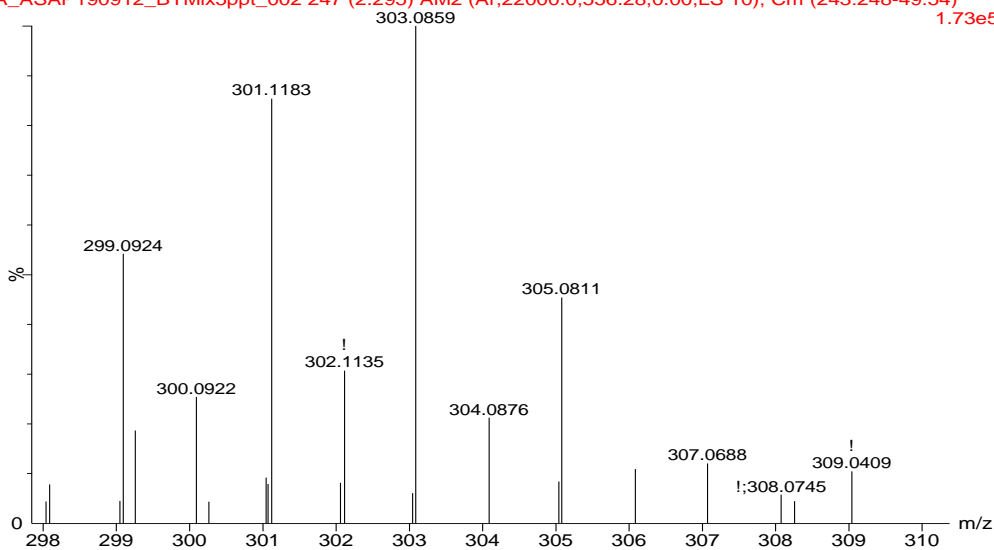


Fig.4-98 ASAP(+) mass spectrum of mix-5 precipitate under optimized conditions showing a dimer of MP-MP

Figure 4-99 shows a dimer of MP-PP at m/z 331.1176 corresponding to a molecular formula C₁₈H₁₈O₆ and structural formula Figure 4-104 (g).

ASAP(+) sen mode MS, lockspray, Probe T=300oC, source 100oC, t=0 IPwCap, B
 JA_ASAP190912_BYMix5ppt_002 287 (2.661) AM2 (Ar,15000.0,556.28,0.00,LS 10); ABS; Cm (2.48e5

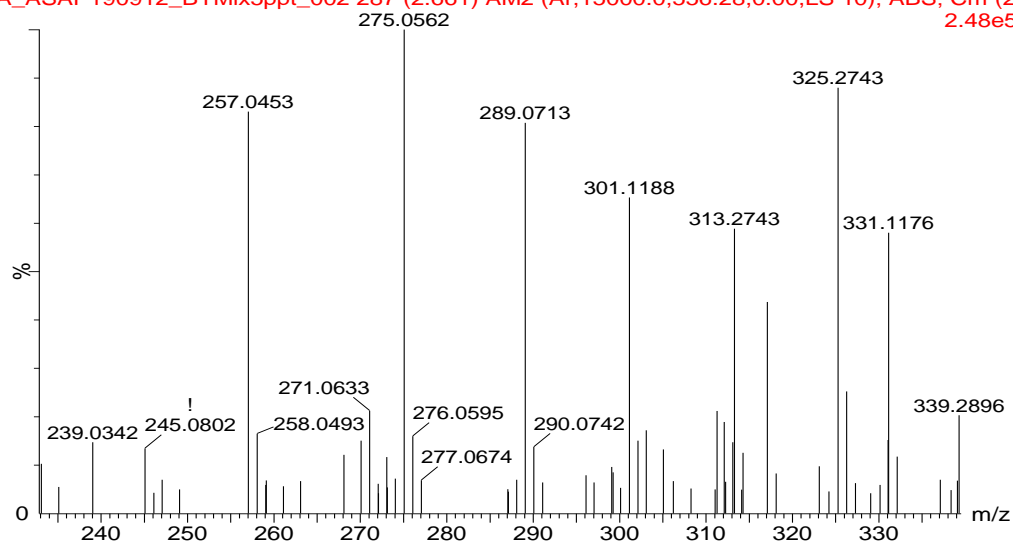


Fig. 4-99 ASAP(+) mass spectrum of mix-5 precipitate under optimized conditions showing a dimer of MP-PP

Figure 4-100 presents a dimer of MP-BP at m/z 345.1328 having the molecular formula $C_{19}H_{20}O_6$ and the structural formula Figure 4-104 (h). Similarly, a homo-

ASAP(+) sen mode MS, lockspray, Probe T=300oC, source 100oC, t=0 IPwCap, B
 JA_ASAP190912_BYMix5ppt_002 287 (2.661) AM2 (Ar,15000.0,556.28,0.00,LS 10); ABS; Cm (2.48e5

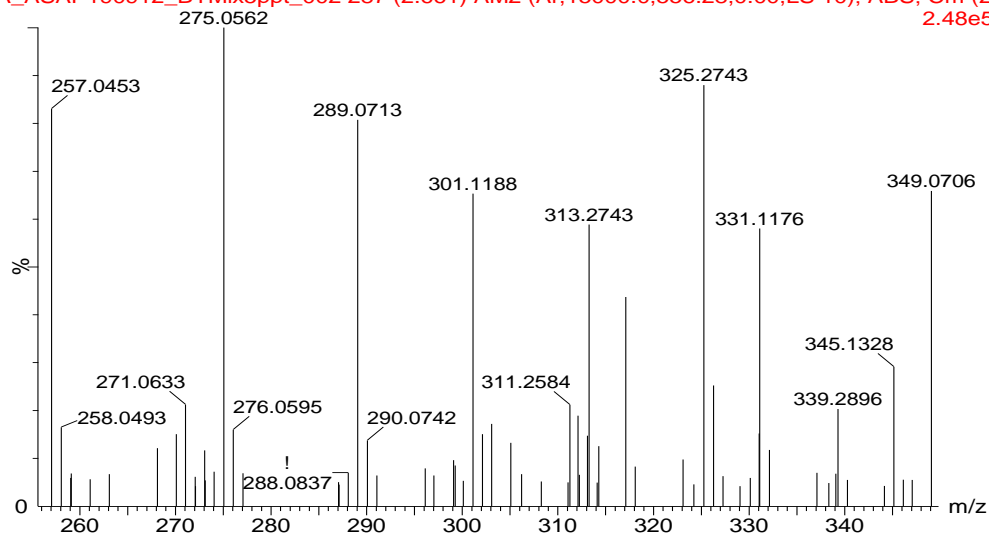


Fig. 4-100 ASAP(+) mass spectrum of mix-5 precipitate under optimized conditions showing a dimer of MP-BP

dimer of PP is seen at m/z 359.1480 (Figure 4-101) having the molecular formula $C_{20}H_{22}O_6$ and a structural formula Figure 4-104 (i).

ASAP(+) sen mode MS, lockspray, Probe T=300oC, source 100oC, t=0 IPwCap, B
JA_ASAP190912_BYMix5ppt_002 287 (2.661) AM2 (Ar,15000.0,556.28,0.00,LS 10); ABS; Cm (2E
2.48e5

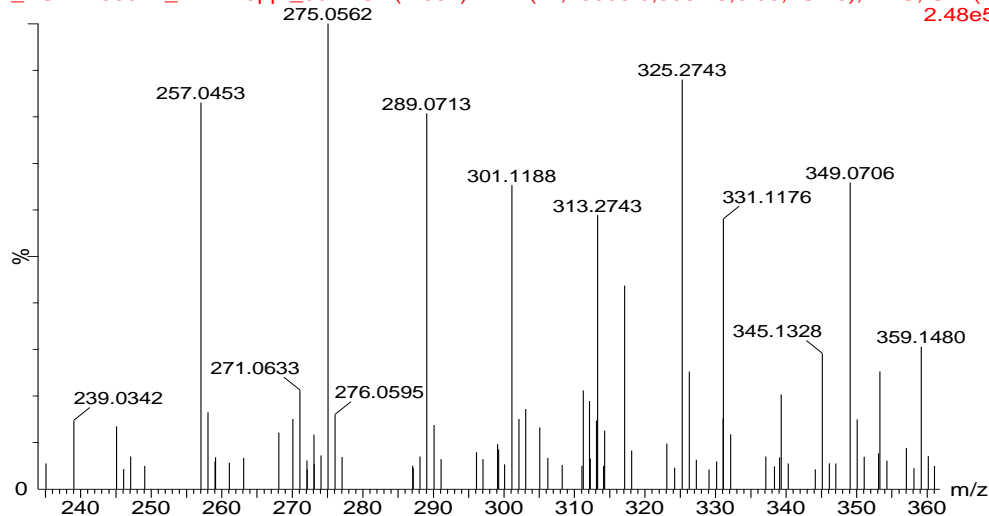


Fig. 4-101 ASAP(+), sen mode mass spectrum of mix-5 precipitate under optimized conditions showing a dimer of PP-PP

The dimer of PP-BP is observed at m/z 373.1647 (Figure 4-102) having a molecular formula $C_{21}H_{24}O_6$ and corresponding to structural formula Figure 4-104 (j). The last

ASAP(+) sen mode MS, lockspray, Probe T=300oC, source 100oC, t=0 IPwCap, B
JA_ASAP190912_BYMix5ppt_002 287 (2.661) AM2 (Ar,15000.0,556.28,0.00,LS 10); ABS; Cm (2E
1.81e5

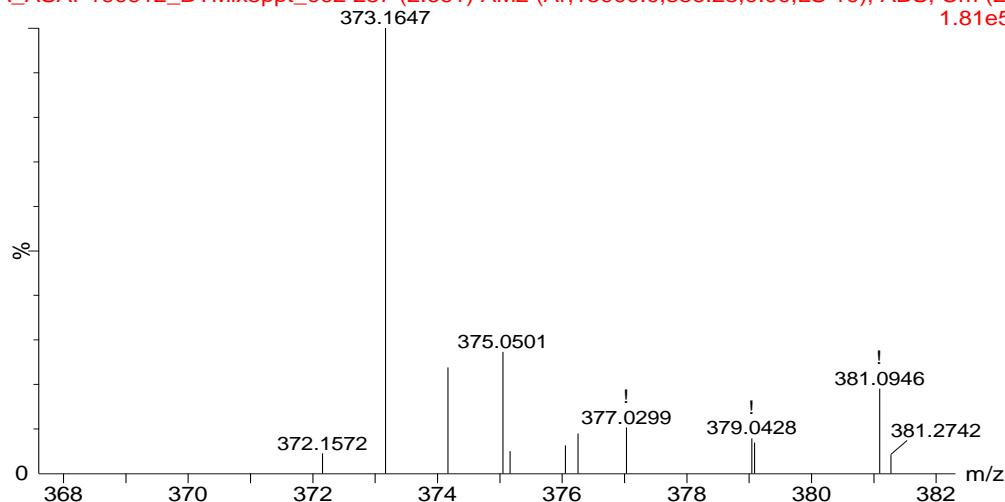


Fig. 4-102 ASAP(+), sen mode mass spectrum of mix-5 precipitate under optimized conditions showing a dimer of PP-BP

among the dimers is a self-coupled dimer of BP, Figure 4-103, at m/z 387.1796 having a molecular formula $C_{22}H_{26}O_6$ and a structural formula Figure 4-104 (k).

ASAP(+) sen mode MS, lockspray, Probe T=300oC, source 100oC, t=0 IPwCap, BYMix5ppt,
JA_ASAP190912_BYMix5ppt_002 309 (2.872) AM2 (Ar,22000.0,556.28,0.00,LS 10); Cm (308:313-49:54)

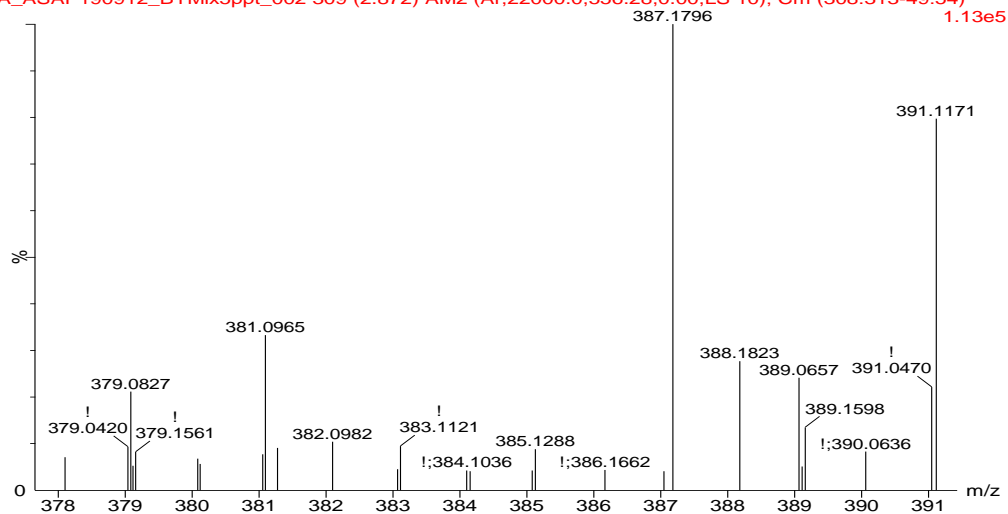


Fig. 4-103 ASAP(+)
mass spectrum of mix-5 precipitate under optimized conditions showing a dimer of BP-BP

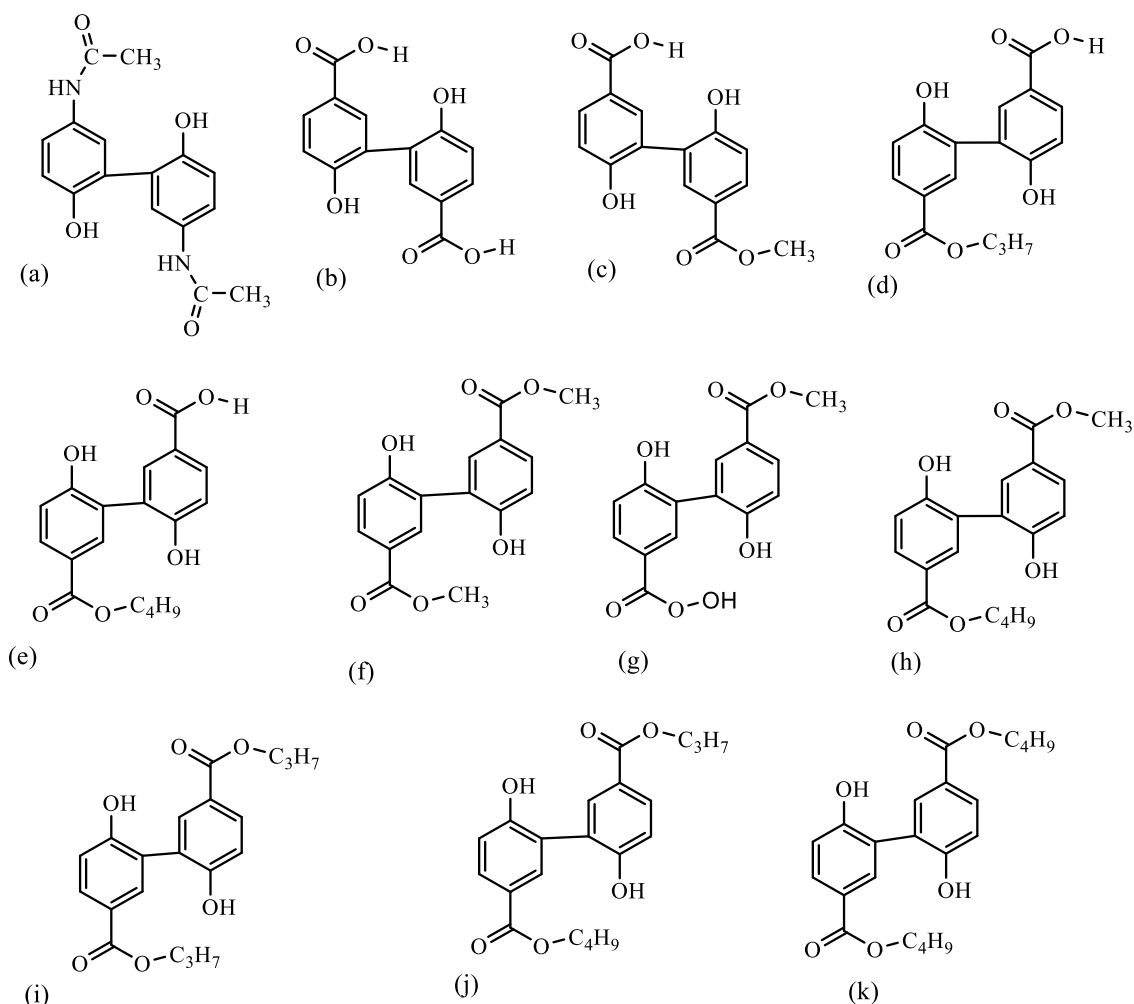


Fig.4-104 Proposed structural formulae for the dimers of mix-5 under optimized conditions

4.8.2 Trimers from mix-5 precipitate

Based on the combinations obtained, 35 different trimers were supposed to be detected from the mix-5 reactions. However, no cross-coupling with acetaminophen was observed, accounting for 15 different trimers. Moreover, due to the poor reactivity of PHBA, no homo-trimer of PHBA was found. A trimer of BP was found in the precipitate but not in the supernatant. This is expected since BP has higher octanol-water partition coefficient than all the other compounds in the mixture, it is expected to easily precipitate when in aqueous solution. Therefore, 19 trimers are represented in Figures 4-105 to 4-123, summarized in Table 4-13, plausible structures Figures 4-124.

Table 4-13 Trimers detected from mix-5 precipitate under optimized conditions using ASAP(+) ionization mode

Combination	Molecular formula	M ⁺ _{theo}	M ⁺ _{expt}	Ppm
PHBA-PHBA-MP	C ₂₂ H ₁₆ O ₉	425.0873	425.0860	-3.1
PHBA-MP-MP	C ₂₃ H ₁₈ O ₉	439.1029	439.1042	3.0
PHBA-PHBA-PP	C ₂₄ H ₂₀ O ₉	453.1186	453.1192	1.3
MP-MP-MP	C ₂₄ H ₂₀ O ₉	453.1186	453.1192	1.3
PHBA-PHBA-BP	C ₂₅ H ₂₂ O ₉	467.1342	467.1353	2.4
PHBA-MP-PP	C ₂₅ H ₂₂ O ₉	467.1342	467.1353	2.4
PHBA-MP-BP	C ₂₆ H ₂₄ O ₉	481.1499	481.1509	2.1
MP-MP-PP	C ₂₆ H ₂₄ O ₉	481.1499	481.1509	2.1
PHBA-PP-PP	C ₂₇ H ₂₆ O ₉	495.1655	495.1646	-1.8
MP-MP-BP	C ₂₇ H ₂₆ O ₉	495.1655	495.1646	-1.8
PHBA-PP-BP	C ₂₈ H ₂₈ O ₉	509.1812	509.1805	-1.4
MP-PP-PP	C ₂₈ H ₂₈ O ₉	509.1812	509.1805	-1.4
PHBA-BP-BP	C ₂₉ H ₃₀ O ₉	523.1968	523.1959	-1.7
MP-PP-BP	C ₂₉ H ₃₀ O ₉	523.1968	523.1959	-1.7
MP-BP-BP	C ₃₀ H ₃₂ O ₉	537.2125	537.2112	-2.4
PP-PP-PP	C ₃₀ H ₃₂ O ₉	537.2125	537.2112	-2.4
PP-PP-BP	C ₃₁ H ₃₄ O ₉	551.2281	551.2271	-1.8
PP-BP-BP	C ₃₂ H ₃₆ O ₉	565.2438	565.2425	-2.3
BP-BP-BP	C ₃₃ H ₃₈ O ₉	579.2594	579.2557	-6.4

The trimer of protonated PHBA-PHBA-MP is found at m/z 425.0860 (Figure 4-105) and corresponds to the molecular formula C₂₂H₁₆O₉ with a structural formula Figure 4-124 (a). Since PHBA is poor in oligomerizing, it is plausible to reason the incoming paraben radical acted as a bridge to link the two molecules together. The m/z peak at 393.0620 is thought to be for a fragment from the loss of -OCH₃ from the MP residue. Figure 4-106 has an m/z peak at 453.1192 with a molecular formula C₂₄H₂₀O₉ that is a

ASAP(+) sen mode MS, lockspray, Probe T=300oC, source 100oC, t=0 IPwCap, I
 JA_ASAP190912_BYMix5ppt_002 287 (2.661) AM2 (Ar,15000.0,556.28,0.00,LS 10); ABS; Cm (z
 1.33e5

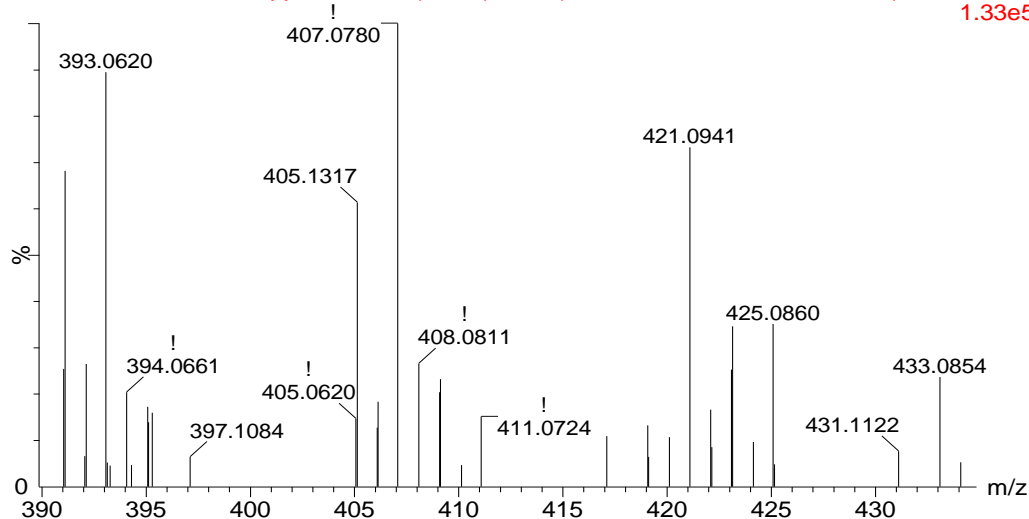


Fig. 4-105 ASAP(+) mass spectrum of mix-5 precipitate under optimized conditions showing a trimer of PHBA-PHBA-MP

trimer of PHBA-PHBA-PP with structural formula Figure 4-124 (b). The loss of -OH and -OC₃H₇ account for the m/z peaks 421.0941 and 393.0620, respectively.

ASAP(+) sen mode MS, lockspray, Probe T=300oC, source 100oC, t=0 IPwCap, I
 JA_ASAP190912_BYMix5ppt_002 287 (2.661) AM2 (Ar,15000.0,556.28,0.00,LS 10); ABS; Cm (z
 2.19e5

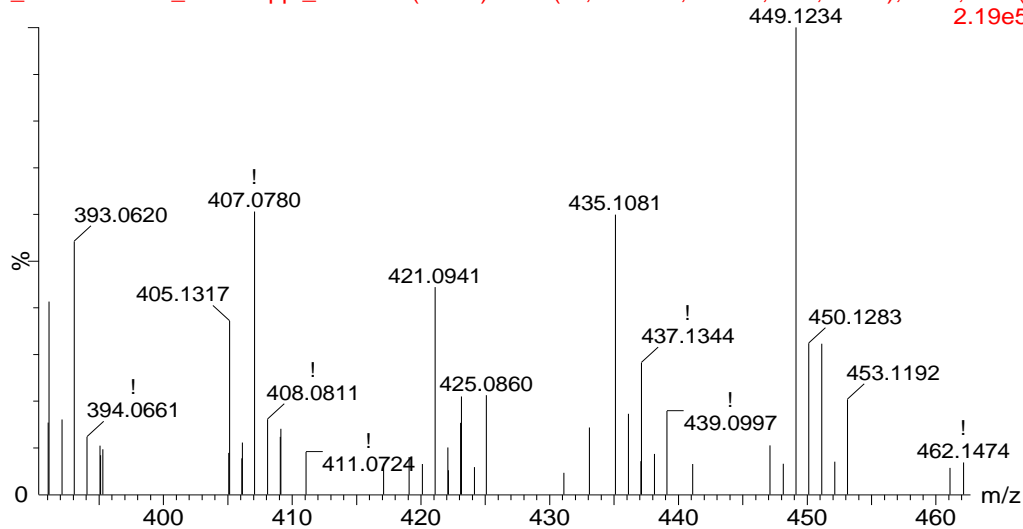


Fig. 4-106 ASAP(+) mass spectrum of mix-5 precipitate under optimized conditions showing a trimer of PHBA-PHBA-PP

Likewise, the m/z peak at 467.1353 in Figure 4-107 corresponds to a trimer of PHBA-PHBA-BP with molecular structure $C_{25}H_{22}O_9$ and molecular formula 4-124 (c). The m/z peak at 393.0620 may be for a fragment from the loss of protonated $-OC_4H_9$ of BP. The

ASAP(+) sen mode MS, lockspray, Probe T=300oC, source 100oC, t=0 IPwCap, I
 JA_ASAP190912_BYMix5ppt_002 287 (2.661) AM2 (Ar,15000.0,556.28,0.00,LS 10); ABS; Cm (z
 2.19e5

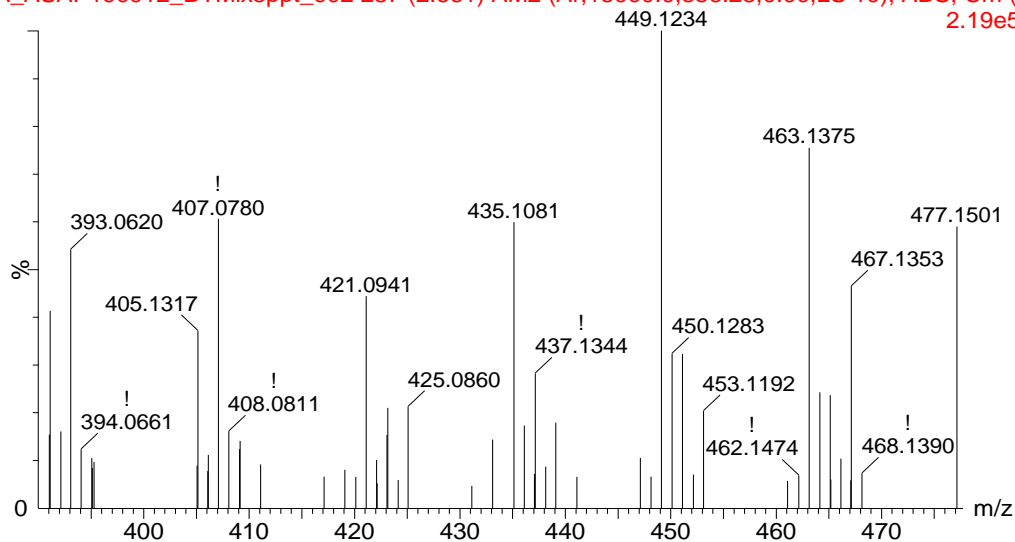


Fig. 4-107 ASAP(+) mass spectrum of mix-5 precipitate under optimized conditions showing a trimer of PHBA-PHBA-BP

consistent pattern of 14 amu peaks downwards the lower side of the mass spectrum, suggests the successive loss of methylene groups from the respective molecular ions. This pattern has been generally observed in the mass spectra, in addition to the alkoxy group fragmentation patterns earlier mentioned. Figure 4-108 shows a trimer of PHBA-MP-MP at m/z 439.1042 corresponding to the molecular formula $C_{23}H_{18}O_9$ with a structural formula Figure

ASAP(+) sen mode MS, lockspray, Probe T=300oC, source 100oC, t=0 IPwCap, B
 JA_ASAP190912_BYMix5ppt_002 170 (1.589) AM2 (Ar,22000.0,556.28,0.00,LS 10); Cm (165:170) 3.12e4

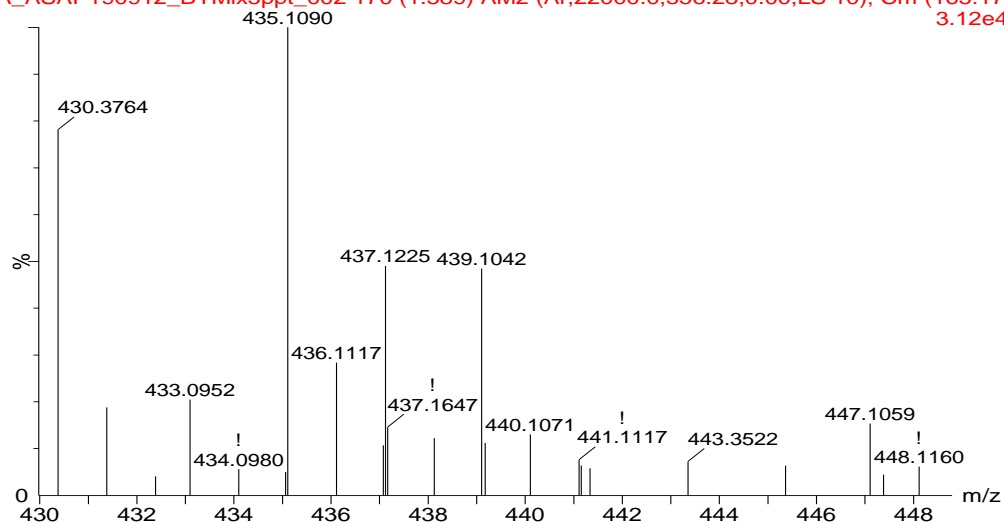


Fig. 4-108 ASAP(+) mass spectrum of mix-5 precipitate under optimized conditions showing a trimer of PHBA-MP-MP

4-124 (d). Similarly, Figure 4-109 shows a trimer of PHBA-MP-PP at m/z 467.1353 with molecular formula $C_{25}H_{22}O_9$ and structural formula Figure-124 (e). In Figure

ASAP(+) sen mode MS, lockspray, Probe T=300oC, source 100oC, t=0 IPwCap, I
 JA_ASAP190912_BYMix5ppt_002 287 (2.661) AM2 (Ar,15000.0,556.28,0.00,LS 10); ABS; Cm (165:170) 2.19e5

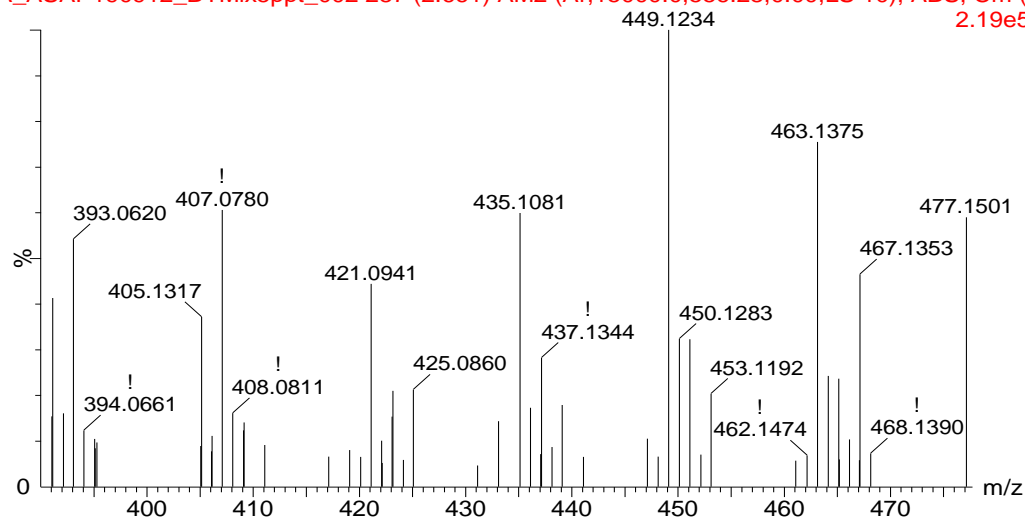


Fig. 4-109 ASAP(+) mass spectrum of mix-5 precipitate under optimized conditions showing a trimer of PHBA-MP-PP

4-110, a trimer of PHBA-MP-BP is seen at m/z 481.1509 with molecular formula $C_{26}H_{24}O_9$ and structural formula Figure 4-124 (f). The m/z peak at 407.0780 may be formed when $-OC_4H_9$ from the BP residue cleaves from the trimer molecule.

ASAP(+) sen mode MS, lockspray, Probe T=300oC, source 100oC, t=0 IPwCap, I
 JA_ASAP190912_BYMix5ppt_002 287 (2.661) AM2 (Ar,15000.0,556.28,0.00,LS 10); ABS; Cm (z
 2.19e5

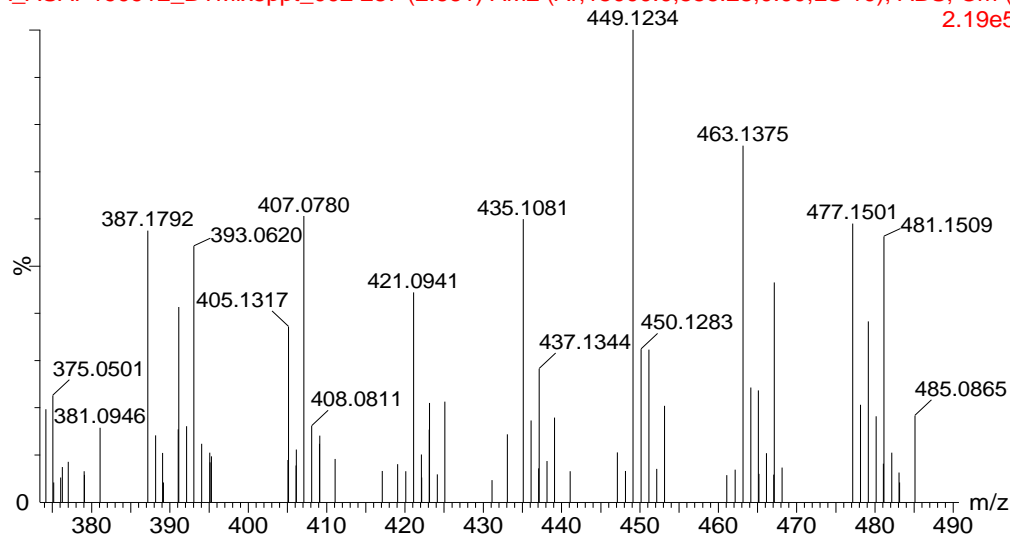


Fig. 4-110 ASAP(+) mass spectrum of mix-5 precipitate under optimized conditions showing a trimer of PHBA-MP-BP

Figure 4-111 shows the trimer of PHBA-PP-PP at m/z 495.1646 with molecular formula $C_{27}H_{26}O_9$ and structural formula Figure 4-124 (g). The m/z peak at 435.1081 corresponds to 60.0575 difference which may be a fragment of protonated $-OC_3H_7$ arising from a PP residue.

ASAP(+) sen mode MS, lockspray, Probe T=300oC, source 100oC, t=0 IPwCap, I
JA_ASAP190912_BYMix5ppt_002 287 (2.661) AM2 (Ar,15000.0,556.28,0.00,LS 10); ABS; Cm (z
2.19e5

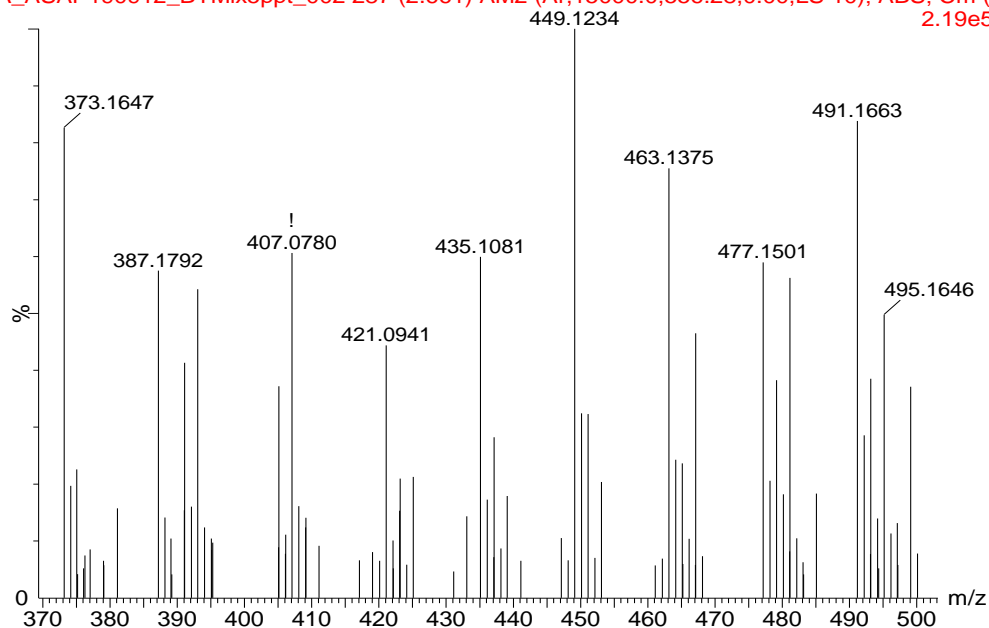


Fig. 4-111 ASAP(+) mass spectrum of mix-5 precipitate under optimized conditions showing a trimer of PHBA-PP-PP

From Figure 4-112, m/z peak at 509.1805 shows a trimer of PHBA-PP-BP. This corresponds to the molecular formula $C_{28}H_{28}O_9$ and structural formula Figure

ASAP(+) sen mode MS, lockspray, Probe T=300oC, source 100oC, t=0 IPwCap, I
JA_ASAP190912_BYMix5ppt_002 287 (2.661) AM2 (Ar,15000.0,556.28,0.00,LS 10); ABS; Cm (z
2.19e5

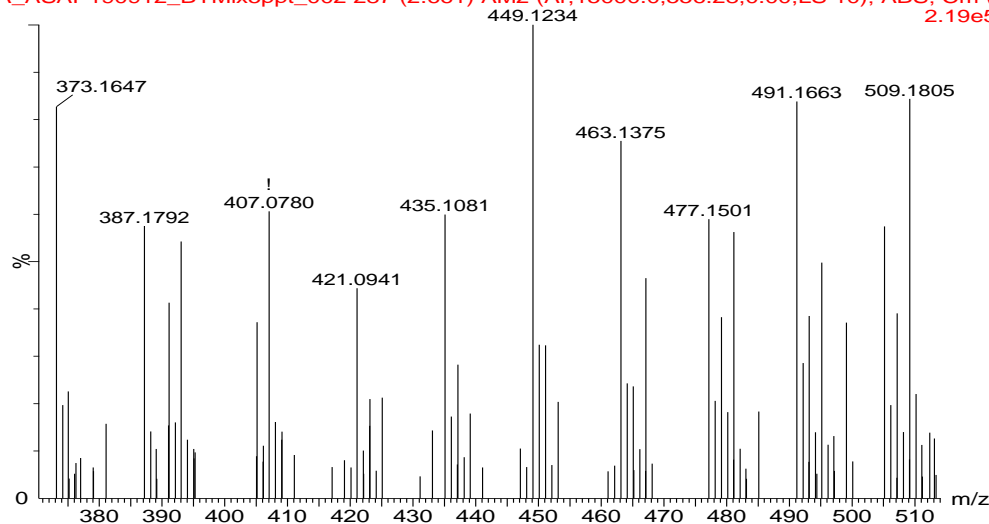
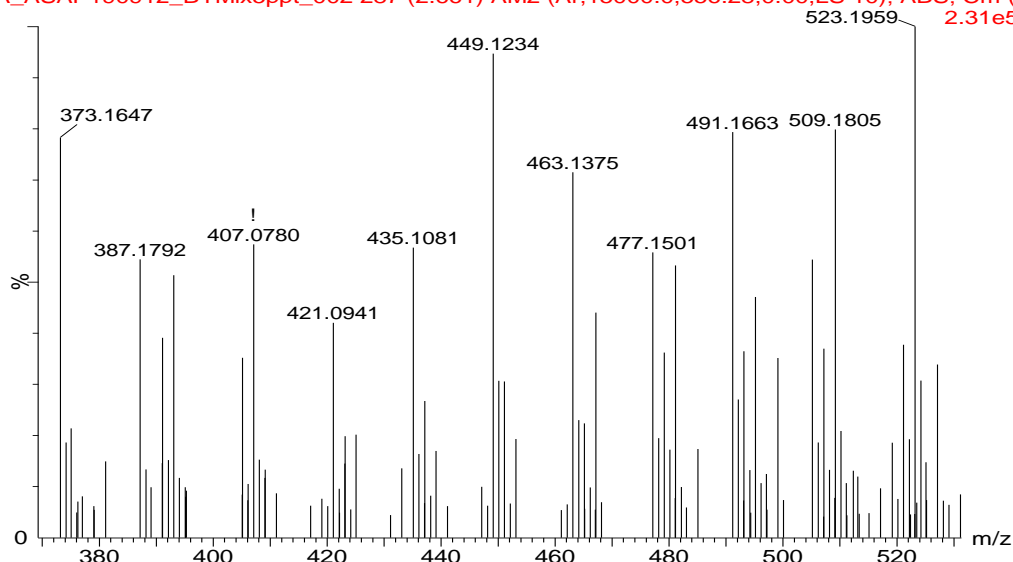


Fig. 4-112 ASAP(+) mass spectrum of mix-5 precipitate under optimized conditions showing a trimer of PHBA-PP-BP

4-124 (h). Again, different fragmentation patterns occur concurrently. Loss of $-\text{OC}_3\text{H}_7$ first accounts for the fragment with m/z 449.1234, followed by loss of $-\text{OC}_4\text{H}_9$ to account for the fragment at m/z 375.0501. Alternatively, with loss of $-\text{OC}_4\text{H}_9$ first, product with m/z peak 435.1081 is formed followed by loss of $-\text{OC}_3\text{H}_7$ to yield a fragment with m/z 375.0501. Since the intensity of 449.1234 is greater, it is thought the fragmentation of the trimer proceeds preferentially through the loss of $-\text{OC}_3\text{H}_7$ followed by $-\text{OC}_4\text{H}_9$. Alternatively, it may also be that there are other oligomers whose fragments give rise to the m/z peak at 449.1234, hence its strong intensity. Figure 4-113 shows the trimer of PHBA-BP-BP at m/z 523.1959 with a molecular formula of $\text{C}_{29}\text{H}_{30}\text{O}_9$ and structural formula Figure 4-124 (i). Fragmentation with successive loss of butyloxy groups produces

ASAP(+) sen mode MS, lockspray, Probe T=300oC, source 100oC, t=0 IPwCap, f
 JA_ASAP190912_BYMix5ppt_002 287 (2.661) AM2 (Ar,15000.0,556.28,0.00,LS 10); ABS; Cm (z
 523.1959 2.31e5



fragments with m/z 449.1234 and 375.0501. A protonated homo-trimer of MP is observed at m/z 453.1192 (Figure 4-114) having the molecular formula $\text{C}_{24}\text{H}_{20}\text{O}_9$ and structural formula Figure 4-124 (j). Cleavage of $-\text{OCH}_3$ groups in accounts for fragments at m/z 421.0941, 389.0638 and 357.0390.

ASAP(+) sen mode MS, lockspray, Probe T=300oC, source 100oC, t=0 IPwCap, I
 JA_ASAP190912_BYMix5ppt_002 287 (2.661) AM2 (Ar,15000.0,556.28,0.00,LS 10); ABS; Cm (2.19e5

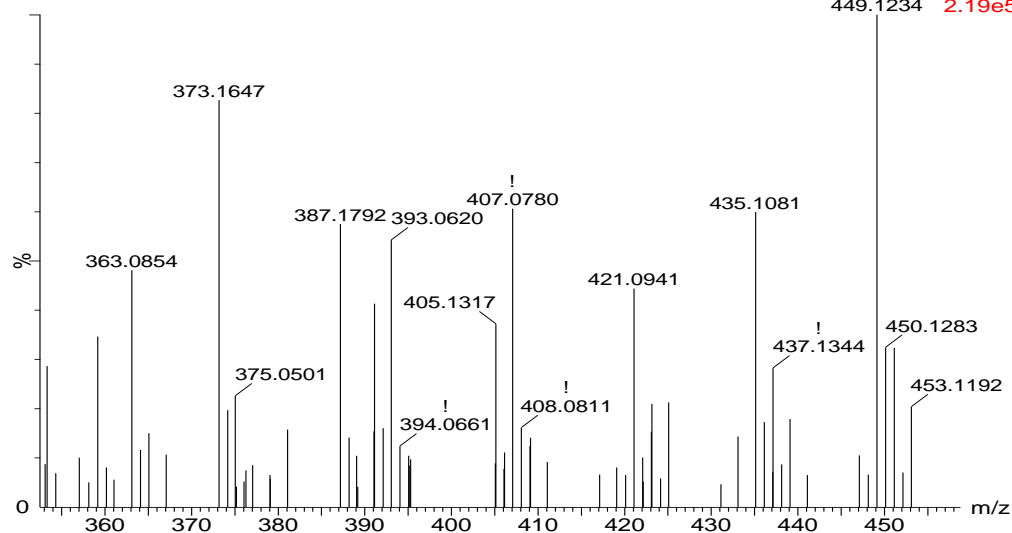


Fig. 4-114 ASAP(+) mass spectrum of mix-5 precipitate under optimized conditions showing a trimer of MP-MP-MP

Figure 4-115 shows m/z peak at 481.1509 corresponding to protonated trimer of MP-MP-PP with molecular formula $C_{26}H_{24}O_9$ and structural formula Figure 4-124 (k). The peak at m/z 421.0941 is consistent with loss of $-OC_3H_7$. Similarly,

ASAP(+) sen mode MS, lockspray, Probe T=300oC, source 100oC, t=0 IPwCap, BYMix5p
 JA_ASAP190912_BYMix5ppt_002 287 (2.661) AM2 (Ar,15000.0,556.28,0.00,LS 10); ABS; Cm (282:287-4:
 2.19e5

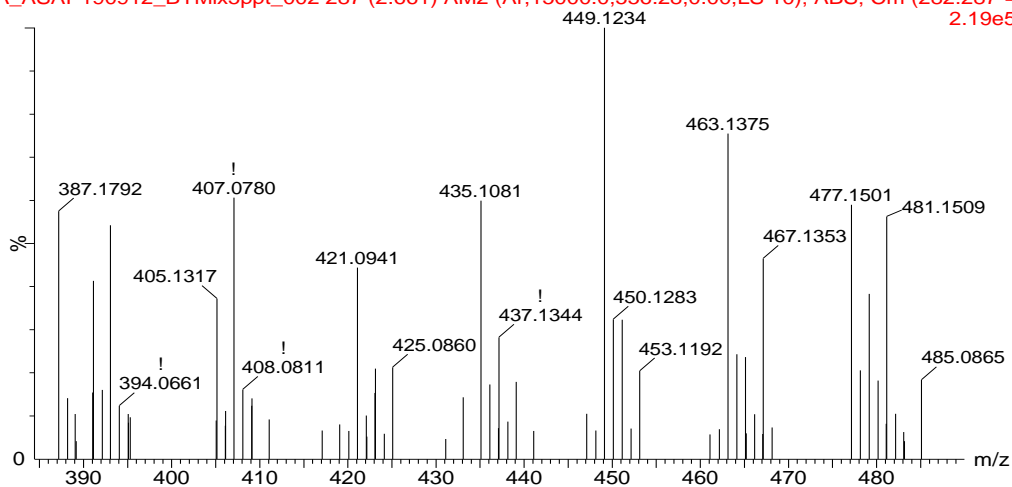


Fig. 4-115 ASAP(+) mass spectrum of mix-5 precipitate under optimized conditions showing a trimer of MP-MP-PP

Figure 4-116 shows a trimer of MP-MP-BP at m/z 495.1646 having a molecular formula $C_{27}H_{26}O_9$ and structural formula Figure 4-124 (l). A difference corresponding to a protonated $-OCH_3$ could be observed between the trimer m/z peak and that at 463.1375.

ASAP(+) sen mode MS, lockspray, Probe T=300oC, source 100oC, t=0 IPwCap, BYMix5;
 JA_ASAP190912_BYMix5ppt_002 287 (2.661) AM2 (Ar,15000.0,556.28,0.00,LS 10); ABS; Cm (282:287-4:
 2.19e5

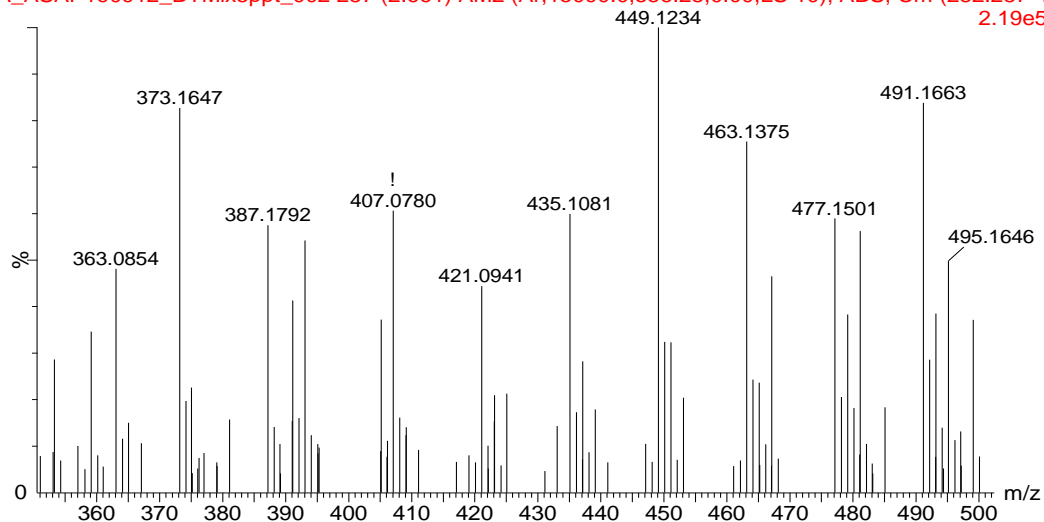


Fig. 4-116 ASAP(+) mass spectrum of mix-5 precipitate under optimized conditions showing a trimer of MP-MP-BP

A trimer of MP-PP-PP is observed at m/z 509.1805 (Figure 4-117) corresponding to a molecular formula $C_{28}H_{28}O_9$ and structural formula Figure 4-124 (m). Loss of protonated $-OC_3H_7$ from either of the PP residues may produce a peak at m/z 449.1234.

ASAP(+) sen mode MS, lockspray, Probe T=300oC, source 100oC, t=0 IPwCap, BYMix5p
JA_ASAP190912_BYMix5ppt_002 287 (2.661) AM2 (Ar,15000.0,556.28,0.00,LS 10); ABS; Cm (282:287-4:
2.19e5

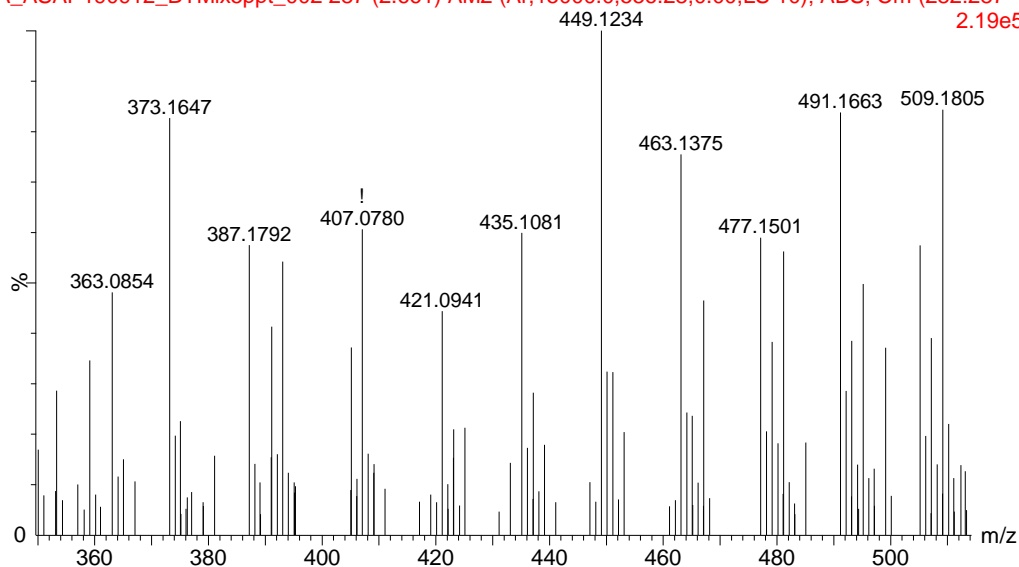


Fig. 4-117 ASAP(+) mass spectrum of mix-5 precipitate under optimized conditions showing a trimer of MP-PP-PP

Figure 4-118 shows a m/z peak at 523.1959 for a trimer of MP-PP-BP having a molecular formula $C_{29}H_{30}O_9$ and structural formula Figure 4-124 (n). Loss of $-OC_4H_9$ group leaves a fragment with m/z 449.1234.

ASAP(+) sen mode MS, lockspray, Probe T=300oC, source 100oC, t=0 IPwCap, BYMix5p
JA_ASAP190912_BYMix5ppt_002 287 (2.661) AM2 (Ar,15000.0,556.28,0.00,LS 10); ABS; Cm (282:287-4:
2.31e5

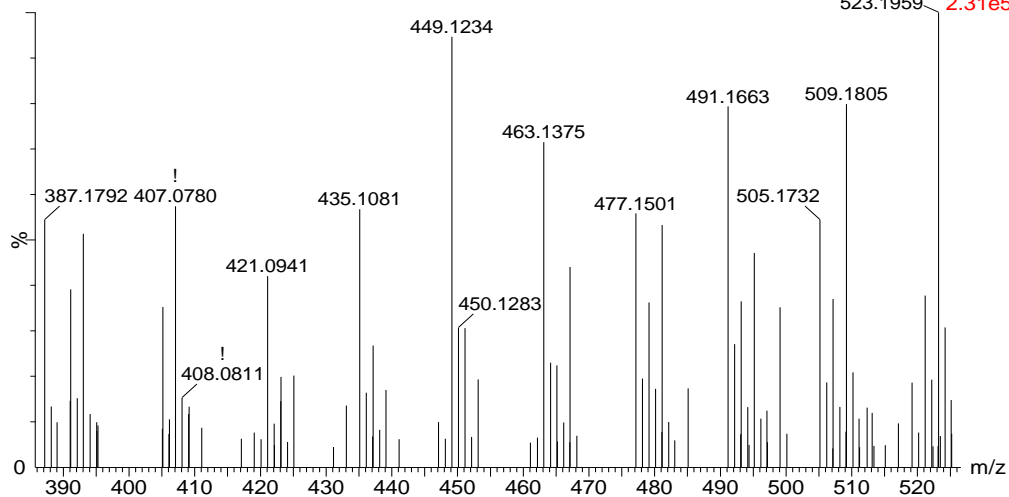


Fig. 4-118 ASAP(+) mass spectrum of mix-5 precipitate under optimized conditions showing a trimer of MP-PP-BP

Figure 4-119 shows a protonated m/z peak for a trimer of MP-BP-BP at 537.2112 having a molecular formula $C_{30}H_{32}O_9$ and structural formula at Figure 4-124 (o). Cleavage of $-OC_4H_9$ from a BP is consistent with a strong peak at m/z 463.1375.

ASAP(+) sen mode MS, lockspray, Probe T=300oC, source 100oC, t=0 IPwCap, BYMix5p; JA_ASAP190912_BYMix5ppt_002 287 (2.661) AM2 (Ar,15000.0,556.28,0.00,LS 10); ABS; Cm (282:287-4: 523.1959 2.31e5

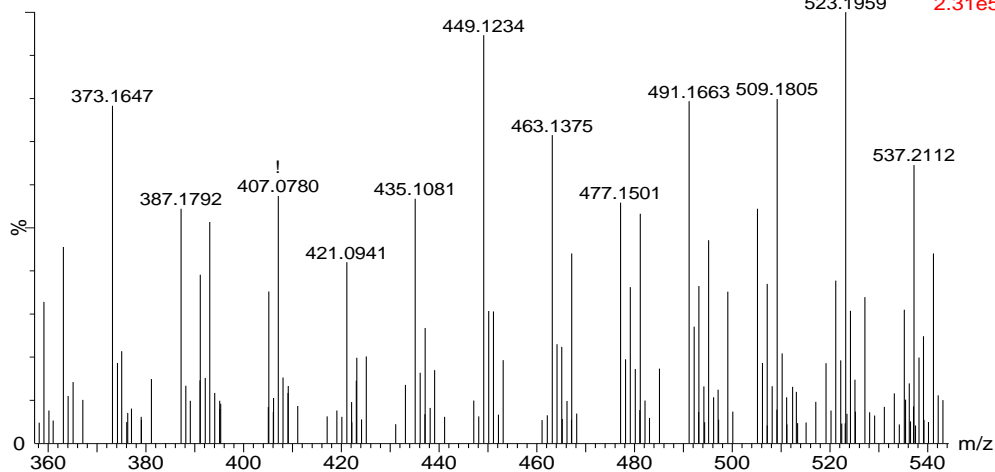


Fig. 4-119 ASAP(+)

 mass spectrum of mix-5 precipitate under optimized conditions showing a trimer of MP-BP-BP

Likewise, a homotrimer of PP is found at $m/z = 537.2112$ (Figure 4-120) assigned

ASAP(+) sen mode MS, lockspray, Probe T=300oC, source 100oC, t=0 IPwCap, BYMix5p; JA_ASAP190912_BYMix5ppt_002 287 (2.661) AM2 (Ar,15000.0,556.28,0.00,LS 10); ABS; Cm (282:287-4: 523.1959 2.31e5

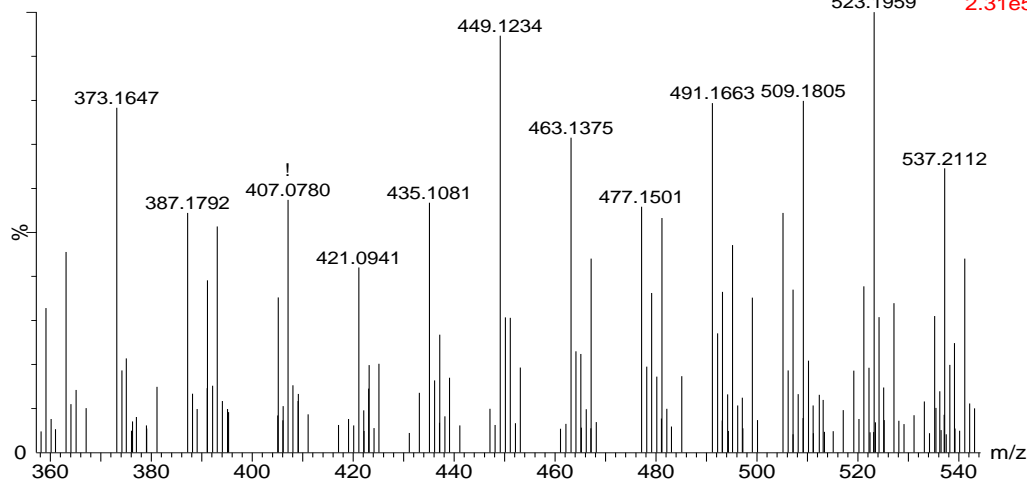


Fig. 4-120 ASAP(+)

 mass spectrum of mix-5 precipitate under optimized conditions showing a trimer of PP-PP-PP

the molecular formula $C_{30}H_{32}O_9$ and structural formula Figure 4-124 (p). Fragmentation of any of the alkyloxy groups would yield a fragment at m/z 477.1501 (with successive alkyloxy losses only noticeable with scale expansion at m/z 417.0963 and 357.0380).

Similarly, Figure 4-121 shows a trimer of PP-PP-BP at m/z 551.2271 assigned molecular formula $C_{31}H_{34}O_9$ and structural formula Figure 4-124 (q). The peak at m/z 491.1663 accounts for loss of $-OC_3H_7$ from the trimer. In Figure 4-122, a trimer of PP-BP-BP is observed at m/z 565.2425 corresponding to a molecular formula $C_{32}H_{36}O_9$ and structural formula Figure 4-124 (r). Loss of $-OC_3H_7$ produced the fragment with m/z 491.1663.

ASAP(+) sen mode MS, lockspray, Probe T=300oC, source 100oC, t=0 IPwCap, BYMix5p
JA_ASAP190912_BYMix5ppt_002 287 (2.661) AM2 (Ar,15000.0,556.28,0.00,LS 10); ABS; Cm (282:287-4;
2.31e5

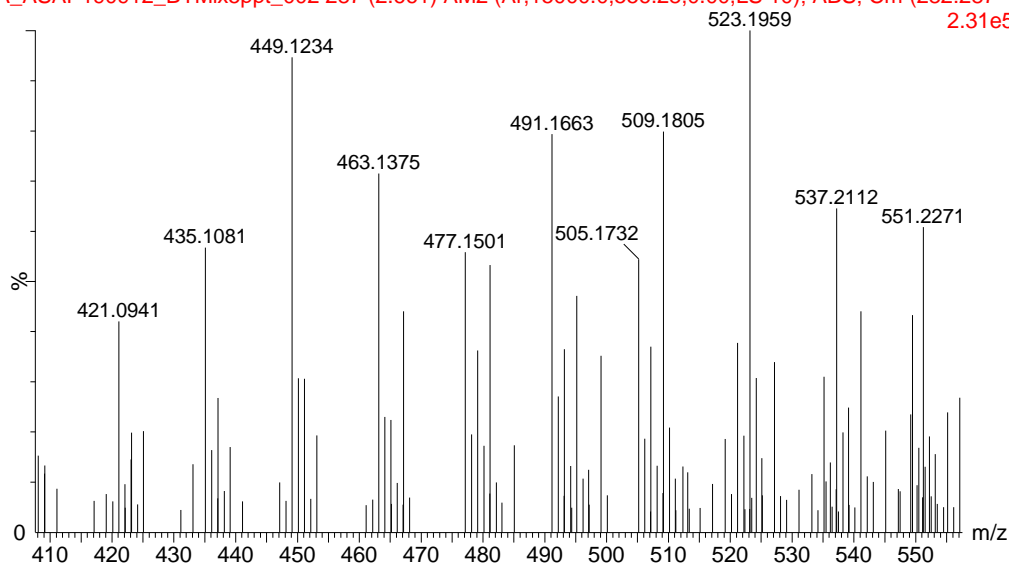


Fig. 4-121 ASAP(+)
mass spectrum of mix-5 precipitate under optimized conditions showing a trimer of PP-PP-BP

ASAP(+) sen mode MS, lockspray, Probe T=300oC, source 100oC, t=0 IPwCap, B
 JA_ASAP190912_BYMix5ppt_002 287 (2.661) AM2 (Ar,15000.0,556.28,0.00,LS 10); ABS; Cm (28
 4.42e5

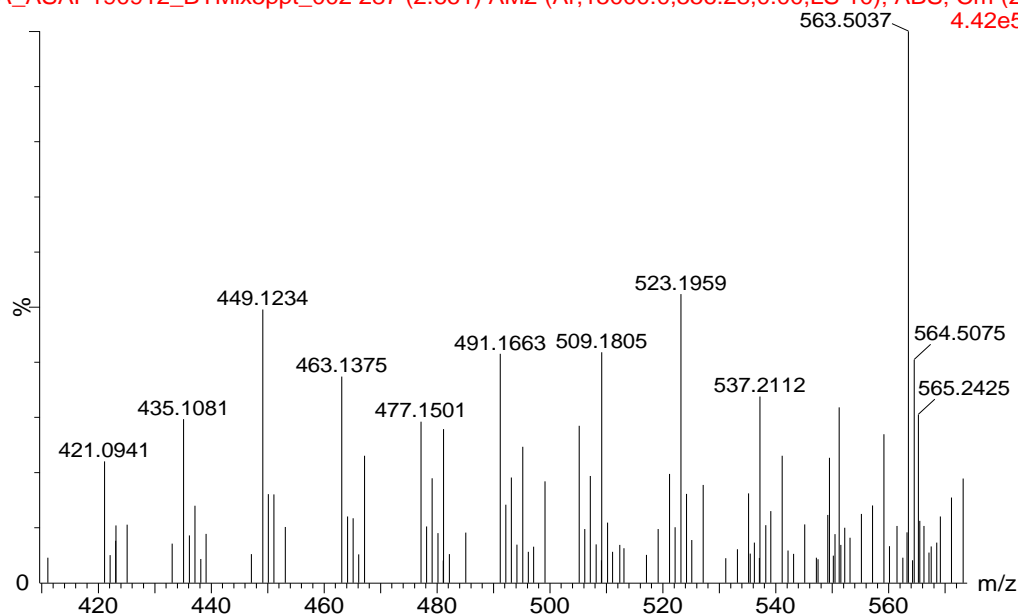


Fig. 4-122 ASAP(+) mass spectrum of mix-5 precipitate under optimized conditions showing a trimer of PP-BP-BP

A homo trimer of BP was noticed having a protonated m/z at 579.2557 (Figure 4-123) and corresponds to a molecular formula $C_{33}H_{38}O_9$ and structural formula Figure 4-124 (s).

ASAP(+) sen mode MS, lockspray, Probe T=300oC, source 100oC, t=0 IPwCap, B
 JA_ASAP190912_BYMix5ppt_002 287 (2.661) AM2 (Ar,15000.0,556.28,0.00,LS 10); ABS; Cm (28
 1.43e5

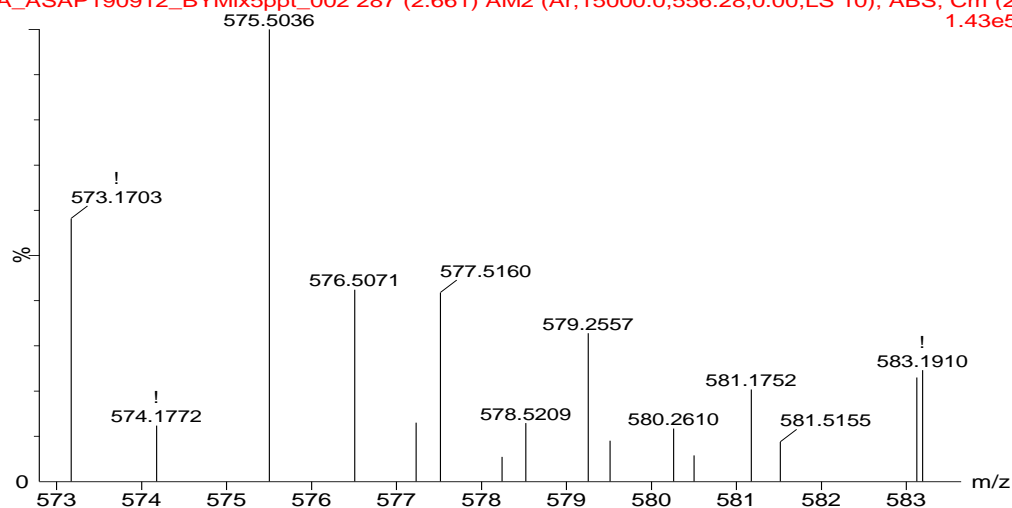


Fig. 4-123 ASAP(+) mass spectrum of mix-5 precipitate under optimized conditions showing a trimer of BP-BP-BP

Plausible structures of the oligomers are presented in Figure 4-124 are based on the monomer residues identified. Other regioisomers are possible and these represent only a diagrammatic illustration of the type of products obtained. Detailed structural analysis of these oligomers are outside the objectives of this study.

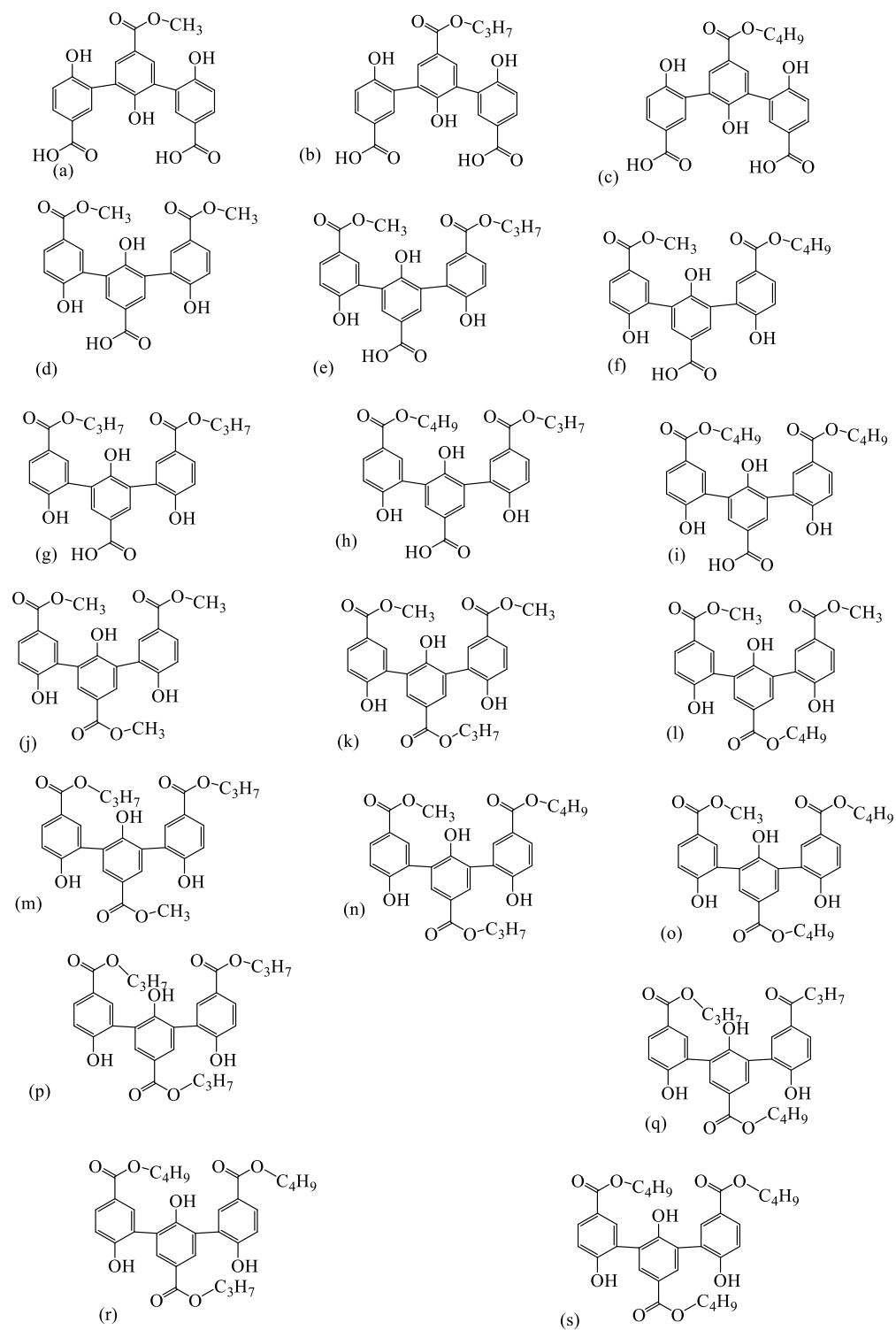


Fig. 4-124. Proposed structural formulae for the trimers of mix-5 under optimized conditions

4.8.3 Tetramers from mix-5 precipitate

Based on the combination patterns generated, 70 tetramers were expected. Acetaminophen cross-coupled oligomers were not detected under the reaction conditions, representing 35 expected combinations. Since a 10-ppm error margin was employed, other oligomers with error deviations above this were rejected. Thus, 20 tetramer oligomers were resolved within the set error limits (Table 4-14).

Table 4-14 Tetramers detected from mix-5 precipitate under optimized conditions using ASAP(+) ionization mode

Combinations	Molecular Formulae	M^{+}_{theo}	M^{+}_{expt}	Ppm
PHBA-PHBA-PHBA-PP	$C_{31}H_{24}O_{12}$	589.1346	589.1322	-4.1
PHBA-MP-MP-MP	$C_{31}H_{24}O_{12}$	589.1346	589.1322	-4.1
PHBA-PHBA-PHBA-BP	$C_{32}H_{26}O_{12}$	603.1503	603.1479	-4.0
PHBA-PHBA-MP-PP	$C_{32}H_{26}O_{12}$	603.1503	603.1479	-4.0
PHBA-PHBA-MP-BP	$C_{33}H_{28}O_{12}$	617.1659	617.1668	1.5
PHBA-MP-MP-PP	$C_{33}H_{28}O_{12}$	617.1659	617.1668	1.5
PHBA-PHBA-PP-PP	$C_{34}H_{30}O_{12}$	631.1816	631.1765	-8.1
PHBA-MP-MP-BP	$C_{34}H_{30}O_{12}$	631.1816	631.1765	-8.1
MP-MP-MP-PP	$C_{34}H_{30}O_{12}$	631.1816	631.1765	-8.1
PHBA-PHBA-PP-BP	$C_{35}H_{32}O_{12}$	645.1972	645.193	-6.5
PHBA-MP-PP-PP	$C_{35}H_{32}O_{12}$	645.1972	645.193	-6.5
MP-MP-MP-BP	$C_{35}H_{32}O_{12}$	645.1972	645.193	-6.5
PHBA-PHBA-BP-BP	$C_{36}H_{34}O_{12}$	659.2129	659.208	-7.4
MP-MP-PP-PP	$C_{36}H_{34}O_{12}$	659.2129	659.208	-7.4
PHBA-MP-PP-BP	$C_{36}H_{34}O_{12}$	659.2129	659.208	-7.4
PHBA-PP-PP-BP	$C_{38}H_{38}O_{12}$	687.2442	687.2373	-10.0
MP-MP-BP-BP	$C_{38}H_{38}O_{12}$	687.2442	687.2373	-10.0
MP-PP-PP-PP	$C_{38}H_{38}O_{12}$	687.2442	687.2373	-10.0
PHBA-PP-BP-BP	$C_{39}H_{40}O_{12}$	701.2598	701.2538	-8.6
MP-PP-PP-BP	$C_{39}H_{40}O_{12}$	701.2598	701.2538	-8.6

Among the twenty, eight isomers comprised of two or more isomers differing only in the distribution of carbons in their acyloxy groups, hereafter dubbed acyloxy carbon count isomers. For example, a tetramer with an acyloxy carbon count of 4 could be comprised of

PHBA-PHBA-PHBA-BP, MP-MP-MP-MP-MP and/or PHBA-PHBA-MP-PP. Detected tetramers from mix-5 precipitate are presented in the following detailed mass spectra on Figures 4-125 to 132. Tentative structures are shown in Figure 4-133.

Figure 4-125 shows a protonated tetramer peak at m/z 589.1322, corresponding to parent molecular formula $C_{31}H_{24}O_{12}$. A plausible structure is shown in Figure 4-133 (a) the tetramer PHBA-PHBA-PHBA-PP (or its acyloxy carbon-count isomer, PHBA-MP-MP-MP which is not drawn). The oligomerization of three monomers of PHBA in the former is thought to be facilitated through PP, which may act as a bridge to connect PHBA residues, since only a dimer of this compound was found in the single-compound study, for which explanations were made earlier. This illustrates the enhanced removal effect on compounds in a mixture treatment process over

ASAP(+) sen mode MS, lockspray, Probe T=300oC, source 100oC, t=0 IPwCap, B'
 JA_ASAP190912_BYMix5ppt_002 287 (2.661) AM2 (Ar,15000.0,556.28,0.00,LS 10); ABS; Cm (2E
 9.52e4

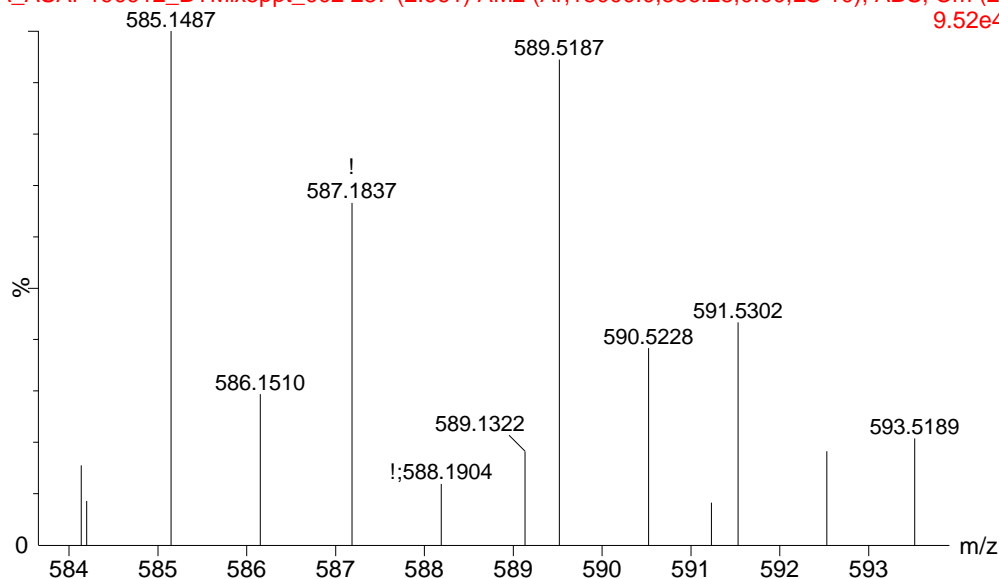


Fig.4-125 ASAP(+) mass spectrum of mix-5 precipitate under optimized conditions showing a tetramer (matching PHBA-PHBA-PHBA-PP and PHBA-MP-MP-MP)

single-compound treatment, as previously reported (Xiang *et al.* 2020, Pylypchuk *et al.* 2018). The peak may as well be only for the latter tetramer since tetramers of MP were observed in the single-compound study. Therefore, all reported structural formulae are plausible predictions based on the monomer residues accounting for the m/z peaks

obtained. Other isomeric patterns, regioselective variances are bound to be obtained other than the tentative structures reported for all the oligomers.

Figure 4-126 shows a protonated m/z peak at 603.1479, matching the parent PHBA-PHBA-PHBA-BP (and/or PHBA-PHBA-MP-PP and/or MP-MP-MP-MP) formula $C_{32}H_{26}O_{12}$, structure Figure 4-133 (b).

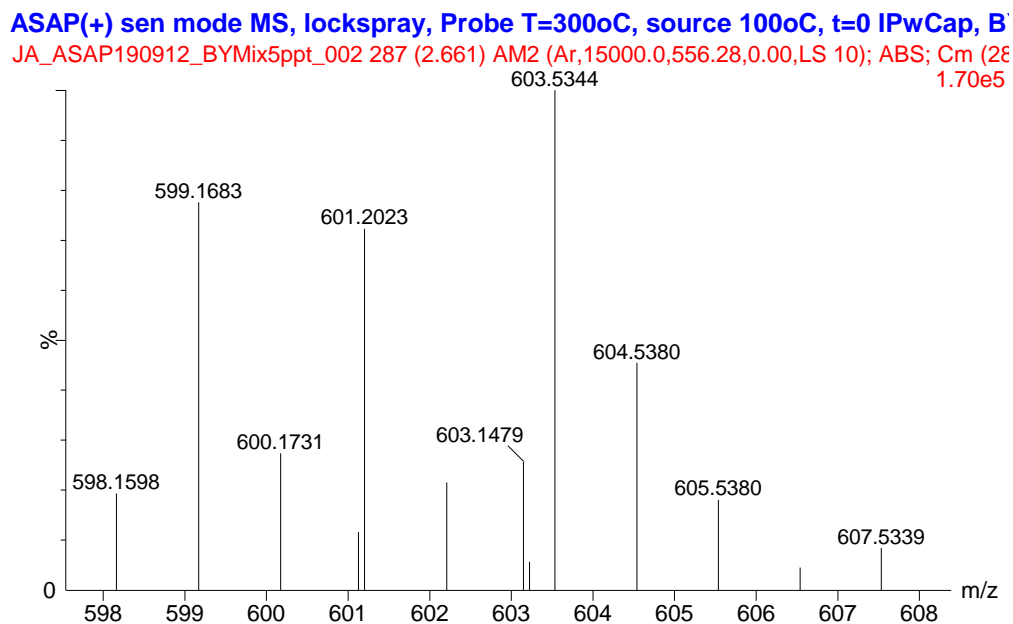


Fig.4-126 ASAP(+) mass spectrum of mix-5 precipitate under optimized conditions showing a tetramer matching PHBA-PHBA-PHBA-BP and acyloxy carbon count isomers

Figure 4-127 shows a protonated m/z peak at 617.1668, matching the parent PHBA-PHBA-MP-BP (and/or PHBA-MP-MP-PP) formula $C_{33}H_{28}O_{12}$, structure Figure 4-133 (c).

ASAP(+) sen mode MS, lockspray, Probe T=300oC, source 100oC, t=0 IPwCap, B'
 JA_ASAP190912_BYMix5ppt_002 287 (2.661) AM2 (Ar,15000.0,556.28,0.00,LS 10); ABS; Cm (28
 1.18e5

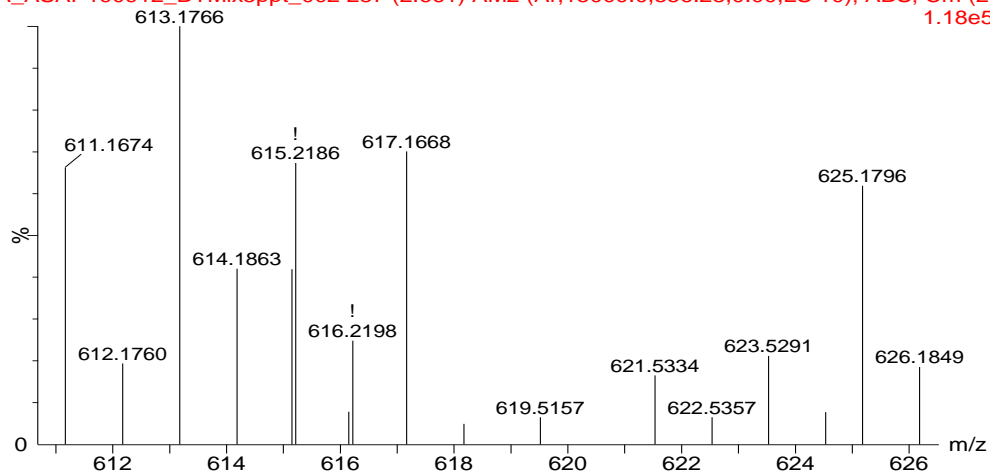


Fig.4-127 ASAP(+) mass spectrum of mix-5 precipitate under optimized conditions showing a tetramer matching PHBA-PHBA-MP-BP and PHBA-MP-MP-PP PHBA-PHBA-MP-BP (and/or PHBA-MP-MP-PP)

Figure 4-128 shows m/z peak at 631.1765, matching with the parent PHBA-PHBA-PP-PP (and/or PHBA-MP-MP-BP and/or MP-MP-MP-PP) formula $C_{34}H_{30}O_{12}$, structure

ASAP(+) sen mode MS, lockspray, Probe T=300oC, source 100oC, t=0 IPwCap, B'
 JA_ASAP190912_BYMix5ppt_002 287 (2.661) AM2 (Ar,15000.0,556.28,0.00,LS 10); ABS; Cm (28
 1.20e5

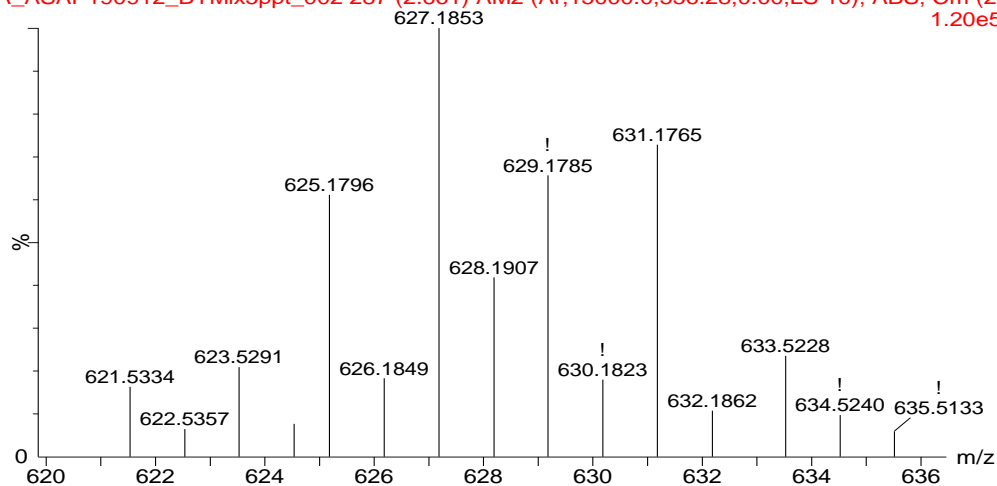


Fig. 4-128 ASAP(+) mass spectrum of mix-5 precipitate under optimized conditions showing tetramer matching to PHBA-PHBA-PP-PP and other acyloxy carbon count isomers

Figure 4-133 (d). Similarly, a tetramer m/z peak at 645.1930 (Figure 4-129) matching the parent PHBA-PHBA-PP-BP (and/or PHBA-MP-PP-PP and/or MP-MP-MP-BP) molecular formula $C_{35}H_{32}O_{12}$, structure Figure 4-133 (e).

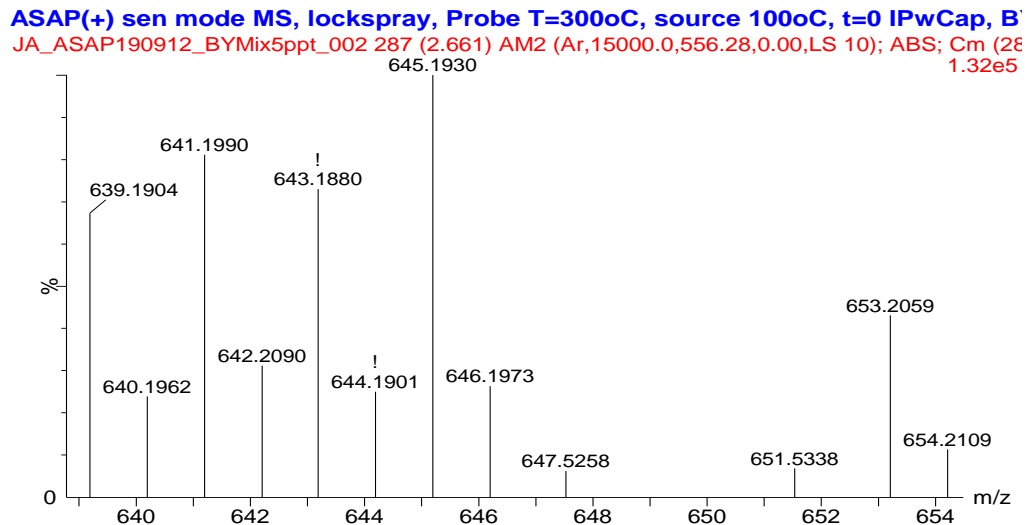


Fig.4-129 ASAP(+) mass spectrum of mix-5 precipitate under optimized conditions showing a tetramer of PHBA-PHBA-PP-BP and other acyloxy carbon count isomers

Figure 4-130 shows m/z peak at 659.2080, corresponding to the protonated

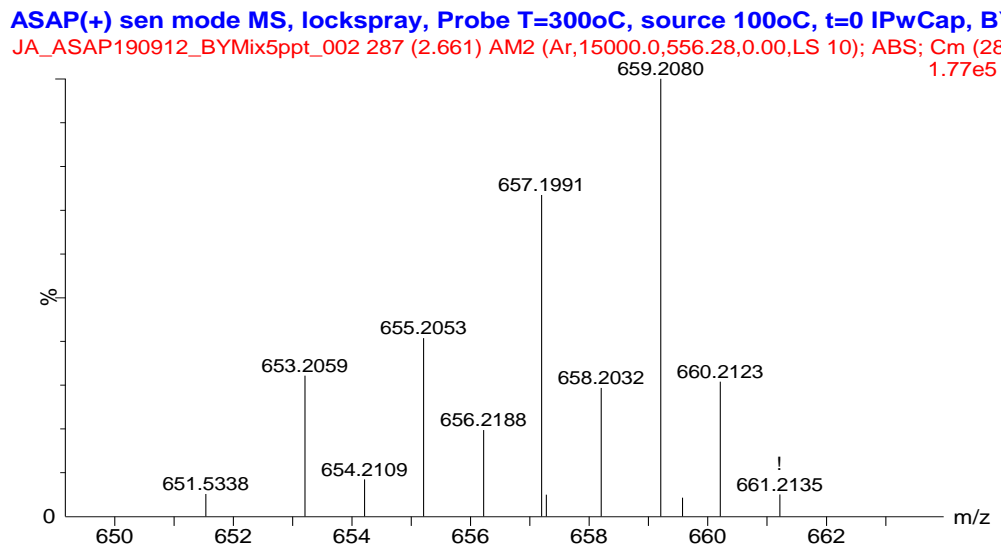


Fig. 4-130 ASAP(+) mass spectrum of mix-5 precipitate under optimized conditions showing a tetramer of PHBA-PHBA-BP-BP and other acyloxy carbon count isomers

molecular formula $C_{36}H_{34}O_{12}$, matching the parent PHBA-PHBA-BP-BP (and/or PHBA-MP-PP-BP and/or MP-MP-PP-PP), structure Figure 4-133 (f). Likewise, m/z peak at 687.2373 (Figure 4-131) matching the parent PHBA-PP-PP-BP, (and/or MP-MP-BP-BP, and/or MP-PP-PP-PP) formula $C_{38}H_{38}O_{12}$, structure Figure 4-133 (g).

ASAP(+) sen mode MS, lockspray, Probe T=300oC, source 100oC, t=0 IPwCap, B
 JA_ASAP190912_BYMix5ppt_002 287 (2.661) AM2 (Ar,15000.0,556.28,0.00,LS 10); ABS; Cm (28
 1.49e5

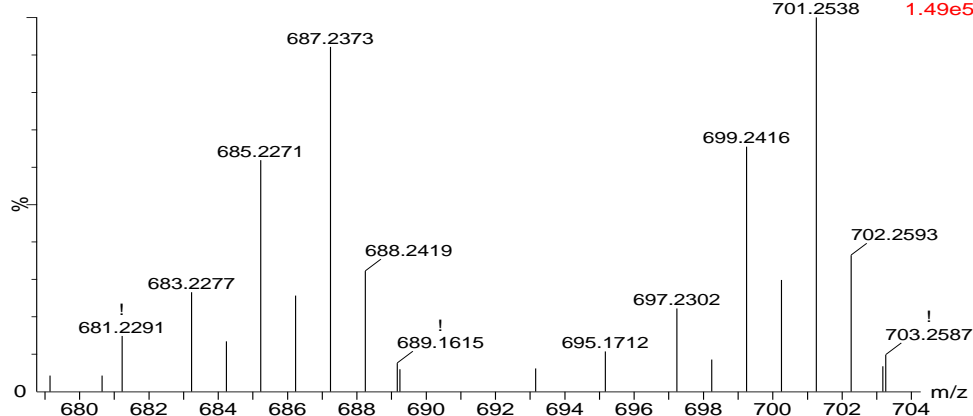


Fig. 4-131 ASAP(+) mass spectrum of mix-5 precipitate under optimized conditions showing a tetramer of PHBA-PP-PP-BP and acyloxy carbon count isomers

Figure 4-132 shows a protonated tetramer peak at m/z 701.2538, matching the parent PHBA-PP-PP-BP and/or MP-PP-PP-BP, formula $C_{39}H_{40}O_{12}$, structure Figure 4-133 (h).

ASAP(+) sen mode MS, lockspray, Probe T=300oC, source 100oC, t=0 IPwCap, B
 JA_ASAP190912_BYMix5ppt_002 287 (2.661) AM2 (Ar,15000.0,556.28,0.00,LS 10); ABS; Cm (28
 1.49e5

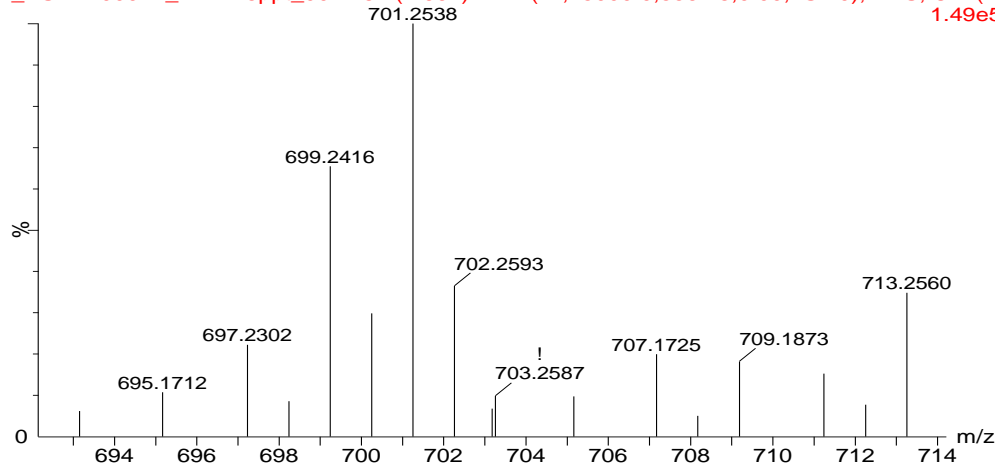


Fig. 4-132 ASAP(+) mass spectrum of mix-5 precipitate under optimized conditions showing a tetramer matching MP-PP-PP-BP and/or PHBA-PP-BP-BP

Proposed structures for these tetramers are presented (Figure 4-133), again, it shows the comprising monomeric units, without any isomeric or regioselective considerations.

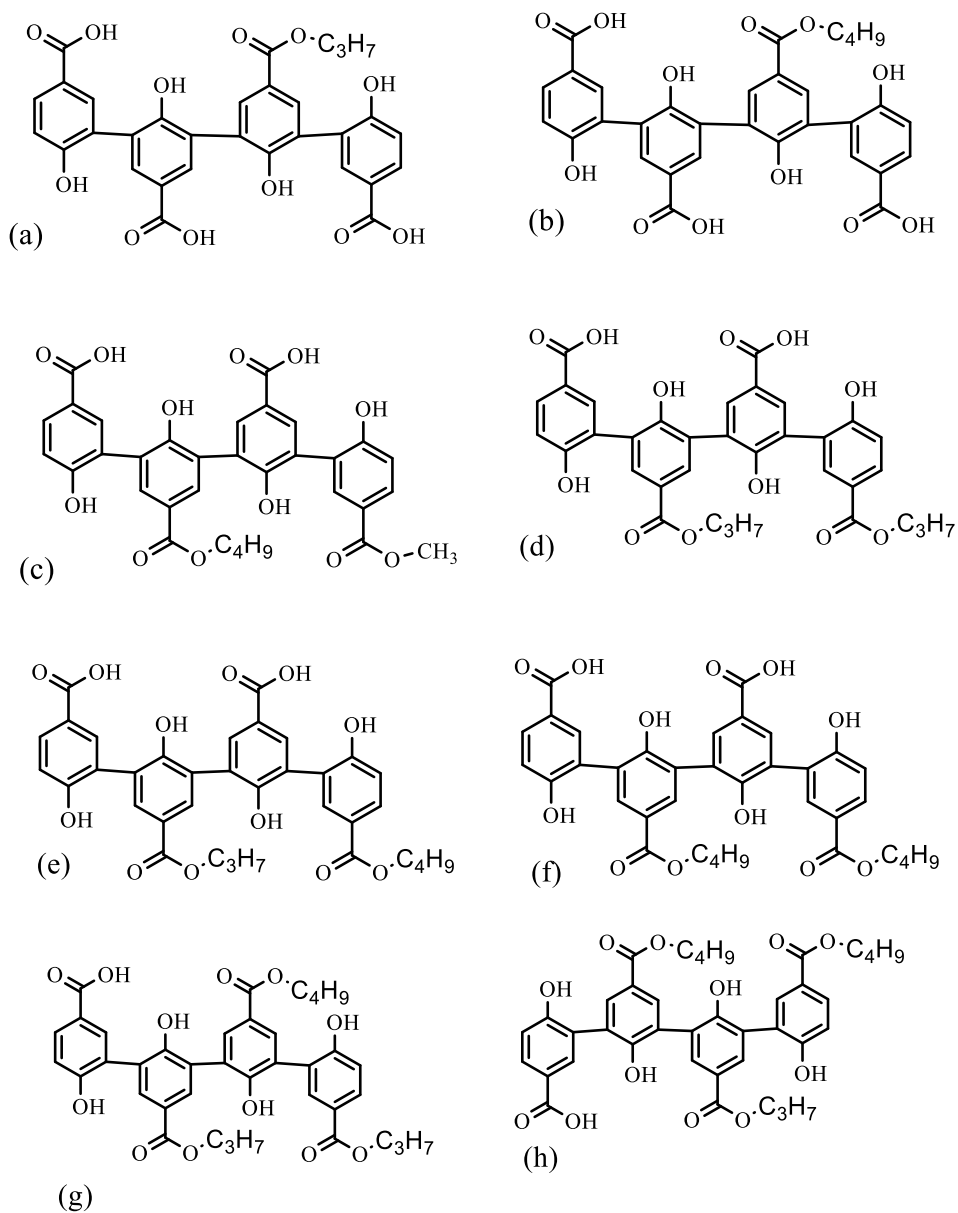


Fig.4-133. Proposed structural formulae for plausible tetramers combinations (but not permutations) of mix-5 under optimized conditions (other regioisomers and acyloxy carbon-count isomers are possible)

4.8.4 Pentamers from mix-5 precipitate

Combination patterns predicted 140 possible pentamers to be formed. Acetaminophen cross coupled oligomers, accounting for 75 pentamers could not be detected under the reaction conditions. Considering the 10-ppm error margin, several other pentamers were filtered out. Yet other combinations comprising those constituting 4 residues of PHBA and BP were also not detected. This may be in respect to the poor oligomerization tendency of PHBA earlier mentioned. The high K_{ow} of BP and reduction in organic reaction volume content from 5% (v/v) in single-compound studies to 1.75% (v/v) in the mixture studies, could also contribute to reducing the extent of oligomerization achieved with these compounds (Ryu and Dordick 1992). Thus, 31 pentamers were identified. Among these, 10 distinct m/z values could be observed. Each of these comprised of two or more acyloxy carbon-count isomers. A summary of the identified pentamers from mix-5 treatment under optimized conditions is presented (Table 4-15). The detailed mass spectra are shown in Figures 4-134 to 4-143, putative structures are shown in Figure 4-144.

Table 4-15 Pentamers detected from mix-5 precipitate under optimized conditions using ASAP(+) ionization mode

Combination	Molecular formula	M ⁺ _{theo}	M ⁺ _{expt}	ppm
PHBA-PHBA-MP-MP-BP	C ₄₁ H ₃₄ O ₁₅	767.1976	767.1926	-6.5
PHBA-MP-MP-MP-PP	C ₄₁ H ₃₄ O ₁₅	767.1976	767.1926	-6.5
PHBA-PHBA-MP-PP-PP	C ₄₂ H ₃₆ O ₁₅	781.2132	781.2095	-4.7
PHBA-MP-MP-MP-BP	C ₄₂ H ₃₆ O ₁₅	781.2132	781.2095	-4.7
MP-MP-MP-MP-PP	C ₄₂ H ₃₆ O ₁₅	781.2132	781.2095	-4.7
PHBA-PHBA-MP-PP-BP	C ₄₃ H ₃₈ O ₁₅	795.2289	795.2281	-1.0
MP-MP-MP-MP-BP	C ₄₃ H ₃₈ O ₁₅	795.2289	795.2281	-1.0
PHBA-MP-MP-PP-PP	C ₄₃ H ₃₈ O ₁₅	795.2289	795.2281	-1.0
PHBA-PHBA-MP-BP-BP	C ₄₄ H ₄₀ O ₁₅	809.2445	809.2417	-3.5
PHBA-PHBA-PP-PP-PP	C ₄₄ H ₄₀ O ₁₅	809.2445	809.2417	-3.5
MP-MP-MP-PP-PP	C ₄₄ H ₄₀ O ₁₅	809.2445	809.2417	-3.5
PHBA-MP-MP-PP-BP	C ₄₄ H ₄₀ O ₁₅	809.2445	809.2417	-3.5
PHBA-MP-MP-BP-BP	C ₄₅ H ₄₂ O ₁₅	823.2602	823.2532	-8.5
PHBA-PHBA-PP-PP-BP	C ₄₅ H ₄₂ O ₁₅	823.2602	823.2532	-8.5
PHBA-MP-PP-PP-PP	C ₄₅ H ₄₂ O ₁₅	823.2602	823.2532	-8.5
PHBA-PHBA-PP-BP-BP	C ₄₆ H ₄₄ O ₁₅	837.2758	837.2688	-8.4
PHBA-MP-PP-PP-BP	C ₄₆ H ₄₄ O ₁₅	837.2758	837.2688	-8.4
MP-MP-MP-BP-BP	C ₄₆ H ₄₄ O ₁₅	837.2758	837.2688	-8.4
MP-MP-PP-PP-PP	C ₄₆ H ₄₄ O ₁₅	837.2758	837.2688	-8.4
PHBA-PHBA-BP-BP-BP	C ₄₇ H ₄₆ O ₁₅	851.2915	851.2852	-7.4
PHBA-MP-PP-BP-BP	C ₄₇ H ₄₆ O ₁₅	851.2915	851.2852	-7.4
PHBA-PP-PP-PP-PP	C ₄₇ H ₄₆ O ₁₅	851.2915	851.2852	-7.4
PHBA-PP-PP-PP-BP	C ₄₈ H ₄₈ O ₁₅	865.3071	865.2997	-8.6
MP-MP-PP-BP-BP	C ₄₈ H ₄₈ O ₁₅	865.3071	865.2997	-8.6
MP-PP-PP-PP-PP	C ₄₈ H ₄₈ O ₁₅	865.3071	865.2997	-8.6
PHBA-PP-PP-BP-BP	C ₄₉ H ₅₀ O ₁₅	879.3228	879.3143	-9.7
MP-MP-BP-BP-BP	C ₄₉ H ₅₀ O ₁₅	879.3228	879.3143	-9.7
MP-PP-PP-PP-BP	C ₄₉ H ₅₀ O ₁₅	879.3228	879.3143	-9.7
PHBA-PP-BP-BP-BP	C ₅₀ H ₅₂ O ₁₅	893.3384	893.3300	-9.4
MP-PP-PP-BP-BP	C ₅₀ H ₅₂ O ₁₅	893.3384	893.3300	-9.4
PP-PP-PP-PP-PP	C ₅₀ H ₅₂ O ₁₅	893.3384	893.3300	-9.4

Figure 4-134 shows protonated m/z peak at 767.1926 matching the parent PHBA-PHBA-MP-MP-BP and/or PHBA-MP-MP-MP-PP, formula $C_{41}H_{34}O_{15}$, structure Figure 4-144 (a).

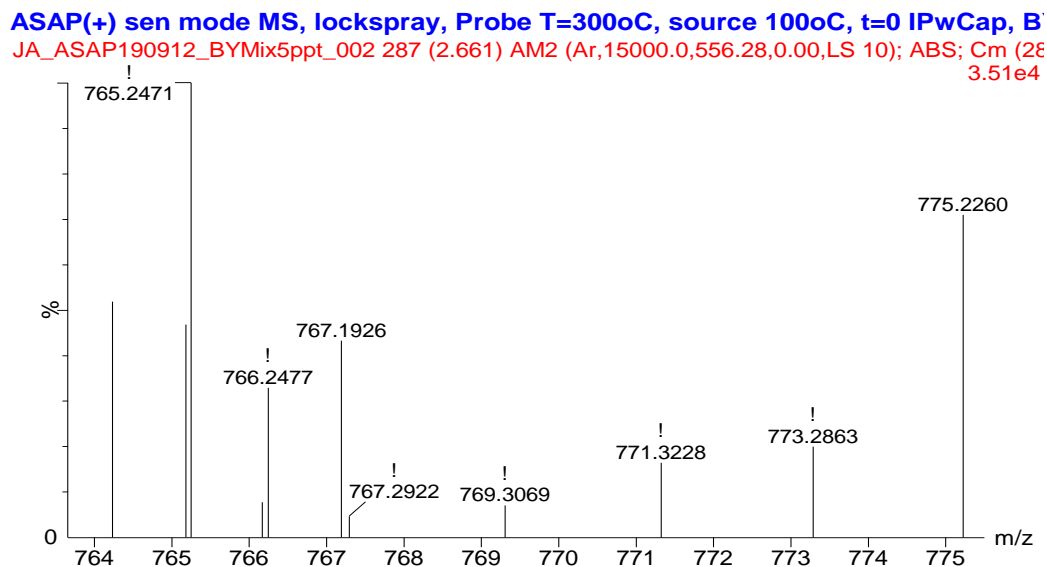


Fig. 4-134 ASAP(+)
 mass spectrum of mix-5 precipitate under optimized conditions showing a pentamer matching PHBA-PHBA-MP-MP-BP and/or PHBA-MP-MP-MP-PP

Figure 4-135 show m/z peak 781.2095 matching the parent PHBA-PHBA-MP-

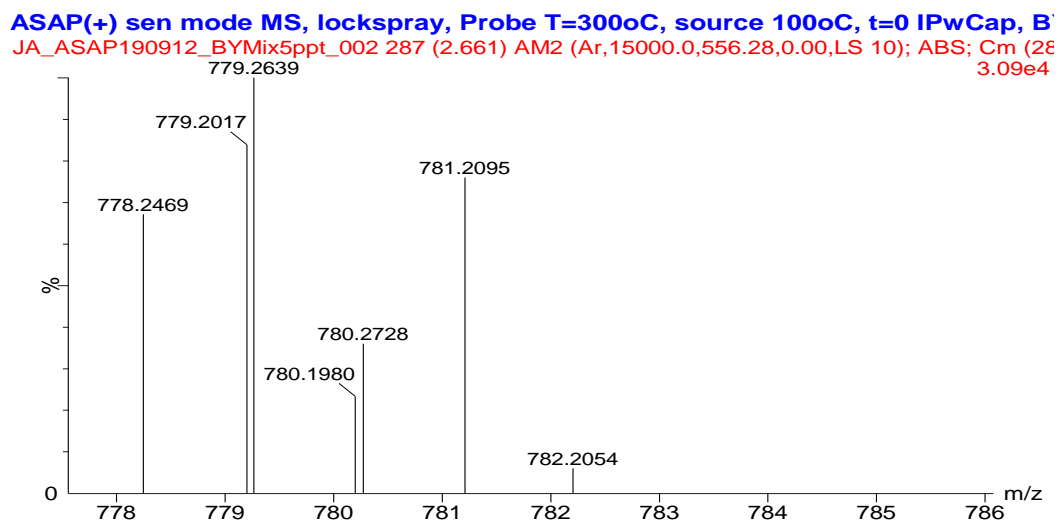


Fig. 4-135 ASAP(+)
 mass spectrum of mix-5 precipitate under optimized conditions showing a pentamer of PHBA-PHBA-MP-PP-PP and other acyloxy carbon-count isomers

PP-PP (and/or PHBA-MP-MP-MP-BP and/or MP-MP-MP-MP-PP) formula $C_{42}H_{36}O_{15}$, structure Figure 4-144 (b). Likewise, Figure 4-136 shows a m/z peak at 795.2281, matching the parent PHBA-PHBA-MP-PP-BP (and/or PHBA-MP-MP-PP-PP and/or MP-MP-MP-MP-BP), formula $C_{43}H_{38}O_{15}$, structure Figure 4-144 (c).

ASAP(+) sen mode MS, lockspray, Probe T=300oC, source 100oC, t=0 IPwCap, B'
 JA_ASAP190912_BYMix5ppt_002 287 (2.661) AM2 (Ar,15000.0,556.28,0.00,LS 10); ABS; Cm (28
 4.96e4

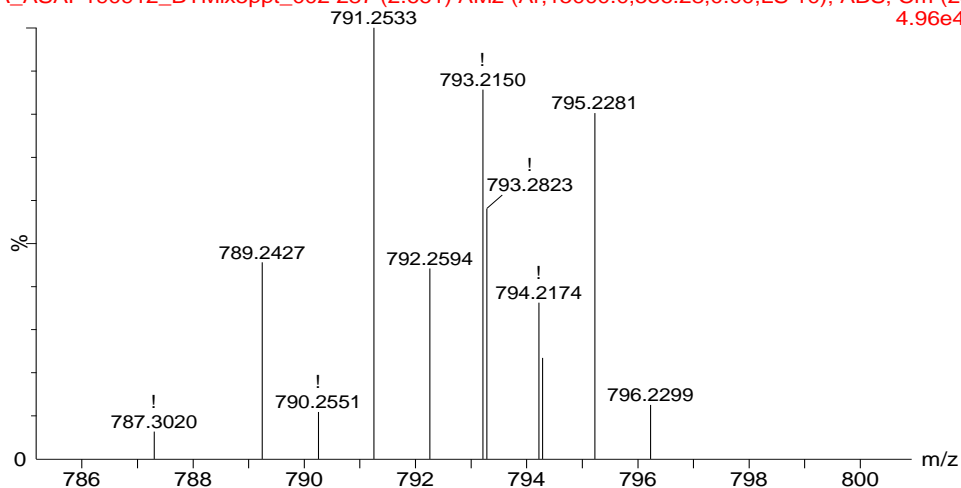


Fig. 4-136 ASAP(+), sen mode mass spectrum of mix-5 precipitate under optimized conditions showing a pentamer matching PHBA-PHBA-MP-PP-BP and other acyloxy carbon-count isomers

Figure 4-137 presents m/z peak at 809.2417 corresponding to formula $C_{44}H_{40}O_{15}$, for parent PHBA-PHBA-MP-BP-BP (and/or PHBA-PHBA-PP-PP-PP and/or PHBA-MP-MP-PP-BP and/or MP-MP-MP-PP-PP), structure Figure 4-144 (d).

ASAP(+) sen mode MS, lockspray, Probe T=300oC, source 100oC, t=0 IPwCap, B'
 JA_ASAP190912_BYMix5ppt_002 287 (2.661) AM2 (Ar,15000.0,556.28,0.00,LS 10); ABS; Cm (28
 6.52e4

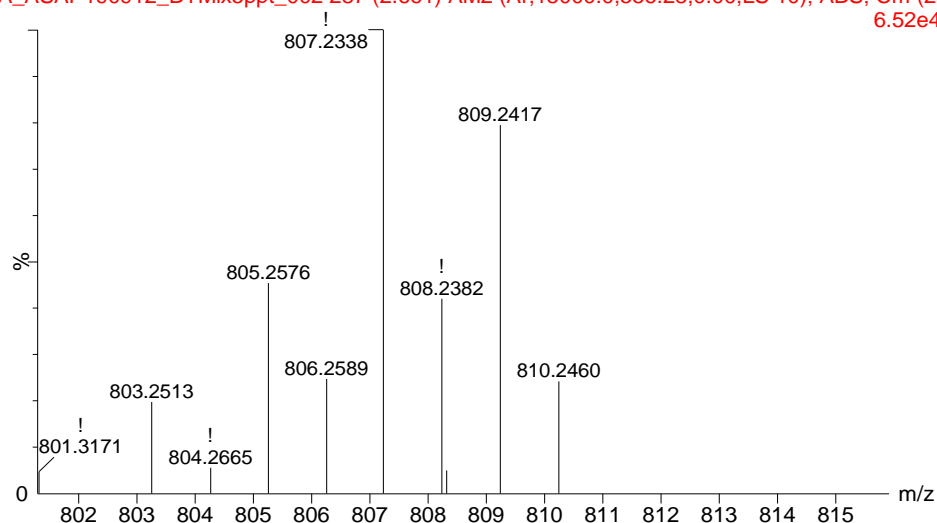


Fig. 4-137 ASAP(+) mass spectrum of mix-5 precipitate under optimized conditions showing a pentamer of PHBA-PHBA-PP-PP-PP and other acyloxy carbon-count isomers

Figure 4-138 shows protonated m/z peak at 823.2532 like the parent PHBA-

ASAP(+) sen mode MS, lockspray, Probe T=300oC, source 100oC, t=0 IPwCap, B'
 JA_ASAP190912_BYMix5ppt_002 287 (2.661) AM2 (Ar,15000.0,556.28,0.00,LS 10); ABS; Cm (28
 5.86e4

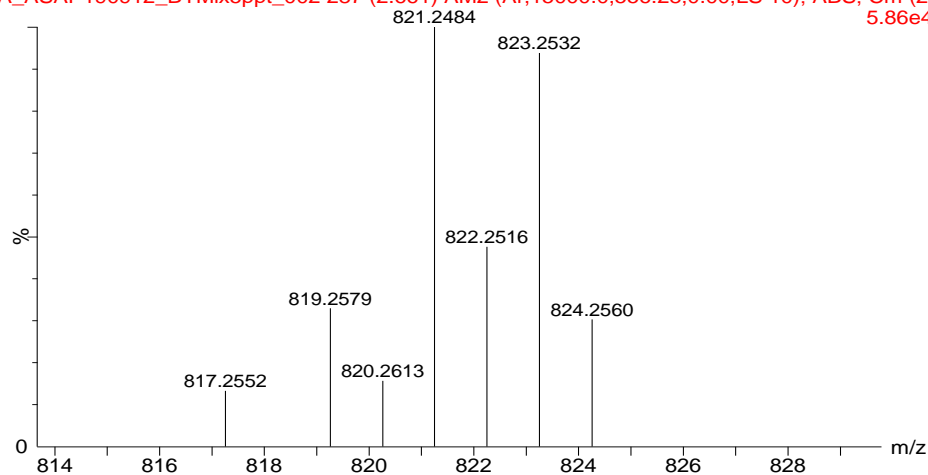


Fig. 4-138 ASAP(+) mass spectrum of mix-5 precipitate under optimized conditions showing a pentamer of PHBA-PHBA-PP-PP-BP and other acyloxy carbon-count isomers

PHBA-PP-PP-BP (and/or PHBA-MP-MP-BP-BP and/or PHBA-MP-PP-PP-PP), formula $C_{45}H_{42}O_{15}$, structure Figure 4-144 (e). Similarly, m/z peak 837.2688 (Figure 4-139) agrees with the formula $C_{46}H_{44}O_{15}$ for parent PHBA-PHBA-PP-BP-BP (and/or PHBA-

MP-PP-PP-BP and/or MP-MP-MP-BP-BP and/or MP-MP-PP-PP-PP), structure Figure 4-144 (f).

ASAP(+) sen mode MS, lockspray, Probe T=300oC, source 100oC, t=0 IPwCap, B'
 JA_ASAP190912_BYMix5ppt_002 287 (2.661) AM2 (Ar,15000.0,556.28,0.00,LS 10); ABS; Cm (2E
 6.95e4

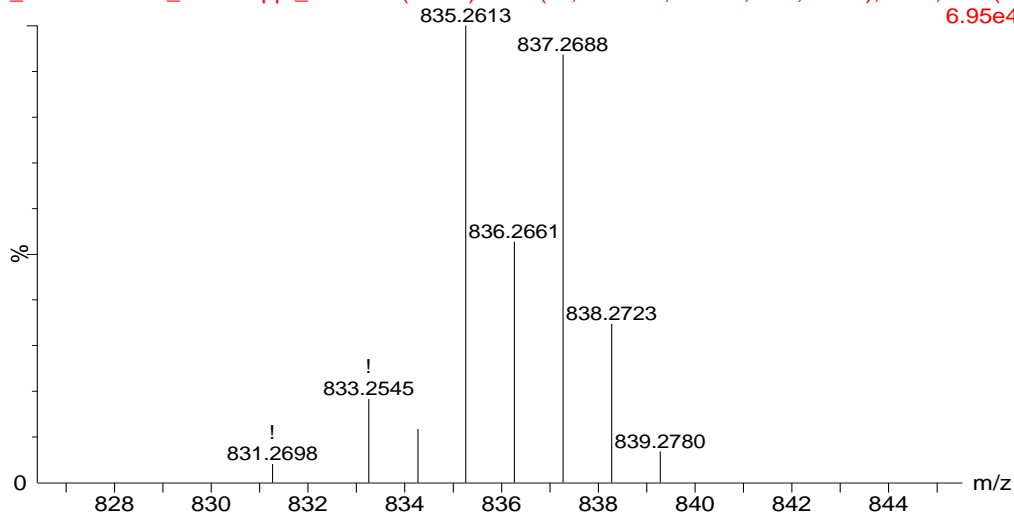


Fig. 4-139 ASAP(+)
 showing a pentamer matching PHBA-PHBA-PP-BP-BP and other acyloxy carbon-count isomers

Figure 4-140 shows protonated pentamer with m/z peak at 851.2852, for parent

ASAP(+) sen mode MS, lockspray, Probe T=300oC, source 100oC, t=0 IPwCap, B'
 JA_ASAP190912_BYMix5ppt_002 287 (2.661) AM2 (Ar,15000.0,556.28,0.00,LS 10); ABS; Cm (2E
 6.88e4

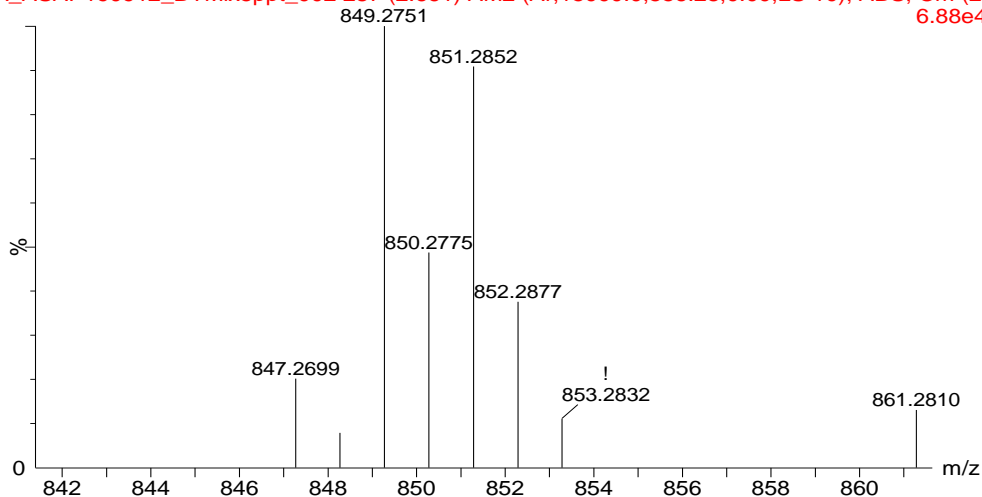


Fig.4-140 ASAP(+)
 showing pentamer matching PHBA-PHBA-BP-BP-BP and other acyloxy carbon-count isomers

PHBA-PHBA-BP-BP-BP (and/or PHBA-MP-PP-BP-BP and/or PHBA-PP-PP-PP-PP) formula $C_{47}H_{46}O_{15}$, structure Figure 4-144 (g). Similarly, Figure 5-141 Shows m/z peak at 865.2997 having a molecular formula $C_{48}H_{48}O_{15}$, corresponding to parent PHBA-PP-PP-PP-BP (and/or MP-MP-PP-BP-BP and/or MP-PP-PP-PP-PP) structure Figure 4-144 (h).

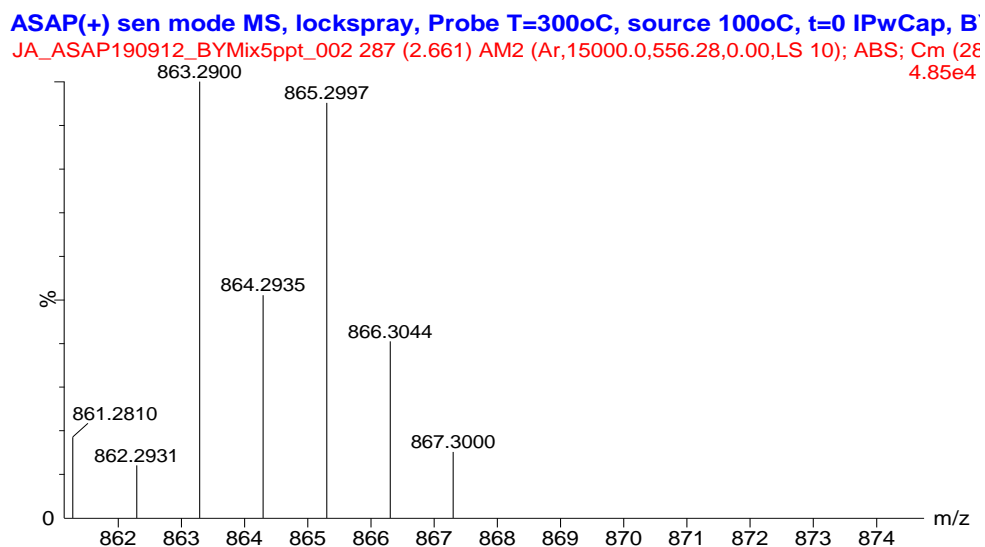


Fig. 4-141 ASAP(+), sen mode mass spectrum of mix-5 precipitate under optimized conditions showing a pentamer of PHBA-PP-PP-PP-BP and other acyloxy carbon-count isomers

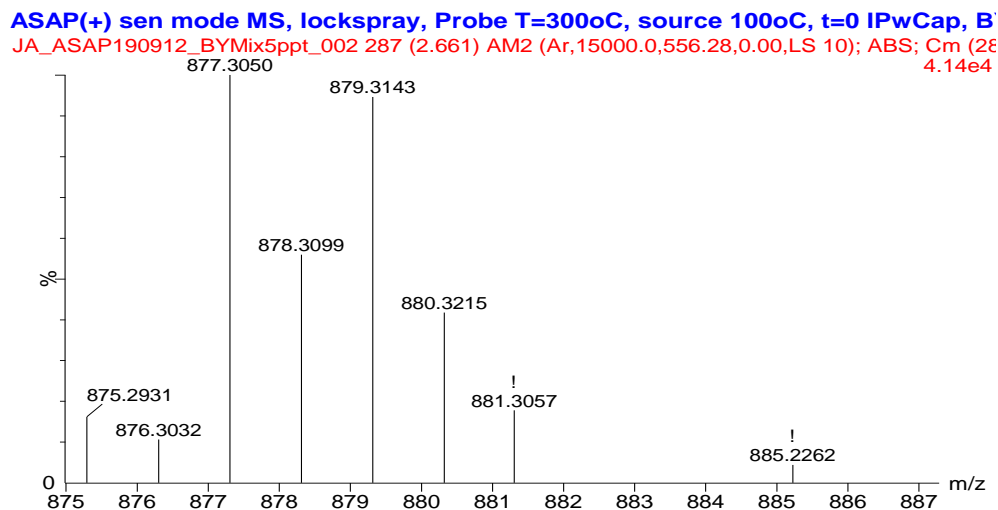


Fig. 4-142 ASAP(+), sen mode mass spectrum of mix-5 precipitate under optimized conditions showing a pentamer of PHBA-PP-PP-BP-BP and other acyloxy carbon-count isomers.

PHBA-PP-PP-BP-BP (and/or MP-MP-BP-BP-BP and/or MP-PP-PP-PP-BP), structure Figure 4-144 (i). Similarly, Figure 4-143 show m/z peak at 893.3300 corresponding to

parent pentamer PHBA-PP-BP-BP-BP (and/or MP-PP-PP-BP-BP and/or PP-PP-PP-PP-PP), formula $C_{50}H_{52}O_{15}$, structure Figure 4-144 (j).

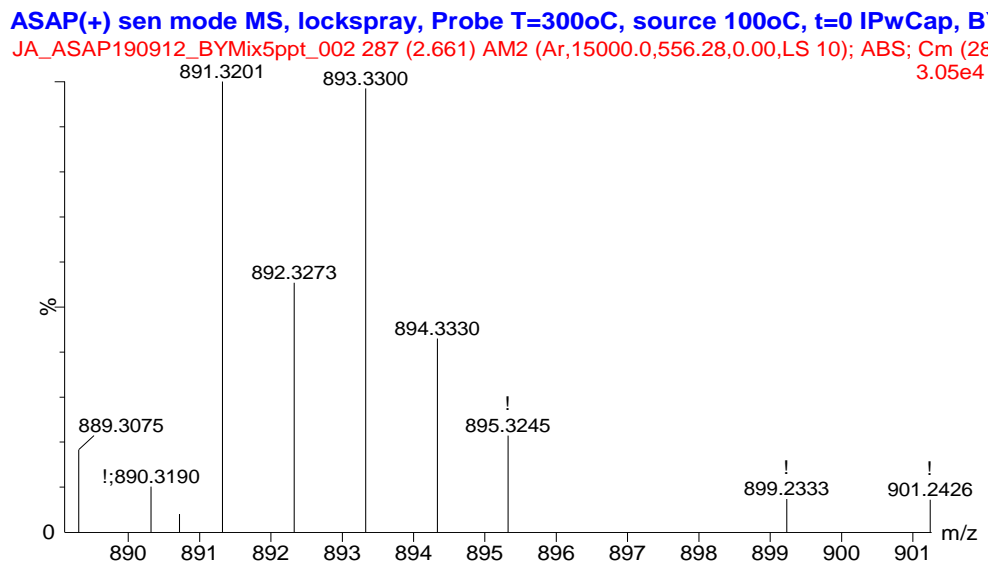


Fig. 4-143 ASAP(+), sen mode mass spectrum of mix-5 precipitate under optimized conditions showing a pentamer of PHBA-PP-BP-BP-BP and other acyloxy carbon-count isomers

Figure 149 represents plausible structural formulae of the pentamers earlier mentioned. While the structures are derived from the combinations generated, other regioisomers and carbon-count isomers may possibly be found on closer structural analysis.

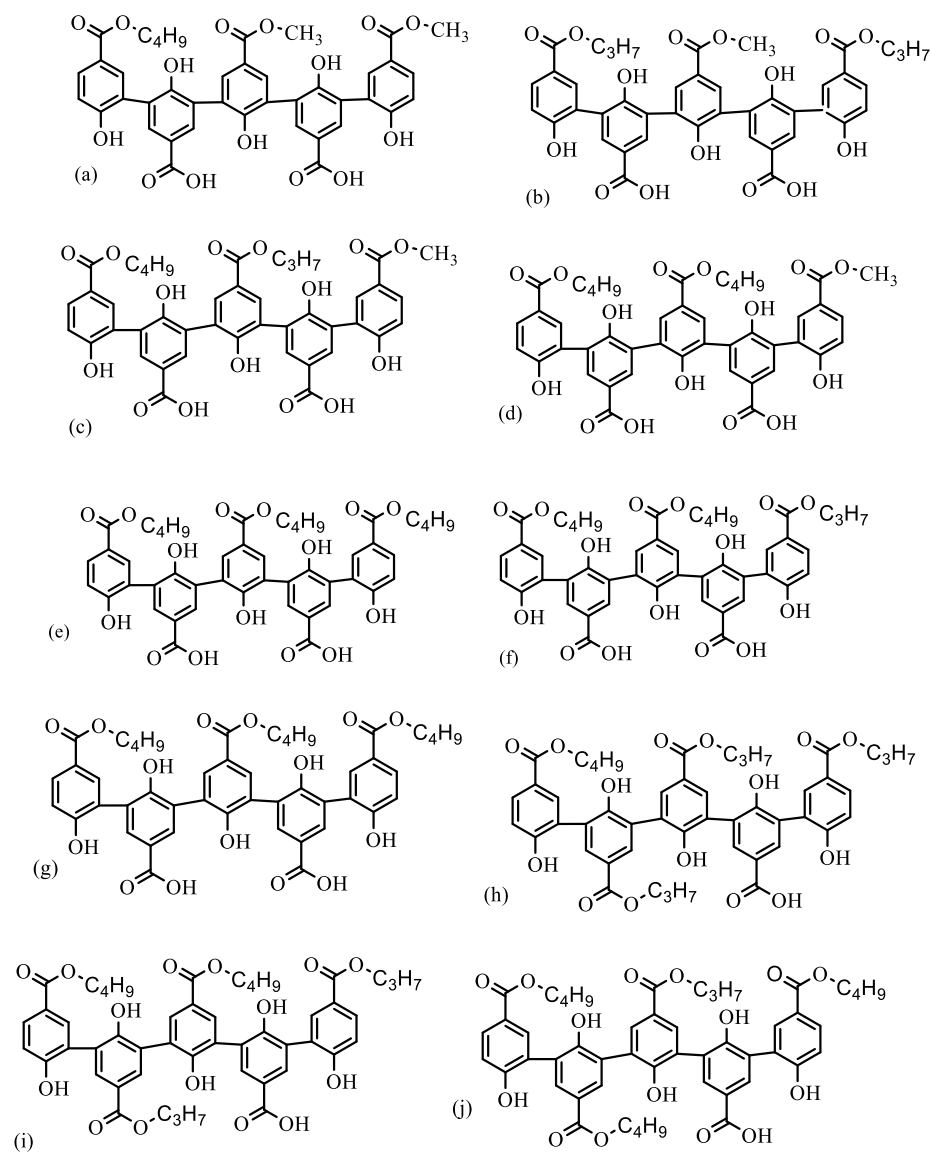


Fig. 4-144 Proposed structural formulae for plausible pentamer combinations (but not permutations) of mix-5 under optimized conditions (other regioisomers are possible)

CHAPTER FIVE

SUMMARY, CONCLUSIONS AND RECOMMENDATIONS

5.0 Summary

Soybean peroxidase-catalyzed oligomerization of selected CECs commonly occurring in the environment and in wastewater effluents was investigated. The selected CECs comprised a pharmaceutically active ingredient, preservatives and their common degradation intermediate. The optimal conditions required to achieve $\geq 95\%$ substrate removal were optimized. Since CECs as natural environmental pollutants do not occur mutually exclusive of other contaminants, a mixture treatment approach is necessary to simulate near-environmental reality conditions in the laboratory setting. Therefore, these compounds were mixed together and studied (mix-5) under similar conditions and targets as the single-compound treatment. The findings are summarized hereunder:

1. Optimal pH for the removal of acetaminophen was at pH 8.0, but it demonstrated a wide effective pH range 6.5-8.5, with steeper decline on the basic side than on the acidic side. The other compounds showed optimal pH at 6.5. All compounds showed optimal pH below their respective hydroxyl-*pK*_a values. The SBP activity used with mix-5 showed acetaminophen removal to below the quantification limits at all the tested pHs between 3.6 and 10.0. All the other compounds showed >95% removal in the mixture at pH 6.5. At all the pH tested, removal was in the order of Acet >> PHBA > BP > PP > MP. However, under stringent SBP conditions, the removal order was changed to Acet >> BP > PP > PHBA > MP with diminishing removal efficiency from acidic to basic pH.
2. For 1.0 mM substrates, acetaminophen showed optimal SBP requirement of 0.006 U/mL, which was 380 times less than MP, with the highest optimal SBP requirement of 2.3 U/mL. The SBP requirement was in the order of Acet << PP = BP < PHBA < MP. Under optimized SBP conditions, removal of compounds (0.2 mM each) in mix-5 was in the order of Acet >> PHBA > BP > PP > MP
3. For 1.0 mM substrate, the required peroxide was highest in PHBA at 2.0 mM and least for PP and BP at 1.15 mM. Required peroxide to substrate ratio was in the increasing order of PP = BP < Acet < MP < PHBA.

4. Under the optimized conditions, removal efficiency was highest with Acet and least with MP, following the decreasing order of Acet>PP>BP=PHBA>MP with a difference of 3.7% between the highest and least removed compounds. The removal of Acet and PHBA were above the target 95%, while MP was less removed than it was in the single-compound study.
5. In all cases where 95% compound removal was not achieved, incremental addition of optimized peroxide doses in four aliquots (to same cumulative [peroxide]) improved the removal of the CECs both in single-compound studies and in mix-5. For instance, under single-compound treatment, MP removal improved from about 88% to 94%. Additions of the optimized peroxide concentration in four aliquots at intervals corresponding to the half-life of BP, the compound with the longest half-life in single-compound studies, showed improved removal to above 95% for all compounds. Specifically, MP the most recalcitrant compound increased from 75% to about 95%
6. The removal of all compounds in the single-compound study followed pseudo-first-order kinetics for the initial treatment period. Normalized rate constants for single-compound and mix-5 treatments followed the order of Acet>>BP≈PP>PHBA≈MP and Acet>>BP>PHBA>PP≈MP, respectively. Note that under both treatment conditions, among the parabens, the order goes from the longest alkyl group paraben, BP, to the shortest, MP.
7. Mass spectroscopy studies on the products were performed using an electrospray (+) ionization technique for acetaminophen, atmospheric solids analysis probe in positive ionization mode (ASAP(+)) for PHBA and mix-5, while ASAP(-) was used for the single-compound studies for MP, PP and BP. The oligomerization of compounds in single-compound studies showed higher oligomers observed in the precipitates than in the supernatants, except for PHBA. Acetaminophen had oligomers to the pentamer stage while only dimers of PHBA were detected in the supernatants. Highest observed oligomers of other compounds included heptamers of MP, hexamers of PP and heptamers of BP and their respective oxygenated derivatives.
8. Oligomers observed in mix-5 ranged from dimers to pentamers, including homo- and hetero- coupled oligomers having a wide range of alkyloxy isomers. Interestingly, Acet showed only the homodimer.

9. Recovery of at least 80% was achieved using a SPE protocol developed and applied to synthetic wastewater.

5.1 Conclusions

This study has provided empirical evidence of SBP-catalyzed oligomerization of phenolic CECs – acetaminophen and selected parabens – for wastewater treatment. For the single compounds, optimal pH was pH 6.5-8.0. SBP requirement varied between 0.006 U/mL and 2.3 U/mL, for the most and least-efficiently removed compounds; peroxide to compound ratio varied between 1.15 and 2.0. Mix-5 reaction (containing 0.2 mM each) at pH 6.5, optimized SBP activity of 1.43 U/mL and 1.56 mM of peroxide, could achieve $\geq 95\%$ removal of compounds provided with step-feeding of peroxide was carried out. Initial reaction rates were pseudo-first-order except for the first 30 seconds of the mix-5 treatment process for acetaminophen and BP, where more than 90% and 55%, respectively, were removed. Mass spectroscopic investigations showed the highest oligomers observed were dimers for PHBA, pentamers for acetaminophen, hexamers for PP and heptamers for MP and BP. Mix-5 produced oligomers up to pentamers in the precipitate, comprised of cross-coupling and self-coupling of monomers. This illustrates that, under mixture conditions, there is indiscriminate reaction of the aryl radicals generated from the peroxidase activity of SBP. Expectedly, more hetero-oligomers were observed than homo-oligomers. Based on the oligomers observed, reaction mechanisms for the five monomer self-couplings were postulated. For practical applications, it is thought the optimal removal achieved could provide an improvement in process cost.

5.2 Recommendations for future studies

Based on the results obtained from this study and the discussions made, it is suggested that some further research directions may improve on the results.

1. Experimental concentrations employed in this study were much higher than reported environmental concentrations. It is important to study environmentally-relevant concentrations – which will depend on the source being considered – to gain knowledge into the removal efficiencies and also understand the effects of polyphenolic precipitates formation on parameter requirements and enzyme inactivation.
2. The Michaelis-Menten kinetics for the individual and mix-5 reactions would provide enzyme-substrate binding affinity data which may help improve process design and optimization procedures.
3. The hypothetical treatment process has been effective for a mixture of 5 compounds however, the real wastewater effluents will present myriad compounds posing different removal dynamics. It is recommended further studies should employ real wastewater effluents.
4. It is important for process design engineers to estimate the cost implication and feasibility of incorporating a treatment chamber based on this technique before effluents are released. This may be before disinfection or after disinfection.
5. Many of the oligomers formed are still soluble. For the full treatment scenario, it would be important to investigate various means of causing their precipitation.
6. It is important to ascertain the toxicity of any soluble oligomers using classical toxicological assays to ensure the oligomers are not toxic. These may include acute and chronic toxicity tests, and/or molecular toxicity studies.
7. Classical chemical structure analytical techniques such as NMR, FTIR should be used to determine the structural formulae of the oligomers formed, especially the alkyloxy isomers to authenticate the monomeric units. This may especially be helpful for the isomers showing up to three monomeric units of PHBA, which would clarify the role of the other monomers in aiding its oligomerization under mixture conditions.
8. Pilot studies comparing CECs removal efficiency of this technique against other commonly used AOP needs to be investigated to highlight comparative merits and demerits.

9. Pilot studies need to be carried out using continuous-flow reactors to ascertain the feasibility of transferring these lab-scale batch reactor experiments to prospective industrial applications employing real wastewater effluents.

REFERENCES

- Abdollahi, K., Yazdani, F., Panahi, R., & Mokhtarani, B. (2018). Biotransformation of phenol in synthetic wastewater using the functionalized magnetic nano-biocatalyst particles carrying tyrosinase. *Biotechnology*, 8(10), 1–10. <https://doi.org/10.1007/s13205-018-1445-2>
- Afsa, S., Hamden, K., Martin, P.A.L., Mansour, H.B. (2020). Occurrence of 40 pharmaceutically active compounds in hospital and urban wastewaters and their contribution to Mahdia coastal seawater contamination. *Environmental Science and Pollution Research International*, 27(2), 1941–1955. <https://doi.org/10.1007/s11356-019-06866-5>
- Alhalib, A. (2017). The use of UV-Visible spectroscopy for the determination of acetaminophen content of different brands of paracetamol tablets. *Journal of Humanities and Applied Science* 30, 113-119
- Alshabib, M., & Onaizi, S. (2019). A review on phenolic wastewater remediation using homogeneous and heterogeneous enzymatic processes: Current status and potential challenges. *Separation and Purification Technology*, 219, 186–207. <https://doi.org/10.1016/j.seppur.2019.03.028>
- Alvarez-Rivera, G., Llompert, M., Garcia-Jares, C., & Lores, M. (2014). Identification of halogenated photoproducts generated after ultraviolet-irradiation of parabens and benzoates in water containing chlorine by solid-phase microextraction and gas chromatography-mass spectrometry. *Journal of Chromatography A*, 1349, 105–115. <https://doi.org/10.1016/j.chroma.2014.05.009>
- Amin, M., Bina, B., Ebrahimi, A., Yavari, Z., Mohammadi, F., & Rahimi, S. (2018). The occurrence, fate, and distribution of natural and synthetic hormones in different types of wastewater treatment plants in Iran. *Chinese Journal of Chemical Engineering*, 26(5), 1132–1139. <https://doi.org/10.1016/j.cjche.2017.09.005>
- An, T., Fang, H., Li, G., Wang, S., & Yao, S. (2014). Experimental and theoretical insights into photochemical transformation kinetics and mechanisms of aqueous propylparaben and risk assessment of its degradation products. *Environmental Toxicology and Chemistry*, 33(8), 1809–1816. <https://doi.org/10.1002/etc.2632>
- Angeles, L., Mullen, R., Huang, I., Wilson, C., Khunjar, W., Sirotkin, H. I., McElroy, A.E., Aga, D. (2020). Assessing pharmaceutical removal and reduction in toxicity provided by advanced wastewater treatment systems. *Environmental Science: Water Research & Technology*, 6(1), 62–77. <https://doi.org/10.1039/c9ew00559e>
- Arbeláez, P., Borrull, F., Pocurull, E., & Marcé, R. (2015). Determination of high-intensity sweeteners in river water and wastewater by solid-phase extraction and liquid chromatography–tandem mass spectrometry. *Journal of Chromatography A*, 1393, 106–114. <https://doi.org/10.1016/j.chroma.2015.03.035>

- Archer, E., Petrie, B., Kasprzyk-Hordern, B. & Wolfaardt, G.M. (2017). The fate of pharmaceuticals and personal care products (PPCPs), endocrine disrupting contaminants (EDCs), metabolites and illicit drugs in a WWTW and environmental waters. *Chemosphere* 174:437–446.
<https://doi.org/10.1016/j.chemosphere.2017.01.1010045-6535>
- Aryal, W.Wood, J., Rjal, I., Deng, D., Jha, M.K. & Ofori-Boadu, A. (2020). Fate of environmental pollutants: A review. *Water Environment Research*, 92(10), 1587–1594. <https://doi.org/10.1002/wer.1404>
- Asgari, E., Esrafil, A., Rostami, R., & Farzadkia, M. (2019). O₃, O₃/UV and O₃/UV/ZnO for abatement of parabens in aqueous solutions: Effect of operational parameters and mineralization/biodegradability improvement. *Process Safety and Environmental Protection*, 125, 238–250.
<https://doi.org/10.1016/j.psep.2019.03.032>
- Aymerich, I., Acuña, V., Barceló, D., García, M.J., Petrovic, M., Poch, M., Rodriguez-Mozaz, S., Rodríguez-Roda, I., Sabater, S., Von Schiller, D., Corominas, Ll. (2016). Attenuation of pharmaceuticals and their transformation products in a wastewater treatment plant and its receiving river ecosystem. (2016). *Water Research*, 100, 126–136. <https://doi.org/10.1016/j.watres.2016.04.022>
- Ayobahan, E., Eilebrecht, A., Baumann, L., Teigeler, M., Hollert, H., Kalkhof, S., Eilebrecheht, E. & Schafers, C. (2020). Detection of biomarkers to differentiate endocrine disruption from hepatotoxicity in zebrafish (*Danio rerio*) using proteomics. *Chemosphere (Oxford)*, 240, 124970–124970.
<https://doi.org/10.1016/j.chemosphere.2019.124970>
- Baek, H.K., & Van Wart, H.E. (1989). Elementary steps in the formation of horseradish peroxidase Compound I: Direct observation of Compound 0, a new intermediate with a hyperporphyrin spectrum. *Biochemistry* 28:5714–5719
- Barabasz, W., Pikulicka, A., Wzorek, Z., Nowak, A.K. (2019). Ecotoxicological aspects of the use of parabens in the production of cosmetics. *Technical Transactions*, 12:99-124 <https://doi:10.4467/235373XCT.19.126.11451>
- Barel-Cohen, K., Shore, L., Shemesh, M., Wenzel, A., Mueller, J., & Kronfeld-Schor, N. (2006). Monitoring of natural and synthetic hormones in a polluted river. *Journal of Environmental Management*, 78(1), 16–23.
<https://doi.org/10.1016/j.jenvman.2005.04.006>
- Bartolomeu, M., Neves, M., Faustino, M., & Almeida, A. (2018). Wastewater chemical contaminants: remediation by advanced oxidation processes. *Photochemical & Photobiological Sciences*, 17(11), 1573–1598. <https://doi.org/10.1039/c8pp00249e>
- Battistuzzi, G., Bellei, M., Bortolotti, C., & Sola, M. (2010). Redox properties of heme peroxidases. *Archives of Biochemistry and Biophysics*, 500(1), 21–36.
<https://doi.org/10.1016/j.abb.2010.03.002>

- Bauer, R., & Fallmann, H. (1997). The Photo-Fenton Oxidation — A cheap and efficient wastewater treatment method. *Research in Chemical Intermediates* 23, 341–354 (1997). <https://doi.org/10.1163/156856797X00565>
- Bayülken, D.G., Tüylü, B. A., Sinan, H., & Sivas, H. (2019). Investigation of genotoxic effects of paraben in cultured human lymphocytes. *Drug and Chemical Toxicology*, 42(4), 349–356. <https://doi.org/10.1080/01480545.2017.1414834>
- Beausse, J. (2004) Selected drugs in solid matrices: a review of environmental occurrence, determination and properties of principal substances. *Trends in Analytical Chemistry* 23 (10–11): 753–761. <https://doi.org/10.1016/j.trac.2004.08.005>
- Becker, D., Rodriguez-Mozaz, S., Insa, S., Schoevaart, R., Barceló, D., de Cazes, M., Belleville, M., Sanchez-Marcano, J., Misovic, A., Oehlmann, J., Wagner, M., & Falque, P. (2017). Removal of Endocrine Disrupting Chemicals in Wastewater by Enzymatic Treatment with Fungal Laccases. *Organic Process Research & Development*, 21(4), 480–491. <https://doi.org/10.1021/acs.oprd.6b00361>
- Bedner, M., Maccrehan, W., & Bedner, M. (2006). Transformation of acetaminophen by chlorination produces the toxicants 1,4-benzoquinone and N-acetyl-p-benzoquinone imine. *Environmental Science & Technology*, 40(2), 516–522. <https://doi.org/10.1021/es0509073>
- Berglund, G., Carlsson, G., Smith, A., Szöke, H., Henriksen, A., & Hajdu, J. (2002). The catalytic pathway of horseradish peroxidase at high resolution. *Nature* (London), 417(6887), 463–468. <https://doi.org/10.1038/417463a>
- Bilal, M., Adeel, M., Rasheed, T., Zhao, Y., & Iqbal, H. (2019). Emerging contaminants of high concern and their enzyme-assisted biodegradation – A review. *Environmental International*, 124, 336–353. <https://doi.org/10.1016/j.envint.2019.01.011>
- Blair, B., Crago, J., Hedman, C., & Klaper, R. (2013). Pharmaceuticals and personal care products found in the Great Lakes above concentrations of environmental concern. *Chemosphere* (Oxford), 93(9), 2116–2123. <https://doi.org/10.1016/j.chemosphere.2013.07.057>
- Bledzka, D., Miller, J., & Ledakowicz, S. (2012). Kinetic Studies of n-Butylparaben Degradation in H₂O₂/UV System. *Ozone-Science & Engineering*, 34(5), 354–358. <https://doi.org/10.1080/01919512.2012.712847>
- Bódalo, A., Gómez, J., Gómez, E., Bastida, J., & Máximo, M. (2006). Comparison of commercial peroxidases for removing phenol from water solutions. *Chemosphere*, 63(4), 626–632. <https://doi.org/10.1016/j.chemosphere.2005.08.007>
- Bosio, M., Souza-Chaves, B., Gomes, J., Gmurek, M., Martins, R., Saggiaro, E., Dezotti, M., Bassin, J., Quinta-Ferreira, M., & Quinta-Ferreira, R. (2020). Electrochemical oxidation of paraben compounds and the effects of by-products on neuronal

- activity. *Energy Reports*, 6(s1), 903–908.
<https://doi.org/10.1016/j.egy.2019.11.156>
- Boyle, E., Guerriero, N., Thiallet, A., Del Vecchio, R., & Blough, N. (2009). Optical Properties of Humic Substances and CDOM: Relation to Structure. *Environmental Science & Technology*, 43(7), 2262–2268.
<https://doi.org/10.1021/es803264g>
- Bracchini, L., Dattilo, A., Hull, V., Loiselle, S., Nannicini, L., Picchi, M., Ricci, M., Santinelli, C., Seritti, A., Tognazzi, A., & Rossi, C. (2010). Spatial and seasonal changes in optical properties of autochthonous and allochthonous chromophoric dissolved organic matter in a stratified mountain lake. *Photochemical & Photobiological Sciences*, 9(3), 304–314. <https://doi.org/10.1039/b9pp00129h>
- Bradley, P.M., Journey, C.A., Button, D.T., Carlisle, D.M., Huffman, B.J., Qi, S.L., Romanok, K.M., Van Metre, P.C. (2020). Multi-region assessment of pharmaceutical exposures and predicted effects in USA wadeable urban-gradient streams. s. *PLoS ONE* 15(1): <https://doi.org/10.1371/journal.pone.0228214>
- Brown, A., & Wong, C. (2018). Distribution and fate of pharmaceuticals and their metabolite conjugates in a municipal wastewater treatment plant. *Water Research*, 144, 774–783. <https://doi.org/10.1016/j.watres.2018.08.034>
- Brzyska, M., Cieszczyk, M., & Łobarzewski, J. (1997). The Effect of the Simultaneous Operation of Two Metal Ions on Soluble and Immobilized Peroxidase. *Journal of Chemical Technology & Biotechnology*, 68(1), 101–109.
[https://doi.org/10.1002/\(SICI\)1097-4660\(199701\)68:13.O.CO;2-V](https://doi.org/10.1002/(SICI)1097-4660(199701)68:13.O.CO;2-V)
- Bugatti, V., Vertuccio, L., Zuppari, F., Vittoria, V., & Gorrasi, G. (2019). PET and Active Coating Based on a LDH Nanofiller Hosting p-Hydroxybenzoate and Food-Grade Zeolites: Evaluation of Antimicrobial Activity of Packaging and Shelf Life of Red Meat. *Nanomaterials (Basel, Switzerland)*, 9(12), 1727–.
<https://doi.org/10.3390/nano9121727>
- Burch, K.D., Han, B., Pichtel, J., Zubkov, T. (2019). Removal efficiency of commonly prescribed antibiotics via tertiary wastewater treatment. *Environmental Science and Pollution Research* 26:6301–6310 <https://doi.org/10.1007/s11356-019-04170-w>
- Bustillo-Lecompte, C., Mehrvar, M. and Quiñones-Bolaños, E. (2016) Slaughterhouse Wastewater Characterization and Treatment: An Economic and Public Health Necessity of the Meat Processing Industry in Ontario, Canada. *Journal of Geoscience and Environment Protection*, 4, 175-186.
<http://dx.doi.org/10.4236/gep.2016.44021>
- Calafat, A., Ye, X., Wong, L., Bishop, A., Needham, L., & Calafat, A. (2010). Urinary concentrations of four parabens in the U.S. population: NHANES 2005-2006. *Environmental Health Perspectives*, 118(5), 679–685.
<https://doi.org/10.1289/ehp.0901560>
- Cavillini, G.S., de Soucsal Vidal, C.M., de Souza J.B., de Campos, S.X. (2015). Fenton coagulation/oxidation using Fe²⁺ and Fe³⁺ ions and peracetic acid for the

- treatment of wastewater. *Orbital – The Electronic Journal of Chemistry* 7(3)
<https://doi.org/10.17807/orbital.v7i3.626>
- Caza, N., Bewtra, J., Biswas, N., & Taylor, K. (1999). Removal of phenolic compounds from synthetic wastewater using soybean peroxidase. *Water Research*, 33(13), 3012–3018. [https://doi.org/10.1016/S0043-1354\(98\)00525-9](https://doi.org/10.1016/S0043-1354(98)00525-9)
- Celente, G.S., Colares, G.S., Araujo, P.S., Machado, E.L., Lobo, E.A. (2020). Acute ecotoxicity and genotoxicity assessment of two wastewater treatment units. *Environmental Science and Pollution Research* 27:10520–10527
<https://doi:10.1007/s11356-019-07308-y>
- Chagas, P., Torres, J., Corrêa, A., & Silva, M. (2015). Immobilized soybean hull peroxidase for the oxidation of phenolic compounds in coffee processing wastewater. *International Journal of Biological Macromolecules*, 81, 568–575.
<https://doi.org/10.1016/j.ijbiomac.2015.08.061>
- Chang, C., Hsieh, Y., Cheng, K., Hsieh, L., Cheng, T., Yao, K., & Chang, C. (2008). Effect of pH on Fenton process using estimation of hydroxyl radical with salicylic acid as trapping reagent. *Water Science and Technology : Journal of the International Association on Water Pollution Research*, 58(4), 873–879.
<https://doi.org/10.2166/wst.2008.429>
- Chen, Y., Zhang, X., Feng, S., & Chen, Y. (2018). Contribution of the Excited Triplet State of Humic Acid and Superoxide Radical Anion to Generation and Elimination of Phenoxy Radical. *Environmental Science & Technology*, 52(15), 8283–8291. <https://doi.org/10.1021/acs.est.8b00890>
- Cheng, W., & Harper Jr, W.F. (2012). Chemical kinetics and interactions involved in horseradish peroxidase-mediated oxidative polymerization of phenolic compounds. *Enzyme and Microbial Technology*, 50(3), 204–208.
<https://doi.org/10.1016/j.enzmictec.2011.12.005>
- Choi, E., Alsop, D. & Wilson, J.Y. (2018). The effects of chronic acetaminophen exposure on the kidney, gill and liver in rainbow trout (*Oncorhynchus mykiss*). *Aquatic Toxicology* 198:20–29 <https://doi.org/10.1016/j.aquatox.2018.02.007>
- Chokwe, T., & Mporetji, S. (2019). Organophosphorus flame retardants in surface and effluent water samples from the Vaal River catchment, South Africa: levels and risk to aquatic life. *Water S.A.*, 45(3), 469–476.
<https://doi.org/10.17159/wsa/2019.v45.i3.6744>
- Chrostowski, P., Dietrich, A., & Suffet, I. (1983). Ozone and oxygen induced oxidative coupling of aqueous phenolics. *Water Research*, 17(11), 1627–1633.
[https://doi.org/10.1016/0043-1354\(83\)90021-0](https://doi.org/10.1016/0043-1354(83)90021-0)

- Cizmas, L., Sharma, V.K., Gray, C.M., McDonald, T.J. (2015). Pharmaceuticals and personal care products in waters: occurrence, toxicity, and risk. *Environmental Chemistry Letters* 13(4): 381–394. <https://doi:10.1007/s10311-015-0524-4>
- Corcoran, S., Metcalfe, C., Sultana, T., Amé, M., & Menone, M. (2020). Pesticides in Surface Waters in Argentina Monitored Using Polar Organic Chemical Integrative Samplers. *Bulletin of Environmental Contamination and Toxicology*, 104(1), 21–26. <https://doi.org/10.1007/s00128-019-02758-z>
- Courteix, A., & Bergel, A. (1995). Horseradish peroxidase—catalyzed hydroxylation of phenol: I. Thermodynamic analysis. *Enzyme and Microbial Technology*, 17(12), 1087–1093. [https://doi.org/10.1016/0141-0229\(95\)00037-2](https://doi.org/10.1016/0141-0229(95)00037-2)
- Cuerda-Correa, E., Dominguez, J., Munoz-Pena, M., Gonzalez, T., & Cuerda-Correa, E. (2016). Degradation of Parabens in Different Aqueous Matrices by Several O₃-Derived Advanced Oxidation Processes. *Industrial & Engineering Chemistry Research*, 55(18), 5161–5172. <https://doi.org/10.1021/acs.iecr.6b00740>
- Darbre, P., & Harvey, P. (2008). Paraben esters: review of recent studies of endocrine toxicity, absorption, esterase and human exposure, and discussion of potential human health risks [Review of Paraben esters: review of recent studies of endocrine toxicity, absorption, esterase and human exposure, and discussion of potential human health risks]. *Journal of Applied Toxicology*, 28(5), 561–578. John Wiley & Sons, Ltd. <https://doi.org/10.1002/jat.1358>
- Daughton, C. (2005) Pharmaceuticals and personal care products in the environment: overarching issues and overview. In: Daughton, C.G. and Jones-Lepp, T. (eds), American Chemical Society, Symposium series 791, Washington, DC, pp .2–38.
- Davies, M.J., & Dean, R.T. (1997). Radical-Mediated Protein Oxidation. From Chemistry to Medicine, Oxford Science Publications, New York (1997).
- De García, S.O., García-Encina, P.A., Irusta-Mata, (2017). The potential ecotoxicological impact of pharmaceutical and personal care products on humans and freshwater, based on USEtox™ characterization factors. A Spanish case study of toxicity impact scores. *Science of the Total Environment* 609:429-445. <https://doi.org/10.1016/j.scitotenv.2017.07.148>
- De Laurentiis, E., Prasse, C., Ternes, T., Minella, M., Maurino, V., Minero, C., Sarakha, M., Brigante, M., & Vione, D. (2014). Assessing the photochemical transformation pathways of acetaminophen relevant to surface waters: Transformation kinetics, intermediates, and modelling. *Water Research*, 53, 235–248. <https://doi.org/10.1016/j.watres.2014.01.016>
- De Luna, M., Veciana, M., Su, C., & Lu, M. (2012). Acetaminophen degradation by electro-Fenton and photoelectro-Fenton using a double cathode electrochemical cell.(Report). *Journal of Hazardous Materials*, 217 218.

- de Salas, F., Cañadas, R., Santiago, G., Virseda-Jerez, A., Vind, J., Gentili, P., Martínez, A., Guallar, V., Muñoz, I., & Camarero, S. (2019). Structural and biochemical insights into an engineered high-redox potential laccase overproduced in *Aspergillus*. *International Journal of Biological Macromolecules*, 141, 855–867. <https://doi.org/10.1016/j.ijbiomac.2019.09.052>
- Decker, H. and Tuczek, F. (2000) Tyrosinase/catecholoxidase activity of hemocyanins: Structural basis and molecular mechanism. *Trends Biochemical Sciences* 25, 392 – 397.
- Deng, Y., & Zhao, R. (2015). Advanced Oxidation Processes (AOPs) in Wastewater Treatment. *Current Pollution Reports*, 1(3), 167–176. <https://doi.org/10.1007/s40726-015-0015-z>
- Ding, R., Liu, S., He, C. & Nie, X. (2020). Paracetamol affects the expression of detoxification- and reproduction-related genes and alters the life traits of *Daphnia magna*. *Ecotoxicology* 29, 398–406 <https://doi.org/10.1007/s10646-020-02199-z>
- Ding, G., Zhang, X., Yang, M., & Pan, Y. (2013). Formation of new brominated disinfection byproducts during chlorination of saline sewage effluents. *Water Research*, 47(8), 2710–2718. <https://doi.org/10.1016/j.watres.2013.02.036>
- Dominguez, J., Gonzalez, T., Cuerda-Correa, E., & Muñoz-Peña, M. (2019). Combating paraben pollution in surface waters with a variety of photocatalyzed systems: Looking for the most efficient technology. *Open Chemistry*, 17(1), 1317–1327. <https://doi.org/10.1515/chem-2019-0133>
- Dordick, J. S., Marletta, M. A., & Klibanov, A. M. (1987). Polymerization of phenols catalyzed by peroxidase in non-aqueous media. *Biotechnology and Bioengineering*, 30(1), 31–36. <https://doi.org/10.1002/bit.260300106>
- Dordick, J.S., Klibanov, A.M., & Marletta, M.A. (1986). Horseradish peroxidase-catalyzed Hydroxylations: Mechanistic Studies. *Biochemistry* 1986 25 (10), 2946–2951 <https://doi.org/10.1021/bi00358a032>
- Du, Z., Zhang, Y., Li, A., & Lv, S. (2014). Rapid identification of polymer additives by atmospheric solid analysis probe with quadrupole time-of-flight mass spectrometry: Identification of polymer additives by ASAP-QTOFMS. *Rapid Communications in Mass Spectrometry*, 28(19), 2035–2042. <https://doi.org/10.1002/rcm.6998>
- Dunford, B.H. (2016) Heme Peroxidase Kinetics *In*: Raven, E. and Dunford, B. (Eds) *Heme Peroxidases*. Royal Society of Chemistry, Cambridge, UK, pp 99–112
- Dunford, H.B. (1999). *Heme Peroxidases*, Wiley and Sons pp. 1–111
- Duran, N., Rosa, M.A., D'Annibale, A., Gianfreda, L., 2002. Applications of laccases and tyrosinases (phenoloxidases) immobilized on different supports: a review. *Enzyme Microbial Technology* 31, 907–931. [https://doi.org/10.1016/S0141-0229\(02\)00214-4](https://doi.org/10.1016/S0141-0229(02)00214-4).

- Durliat, H., Courteix, A., Comtat, M., & Séris, J. (1992). Role of horseradish peroxidase in the catalytic hydroxylation of phenol. *Journal of Molecular Catalysis*, 75(3), 357–369. [https://doi.org/10.1016/0304-5102\(92\)80137-6](https://doi.org/10.1016/0304-5102(92)80137-6)
- Ebele, A.J., Abdallah, M.A., Harrad, S. (2017). Pharmaceuticals and personal products in the aquatic freshwater environment. *Emerging contaminants*, 3:1-16
<https://doi.org/10.1016/j.emcon.2016.12.004>
- Echeveste, P., Dachs, J., Berrojalbiz, N., & Agustí, S. (2010). Decrease in the abundance and viability of oceanic phytoplankton due to trace levels of complex mixtures of organic pollutants. *Chemosphere* (Oxford), 81(2), 161–168.
<https://doi.org/10.1016/j.chemosphere.2010.06.072>
- Eker, B., Zagorevski, D., Zhu, G., Linhardt, R., & Dordick, J. (2009). Enzymatic polymerization of phenols in room-temperature ionic liquids. *Journal of Molecular Catalysis. B, Enzymatic*, 59(1), 177–184.
<https://doi.org/10.1016/j.molcatb.2009.02.018>
- Ely, C., Lourdes Borba Magalhães, M., Henrique Lemos Soares, C., & Skoronski, E. (2017). Optimization of Phenol Removal from Biorefinery Effluent Using Horseradish Peroxidase. *Journal of Environmental Engineering*, 143(12), 4017075–. [https://doi.org/10.1061/\(ASCE\)EE.1943-7870.0001279](https://doi.org/10.1061/(ASCE)EE.1943-7870.0001279)
- European Union (EU) (2011). Parabens used in cosmetics.
https://ec.europa.eu/health/scientific_committees/docs/citizens_parabens_en.pdf
- Fang, W., Peng, Y., Muir, D., Lin, J., & Zhang, X. (2019). A critical review of synthetic chemicals in surface waters of the US, the EU and China. *Environment International*, 131, 104994. <https://doi.org/10.1016/j.envint.2019.104994>
- Fast, S., Gude, V., Truax, D., Martin, J., & Magbanua, B. (2017). A Critical Evaluation of Advanced Oxidation Processes for Emerging Contaminants Removal. *Environmental Processes*, 4(1), 283–302. <https://doi.org/10.1007/s40710-017-0207-1>
- Faust, B.C., & Holgne, J. (1987). Sensitized photooxidation of phenols by fulvic acid and in natural waters. *Environmental Science & Technology*, 21(10), 957–964.
<https://doi.org/10.1021/es50001a008>
- Feng, W., Taylor, K., Biswas, N., & Bewtra, J. (2013). Soybean peroxidase trapped in product precipitate during phenol polymerization retains activity and may be recycled. *Journal of Chemical Technology and Biotechnology* (1986), 88(8), 1429–1435. <https://doi.org/10.1002/jctb.4075>
- Fernandes, M., Souza, D., Henriques, R., Alves, M., Skoronski, E., & Junior, A. (2020). Obtaining soybean peroxidase from soybean hulls and its application for detoxification of 2,4-dichlorophenol contaminated water. *Journal of Environmental Chemical Engineering*, 8(3), 103786–.
<https://doi.org/10.1016/j.jece.2020.103786>

- Fernández, M.F., Arrebola, J.P., Jiménez-Díaz, I., Sáenz, J.M., Molina-Molina, J.M., Ballesteros, O. Kortenkamp, A., Olea, N. (2015). Bisphenol A and other phenols in human placenta from children with cryptorchidism or hypospadias. *Reproductive Toxicology* 59:89-95. <http://doi:10.1016/j.reprotox.2015.11.002>
- Fisher, M., Macpherson, S., Braun, J., Hauser, R., Walker, M., Feeley, M., Mallick, R., Bérubé, R., Arbuckle, T., & Fisher, M. (2017). Paraben Concentrations in Maternal Urine and Breast Milk and Its Association with Personal Care Product Use. *Environmental Science & Technology*, 51(7), 4009–4017. <https://doi.org/10.1021/acs.est.6b04302>
- Forero, J.E. Duque, J.J., & Diaz, J. (2001). Ozone for phenol treatment in industrial wastewater. *Ciencia, Tecnología y Futuro* 2(2):17-26.
- Frederiksen, H., Nielsen, J., Mørck, T., Hansen, P., Jensen, J., Nielsen, O., Andersson, A., & Knudsen, L. (2013). Urinary excretion of phthalate metabolites, phenols and parabens in rural and urban Danish mother–child pairs. *International Journal of Hygiene and Environmental Health*, 216(6), 772–783. <https://doi.org/10.1016/j.ijheh.2013.02.006>
- Frontistis, Z. (2020). Sonoelectrochemical Degradation of Propyl Paraben: An Examination of the Synergy in Different Water Matrices. *International Journal of Environmental Research and Public Health*, 17(8). <https://doi.org/10.3390/ijerph17082621>
- Gajhede, M., Schuller, D.J., Henriksen, A., Smith, A.T., Poulos, T.L. (1997). Crystal structure of horseradish peroxidase C at 2.15 Å resolution. *Nature Structural Biology*, 4(12):1032-1038. <https://doi:10.1038/nsb1297-1032>
- Galindo-Miranda, J., Guízar-González, C., Becerril-Bravo, E., Moeller-Chávez, G., & León-Becerril, E. (2019). Occurrence of emerging contaminants in environmental surface waters and their analytical methodology – a review. *Water Science & Technology*, 19(7), 1871–1884. <https://doi.org/10.2166/ws.2019.087>
- Galindo-Miranda, J., Guízar-González, C., Becerril-Bravo, E., Moeller-Chávez, G., & León-Becerril, E. (2019). Occurrence of emerging contaminants in environmental surface waters and their analytical methodology – a review. *Water Science & Technology*, 19(7), 1871–1884. <https://doi.org/10.2166/ws.2019.087>
- Ganiyu, S., Zhou, M., & Martínez-Huitle, C. (2018). Heterogeneous electro-Fenton and photoelectro-Fenton processes: A critical review of fundamental principles and application for water/wastewater treatment. *Applied Catalysis B: Environmental*, 235, 103–129. <https://doi.org/10.1016/j.apcatb.2018.04.044>
- Gasser, C., Ammann, E., Shahgaldian, P., & Corvini, P. (2014). Laccases to take on the challenge of emerging organic contaminants in wastewater. *Applied Microbiology and Biotechnology*, 98(24), 9931–9952. <https://doi.org/10.1007/s00253-014-6177-6>

- Geng, Z., Jagannadha Rao, K., Bassi, A., Gijzen, M., & Krishnamoorthy, N. (2001). Investigation of biocatalytic properties of soybean seed hull peroxidase. *Catalysis Today*, 64(3), 233–238. [https://doi.org/10.1016/S0920-5861\(00\)00527-7](https://doi.org/10.1016/S0920-5861(00)00527-7)
- Ghoshdastidar, A., Fox, S., & Tong, A. (2015). The presence of the top prescribed pharmaceuticals in treated sewage effluents and receiving waters in Southwest Nova Scotia, Canada. *Environmental Science and Pollution Research*, 22(1), 689–700. <https://doi.org/10.1007/s11356-014-3400-z>
- Ginebreda, A., Kuzmanovic, M., Guasch, H., Alda, M.L., Lopez-Doval, J.C., Munoz, I., Ricart, M., Romani, A.M., Sabater, S., Barcelo, D. (2014). Assessment of multi-chemical pollution in aquatic ecosystems using toxic units: Compound prioritization, mixture characterization and relationships with biological descriptors. *Science of the Total Environment* 468-469:715-723 <https://doi.org/10.1016/j.scitotenv.2013.08.086>
- Glaze, W. (1987). Drinking-water treatment with ozone. *Environmental Science & Technology*, 21(3), 224–230. <https://doi.org/10.1021/es00157a001>
- Gmurek, M., Gomes, J., Martins, R., Quinta-Ferreira, R., & Gmurek, M. (2019). Comparison of radical-driven technologies applied for paraben mixture degradation: mechanism, biodegradability, toxicity and cost assessment. *Environmental Science and Pollution Research International*, 26(36), 37174–37192. <https://doi.org/10.1007/s11356-019-06703-9>
- Golanoski, K., Fang, S., Del Vecchio, R., Blough, N., & Golanoski, K. (2012). Investigating the mechanism of phenol photooxidation by humic substances. *Environmental Science & Technology*, 46(7), 3912–3920. <https://doi.org/10.1021/es300142y>
- Gomes, J., Quinta-Ferreira, M., Costa, R., Quinta-Ferreira, R., & Martins, R. (2018a). Paraben degradation using catalytic ozonation over volcanic rocks. *Environmental Science and Pollution Research*, 25(8), 7346–7357. <https://doi.org/10.1007/s11356-017-1025-8>
- Gomes, F., Bergo, P., Trap, M., Spadoto, M., Galinaro, C., Rodrigues-Filho, E., Leitão, A., & Tremiliosi-Filho, G. (2018b). Photolysis of parabens using medium-pressure mercury lamps: Toxicity effects in MCF7, Balb/c 3T3 cells and *Ceriodaphnia dubia*. *Chemosphere* (Oxford), 208, 325–334. <https://doi.org/10.1016/j.chemosphere.2018.05.135>
- Gomes, F., de Souza, N., Galinaro, C., Arriveti, L., de Assis, J., & Tremiliosi-Filho, G. (2016). Electrochemical degradation of butyl paraben on platinum and glassy carbon electrodes. *Journal of Electroanalytical Chemistry*, 769, 124–130. <https://doi.org/10.1016/j.jelechem.2016.03.016>
- Gomes, J., Frasson, D., Pereira, J., Gonçalves, F., Castro, L., Quinta-Ferreira, R., & Martins, R. (2019). Ecotoxicity variation through parabens degradation by single

- and catalytic ozonation using volcanic rock. *Chemical Engineering Journal*, 360, 30–37. <https://doi.org/10.1016/j.cej.2018.11.194>
- Gomori G. (1955). Preparation of buffers for use in enzyme studies. *Methods in Enzymology* 1, 138-146.
- Gong, T., & Zhang, X. (2015). Detection, identification and formation of new iodinated disinfection byproducts in chlorinated saline wastewater effluents. *Water Research*, 68, 77–86. <https://doi.org/10.1016/j.watres.2014.09.041>
- Goodwin, D., Yamazaki, I., Aust, S., & Grover, T. (1995). Determination of Rate Constants for Rapid Peroxidase Reactions. *Analytical Biochemistry*, 231(2), 333–338. <https://doi.org/10.1006/abio.1995.0059>
- Gotardo, F., Cocca, L., Acunha, T., Longoni, A., Toldo, J., Gonçalves, P., Iglesias, B., & De Boni, L. (2017). Investigating the intersystem crossing rate and triplet quantum yield of Protoporphyrin IX by means of pulse train fluorescence technique. *Chemical Physics Letters*, 674, 48–57. <https://doi.org/10.1016/j.cplett.2017.02.055>
- Gray, J., & Montgomery, R. (2006). Asymmetric glycosylation of soybean seed coat peroxidase. *Carbohydrate Research*, 341(2), 198–209. <https://doi.org/10.1016/j.carres.2005.11.016>
- Gray, J., Yang, B., Hull, S., Venzke, D., & Montgomery, R. (1996). The glycans of soybean peroxidase. *Glycobiology*, 6(1), 23–32. <https://doi.org/10.1093/glycob/6.1.23>
- Gros, M., Mas-Pla, J., Boy-Roura, M., Geli, I., Domingo, F., & Petrović, M. (2019). Veterinary pharmaceuticals and antibiotics in manure and slurry and their fate in amended agricultural soils: Findings from an experimental field site (Baix Empordà, NE Catalonia). *Science of the Total Environment*, 654, 1337–1349. <https://doi.org/10.1016/j.scitotenv.2018.11.061>
- Gryglik, D., & Gmurek, M. (2018). The photosensitized oxidation of mixture of parabens in aqueous solution. *Environmental Science and Pollution Research*, 25(4), 3009–3019. <https://doi.org/10.1007/s11356-014-4059-1>
- Guiloski, I.C., Ribasa, J.L.C., Piancinib, L.D.S., Dagostimb, A.C., Cirioc, S.M., Favorod, L.F., Boschen, S.L., Cestari, M.M., Cunha, C., Silva de Assisa, H.C. (2017). Paracetamol causes endocrine disruption and hepatotoxicity in male fish *Rhamdia quelen* after subchronic exposure. *Environmental Toxicology and Pharmacology* 53:111-120. <https://doi.org/10.1016/j.etap.2017.05.005>
- Gunne, M., Hoppner, A., Hagedoorn, P., & Urlacher, V. (2014). Structural and redox properties of the small laccase Ssl1 from *Streptomyces sviveus*.(Report). *FEBS Journal*, 281(18), 4307–4318. <https://doi.org/10.1111/febs.12755>
- Hachi, M., Chergui, A., Yeddou, A., Selatnia, A., & Cabana, H. (2017). Removal of acetaminophen and carbamazepine in single and binary systems with immobilized

- laccase from *Trametes hirsuta*. *Biocatalysis and Biotransformation*, 35(1), 51–62. <https://doi.org/10.1080/10242422.2017.1280032>
- Hailu, G., Weersink, A. & Cahlik, F. (2010). Examining the Prospects for Commercialization of Soybean Peroxidase. *AgBioForum*, 13(3): 263-273
- Halling-Sørensen, B., Nors Nielsen, S., Lanzky, P., Ingerslev, F., Holten Lützhøft, H., & Jørgensen, S. (1998). Occurrence, fate and effects of pharmaceutical substances in the environment- A review. *Chemosphere*, 36(2), 357–393. [https://doi.org/10.1016/S0045-6535\(97\)00354-8](https://doi.org/10.1016/S0045-6535(97)00354-8)
- Han, Q.F., Zhao, S., Zhang, X.R., Wang, X.L., Song, C., Wang, S.G. (2020). Distribution, combined pollution and risk assessment of antibiotics in typical marine aquaculture farms surrounding the Yellow Sea, North China. *Environment International* 138: 105551 <https://doi.org/10.1016/j.envint.2020.105551>
- Hansen, K., Andersen, H., Ledin, A., & Hansen, K. (2010). Ozonation of estrogenic chemicals in biologically treated sewage. *Water Science & Technology*, 62(3), 649–657. <https://doi.org/10.2166/wst.2010.919>
- Hansen, K.M.S., & Andersen, H.R. (2012). Energy Effectiveness of Direct UV and UV/H₂O₂ Treatment of Estrogenic Chemicals in Biologically Treated Sewage. *International Journal of Photoenergy*, 2012(2012), 1–9. <https://doi.org/10.1155/2012/270320>
- Harada, T., Kimura, E., Hirata-Koizumi, M., Hirose, A., Kamata, D., Ema, M. (2008). Reproductive and developmental toxicity screening study of 4-aminophenol in rats. *Drug Chemical Toxicology* 31 (4), 473-486.
- Heffernan, A., Baduel, C., Toms, L., Calafat, A., Ye, X., Hobson, P., Broomhall, S., & Mueller, J. (2015). Use of pooled samples to assess human exposure to parabens, benzophenone-3 and triclosan in Queensland, Australia. *Environment International*, 85, 77–83. <https://doi.org/10.1016/j.envint.2015.09.001>
- Heidler, J., Sapkota, A., & Halden, R. (2006). Partitioning, persistence, and accumulation in digested sludge of the topical antiseptic triclocarban during wastewater treatment. *Environmental Science & Technology*, 40(11), 3634–3639. <https://doi.org/10.1021/es052245n>
- Henriksen, A., Mirza, O., Indiani, C., Teilum, K., Smulevich, G., Welinder, K., & Gajhede, M. (2001). Structure of soybean seed coat peroxidase: A plant peroxidase with unusual stability and haem-apoprotein interactions. *Protein Science*, 10(1), 108–115. <https://doi.org/10.1110/ps.37301>
- Hersleth, H.P., Ryde, U., Rydberg, P., Görbitz, C.H., Andersson, K.K. (2006). Structures of the high-valent metal-ion haem-oxygen intermediates in peroxidases,

- oxygenases and catalases. *Journal of Inorganic Biochemistry*, 100(4):460-476. <https://doi:10.1016/j.jinorgbio.2006.01.018>
- Hewavitharana, A., Lee, S., Dawson, P., Markovich, D., & Shaw, P. (2008). Development of an HPLC–MS/MS method for the selective determination of paracetamol metabolites in mouse urine. *Analytical Biochemistry*, 374(1), 106–111. <https://doi.org/10.1016/j.ab.2007.11.011>
- Hines, E., Mendola, P., Von Ehrenstein, O., Ye, X., Calafat, A., & Fenton, S. (2015). Concentrations of environmental phenols and parabens in milk, urine and serum of lactating North Carolina women. *Reproductive Toxicology*, 54, 120–128. <https://doi.org/10.1016/j.reprotox.2014.11.006>
- Howard, P.H., Muir, D.C.G. (2011). Identifying New Persistent and Bioaccumulative Organics Among Chemicals in Commerce II: Pharmaceuticals. *Environmental Science and Technology* 45:6938–6946. <https://doi.org/10.1021/es201196x>
- Howes, B., Heering, H., Roberts, T., Schneider-Belhadadd, F., Smith, A., & Smulevich, G. (2001). Mutation of residues critical for benzohydroxamic acid binding to horseradish peroxidase isoenzyme C. *Biopolymers*, 62(5), 261–267. <https://doi.org/10.1002/bip.1021>
- Hu, Y., Li, Z., Yang, J., & Zhu, H. (2019). Degradation of methylparaben using BiOI-hydrogel composites activated peroxymonosulfate under visible light irradiation. *Chemical Engineering Journal (Lausanne, Switzerland)*, 360, 200–211. <https://doi.org/10.1016/j.cej.2018.11.217>
- Huixian, Z., & Taylor, K. (1994). Products of oxidative coupling of phenol by horseradish peroxidase. *Chemosphere*, 28(10), 1807–1817. [https://doi.org/10.1016/0045-6535\(94\)90028-0](https://doi.org/10.1016/0045-6535(94)90028-0)
- Humer, D., & Spadiut, O. (2019). Improving the Performance of Horseradish Peroxidase by Site-Directed Mutagenesis. *International Journal of Molecular Sciences*, 20(4). <https://doi.org/10.3390/ijms20040916>
- Ibrahim, M., Ali, H., Taylor, K., Biswas, N., & Bewtra, J. (2001). Enzyme-Catalyzed Removal of Phenol from Refinery Wastewater: Feasibility Studies. *Water Environment Research*, 73(2), 165–172. <https://doi.org/10.2175/106143001X138822>
- Ike, I., Karanfil, T., Cho, J., & Hur, J. (2019). Oxidation byproducts from the degradation of dissolved organic matter by advanced oxidation processes – A critical review. *Water Research*, 164, 114929. <https://doi.org/10.1016/j.watres.2019.114929>
- Jamal, A., Rastkari, N., Dehghaniathar, R., Aghaei, M., Nodehi, R., Nasser, S., Kashani, H., & Yunesian, M. (2019). Prenatal exposure to parabens and anthropometric birth outcomes: A systematic review. *Environmental Research*, 173, 419–431. <https://doi.org/10.1016/j.envres.2019.02.044>
- Janusz, G., Pawlik, A., Świdarska-Burek, U., Polak, J., Sulej, J., Jarosz-Wilkolazka, A., Paszczyński, A., & Janusz, G. (2020). Laccase Properties, Physiological Functions, and Evolution. *International Journal of Molecular Sciences*, 21(3). <https://doi.org/10.3390/ijms21030966>

- Jelic', A., Gros, M., Petrovic', M., Ginebreda, A., & Barcelo, D. (2012). Occurrence and Elimination of Pharmaceuticals During Conventional Wastewater Treatment *In* H. Guasch et al. . (eds.), *Emerging and Priority Pollutants in Rivers*, Handbook of Environmental Chemistry 19: 1–24, https://DOI.org/10.1007/978-3-642-25722-3_1 Springer-Verlag Berlin Heidelberg.
- Jones, O., Voulvoulis, N., & Lester, J. (2006). Partitioning Behavior of Five Pharmaceutical Compounds to Activated Sludge and River Sediment. *Archives of Environmental Contamination and Toxicology*, 50(3), 297–305. <https://doi.org/10.1007/s00244-005-1095-3>
- Juliano, C., & Magrini, G. (2017). Cosmetic Ingredients as Emerging Pollutants of Environmental and Health Concern. A Mini-Review. *Cosmetics*, 4(2). <https://doi.org/10.3390/cosmetics4020011>
- Ju-nam, Y., and Lead, J.R. (2008). Manufactured nanoparticles: an overview of chemistry, interactions and potential environmental implications. *Science of the Total Environment*, 400, 396-414. <https://doi.org/10.1016/j.scitotenv.2008.06.042>
- K'Oreje, K., Kandie, F., Vergeynst, L., Abira, M., Van Langenhove, H., Okoth, M., & Demeestere, K. (2018). Occurrence, fate and removal of pharmaceuticals, personal care products and pesticides in wastewater stabilization ponds and receiving rivers in the Nzoia Basin, Kenya. *Science of the Total Environment*, 637-638, 336–348. <https://doi.org/10.1016/j.scitotenv.2018.04.331>
- K'Oreje, K., Okoth, M., Van Langenhove, H., & Demeestere, K. (2020). Occurrence and treatment of contaminants of emerging concern in the African aquatic environment: Literature review and a look ahead. *Journal of Environmental Management*, 254, 109752. <https://doi.org/10.1016/j.jenvman.2019.109752>
- Kadirvelu, K., Thamaraiselvi, K., & Namasivayam, C. (2001). Removal of heavy metals from industrial wastewaters by adsorption onto activated carbon prepared from an agricultural solid waste. *Bioresource Technology*, 76(1), 63–65. [https://doi.org/10.1016/S0960-8524\(00\)00072-9](https://doi.org/10.1016/S0960-8524(00)00072-9)
- Kamal, J.K., & Behere, D.V. (2003). Activity, stability and conformational flexibility of seed coat soybean peroxidase. *Journal of Inorganic Biochemistry*, 94(3):236-42. [https://doi.org/10.1016/s0162-0134\(03\)00004-7](https://doi.org/10.1016/s0162-0134(03)00004-7)
- Kamal, J.K.A., & Behere, D.V. (2002). Thermal and conformational stability of seed coat soybean peroxidase. *Biochemistry*, 41, 9034–9042. <http://doi.org/10.1021/bi025621e>
- Kanteev, M., Goldfeder, M., & Fishman, A. (2015). Structure–function correlations in tyrosinases [Review of Structure–function correlations in tyrosinases]. *Protein Science*, 24(9), 1360–1369. <https://doi.org/10.1002/pro.2734>

- Kaonga, C., Chidya, R., Kosamu, I., Abdel-dayem, S., Mapoma, H., Thole, B., ... Sakugawa, H. (2018). Trends in usage of selected fungicides in Japan between 1962 and 2014: a review. *International Journal of Environmental Science and Technology*, 15(8), 1801–1814. <https://doi.org/10.1007/s13762-017-1565-y>
- Karthikraj, R., Borkar, S., Lee, S., Kannan, K., & Karthikraj, R. (2018). Parabens and Their Metabolites in Pet Food and Urine from New York State, United States. *Environmental Science & Technology*, 52(6), 3727–3737. <https://doi.org/10.1021/acs.est.7b05981>
- Karthikraj, R., Vasu, A., Balakrishna, K., Sinha, R., & Kannan, K. (2017). Occurrence and fate of parabens and their metabolites in five sewage treatment plants in India. *Science of the Total Environment*, 593-594, 592–598. <https://doi.org/10.1016/j.scitotenv.2017.03.173>
- Kaur, T. Taylor, K.E., Biswas, N. (2020). Soybean peroxidase-catalyzed degradation of a sulfonated dye and its azo-cleavage product. *Journal of Chemical Technology and Biotechnology (1986)*. <https://doi.org/10.1002/jctb.6555>
- Keerthanan, S., Jayasinghe, C., Biswas, J.K. & Vithanage, M. (2020). Pharmaceutical and Personal Care Products (PPCPs) in the environment: Plant uptake, translocation, bioaccumulation, and human health risks. *Critical Reviews in Environmental Science and Technology*, ahead-of-print(ahead-of-print), 1–38. <https://doi.org/10.1080/10643389.2020.1753634>
- Kim, D., Cui, R., Moon, J., Kwak, J., Kim, S., Kim, D., An, Y., & Kim, D. (2018). Estimation of the soil hazardous concentration of methylparaben using a species sensitivity approach. *Environmental Pollution (Barking, Essex : 1987)*, 242(Pt A), 1002–1009. <https://doi.org/10.1016/j.envpol.2018.07.053>
- Klein, E.Y., Van Boeckel, T.P., Martinez, E.M., Pant, S., Gandra, S., Levin, S.A., Goossens, H. and Laxminarayan, R., 2018. Global increase and geographic convergence in antibiotic consumption between 2000 and 2015. *Proceedings of the National Academy of Science*, U.S.A. 115, E3463-e3470
- Kleywegt, Payne, Ng, Fletcher, T. (2019). Environmental loadings of Active Pharmaceutical Ingredients from manufacturing facilities in Canada. *Science of the Total Environment* 646:257-264. <https://doi.org/10.1016/j.scitotenv.2018.07.240>
- Klibanov, A., & Klibanov, A. (1997). Why are enzymes less active in organic solvents than in water? *Trends in Biotechnology*, 15(3), 97–101. [https://doi.org/10.1016/S0167-7799\(97\)01013-5](https://doi.org/10.1016/S0167-7799(97)01013-5)
- Klonowska, A., Gaudin, C., Fournel, A., Asso, M., Le Petit, J., Giorgi, M., & Tron, T. (2002). Characterization of a low redox potential laccase from the basidiomycete

- C30. *European Journal of Biochemistry*, 269(24), 6119–6125.
<https://doi.org/10.1046/j.1432-1033.2002.03324.x>
- Kluge, M., Ullrich, R., Dolge, C., Scheibner, K., & Hofrichter, M. (2009). Hydroxylation of naphthalene by aromatic peroxygenase from *Agroclybe aegerita* proceeds via oxygen transfer from H₂O₂ and intermediary epoxidation. *Applied Microbiology and Biotechnology*, 81(6), 1071–1076. <https://doi.org/10.1007/s00253-008-1704-y>
- Kobayashi S., Shoda S., Uyama H. (1995) Enzymatic polymerization and oligomerization. In: *Polymer Synthesis/Polymer Engineering. Advances in Polymer Science*, vol 121. Springer, Berlin, Heidelberg. Pp 1-30.
<https://doi.org/10.1007/BFb0018577>
- Koehler, B., Barsotti, F., Minella, M., Landelius, T., Minero, C., Tranvik, L., & Vione, D. (2018). Simulation of photoreactive transients and of photochemical transformation of organic pollutants in sunlit boreal lakes across 14 degrees of latitude: A photochemical mapping of Sweden. *Water Research*, 129, 94–104.
<https://doi.org/10.1016/j.watres.2017.10.064>
- Koplin, D.A., Furlong, E.T., Meyer, M.T., Thurman, E.M., Zaugg, S.D., Barber, L.B., Buxton, H.T. (2002). Pharmaceuticals, hormones, and other organic wastewater contaminants in U.S. streams, 1999-2000: A national reconnaissance. *Environmental Science & Technology* 36:1202-1211
<https://doi.org/10.1021/es011055j>
- Kunkel, U., & Radke, M. (2012). Fate of pharmaceuticals in rivers: Deriving a benchmark dataset at favorable attenuation conditions. *Water Research*, 46(17), 5551–5565. <https://doi.org/10.1016/j.watres.2012.07.033>
- Le, T.X.H., Nguyen, T.V., Amadou, Y.Z., Zoungrana, L., Avril, F., Nguyen, D.L., Petit, E., Mendret, J., Bonniol, V., Bechelany, M., Lacour, S., Lesage, G., Cretin, M. (2017). Correlation between degradation pathway and toxicity of acetaminophen and its by-products by using the electro-Fenton process in aqueous media. *Chemosphere*, 172:1-9
<https://doi.org/10.1016/j.chemosphere.2016.12.060>
- Lee, J., Bang, S.H., Kim, Y., & Min, J. (2018). Toxicities of Four Parabens and Their Mixtures to *Daphnia magna* and *Aliivibrio fischeri*. *Environmental Health and Toxicology*, 33(4), e2018018. <https://doi.org/10.5620/eht.e2018018>
- Lee, S., Hong, S., & Sung, M. (1996). Removal and bioconversion of phenol in wastewater by a thermostable β -tyrosinase. *Enzyme and Microbial Technology*, 19(5), 374–377. [https://doi.org/10.1016/S0141-0229\(96\)00001-4](https://doi.org/10.1016/S0141-0229(96)00001-4)
- Li, J., Ye, Q., Gan, J., & Li, J. (2014). Degradation and transformation products of acetaminophen in soil. *Water Research*, 49, 44–52.
<https://doi.org/10.1016/j.watres.2013.11.008>
- Li, X., Chen, W., Ma, L., Wang, H., & Fan, J. (2018b). Industrial wastewater advanced treatment via catalytic ozonation with an Fe-based catalyst. *Chemosphere*, 195, 336–343. <https://doi.org/10.1016/j.chemosphere.2017.12.080>

- Li, Y., Pan, Y., Lian, L., Yan, S., Song, W., & Yang, X. (2017). Photosensitized degradation of acetaminophen in natural organic matter solutions: The role of triplet states and oxygen. *Water Research*, 109, 266–273. <https://doi.org/10.1016/j.watres.2016.11.049>
- Li, Y., Zhang, L., Liu, X., Ding, J. (2019). Ranking and prioritizing pharmaceuticals in the aquatic environment of China. *Science of the Total Environment* 658: 333–342 <https://doi.org/10.1016/j.scitotenv.2018.12.048>
- Li, Z., Sobek, A., Radke, M., & Li, Z. (2016). Fate of Pharmaceuticals and Their Transformation Products in Four Small European Rivers Receiving Treated Wastewater. *Environmental Science & Technology*, 50(11), 5614–5621. <https://doi.org/10.1021/acs.est.5b06327>
- Liang, C., Lan, Z., Zhang, X., & Liu, Y. (2016). Mechanism for the primary transformation of acetaminophen in a soil/water system. *Water Research*, 98, 215–224. <https://doi.org/10.1016/j.watres.2016.04.027>
- Liao, C., Liu, F., Kannan, K., & Liao, C. (2013). Occurrence of and dietary exposure to parabens in foodstuffs from the United States. *Environmental Science & Technology*, 47(8), 3918–3925. <https://doi.org/10.1021/es400724s>
- Liu, H., Wang, H., Zhou, X., Fan, J., Liu, Y., & Yang, Y. (2019a). A comprehensive index for evaluating and enhancing effective wastewater treatment in two industrial parks in China. *Journal of Cleaner Production*, 230, 854–861. <https://doi.org/10.1016/j.jclepro.2019.05.134>
- Liu, Y., Hu, C., & Lo, S. (2019b). Direct and indirect electrochemical oxidation of amine-containing pharmaceuticals using graphite electrodes. *Journal of Hazardous Materials*, 366, 592–605. <https://doi.org/10.1016/j.jhazmat.2018.12.037>
- Loeffler, D., Roembke, J., Meller, M., & Ternes, T. (2005). Environmental Fate of Pharmaceuticals in Water/sediment Systems. *Environmental Science & Technology*, 39(14), 5209–5218. <https://doi.org/10.1021/es0484146>
- Loiselle, S., Vione, D., Minero, C., Maurino, V., Tognazzi, A., Dattilo, A., Rossi, C., & Bracchini, L. (2012). Chemical and optical photo-transformation of dissolved organic matter. *Water Research*, 46(10), 3197–3207. <https://doi.org/10.1016/j.watres.2012.02.047>
- Lu, B., Iwuoha, E., Smyth, M., & O’Kennedy, R. (1997). Effects of acetonitrile on horseradish peroxidase (HRP)-anti HRP antibody interaction. *Biosensors and Bioelectronics*, 12(7), 619–625. [https://doi.org/10.1016/S0956-5663\(97\)00015-8](https://doi.org/10.1016/S0956-5663(97)00015-8)
- Lu, J., & Huang, Q. (2009). Removal of Acetaminophen Using Enzyme-Mediated Oxidative Coupling Processes: II. Cross-Coupling with Natural Organic Matter. *Environmental Science & Technology*, 43(18), 7068–7073. <https://doi.org/10.1021/es9001295>
- Lu, J., Li, H., Luo, Z., Lin, H., & Yang, Z. (2018). Occurrence, distribution, and environmental risk of four categories of personal care products in the Xiangjiang

- River, China. *Environmental Science and Pollution Research*, 25(27), 27524–27534. <https://doi.org/10.1007/s11356-018-2686-7>
- Lu, Y., Yang, Q., Wang, L., Zhang, M., Guo, W., Cai, Z., Wang, D., Yang, W., & Chen, Y. (2017). Enhanced Activity of Immobilized Horseradish Peroxidase by Carbon Nanospheres for Phenols Removal. *CLEAN: Soil, Air, Water*, 45(2), 1600077–n/a. <https://doi.org/10.1002/clen.201600077>
- Lucas, M., & Peres, J. (2015). Removal of Emerging Contaminants by Fenton and UV-Driven Advanced Oxidation Processes. *Water, Air, & Soil Pollution*, 226(8), 1–9. <https://doi.org/10.1007/s11270-015-2534-z>
- Ma, K., Qin, Z., Zhao, Z., Zhao, C., & Liang, S. (2016). Toxicity evaluation of wastewater collected at different treatment stages from a pharmaceutical industrial park wastewater treatment plant. *Chemosphere*, 158, 163–170. <https://doi.org/10.1016/j.chemosphere.2016.05.052>
- Machulek, A., Oliveira, S.C., Osugi, M.E., Ferreira, V.S., Quina, F.H., Dantas, R.F., Oliveira, S.L., Casagrande, G.A., Anaissi, F.J., Silva, V.O., Cavalcante, R.P., Gozzi, F., Ramos, D.D., da Rosa, A.P.P., Santos, A.P.F., de castro, D.C., & Nogueira, J.A. (2013). Application of different advanced oxidation processes for the degradation of organic pollutants, in *Organic pollutants - monitoring, risk and treatment*, ed. M. Nageeb Rashed, InTech, 2013. (Available from: <http://www.intechopen.com/books/organic-pollutants-monitoring-risk-and-treatment/applicationof-different-advanced-oxidation-processes-for-the-degradationof-organic-pollutants>) Accessed July 22, 2020
- Madarshahian, S., Pophristic, M., & McEwen, C. N. (2017). Infrared atmospheric solids analysis probe (IR-ASAP) mass spectrometry for ambient analysis of volatile compounds without heated gas. *Analytical Methods*, 9(34), 5009–5014. <https://doi.org/10.1039/C7AY00874K>
- Maeng, S., Sharma, S., Lekkerkerker-Teunissen, K., & Amy, G. (2011). Occurrence and fate of bulk organic matter and pharmaceutically active compounds in managed aquifer recharge: A review. *Water Research*, 45(10), 3015–3033. <https://doi.org/10.1016/j.watres.2011.02.017>
- Mao, Q., Ji, F., Wang, W., Wang, Q., Hu, Z., & Yuan, S. (2016). Chlorination of parabens: reaction kinetics and transformation product identification. *Environmental Science and Pollution Research*, 23(22), 23081–23091. <https://doi.org/10.1007/s11356-016-7499-y>
- Marchisio, A., Minella, M., Maurino, V., Minero, C., & Vione, D. (2015). Photogeneration of reactive transient species upon irradiation of natural water samples: Formation quantum yields in different spectral intervals, and implications for the photochemistry of surface waters. *Water Research*, 73, 145–156. <https://doi.org/10.1016/j.watres.2015.01.016>

- Márquez, G., Rodríguez, E., Beltrán, F., & Álvarez, P. (2014). Solar photocatalytic ozonation of a mixture of pharmaceutical compounds in water. *Chemosphere*, 113, 71–78. <https://doi.org/10.1016/j.chemosphere.2014.03.093>
- Martínez-Huitle, C.A. & Andrade, L.S. (2011). Electrocatalysis in wastewater treatment: recent mechanism advances. *Química Nova*, 34(5), 850–858. <https://doi.org/10.1590/S0100-40422011000500021>
- Martins, R., & Quinta-Ferreira, R. (2009). Catalytic ozonation of phenolic acids over a Mn–Ce–O catalyst. *Applied Catalysis B, Environmental*, 90(1-2), 268–277. <https://doi.org/10.1016/j.apcatb.2009.03.023>
- Mashhadi, N. (2019). "Oxidative Polymerization of Heterocyclic Aromatics Using Soybean Peroxidase for Treatment of Wastewater" (2019). *Electronic Theses and Dissertations*. 7646. <https://scholar.uwindsor.ca/etd/7646>
- Mashhadi, N., Taylor, K., Biswas, N., Meister, P., & Gauld, J. (2019). Oligomerization of 3-substituted quinolines by catalytic activity of soybean peroxidase as a wastewater treatment. Product formation and computational studies. *Chemical Engineering Journal*, 364, 340–348. <https://doi.org/10.1016/j.cej.2019.01.184>
- McCabe, A.J. & Arnold, W.A. (2017). Reactivity of triplet excited states of dissolved natural organic matter in stormflow from mixed-use watersheds. *Environmental Science & Technology*, 51(17), 9718–9728. <https://doi.org/10.1021/acs.est.7b01914>
- McEldoon, J., & Dordick, J. (1996). Unusual Thermal Stability of Soybean Peroxidase. *Biotechnology Progress*, 12(4), 555–558. <https://doi.org/10.1021/bp960010x>
- McNeill, K., & Canonica, S. (2016). Triplet state dissolved organic matter in aquatic photochemistry: reaction mechanisms, substrate scope, and photophysical properties. *Environmental Science: Processes & Impact* 18:1381–1399 <https://doi.org/10.1039/C6EM00408C>
- Meeker, J., Cantonwine, D., Rivera-González, L., Ferguson, K., Mukherjee, B., Calafat, A., Ye, X., Anzalota Del Toro, L., Crespo-Hernández, N., Jiménez-Vélez, B., Alshawabkeh, A., Cordero, J., & Meeker, J. (2013). Distribution, variability, and predictors of urinary concentrations of phenols and parabens among pregnant women in Puerto Rico. *Environmental Science & Technology*, 47(7), 3439–3447. <https://doi.org/10.1021/es400510g>
- Meeker, J., Yang, T., Ye, X., Calafat, A., & Hause, R. (2011). Urinary concentrations of parabens and serum hormone levels, semen quality parameters, and sperm DNA damage. (Research)(Report). *Environmental Health Perspectives*, 119(2), 252–257. <https://doi.org/10.1289/ehp.1002238>
- Melo, L., & Queiroz, M. (2010). Simultaneous analysis of parabens in cosmetic products by stir bar sorptive extraction and liquid chromatography. *Journal of Separation Science*, 33(12), 1849–1855. <https://doi.org/10.1002/jssc.201000024>
- Metcalf & Eddy, (2014) *Wastewater engineering: treatment and resource recovery*, 5th edn. McGraw-Hill Education, New York

- Metch, J., Ma, Y., Pruden, A., & Vikesland, P. (2015). Enhanced disinfection by-product formation due to nanoparticles in wastewater treatment plant effluents. *Environmental Science: Water Research & Technology*, 1(6), 823–831. <https://doi.org/10.1039/c5ew00114e>
- Miklos, D., Remy, C., Jekel, M., Linden, K., Drewes, J., & Hübner, U. (2018). Evaluation of advanced oxidation processes for water and wastewater treatment – A critical review. *Water Research*, 139, 118–131. <https://doi.org/10.1016/j.watres.2018.03.042>
- Milstead, R.P., Nance, K.T., Tarnas, K.S., Egelhofer, K.E., Griffith, D.R. (2018). Photochemical degradation of halogenated estrogens under natural solar irradiance. *Environmental Sciences: Process and Impacts* 20(10):1350-1360. <https://doi.org/10.1039/C8EM00275D>
- Mina, O., Gall, H., Elliott, H., Watson, J., Mashtare, M., Langkilde, T., ... Boyer, E. (2018). Estrogen occurrence and persistence in vernal pools impacted by wastewater irrigation practices. *Agriculture, Ecosystems & Environment*, 257. Retrieved from <http://search.proquest.com/docview/2057956487/>
- Monteiro, S.C., Boxall, A.B. (2010). Occurrence and fate of human pharmaceuticals in the environment. *Reviews of Environmental Contamination and Toxicology*: Springer; 2010. p. 53–154. https://doi.org/10.1007/978-1-4419-1157-5_2 [PMID:19898761](https://pubmed.ncbi.nlm.nih.gov/19898761/)
- Moos, R., Angerer, J., Wittsiepe, J., Wilhelm, M., Brüning, T., & Koch, H. (2014). Rapid determination of nine parabens and seven other environmental phenols in urine samples of German children and adults. *International Journal of Hygiene and Environmental Health*, 217(8), 845–853. <https://doi.org/10.1016/j.ijheh.2014.06.003>
- Morsi, R., Bilal, M., Iqbal, H., & Ashraf, S. (2020). Laccases and peroxidases: The smart, greener and futuristic biocatalytic tools to mitigate recalcitrant emerging pollutants. *Science of the Total Environment*, 714, 136572. <https://doi.org/10.1016/j.scitotenv.2020.136572>
- Mukai, M., Nagano, S., Tanaka, M., Ishimori, K., Morishima, I., Ogura, T., Watanabe, Y., & Kitagawa, T. (1997). Effects of concerted hydrogen bonding of distal histidine on active site structures of horseradish peroxidase. Resonance Raman studies with Asn70 mutants. *Journal of the American Chemical Society*, 119(7), 1758–1766. <https://doi.org/10.1021/ja962551o>
- Munk, L., Sitarz, A., Kalyani, D., Mikkelsen, J., & Meyer, A. (2015). Can laccases catalyze bond cleavage in lignin? *Biotechnology Advances*, 33(1), 13–24. <https://doi.org/10.1016/j.biotechadv.2014.12.008>
- Nagano, S., Tanaka, M., Ishimori, K., Watanabe, Y., Morishima, I., & Nagano, S. (1996). Catalytic roles of the distal site asparagine-histidine couple in peroxidases. *Biochemistry*, 35(45), 14251–14258. <https://doi.org/10.1021/bi961740g>

- Nakajima, R., & Yamazaki, I. (1980). The conversion of horseradish peroxidase C to a verdohemoprotein by a hydroperoxide derived enzymatically from indole-3-acetic acid and by m-nitroperoxybenzoic acid. *Journal of Biological Chemistry*, 255(5), 2067–2071.
- Nakamoto, S., & Machida, N. (1992). Phenol removal from aqueous solutions by peroxidase-catalyzed reaction using additives. *Water Research*, 26(1), 49–54. [https://doi.org/10.1016/0043-1354\(92\)90110-P](https://doi.org/10.1016/0043-1354(92)90110-P)
- Narotsky, M., Klinefelter, G., Goldman, J., Deangelo, A., Best, D., Mcdonald, A., ... Simmons, J. (2015). Reproductive Toxicity of a Mixture of Regulated Drinking-Water Disinfection By-Products in a Multigenerational Rat Bioassay. *Environmental Health Perspectives (Online)*, 123(6), 564. <https://doi.org/10.1289/ehp.1408579>
- Nawrocki, J. (2013). Catalytic ozonation in water: Controversies and questions. Discussion paper. *Applied Catalysis B: Environmental*, 142-143, 465–471. <https://doi.org/10.1016/j.apcatb.2013.05.061>
- Valkova, N., Lépine, F., Valeanu, L., Dupont, M., Labrie, L., Bisailon, J., Beudet, J., Shareck, F., & Villemur, F. (2001). Hydrolysis of 4-Hydroxybenzoic Acid Esters (Parabens) and Their Aerobic Transformation into Phenol by the Resistant *Enterobacter cloacae* Strain EM. *Applied and Environmental Microbiology*, 67(6), 2404–2409. <https://doi.org/10.1128/AEM.67.6.2404-2409.2001>
- Newmyer, S., de Montellano, P., & Newmyer, S. (1996). Rescue of the catalytic activity of an H42A mutant of horseradish peroxidase by exogenous imidazoles. *The Journal of Biological Chemistry*, 271(25), 14891–14896. <https://doi.org/10.1074/jbc.271.25.14891>
- Nicell, J., & Wright, H. (1997). A model of peroxidase activity with inhibition by hydrogen peroxide. *Enzyme and Microbial Technology*, 21(4), 302–310. [https://doi.org/10.1016/S0141-0229\(97\)00001-X](https://doi.org/10.1016/S0141-0229(97)00001-X)
- Nicolescu, T.O. (2017) Interpretation of mass spectra. In: Aliofkhazraei, M. (ed) *Mass spectrometry*. IntechOpen. <https://doi.10.5772/intechopen.68595>
- Niegowski, S. (1953). Destruction of Phenols by Oxidation of Ozone. *Industrial & Engineering Chemistry*, 45(3), 632–634. <https://doi.org/10.1021/ie50519a046>
- Nogueira, R., Trovo, A., Da Silva, M., Villa, R., & de Oliveira, M. (2007). Fundamentals and environmental applications of fenton and photo-Fenton processes [Review of Fundamentals and environmental applications of fenton and photo-Fenton processes]. *Quimica Nova*, 30(2), 400–408. SOC BRASILEIRA QUIMICA.
- Noguera-Oviedo, K., & Aga, D. (2016). Lessons learned from more than two decades of research on emerging contaminants in the environment. *Journal of Hazardous Materials*, 316, 242–251. <https://doi.org/10.1016/j.jhazmat.2016.04.058>

- Nowak, K., Jabłońska, E., Radziwon, P., Ratajczak-Wrona, W., & Nowak, K. (2020). Identification of a novel target for the action of endocrine disrupting chemicals: inhibitory effect of methylparaben on human neutrophil functions. *Environmental Science and Pollution Research International*, 27(6), 6540–6548. <https://doi.org/10.1007/s11356-019-07388-w>
- Nowak, K., Ratajczak-Wrona, W., Górska, M., Jabłońska, E. (2018). Parabens and their effects on the endocrine system. *Molecular and Cellular Endocrinology* 474, 238–251. <https://doi.org/10.1016/j.mce.2018.03.014>
- Ohoru, A. Adeniji, A., Okoh, A.I., & Okoh, O.O. (2019). Distribution and chemical analysis of pharmaceuticals and personal care products (PPCPs) in the environmental systems: A review. *International Journal of Environmental Research and Public Health*, 16(17), 3026–. <https://doi.org/10.3390/ijerph16173026>
- Oputu, O., Fatoki, O., Opeolu, B., & Akharam, M. (2020). Degradation Pathway of Ozone Oxidation of Phenols and Chlorophenols as Followed by LC-MS-TOF. *Ozone: Science & Engineering*, 42(4), 294–318. <https://doi.org/10.1080/01919512.2019.1660617>
- Orak, C., Atalay, S., & Ersöz, G. (2017). Photocatalytic and photo-Fenton-like degradation of methylparaben on monolith-supported perovskite-type catalysts. *Separation Science and Technology*, 52(7), 1310–1320. <https://doi.org/10.1080/01496395.2017.1284866>
- Ouda, K., Kadadou, D., Swaidan, B., Al-Othman, A., Al-Asheh, S., Banat, F. & Hasan, S.W. (2021). Emerging contaminants in the water bodies of the Middle East and North Africa (MENA): A critical review. *The Science of the Total Environment*, 754, 142177–. <https://doi.org/10.1016/j.scitotenv.2020.142177>
- Oyama, S.T. (2000). Chemical and catalytic properties of ozone. *Catalysis Reviews*, 42:3, 279-322, <https://doi.org/10.1081/CR-100100263>
- Padri, S. & Tamzil, S. M. (2019). Fate and Transport of PPCPs in the Environment: A Review on Occurrences, Sources, and Cases. *Materials Science Forum*, 967, 179–188. <https://doi.org/10.4028/www.scientific.net/msf.967.179>
- Pan, M., Wong, C.K.C., Chu, L.M. (2014). Distribution of Antibiotics in Wastewater-Irrigated Soils and Their Accumulation in Vegetable Crops in the Pearl River Delta, Southern China. *Journal of Agricultural and Food Chemistry*, 62(46):11062-11069. <https://doi.org/10.1021/jf503850v>
- Parezanović, G., Lalic-Popovic, M., Golocorbin-Kon, S., Vasovic, V., Milijašević, B., Al-Salami, H., & Mikov, M. (2019). Environmental Transformation of Pharmaceutical Formulations: A Scientific Review. *Archives of Environmental Contamination and Toxicology*, 77(2), 155–161. <https://doi.org/10.1007/s00244-019-00630-z>

- Pereira, M., Oliveira, L., & Murad, E. (2012). Iron oxide catalysts: Fenton and Fentonlike reactions—a review. *Clay Minerals*, 47(3), 285–302. <https://doi.org/10.1180/claymin.2012.047.3.01>
- Perumalla, S.R., Shi, L., & Sun, C.C. (2012). Ionized form of acetaminophen with improved compaction properties. *Crystal Engineering Communications*, 14:2389–2390 <https://doi.org/10.1039/C1CE06278F>
- Petrie, B., Mcadam, E., Lester, J., & Cartmell, E. (2014). Obtaining process mass balances of pharmaceuticals and triclosan to determine their fate during wastewater treatment. *Science of the Total Environment*, 497–498, 553–560. <https://doi.org/10.1016/j.scitotenv.2014.08.003>
- Philip, J., Aravind, U., & Aravindakumar, C. (2018). Emerging contaminants in Indian environmental matrices – A review. *Chemosphere* (Oxford), 190, 307–326. <https://doi.org/10.1016/j.chemosphere.2017.09.120>
- Pipolo, M., Gmurek, M., Corceiro, V., Costa, R., Emília Quinta-Ferreira, M., Ledakowicz, S., Quinta-Ferreira, R., & Martins, R. (2017). Ozone-Based Technologies for Parabens Removal from Water: Toxicity Assessment. *Ozone: Science & Engineering*, 39(4), 233–243. <https://doi.org/10.1080/01919512.2017.1301246>
- Polcaro, A., Mascia, M., Palmas, S., & Vacca, A. (2002). Kinetic Study on the Removal of Organic Pollutants by an Electrochemical Oxidation Process. *Industrial & Engineering Chemistry Research*, 41(12), 2874–2881. <https://doi.org/10.1021/ie010669u>
- Postigo, C., Emiliano, P., Barceló, D., & Valero, F. (2018). Chemical characterization and relative toxicity assessment of disinfection byproduct mixtures in a large drinking water supply network. *Journal of Hazardous Materials*, 359, 166–173. <https://doi.org/10.1016/j.jhazmat.2018.07.022>
- Potter, D.W., Miller, D.W., Hinson, J.A. (1985). Identification of acetaminophen polymerization products catalyzed by horseradish peroxidase. *The Journal of Biological Chemistry*, (22):12174–12180.
- Poulos, T., & Kraut, J. (1980). The stereochemistry of peroxidase catalysis. *Journal of Biological Chemistry*, 255(17), 8199–8205.
- Pylypchuk, I., Daniel, G., Kessler, V., & Seisenbaeva, G. (2020). Removal of Diclofenac, Paracetamol, and Carbamazepine from Model Aqueous Solutions by Magnetic Sol–Gel Encapsulated Horseradish Peroxidase and Lignin Peroxidase Composites. *Nanomaterials (Basel, Switzerland)*, 10(2), 282–. <https://doi.org/10.3390/nano10020282>
- Pylypchuk, I., Kessler, V., & Seisenbaeva, G. (2018). Simultaneous Removal of Acetaminophen, Diclofenac, and Cd(II) by *Trametes versicolor* Laccase Immobilized on Fe₃O₄/SiO₂-DTPA Hybrid Nanocomposites. *ACS Sustainable*

- Chemistry & Engineering*, 6(8), 9979–9989.
<https://doi.org/10.1021/acssuschemeng.8b01207>
- Quach-Cu, J., Herrera-Lynch, B., Marciniak, C., Adams, S., Simmerman, A., Reinke, R.A. (2018). The effect of primary, secondary, and tertiary wastewater treatment processes on antibiotic resistance gene (ARG) concentrations in solid and dissolved wastewater fractions. *Water* 10(1):37 <https://doi.org/10.3390/w10010037>
- Raja, G. L., Subhashree, K. D., Lite, C., Santosh, W., Barathi, S., & Raja, G. L. (2019). Transient exposure of methylparaben to zebrafish (*Danio rerio*) embryos altered cortisol level, acetylcholinesterase activity and induced anxiety-like behaviour. *General and Comparative Endocrinology*, 279, 53–59.
<https://doi.org/10.1016/j.ygcen.2018.11.001>
- Ramachandran, A. & Jaeschke, H. (2018). Acetaminophen toxicity: Novel insights into mechanisms and future perspective. *The Journal of Liver Research* 18(1):19-30
<https://doi.org/10.3727/105221617X15084371374138>
- Ramos, A.S., Correia, A.T., Antunes, S.C., Goncalves, F., Nunes, B. (2014). Effect of acetaminophen exposure in *Oncorhynchus mykiss* gills and liver: Detoxification mechanisms, oxidative defence system and peroxidative damage. *Environmental Toxicology and Pharmacology* 37(3):1221-1228
<https://doi.org.10.1016/j.etap.2014.04.005>
- Richardson, M.L., and Bowron, J.M. (1985). The fate of pharmaceutical chemicals in the aquatic environment. *Journal of pharmacy and pharmacology*, 37: 1-12
- Rizzo, L., Malato, S., Antakyali, D., Beretsou, V., Đolić, M., Gernjak, W., Heath, E., Ivancev-Tumbas, I., Karaolia, P., Lado, R., Ana, R., Mascolo, G., Mcardell, C.S., Schaar, H., Silva, A.M.T., Fatta-Kassinos, D. (2019). Consolidated vs new advanced treatment methods for the removal of contaminants of emerging concern from urban wastewater. *Science of the Total Environment*, 655, 986–1008. <https://doi.org/10.1016/j.scitotenv.2018.11.265>
- Rodríguez-López, J., Fenoll, L., Peñalver, M., García-Ruiz, P., Varón, R., & Martínez-Ortíz, F. (2001). Tyrosinase action on monophenols: evidence for direct enzymatic release of o-diphenol. *Biochimica et Biophysica Acta (BBA)/Protein Structure and Molecular Enzymology*, 1548(2), 238–256.
[https://doi.org/10.1016/S0167-4838\(01\)00237-0](https://doi.org/10.1016/S0167-4838(01)00237-0)
- Rodriguez-Lopez, J., Smith, A., Thorneley, R., & Rodriguez-Lopez, J. (1996). Role of arginine 38 in horseradish peroxidase. A critical residue for substrate binding and catalysis. *The Journal of Biological Chemistry*, 271(8), 4023–4030.
<https://doi.org/10.1074/jbc.271.8.4023>

- Roongtanakiat, N., Tangruangkiat, S., & Meesat, R. (2007). Utilization of vetiver grass (*Vetiveria zizanioides*) for removal of heavy metals from industrial wastewaters. *Science Asia*, 33(4), 397–403. <https://doi.org/10.2306/scienceasia1513-1874.2007.33.397>
- Rosales, E., Buftia, G., Pazos, M., Lazar, G., & Sanromán, M. (2018). Highly active based iron-carbonaceous cathodes for heterogeneous electro-Fenton process: Application to degradation of parabens. *Process Safety and Environmental Protection*, 117, 363–371. <https://doi.org/10.1016/j.psep.2018.05.014>
- Roudi, A.M., Chelliapan, S., Wan Mohtar, W.M., & Kamyab, H. (2018). Prediction and Optimization of the Fenton Process for the Treatment of Landfill Leachate Using an Artificial Neural Network. *Water (Basel)*, 10(5). <https://doi.org/10.3390/w10050595>
- Ryan, B., Carolan, N., & Ó'fágáin, C. (2006). Horseradish and soybean peroxidases: comparable tools for alternative niches? *Trends in Biotechnology*, 24(8), 355–363. <https://doi.org/10.1016/j.tibtech.2006.06.007>
- Ryu, K., & Dordick, J.S. (1992). How do organic solvents affect peroxidase structure and function? *Biochemistry* 31(9):2588-2598. <https://doi:10.1021/bi00124a020>.
- Saleh, A. A., Jamal, A., Djamel, G. (2019). On the Perspective of Applying of a New Method for Wastewater Treatment Technology: Modification of the Third Traditional Stage with Two Units, One by Cultivating Microalgae and Another by Solar Vaporization. *International Journal of Environmental Science and Natural Research*. 16(2): 555934. <https://doi.org/10.19080/IJESNR.2019.16.555934>
- Salimi, M., Esrafil, A., Gholami, M., Jonidi Jafari, A., Rezaei Kalantary, R., Farzadkia, M., Kermani, M., & Sobhi, H. (2017). Contaminants of emerging concern: a review of new approach in AOP technologies. *Environmental Monitoring and Assessment*, 189(8), 1–22. <https://doi.org/10.1007/s10661-017-6097-x>
- Sanchez-Ferrer, A., Rodriguez-Lopez, J. N., Garcia-Canovas, F. and Garcia-Carmona, F. (1995) Tyrosinase: A comprehensive review of its mechanism. *Biochimica et Biophysica Acta*, 1247, 1 – 11. [https://doi.10.1016/0167-4838\(94\)00204-t](https://doi.10.1016/0167-4838(94)00204-t)
- Sanganyado, E., Lu, Z., Fu, Q., Schlenk, D., & Gan, J. (2017). Chiral pharmaceuticals: A review on their environmental occurrence and fate processes. *Water Research*, 124, 527–542. <https://doi.org/10.1016/j.watres.2017.08.003>
- Sanganyado, E., Lu, Z., Fu, Q., Schlenk, D., & Gan, J. (2017). Chiral pharmaceuticals: A review on their environmental occurrence and fate processes. *Water Research*, 124, 527–542. <https://doi.org/10.1016/j.watres.2017.08.003>
- Sauvé, S., & Desrosiers, M. (2014). A review of what is an emerging contaminant. *Chemistry Central Journal*, 8(1), 1–7. <https://doi.org/10.1186/1752-153X-8-15>
- SCCS (Scientific Committee on Consumer Safety) (2011). Opinion on parabens, 14 December 2010, revision of 22 March 2011.

https://ec.europa.eu/health/sites/health/files/scientific_committees/consumer_safety/docs/sccs_o_041.pdf

- Schmitz, N., Huystee, R., & Gijzen, M. (1997). Characterization of anionic soybean (Glycine max) seed coat peroxidase. *Canadian Journal of Botany*, 75(8), 1336–1341. <https://doi.org/10.1139/b97-845>
- Scinicariello, F., & Buser, M. (2016). Serum testosterone concentrations and urinary bisphenol A, benzophenone-3, triclosan, and paraben levels in male and female children and adolescents: NHANES 2011-2012.(Report). *Environmental Health Perspectives*, 124(12), 1898–1904. <https://doi.org/10.1289/EHP150>
- Sedlak, D., Gray, J., Pinkston, K., & Sedlak, D. (2000). Peer reviewed: understanding microcontaminants in recycled water. *Environmental Science & Technology*, 34(23), 508A–15A. <https://doi.org/10.1021/es003513e>
- Shalaby, S., El-Saadany, S., Abo-Eyta, A., Abdel-Satar, A., Al-Afify, A., & Abd El-Gleel, W. (2018). Levels of pesticide residues in water, sediment, and fish samples collected from Nile River in Cairo, Egypt. *Environmental Forensics*, 19(4), 228–238. <https://doi.org/10.1080/15275922.2018.1519735>
- Shanmugam, G., Ramaswamy, B., Radhakrishnan, V., & Tao, H. (2010). GC–MS method for the determination of paraben preservatives in the human breast cancerous tissue. *Microchemical Journal*, 96(2), 391–396. <https://doi.org/10.1016/j.microc.2010.07.005>
- Shargil, D., Gerstl, Z., Fine, P., Nitsan, I., & Kurtzman, D. (2015). Impact of biosolids and wastewater effluent application to agricultural land on steroidal hormone content in lettuce plants. *Science of the Total Environment*, 505, 357–366. <https://doi.org/10.1016/j.scitotenv.2014.09.100>
- Shi, Y., Gao, L., Li, Y.W., Liu, J., & Cai, Y. (2016). Occurrence, distribution and seasonal variation of organophosphate flame retardants and plasticizers in urban surface water in Beijing, China. *Environmental Pollution*, 209:1-10.
- Shin, M., Shin, C., Choi, J., Lee, J., Lee, S., & Kim, S. (2019). Pharmacokinetic profile of propyl paraben in humans after oral administration. *Environment International*, 130, 104917–. <https://doi.org/10.1016/j.envint.2019.104917>
- Silva, M. C., Torres, J. A., Sá, L. R., Chagas, P. M., Ferreira-Leitão, V. S., & Corrêa, A. D. (2013). The use of soybean peroxidase in the decolourization of Remazol Brilliant Blue R and toxicological evaluation of its degradation products. *Journal of Molecular Catalysis B: Enzymatic*, 89, 122-129.
- Skálová, T., Dušková, J., Hašek, J., Štěpánková, A., Koval', T., Østergaard, L., & Dohnálek, J. (2011). Structure of laccase from *Streptomyces coelicolor* after soaking with potassium hexacyanoferrate and at an improved resolution of 2.3 Å. *Acta Crystallographica Section F*, 67(1), 27–32. <https://doi.org/10.1107/S1744309110046099>

- Smith, A., & Veitch, N. (1998). Substrate binding and catalysis in heme peroxidases. *Current Opinion in Chemical Biology*, 2(2), 269–278.
[https://doi.org/10.1016/S1367-5931\(98\)80069-0](https://doi.org/10.1016/S1367-5931(98)80069-0)
- Smith, A., Santama, N., Dacey, S., Edwards, M., Bray, R., Thorneley, R., Burke, J., & Smith, A. (1990). Expression of a synthetic gene for horseradish peroxidase C in *Escherichia coli* and folding and activation of the recombinant enzyme with Ca²⁺ and heme. *The Journal of Biological Chemistry*, 265(22), 13335–13343.
<http://search.proquest.com/docview/79905987/>
- Smith, K., Braun, J., Williams, P., Ehrlich, S., Correia, K., Calafat, A., Ye, X., Ford, J., Keller, M., Meeker, J., & Hauser, R. (2012). Predictors and variability of urinary paraben concentrations in men and women, including before and during pregnancy.(Research)(Report). *Environmental Health Perspectives*, 120 (11), 1538–1543. <https://doi.org/10.1289/ehp.1104614>
- Smith, M., Cameron, N., & Mosely, J. (2012). Evaluating Atmospheric pressure Solids Analysis Probe (ASAP) mass spectrometry for the analysis of low molecular weight synthetic polymers. *Analyst (London)*, 137(19), 4524–4530.
<https://doi.org/10.1039/c2an35556f>
- Solomon, E., Baldwin, M., & Lowery, M. (1992). Electronic structures of active sites in copper proteins: contributions to reactivity. *Chemical Reviews*, 92(4), 521.
- Song, N., & Jiang, H. (2020). Coordinated photodegradation and biodegradation of organic matter from macrophyte litter in shallow lake water: Dual role of solar irradiation. *Water Research*, 172, 115516.
<https://doi.org/10.1016/j.watres.2020.115516>
- Soni, M.G., Carabin, I.G., & Burdock, G.A. (2005). Safety assessment of esters of p-hydroxybenzoic acid (parabens). *Food Chemistry Toxicology* 43:985–1015.
<https://doi:10.1016/j.fct.2005.01.020>
- Spahr, S., Teixido, M., Sedlak, D.L, Luthy, R.G. (2020). Hydrophilic trace organic contaminants in urban stormwater: occurrence, toxicological relevance, and the need to enhance green stormwater infrastructure. *Environmental Science Water Research & Technology*, 6:15 <https://doi:10.1039/c9ew00674e>
- Steevensz, A., Al-Ansari, M., Taylor, K., Bewtra, J., & Biswas, N. (2009). Comparison of soybean peroxidase with laccase in the removal of phenol from synthetic and refinery wastewater samples. *Journal of Chemical Technology & Biotechnology*, 84(5), 761–769. <https://doi.org/10.1002/jctb.2109>
- Steevensz, A., Madur, S., Al-Ansari, M., Taylor, K., Bewtra, J., & Biswas, N. (2013). A simple lab-scale extraction of soybean hull peroxidase shows wide variation among cultivars. *Industrial Crops and Products*, 48, 13–18.
<https://doi.org/10.1016/j.indcrop.2013.03.030>
- Steter, J., Brillas, E., & Sires, I. (2018). Solar photoelectro-Fenton treatment of a mixture of parabens spiked into secondary treated wastewater effluent at low input

- current. *Applied Catalysis B-Environmental*, 224, 410–418.
<https://doi.org/10.1016/j.apcatb.2017.10.060>
- Steter, J., Dionisio, D., Lanza, M., & Motheo, A. (2014b). Electrochemical and sonoelectrochemical processes applied to the degradation of the endocrine disruptor methyl paraben. *Journal of Applied Electrochemistry*, 44(12), 1317–1325. <https://doi.org/10.1007/s10800-014-0742-7>
- Steter, J., Rocha, R., Dionisio, D., Lanza, M., & Motheo, A. (2014a). Electrochemical oxidation route of methyl paraben on a boron-doped diamond anode. *Electrochimica Acta*, 117.
- Strutt, J., Wilson, S., Shorney-Darby, H., Shaw, A., & Byers, A. (2008). Assessing the carbon footprint of water production. *Journal - American Water Works Association*, 100(6), 80–91. <https://doi.org/10.1002/j.1551-8833.2008.tb09654.x>
- Su, C., Cada, C., Dalida, M., & Lu, M. (2013). Effect of Electrochemical Oxidation Processes on Acetaminophen Degradation in Various Electro-Fenton Reactors. *Journal of The Electrochemical Society*, 160(4), H207–H212.
<https://doi.org/10.1149/2.038304jes>
- Su, Y., Chen, F., & Liu, Z. (2015). Comparison of optical properties of chromophoric dissolved organic matter (CDOM) in alpine lakes above or below the tree line: insights into sources of CDOM. *Photochemical & Photobiological Sciences*, 14(5), 1047–1062. <https://doi.org/10.1039/c4pp00478g>
- Talib, A., & Randhir, T. (2017). Managing emerging contaminants in watersheds: Need for comprehensive, systems-based strategies. *Sustainability of Water Quality and Ecology*, 9-10, 1–8. <https://doi.org/10.1016/j.swaqe.2016.05.002>
- Tan, C., Gao, N., Zhou, S., Xiao, Y., & Zhuang, Z. (2014). Kinetic study of acetaminophen degradation by UV-based advanced oxidation processes. *Chemical Engineering Journal*, 253, 229–236.
<https://doi.org/10.1016/j.cej.2014.05.013>
- Tay, K., Rahman, N., & Abas, M. (2010). Ozonation of parabens in aqueous solution: Kinetics and mechanism of degradation. *Chemosphere*, 81(11), 1446–1453.
<https://doi.org/10.1016/j.chemosphere.2010.09.004>
- Tay, K., Rahman, N., & Abas, M. (2010). Ozonation of parabens in aqueous solution: Kinetics and mechanism of degradation. *Chemosphere (Oxford)*, 81(11), 1446–1453. <https://doi.org/10.1016/j.chemosphere.2010.09.004>
- Tony, M.A. & Bedri, Z. (2014). Experimental design of photo-Fenton reactions for the treatment of car wash wastewater effluents by response surface methodological analysis. *Advances in Environmental Chemistry*.
<http://dx.doi.org/10.1155/2014/958134>
- Tran, N.H., Reinhard, M. & Gin, K.Y.H. (2018). Occurrence and fate of emerging contaminants in municipal wastewater treatment plants from different geographical

- Ullrich, R., & Hofrichter, M. (2007). Enzymatic hydroxylation of aromatic compounds. *Cellular and Molecular Life Sciences* 64, 271–293 (2007).
<https://doi.org/10.1007/s00018-007-6362-1>
- United Nations, Department of Economic and Social Affairs, Population Division (2019). World Population Prospects 2019: Highlights (ST/ESA/SER.A/423). Available at https://population.un.org/wpp/Publications/Files/WPP2019_Highlights.pdf
- United States Environmental Protection Agency (US EPA) (1998). How wastewater treatment works... the basics. EPA 4204, Washington DC, 20460-0001. US EPA
<https://www3.epa.gov/npdes/pubs/bastre.pdf>
- United States Environmental Protection Agency (US EPA) (2021). Toxics release inventory (TRI) program. (<https://www.epa.gov/toxics-release-inventory-tri-program/list-pfas-added-tri-ndaa>). Accessed January 15th, 2021
- United States Department of Agriculture (USDA). (2020) Newsroom. <https://www.nass.usda.gov/Newsroom/2020/> Accessed November 24th 2020
- Vahatalo, A.V. (2009). Light, photolytic reactivity and chemical products. *Encyclopedia of Inland Waters*, pp 761-773. <https://doi.org/10.1016/B978-012370626-3.00110-1>
- Valderrama, B., Ayala, M., & Vazquez-Duhalt, R. (2002). Suicide inactivation of peroxidases and the challenge of engineering more robust enzymes. *Chemistry & Biology*, 9(5), 555-565 [https://doi.org/10.1016/S1074-5521\(02\)00149-7](https://doi.org/10.1016/S1074-5521(02)00149-7)
- Veitch, N. C. (2004). Horseradish peroxidase: a modern view of a classic enzyme. *Phytochemistry*, 65(3), 249–259. <https://doi.org/10.1016/j.phytochem.2003.10.022>
- Verloop, A., Vincken, J., & Gruppen, H. (2016). Peroxidase Can Perform the Hydroxylation Step in the “Oxidative Cascade” during Oxidation of Tea Catechins. *Journal of Agricultural and Food Chemistry*, 64(42), 8002–8009.
<https://doi.org/10.1021/acs.jafc.6b03029>
- Viswanath, B., Rajesh, B., Janardhan, A., Kumar, A., Narasimha, G., & Viswanath, B. (2014). Fungal laccases and their applications in bioremediation. *Enzyme Research*, 2014(2014), 163242–163242. <https://doi.org/10.1155/2014/163242>
- Vlasits, J., Jakopitsch, C., Bernroitner, M., Zamocky, M., Furtmüller, P., & Obinger, C. (2010). Mechanisms of catalase activity of heme peroxidases. *Archives of Biochemistry and Biophysics*, 500(1), 74–81.
<https://doi.org/10.1016/j.abb.2010.04.018>
- Vo, T., Jung, E., Choi, K., Yu, F., & Jeung, E. (2011). Estrogen receptor α is involved in the induction of Calbindin-D9k and progesterone receptor by parabens in GH3 cells: A biomarker gene for screening xenoestrogens. *Steroids*, 76(7), 675–681.
<https://doi.org/10.1016/j.steroids.2011.03.006>

- Vrbova, M., Rousarova, E., Bruckova, L., P. Cesla, P. & Rousar, T. (2016). Characterization of Acetaminophen Toxicity in Human Kidney HK-2 Cells. *Physiology Research* 65: 627-635.
- Wada, S., Ichikawa, H., & Tastsumi, K. (1995). Removal of phenols and aromatic amines from wastewater by a combination treatment with tyrosinase and a coagulant. *Biotechnology and Bioengineering*, 45(4), 304–309.
<https://doi.org/10.1002/bit.260450404>
- Wagner, M., & Nicell, J. (2002). Detoxification of phenolic solutions with horseradish peroxidase and hydrogen peroxide. *Water Research*, 36(16), 4041–4052.
[https://doi.org/10.1016/S0043-1354\(02\)00133-1](https://doi.org/10.1016/S0043-1354(02)00133-1)
- Wang, L., Asimakopulos, A., & Kannan, K. (2015). Accumulation of 19 environmental phenolic and xenobiotic heterocyclic aromatic compounds in human adipose tissue. *Environment International*, 78, 45–50.
<https://doi.org/10.1016/j.envint.2015.02.015>
- Wang, L., Liao, C., Liu, F., Wu, Q., Guo, Y., Moon, H., Nakata, H., Kannan, K., & Wang, L. (2012). Occurrence and human exposure of p-hydroxybenzoic acid esters (parabens), bisphenol A diglycidyl ether (BADGE), and their hydrolysis products in indoor dust from the United States and three East Asian countries. *Environmental Science & Technology*, 46(21), 11584–11593.
<https://doi.org/10.1021/es303516u>
- Wang, L., Wu, Y., Zhang, W., Kannan, K., & Wang, L. (2013). Characteristic profiles of urinary p-hydroxybenzoic acid and its esters (parabens) in children and adults from the United States and China. *Environmental Science & Technology*, 47(4), 2069–2076. <https://doi.org/10.1021/es304659r>
- Wang, X., Xiang, W., Wang, S., Ge, J., Qu, R. and Wang, Z. (2020). Oxidative Oligomerization of Phenolic Endocrine Disrupting Chemicals Mediated by Mn(III)-L Complexes and the Role of Phenoxyl Radicals in the Enhanced Removal: Experimental and Theoretical Studies. *Environmental Science & Technology*, 54 (3), 1573-1582. <https://doi.org/10.1021/acs.est.9b05423>
- Wang, Y., & Hasebe, Y. (2011). Amperometric flow-biosensor for cyanide based on an inhibitory effect upon bioelectrocatalytic reduction of oxygen by peroxidase-modified carbon-felt. *Electroanalysis*, 23(7), 1631–1637.
<https://doi.org/10.1002/elan.201100005>
- Weizel, A., Schlüsener, M., Dierkes, G., & Ternes, T. (2018). Occurrence of Glucocorticoids, Mineralocorticoids, and Progestogens in Various Treated Wastewater, Rivers, and Streams. *Environmental Science & Technology*, 52(9), 5296–5307. <https://doi.org/10.1021/acs.est.7b06147>
- Welinder, K. (1979). Amino acid sequence studies of horseradish peroxidase. Amino and carboxyl termini, cyanogen bromide and tryptic fragments, the complete sequence, and some structural characteristics of horseradish peroxidase C.

- European Journal of Biochemistry*, 96(3), 483–502. <https://doi.org/10.1111/j.1432-1033.1979.tb13061.x>
- Welinder, K.G. (1992). Superfamily of plant, fungal and bacterial peroxidases. *Current opinion in Structural Biology*, 2(3):388-393 [https://doi.org/10.1016/0959-440X\(92\)90230-5](https://doi.org/10.1016/0959-440X(92)90230-5)
- Wright, H., & Nicell, J. (1999). Characterization of soybean peroxidase for the treatment of aqueous phenols. *Bioresource Technology*, 70(1), 69–79. [https://doi.org/10.1016/S0960-8524\(99\)00007-3](https://doi.org/10.1016/S0960-8524(99)00007-3)
- Wu, Y., Taylor, K., Biswas, N., & Bewtra, J. (1997). Comparison of additives in the removal of phenolic compounds by peroxidase-catalyzed polymerization. *Water Research*, 31(11), 2699–2704. [https://doi.org/10.1016/S0043-1354\(97\)00119-X](https://doi.org/10.1016/S0043-1354(97)00119-X)
- Wu, Y., Taylor, K., Biswas, N., & Bewtra, J. (1997). Comparison of additives in the removal of phenolic compounds by peroxidase-catalyzed polymerization. *Water Research*, 31(11), 2699–2704. [https://doi.org/10.1016/S0043-1354\(97\)00119-X](https://doi.org/10.1016/S0043-1354(97)00119-X)
- Wu, Y., Taylor, K., Biswas, N., & Bewtra, J. (1998). A model for the Protective Effect of Additives on the Activity of Horseradish Peroxidase in the Removal of Phenol. *Enzyme and Microbial Technology*, 22(5), 315–322. [https://doi.org/10.1016/S0141-0229\(97\)00197-X](https://doi.org/10.1016/S0141-0229(97)00197-X)
- Xiang, W., Qu, R., Wang, X., Wang, Z., Bin-Jumah, M., Allam, A., Zhu, F., & Huo, Z. (2020). Removal of 4-chlorophenol, bisphenol A and nonylphenol mixtures by aqueous chlorination and formation of coupling products. *Chemical Engineering Journal (Lausanne, Switzerland: 1996)*, 402, 126140–. <https://doi.org/10.1016/j.cej.2020.126140>
- Xiao, J., Xie, Y., & Cao, H. (2015). Organic pollutants removal in wastewater by heterogeneous photocatalytic ozonation. *Chemosphere*, 121(C), 1–17. <https://doi.org/10.1016/j.chemosphere.2014.10.072>
- Xie, H., Hao, H., Xu, N., Liang, X., Gao, D., Xu, Y., ... Wong, M. (2019). Pharmaceuticals and personal care products in water, sediments, aquatic organisms, and fish feeds in the Pearl River Delta: Occurrence, distribution, potential sources, and health risk assessment. *Science of the Total Environment*, 659, 230–239. <https://doi.org/10.1016/j.scitotenv.2018.12.222>
- Xue, J., Wu, Q., Sakthivel, S., Pavithran, P., Vasukutty, J., & Kannan, K. (2015). Urinary levels of endocrine-disrupting chemicals, including bisphenols, bisphenol A diglycidyl ethers, benzophenones, parabens, and triclosan in obese and non-obese Indian children. *Environmental Research*, 137, 120–128. <https://doi.org/10.1016/j.envres.2014.12.007>
- Yamamoto, H., Tamura, I., Hirata, Y., Kato, J., Kagota, K., Katsuki, S., Yamamoto, A., Kagami, Y., & Tatarazako, N. (2011). Aquatic toxicity and ecological risk assessment of seven parabens: Individual and additive approach. *Science of the Total Environment*, 410(411), 102–111. <https://doi.org/10.1016/j.scitotenv.2011.09.040>

- Yang, H., Bever, C., Zhang, H., Mari, G., Li, H., Zhang, X., Guo, L., Wang, Z., Luo, P., & Wang, Z. (2019). Comparison of soybean peroxidase with horseradish peroxidase and alkaline phosphatase used in immunoassays. *Analytical Biochemistry*, 581, 113336–. <https://doi.org/10.1016/j.ab.2019.06.007>
- Yang, H., Lu, G., Yan, Z., Liu, J., Dong, H., Bao, X., Zhang, X., Sun, Y. (2020). Residues, bioaccumulation, and trophic transfer of pharmaceuticals and personal care products in highly urbanized rivers affected by water diversion. *Journal of Hazardous Materials*, 391:122245 <https://doi.org/10.1016/j.jhazmat.2020.122245>
- Yarahmadi, H., Duy, S., Hachad, M., Dorner, S., Sauvé, S., & Prévost, M. (2018). Seasonal variations of steroid hormones released by wastewater treatment plants to river water and sediments: Distribution between particulate and dissolved phases. *Science of the Total Environment*, 635, 144–155. <https://doi.org/10.1016/j.scitotenv.2018.03.370>
- Ye, M. & Schuler, R.H. (1989). Second-order combination reaction of phenols. *Journal of Physical Chemistry*, 93(5) 1898-1902. <https://doi.org/10.1021/j100342a040>
- Yu, J., Taylor, K., Zou, H., Biswas, N., & Bewtra, J. (1994). Phenol Conversion and Dimeric Intermediates in Horseradish Peroxidase-Catalyzed Phenol Removal from Water. *Environmental Science & Technology*, 28(12), 2154–2160. <https://doi.org/10.1021/es00061a025>
- Yu, J., Taylor, K., Zou, H., Biswas, N., & Bewtra, J. (1994). Phenol Conversion and Dimeric Intermediates in Horseradish Peroxidase-Catalyzed Phenol Removal from Water. *Environmental Science & Technology*, 28(12), 2154–2160. <https://doi.org/10.1021/es00061a025>
- Zaidi, K., Ali, A., Ali, S., Naaz, I., & Zaidi, K. (2014). Microbial tyrosinases: promising enzymes for pharmaceutical, food bioprocessing, and environmental industry. *Biochemistry Research International*, 2014(2014), 854687–854687. <https://doi.org/10.1155/2014/854687>
- Zavala, M., & Estrada, E. (2016). Degradation of Acetaminophen and Its Transformation Products in Aqueous Solutions by Using an Electrochemical Oxidation Cell with Stainless Steel Electrodes. *Water*, 8(9), 383. <https://doi.org/10.3390/w8090383>
- Zha, D., Li, Y., Yang, C., & Yao, C. (2018). Assessment of organophosphate flame retardants in surface water and sediment from a freshwater environment (Yangtze River, China). *Environmental Monitoring and Assessment*, 190(4), 1–11. <https://doi.org/10.1007/s10661-018-6587-5>
- Zhang, L., Dong, L., Ding, S., Qiao, P., Wang, C., Zhang, M., Zhang, L., Du, Q., Li, Y., Tang, N., & Chang, B. (2014). Effects of n-butylparaben on steroidogenesis and spermatogenesis through changed E2 levels in male rat offspring. *Environmental Toxicology and Pharmacology*, 37(2), 705–717. <https://doi.org/10.1016/j.etap.2014.01.016>
- Zhao, J., Biswas, M., & Oh, W. (2019). A novel BiVO₄-GO-TiO₂-PANI composite for upgraded photocatalytic performance under visible light and its non-toxicity.

- Environmental Science and Pollution Research*, 26(12), 11888–11904.
<https://doi.org/10.1007/s11356-019-04441-6>
- Zhao, P., Wang, Z., Li, K., Guo, X., & Zhao, L. (2018). Multi-residue enantiomeric analysis of 18 chiral pesticides in water, soil and river sediment using magnetic solid-phase extraction based on amino modified multiwalled carbon nanotubes and chiral liquid chromatography coupled with tandem mass spectrometry. *Journal of Chromatography A*, 1568, 8–21.
<https://doi.org/10.1016/j.chroma.2018.07.022>
- Zheng, W., & Colosi, L. (2011). Peroxidase-mediated removal of endocrine disrupting compound mixtures from water. *Chemosphere* (Oxford), 85(4), 553–557.
<https://doi.org/10.1016/j.chemosphere.2011.06.064>
- Zhong, Y., Gan, W., Du, Y., Huang, H., Wu, Q., Xiang, Y., Yang, X. (2019). Disinfection byproducts and their toxicity in wastewater effluents treated by the mixing oxidant of ClO₂/Cl₂. *Water Research*, 162, 471–481.
<https://doi.org/10.1016/j.watres.2019.07.012>
- Zhou, H., Lian, L., Yan, S., Song, W. (2017). Insights into the photo-induced formation of reactive intermediates from effluent organic matter: The role of chemical constituents. *Water Research*, 112:120-128.
<https://doi.org/10.1016/j.watres.2017.01.048>
- Zhou, H., Yan, S., Lian, L. Song, W. (2019). Triplet-state photochemistry of dissolved organic matter: Triplet-state energy distribution and surface electric charge conditions. *Environmental Science and Technology*. 53(5): 2482-2490.
<https://doi.org/10.1021/acs.est.8b06574>
- Zúñiga-Benítez, H., Muñoz-Calderón, A., & Peñuela, G. (2018). Removal of a mix of benzophenones and parabens using solar photo-Fenton and a cylinder parabolic collector in aqueous solutions. *Journal of Environmental Chemical Engineering*, 6(6), 7347–7357. <https://doi.org/10.1016/j.jece.2018.08.039>

APPENDICES

Appendix A: SBP Assay – reagents, procedure and SBP activity calculation

A colorimetric method was adapted to assay for SBP activity. The principle behind this is the formation of a chromophore which absorbs UV light maximally at 510 nm, hence its initial rate of formation is exploited for quantitative gains. One SBP activity unit is defined as the amount of SBP consuming 1.0 μmol of hydrogen peroxide per minute under the assay conditions. To avoid color development while standing, freshly prepared reagents were used each time for the assay, and formulated as shown below:

1. 5.0 mL of 10x phenol reagent was prepared by mixing 0.9410 g (100 mM) of phenol, 1.3105 g and 3.7479 g of monobasic and dibasic sodium phosphate salts, respectively to 100 mL of water. This gives a 0.5 M, pH 7.4 phosphate buffer
2. 25 mg of 4-aminoantipyrene (4-AAP)
3. 100 μL of hydrogen peroxide (from a 30% stock of H_2O_2 , 510 μL was measured out into a 50 mL volumetric flask, mixed thoroughly and stored at 4°C while awaiting to be used).
4. These were made up to 50.0 mL.

Calculation of the SBP Activity

Given the molar absorptivity of the chromophore is $6000 \text{ M}^{-1}\text{cm}^{-1}$, (Ibrahim *et al.* 2001),
SBP sample activity (U/mL) = SBP activity observed in the cuvette * Absorbance

$$\begin{aligned} & \text{activity in cuvette} \left(\frac{U}{\text{mL}} \right) \\ &= \frac{\text{initial rate} \left(\frac{Au}{s} \right) * \left(\frac{60 s}{1 \text{ min}} \right) * \text{dilution factor in cuvette}}{6 \text{ mM}^{-1} * \text{cm}^{-1}} \end{aligned}$$

Since dilution factor in cuvette is =20, substituting in the equation above,

$$\text{SBP activity in cuvette} = \text{initial rate} * 200 \text{ (U/mL)}$$

$$\text{Activity of SBP sample} = \text{SBP activity} * \text{SBP dilution factor}$$

The observed chromophore is formed thus:

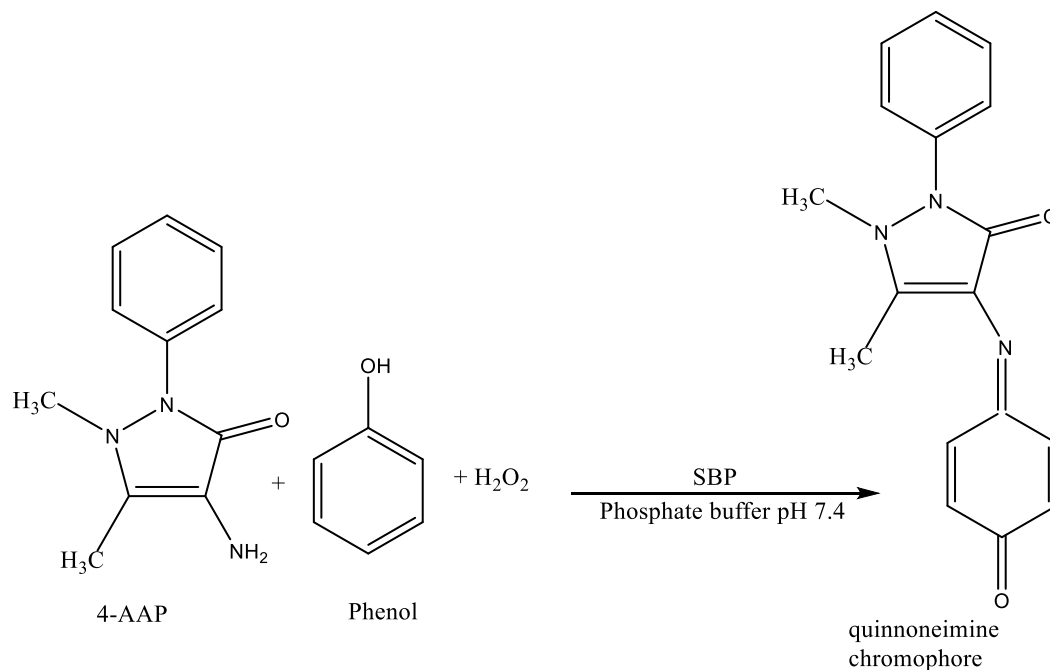


Fig. A-1: SBP catalyzed formation of quinoneimine chromophore from phenol and SBP

Procedure of SBP activity assay

Prepare fresh reagent and dilutions of SBP extract to have a dilution factor of 30, 40 and 50. All assays are performed in triplicate.

1. Set up the software to read enzyme kinetics assay
2. Blank the instrument at 510 nm by measuring 50 μ L of water into a quartz cuvette set in the cuvette holder. Quickly dispense 0.95 mL the reagent and wait for 30 seconds
3. Dry the cuvette and repeat (2) above, replacing water with dilute SBP solution
4. Monitor the progress line indicating color formation over time at 5 s intervals to 30 s at which time the UV-Vis is programmed on auto stop.
5. Checks: carefully performed activity assay should show SBP activity within 5.0 U/mL of each other, irrespective of the dilution factor. The intercept on the y axis should ideally be

under 0.05. Activity below 0.1 U/mL should have higher sample volume used, such as in residual SBP assays.

Note: The process is time-sensitive and is performed in a manner that minimizes time loss between the addition of the reagent and the start of data collection.

Appendix B: Hydrogen peroxide assay

Residual hydrogen peroxide was determined by a colorimetric method, whose principle is like that described in Appendix A. Thus in this protocol, the quinoneimine chromophore, with maximal absorption at 510 nm is being formed from the radical generating activity of ARP on the phenol present, which in turn diffuses into solution from the enzyme active site and undergoes oxidative coupling non-enzymatically with 4-AAP. Different hydrogen peroxide concentrations were used, in keeping to the highest linear limit of linearity (100 μmol) (Wu *et al.* 1998).

Reagent formulation

Target total volume: 20 mL

1. 10 mL of 10x phenol reagent formulated using 0.941 g, giving 100 mM of phenol in a 0.5 M phosphate buffer, pH 7.4 (monobasic sodium phosphate and dibasic sodium phosphate)
2. Approximately 0.51 g of 4-AAP
3. 250 μL of ARP concentrate stored at 4°C
4. Distilled water 20.0 mL

Analytical procedure:

To determine the residual hydrogen peroxide, a calibration curve was constructed, targeting cuvette concentrations between 5 μmol and 100 μmol , in triplicate, from three freshly prepared standard stock solutions (to account for any error arising from the gravimetric and volumetric measurements). 100 μL or 200 μL of sample solution was measured into the quartz cuvette and fixed in the cuvette holder, to which an appropriate volume of water was added to be complemented by 200 μL of reagent, giving a total volume of 1000 μL . For the blank, the sample volume was replaced with water.

1. Set up software to read absorbance at fixed wavelength of 510 nm.
2. Blank the UV-Vis spectrophotometer with the reagent blank
3. Insert the quartz cuvette into the cuvette holder and add to it already pre-incubated reaction mixture
4. Read absorbance after 18 minutes

The mean and standard deviations of the triplicate readings at each concentration were determined and the data plotted in a calibration curve as shown in Figure A-2.

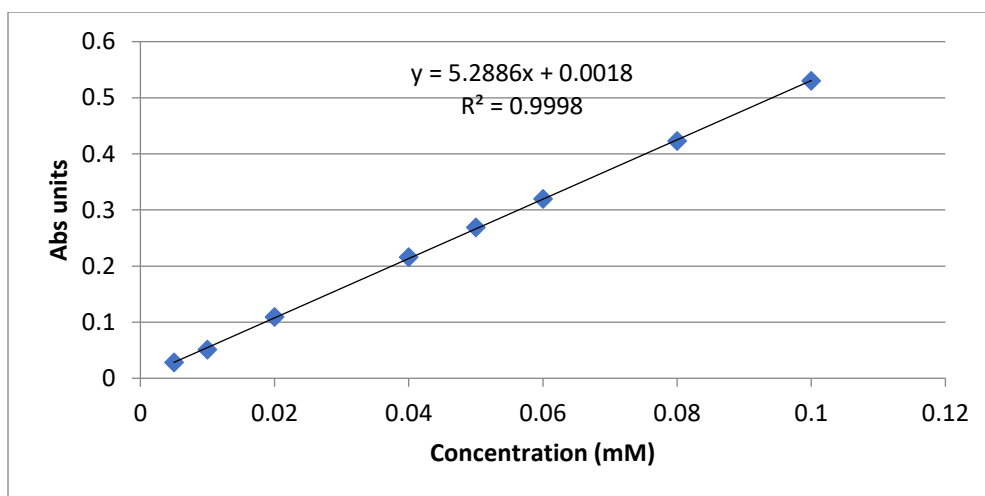


Fig. B-1 Calibration Curve for Hydrogen Peroxide

For residual hydrogen peroxide determination following 3 h oligomerization reactions, the sample size was varied until a substantial absorbance reading within the range of the calibration curve was obtained and used. Peroxide analysis for batch reactor samples were accompanied with a no-peroxide blank to serve as the UV-Vis blank at 510 nm, before sample readings were done.

Determination of actual concentration

Since cuvette concentrations were determined here, actual sample concentration was calculated thus:

$$\begin{aligned} & \text{sample concentration (mmol)} \\ & = \text{Cuvette sample concentration (mmol)} * \text{Dilution factor} \end{aligned}$$

Where cuvette sample concentration was derived by calculation from the equation of the calibration curve.

Appendix C HPLC calibration curves for single-compound analysis

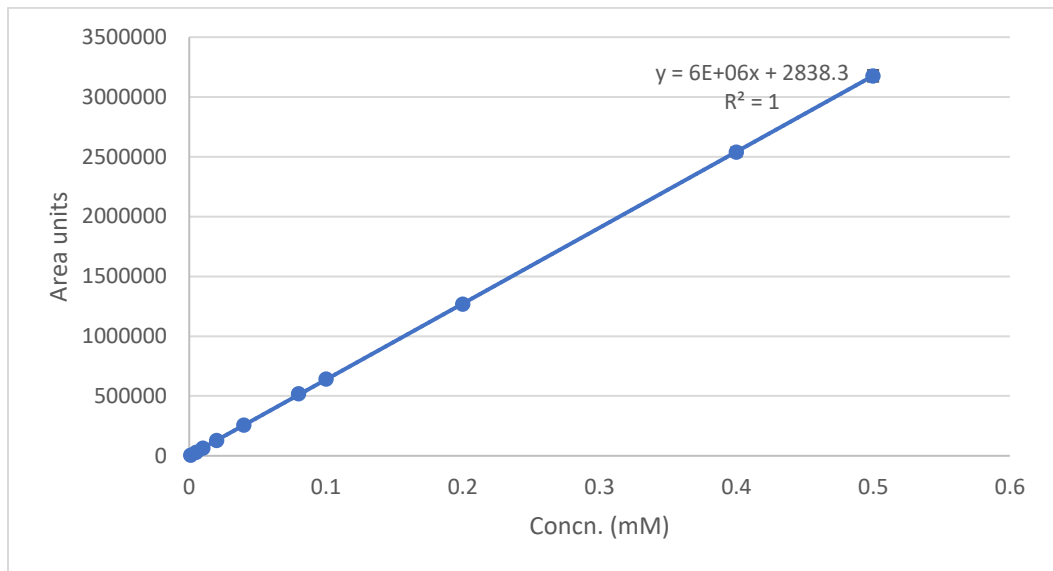


Fig. C-1 Calibration curve for acetaminophen for single-compound analysis

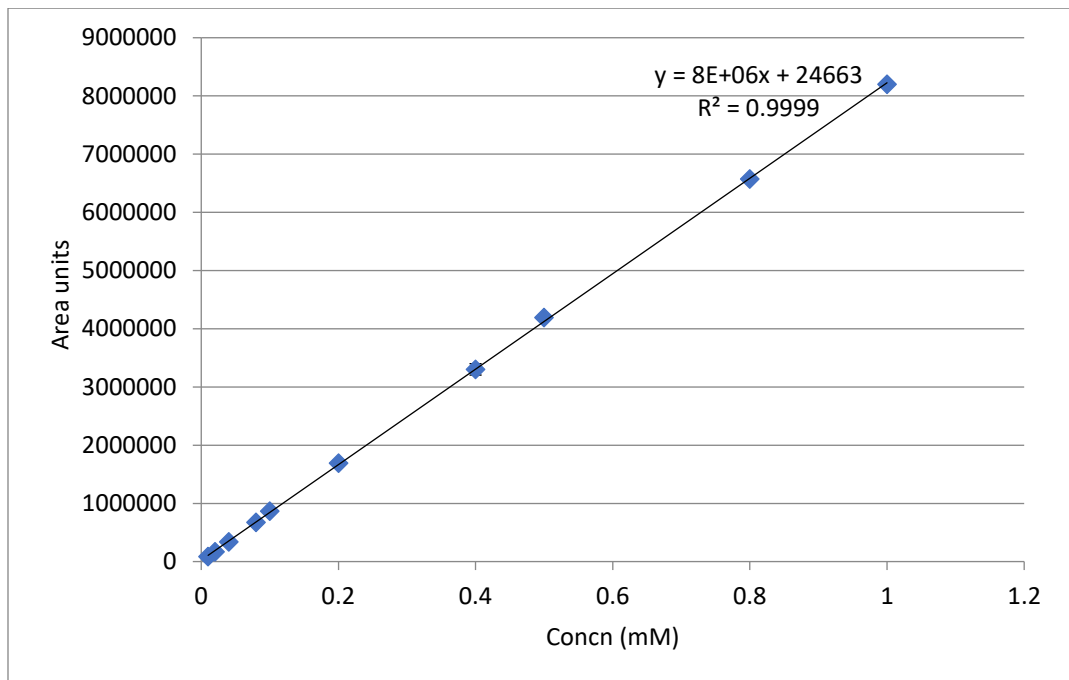


Fig. C-2 Calibration curve for PHBA for single-compound analysis

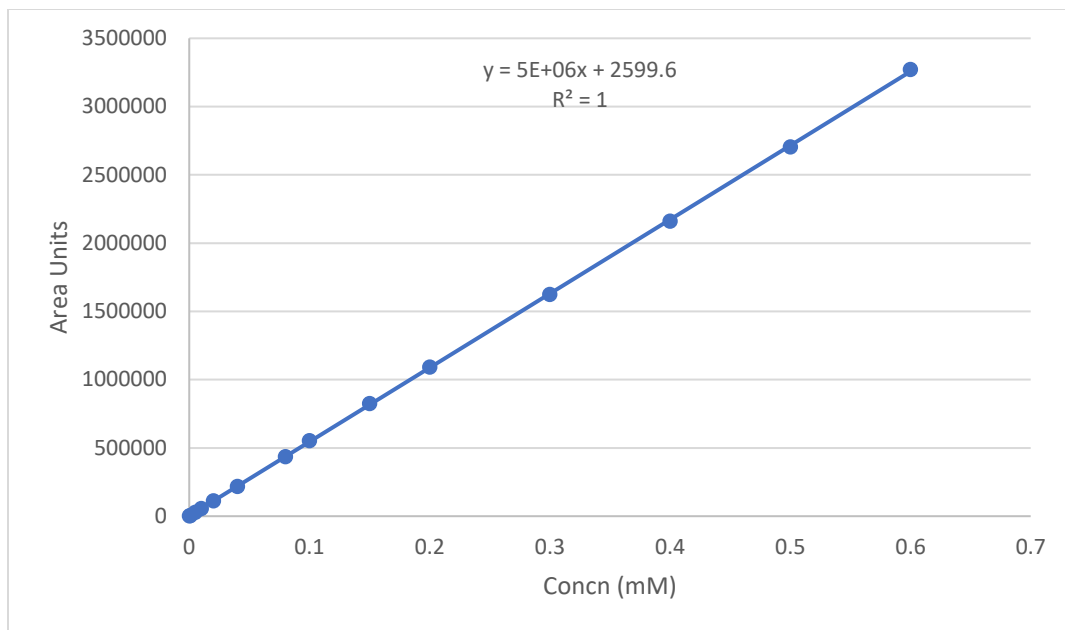


Fig. C-3 Calibration curve of MP for single-compound analysis

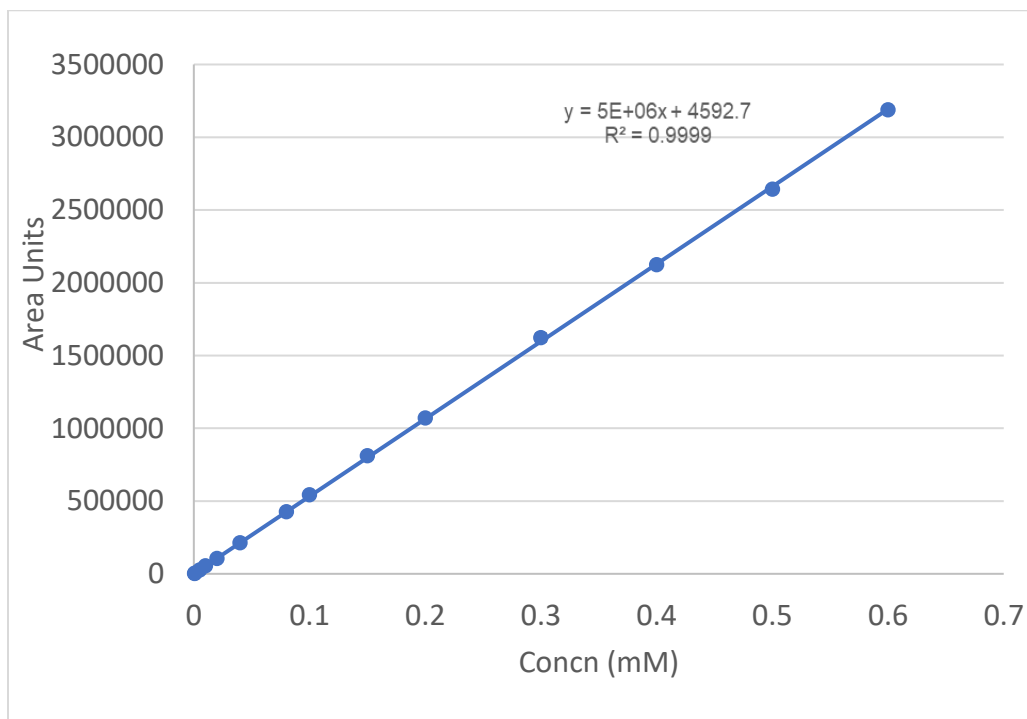


Fig. C-4 Calibration curve of PP for single-compound analysis

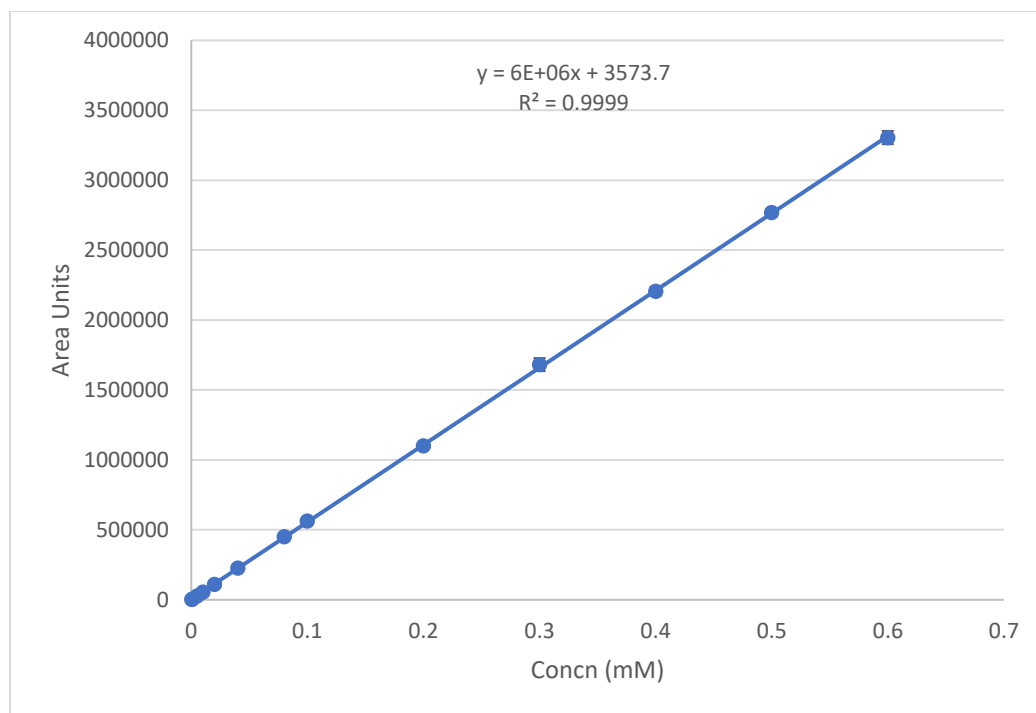


Fig. C-5 Calibration curve of BP for single-compound analysis

Table C-1 Summary of analytical parameters for single-compound analysis of studied CECs

CEC	Analytical wavelength (nm)	Ext. coef. ($M^{-1} \text{ cm}^{-1}$) ($\times 10^3$)	Intercept ($\times 10^3$)	r^2	t_R (min.)	LOD (mM)	LOQ (mM)
Acet	247	6400 \pm 8	2.80 \pm 1.7	0.9999	4.56	0.001	0.003
PHBA	255	8200 \pm 3	24.6 \pm 13	0.9999	3.78	0.005	0.016
MP	270	5400 \pm 10	2.60 \pm 2.6	0.9999	3.96	0.002	0.005
PP	270	5300 \pm 14	4.60 \pm 3.7	0.9999	3.35	0.002	0.007
BP	270	5500 \pm 13	3.60 \pm 3.2	0.9999	4.34	0.002	0.006

Appendix D: HPLC Calibration curves for compounds analysis in mix-5

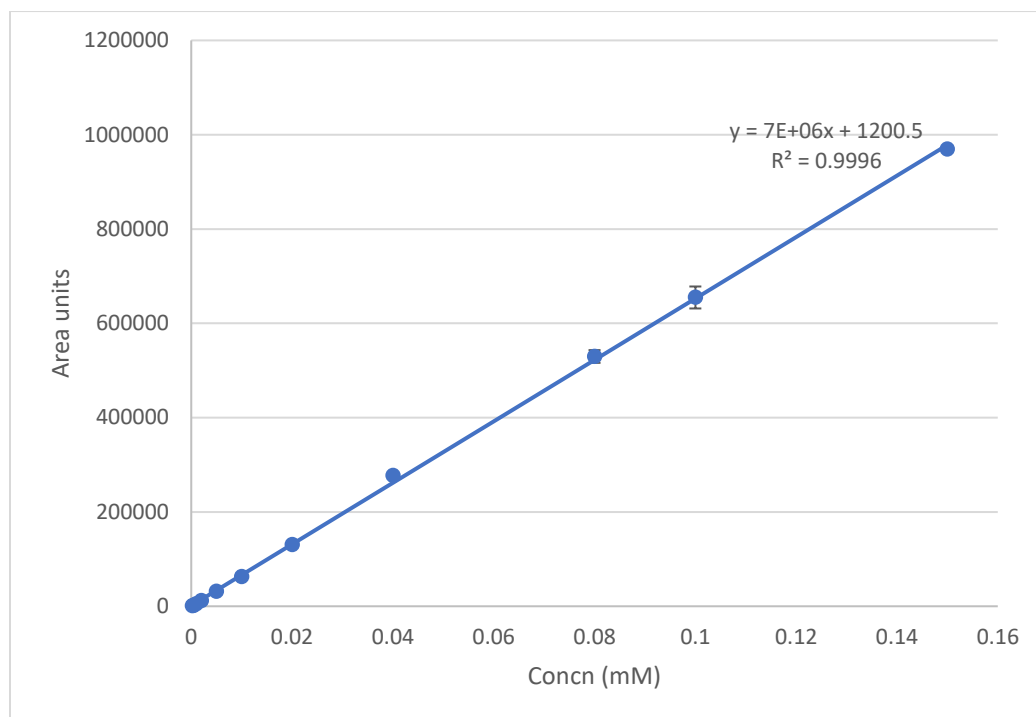


Fig. D-1 Calibration curve of Acet in mix-5

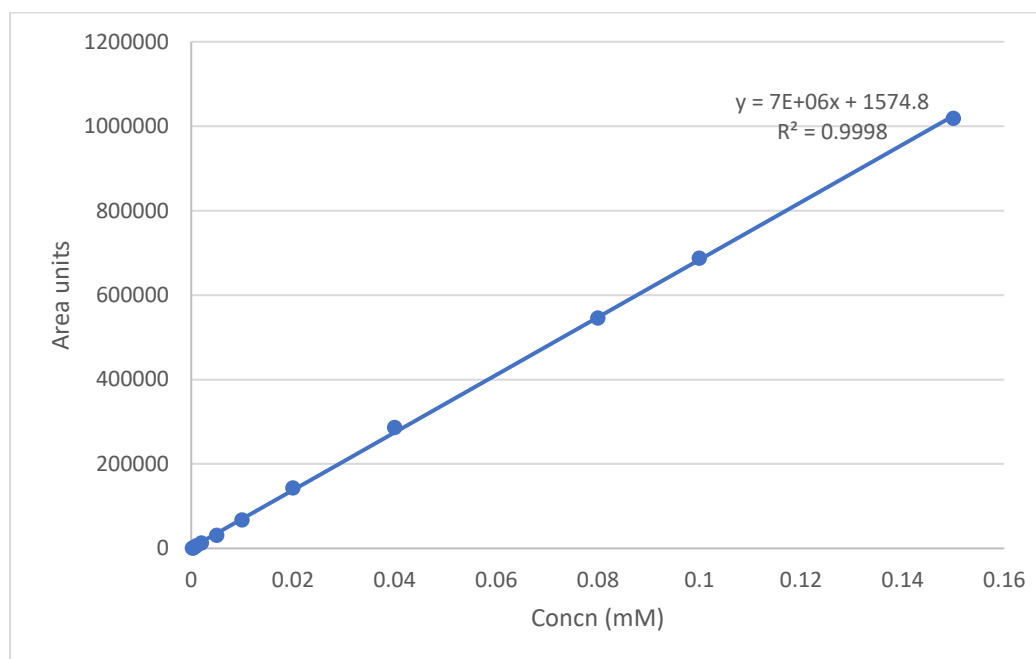


Fig. D-2 Calibration curve of PHBA in mix-5

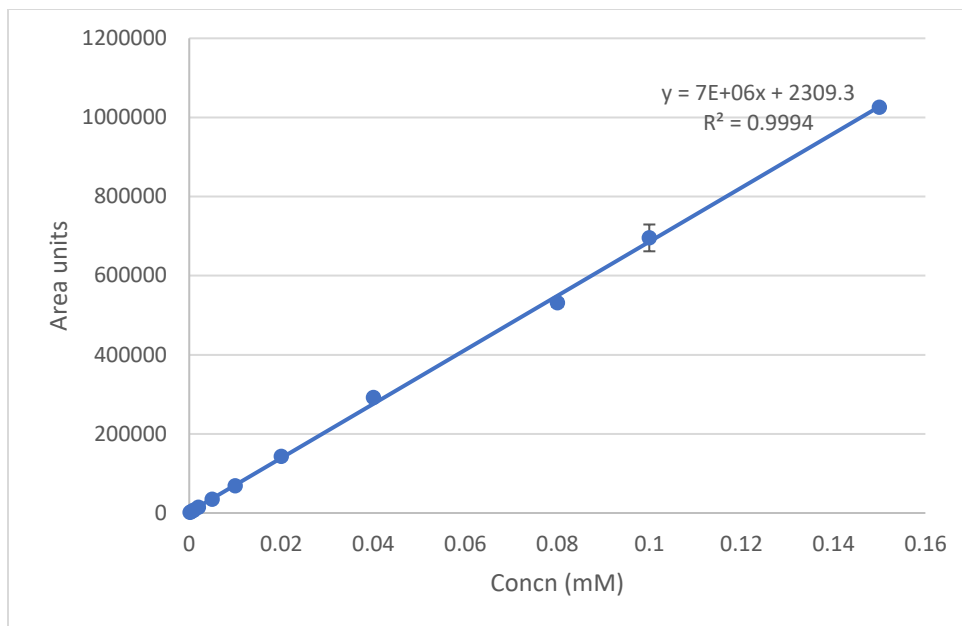


Fig. D-3 Calibration curve of MP in mix-5

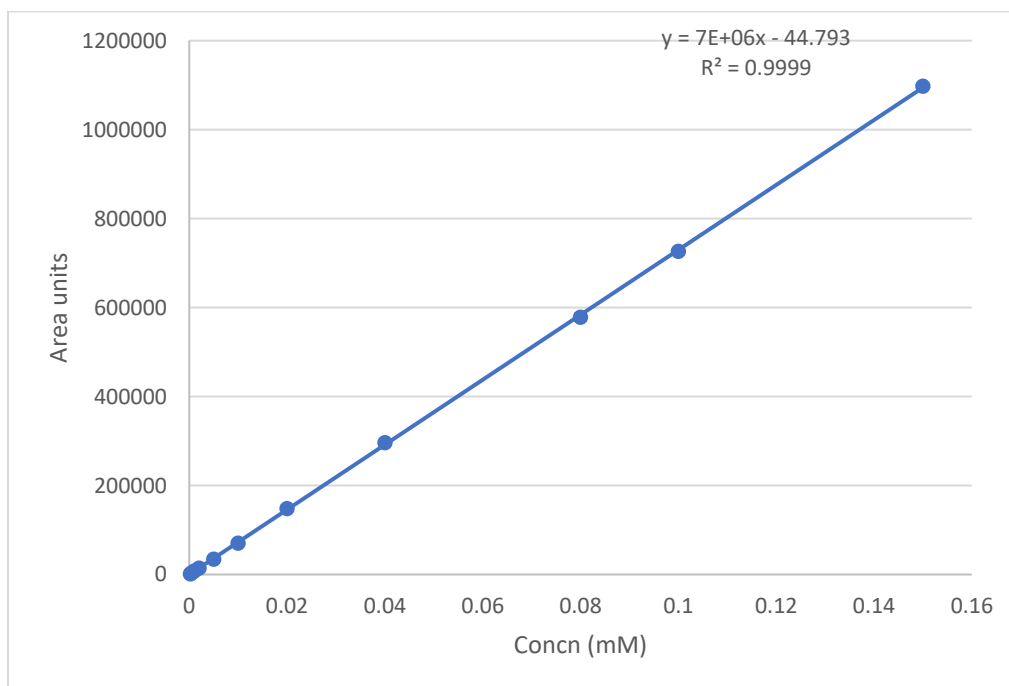


Fig. D-4 Calibration curve of PP in mix-5

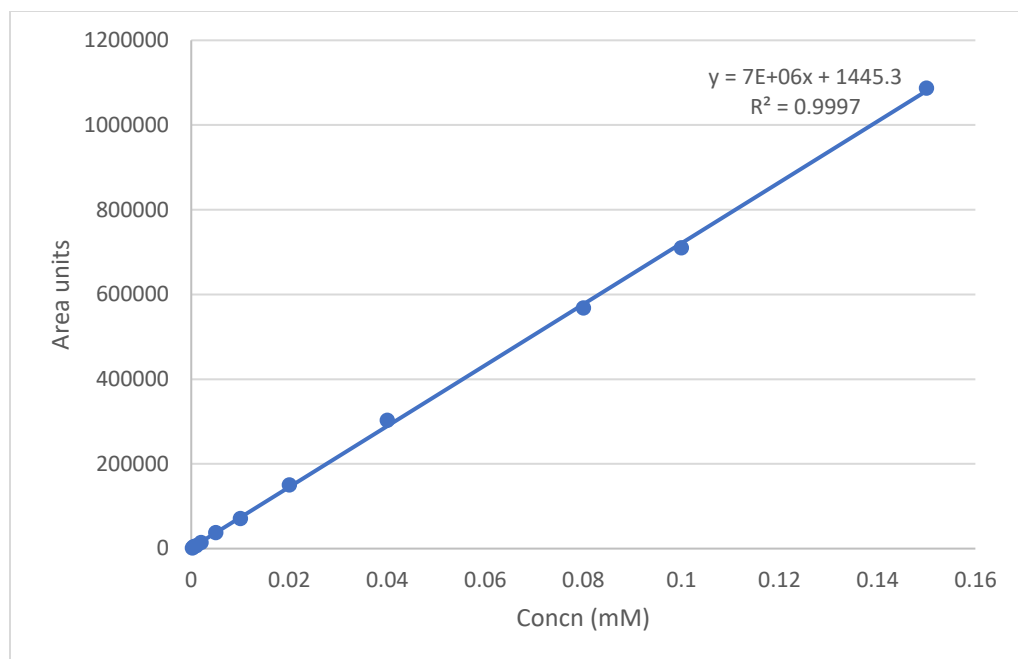


Fig. D-5 Calibration curve of BP in mix-5

Table D-1 Summary of retention times and calibration curves' properties of CECs in mix-5 at 247 nm

CEC	Ext. coef. ($M^{-1} cm^{-1}$) ($\times 10^3$)	Intercept	r^2 value	Concn Range (μmol)	t_R (min)	LOD (mM)	LOQ (mM)
Acet.	6514 \pm 43	1200 \pm 2595	0.9996	0.5 - 150	2.63	0.001	0.004
PHBA	6819 \pm 35	1574 \pm 2118	0.9998	0.5 - 150	4.06	0.001	0.003
MP	6834 \pm 56	2309 \pm 3433	0.9994	0.2 - 150	7.37	0.002	0.005
PP	7307 \pm 16	137 \pm 9610	0.9999	0.2 - 150	10.1	0.001	0.002
BP	7193 \pm 44	1445 \pm 2684	0.9997	0.2 - 150	11.4	0.001	0.004

Appendix E Effects of varying SBP and peroxide on compounds removal in mix-5

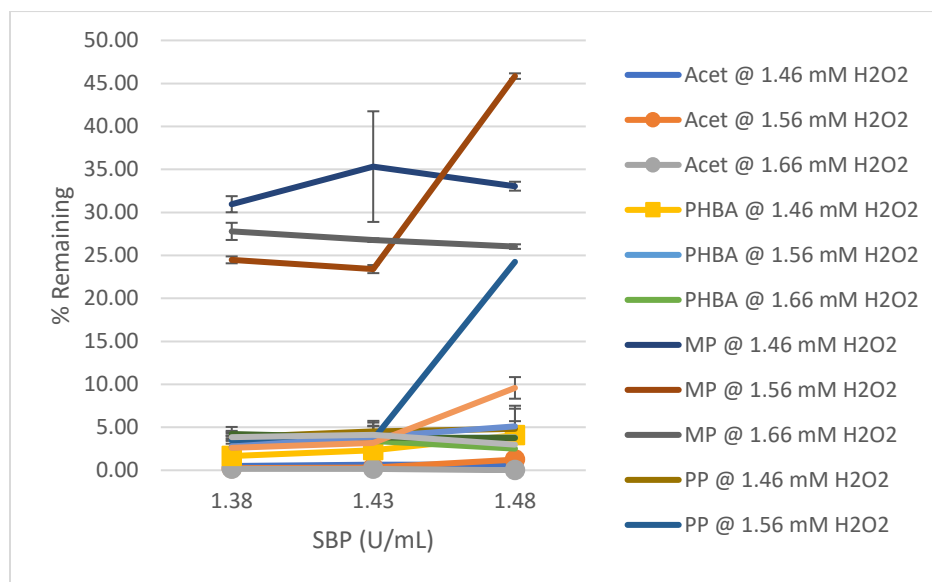


Fig. E-1 Effect of Varying amount of SBP and H₂O₂ concentrations on removal of contaminants. Conditions: 0.2 mM each of the compounds, 40 mM pH 6.5 phosphate buffer incubated for 3 h at the respective concentrations of H₂O₂ and SBP

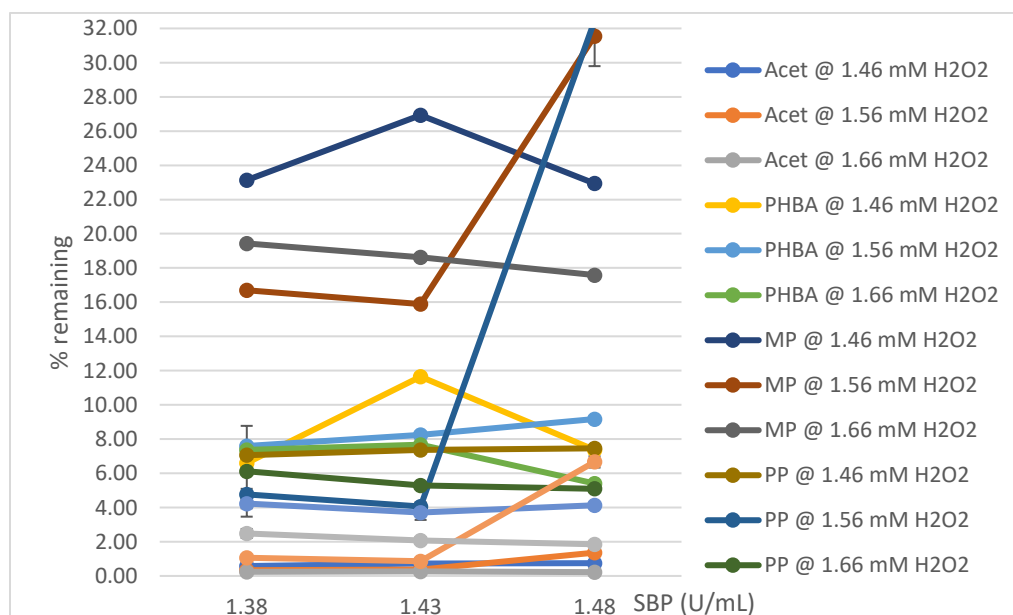


Fig. E-2 Effect of Varying amount of SBP and H₂O₂ concentrations on removal of contaminants. Conditions: 0.2 mM each of the compounds, 40 mM pH 6.5 phosphate buffer incubated for 5 h at the respective concentrations of H₂O₂ and SBP

Appendix F: ASAP(-) mass spectra of MP, PP and BP detected in supernatants of single-compound SBP treatments

ASAP(-) sen mode MS, lockspray, Probe T=300oC, source 100oC, t=(
JA_ASAPneg190911_BYMPsol_001 152 (1.498) AM2 (Ar,22000.0,554.26,0.00,LS
4.99e5

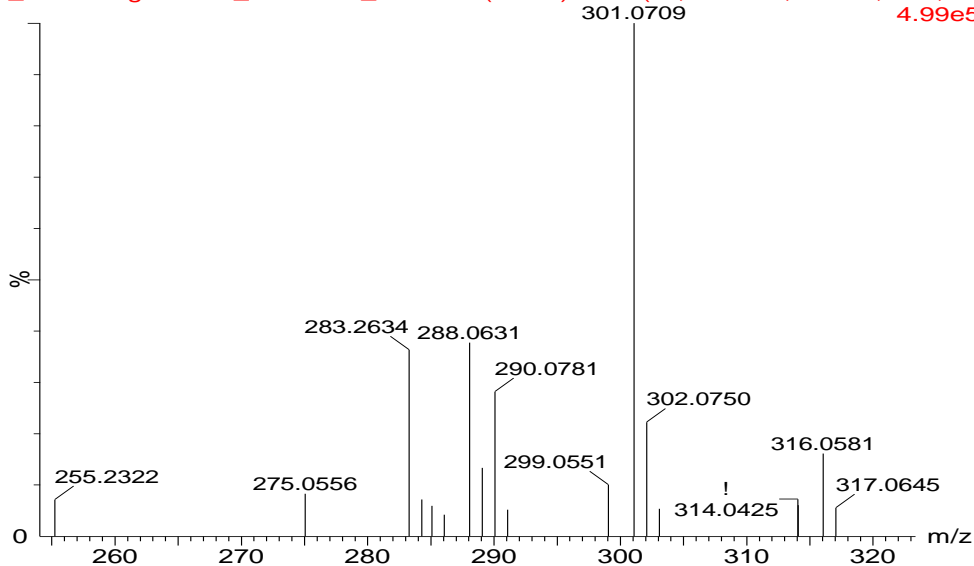


Fig. F-1 ASAP(-) mass spectrum of MP supernatant showing dimer and oxygenated dimer at m/z 301.0709 and 316.0581

ASAP(-) sen mode MS, lockspray, Probe T=300oC, source 100oC, t=(
JA_ASAPneg190911_BYMPsol_001 122 (1.202) AM2 (Ar,22000.0,554.26,0.00,LS
2.78e4

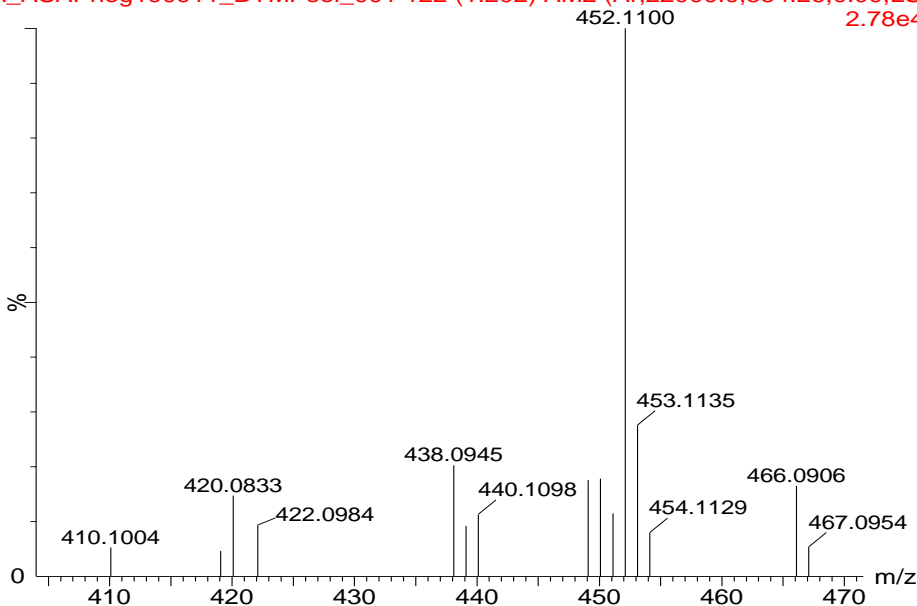


Fig. F-2 ASAP(-) mass spectrum of MP supernatant showing trimer and oxygenated trimer at m/z 451.1015 and 466.0906, respectively

ASAP(-) sen mode MS, lockspray, Probe T=300oC, source 100oC, t=(
JA_ASAPneg190911_BYMPsol_001 155 (1.524) AM2 (Ar,22000.0,554.26,0.00,LS
1.88e5

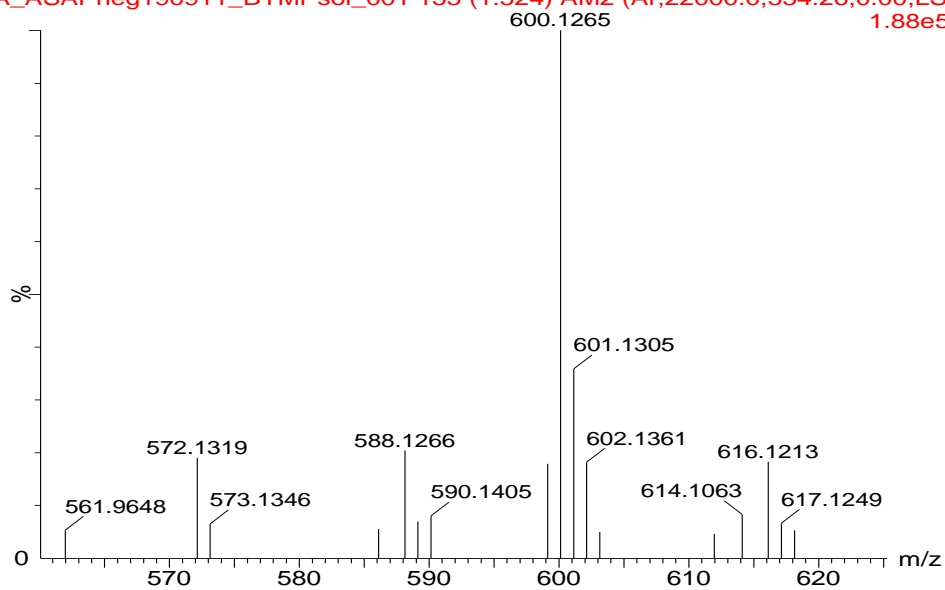


Fig. F-3 ASAP(-) mass spectrum of MP supernatant showing tetramer and oxygenated tetramer at m/z 601.1305 and 616.1213, respectively

ASAP(-) sen mode MS, lockspray, Probe T=300oC, source 100oC, t=(
JA_ASAPneg190911_BYMPsol_001 155 (1.524) AM2 (Ar,22000.0,554.26,0.00,LS
3.37e3

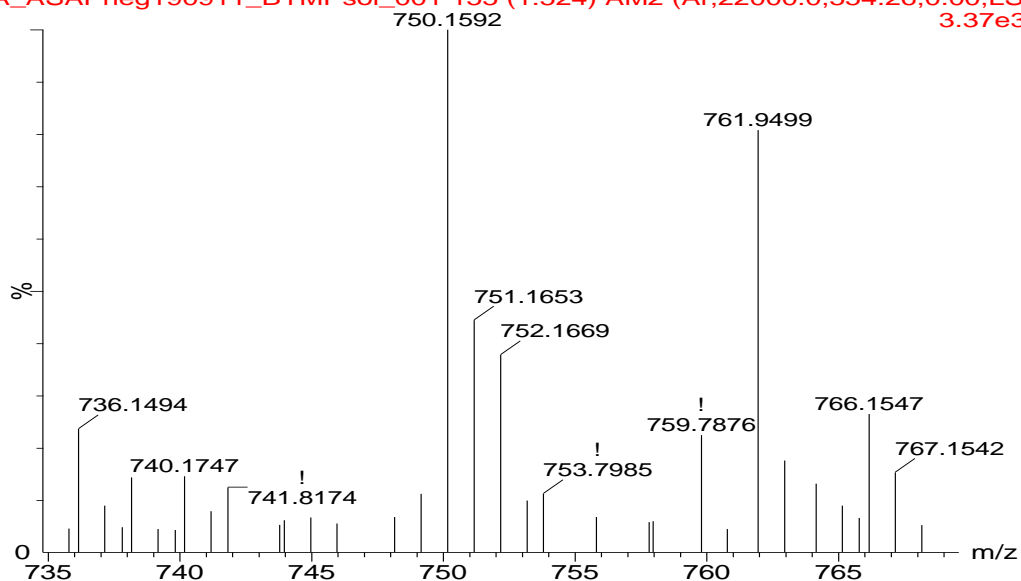


Fig. F-4 ASAP(-) mass spectrum of MP supernatant showing pentamer and oxygenated pentamer at m/z = 751.1653 and 766.1547, respectively

ASAP(-) sen mode MS, lockspray, Probe T=300oC, source 100oC, t=(
JA_ASAPneg190911_BYMPsol_002 176 (1.724) AM2 (Ar,22000.0,554.26,0.00,LS
1.37e3

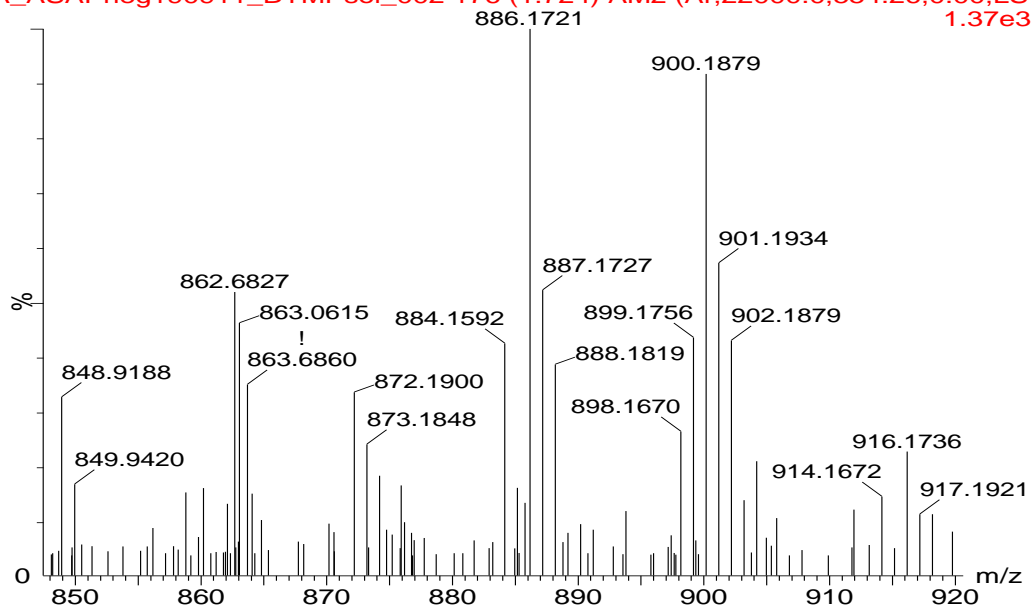


Fig. F-5 ASAP(-) mass spectrum of MP supernatant showing hexamer and oxygenated hexamer at m/z = 901.1934 and 916.1736, respectively

ASAP(-) sen mode MS, lockspray, Probe T=300oC, source 100oC, t=0 IP
JA_ASAPneg190911_BYPPsol_002 167 (1.647) AM2 (Ar,22000.0,554.26,0.00,LS 10);
4.59e5

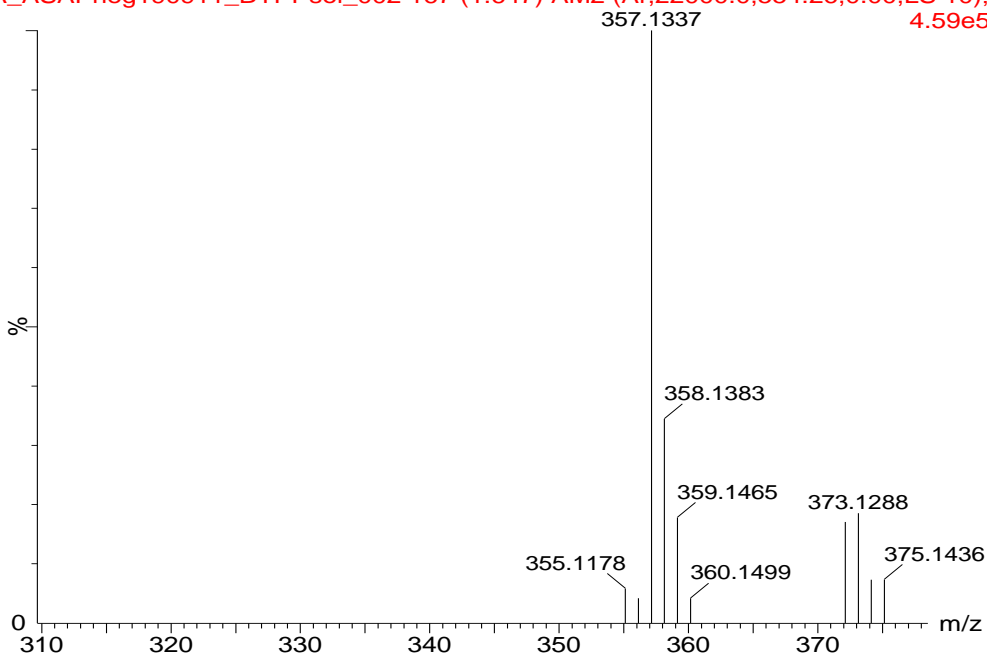


Fig. F-6 ASAP(-) mass spectrum of PP supernatant showing dimer at m/z 357.1337

ASAP(-) sen mode MS, lockspray, Probe T=300oC, source 100oC, t=0 IP
JA_ASAPneg190911_BYPPsol_002 167 (1.647) AM2 (Ar,22000.0,554.26,0.00,LS 10);
1.28e5

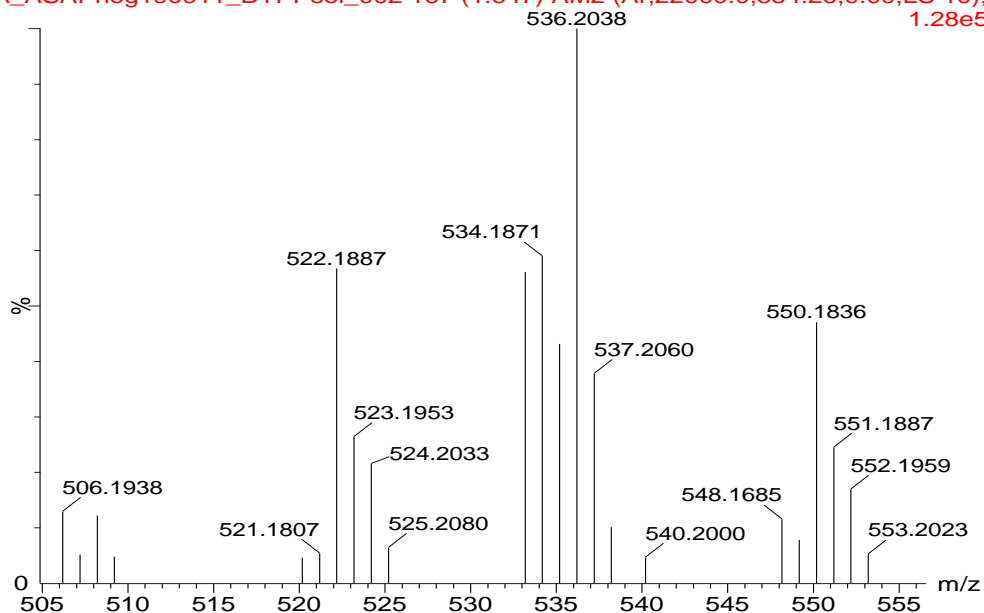


Fig. F-7 ASAP(-) mass spectrum of PP supernatant showing trimer and oxygenated trimer at m/z 535.1945 and 550.1836, respectively

ASAP(-) sen mode MS, lockspray, Probe T=300oC, source 100oC, t=0 IP
JA_ASAPneg190911_BYPPsol_001 148 (1.464) AM2 (Ar,22000.0,554.26,0.00,LS 10);
2.54e4

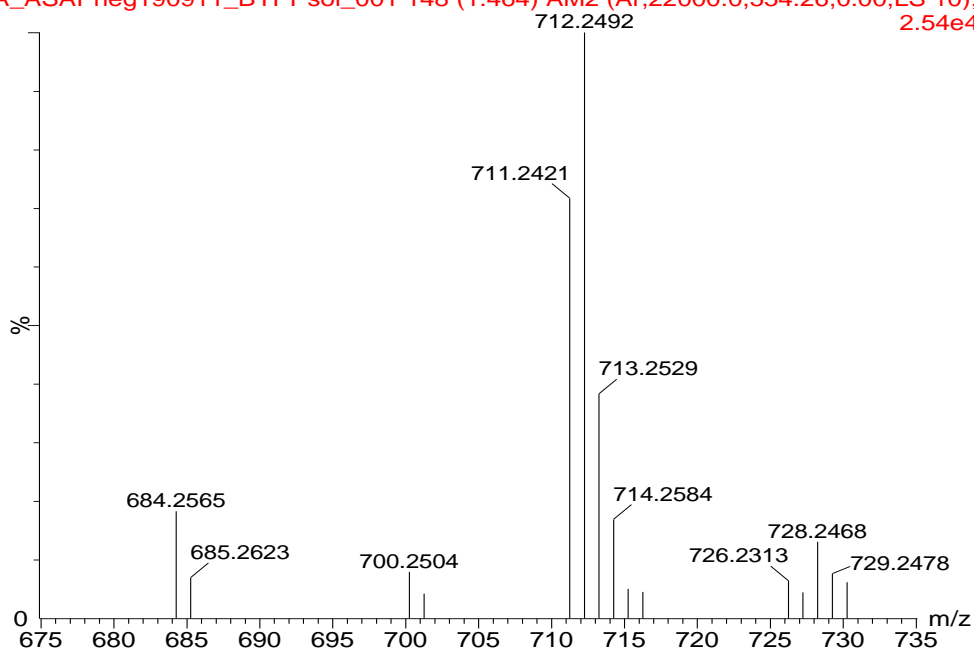


Fig. F-8 ASAP(-) mass spectrum of PP supernatant showing tetramer and oxygenated tetramer at m/z 713.2529 and 728.2468, respectively

ASAP(-) sen mode MS, lockspray, Probe T=300oC, source 100oC, t=0 IPwCap, BY
JA_ASAPneg190909_BYBPsol_004 281 (2.743) AM2 (Ar,22000.0,554.26,0.00,LS 10); Cm (276:28
2.95e5

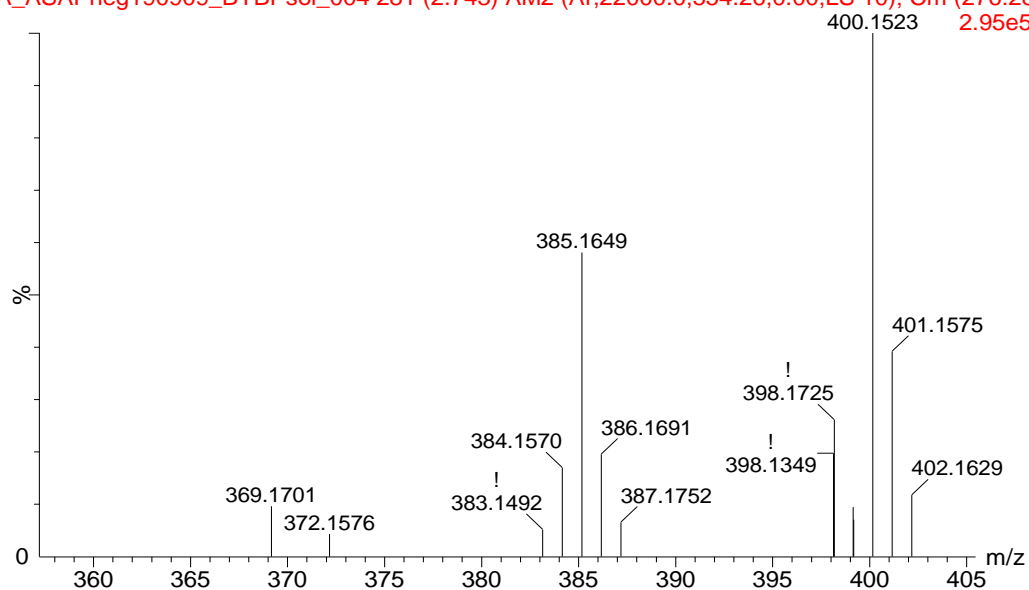


Fig. F-9 ASAP(-) mass spectrum of BP supernatant showing dimer and oxygenated dimer at m/z=385.1649 and 400.1523, respectively

ASAP(-) sen mode MS, lockspray, Probe T=300oC, source 100oC, t=0 IPwCap, BY
JA_ASAPneg190909_BYBPsol_004 281 (2.743) AM2 (Ar,22000.0,554.26,0.00,LS 10); Cm (276:28
3.25e5

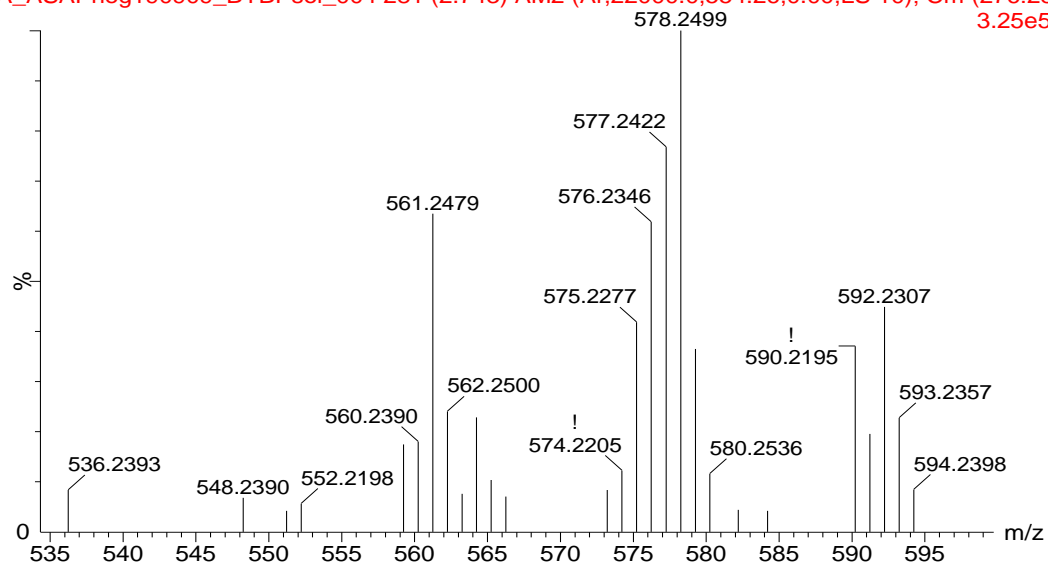


Fig. F-10 ASAP(-) mass spectrum of BP supernatant under optimized conditions showing trimer and oxygenated trimer at m/z 577.2422 and 592.2307, respectively

ASAP(-) sen mode MS, lockspray, Probe T=300oC, source 100oC, t=0 IPwC
JA_ASAPneg190909_BYBPsol_004 170 (1.672) AM2 (Ar,22000.0,554.26,0.00,LS 10); ABS
1.08e6

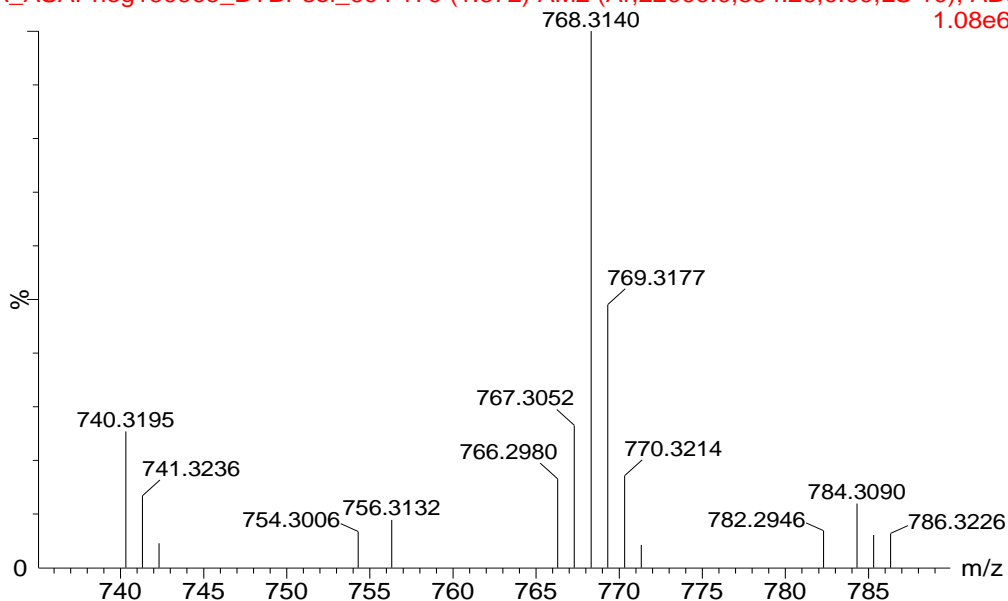


Fig. F-11 ASAP(-) mass spectrum of BP supernatant under optimized conditions showing tetramer and oxygenated tetramer at 769.3177 and 784.3090, respectively

ASAP(-) sen mode MS, lockspray, Probe T=300oC, source 100oC, t=0 IPwC
JA_ASAPneg190909_BYBPsol_004 170 (1.672) AM2 (Ar,22000.0,554.26,0.00,LS 10); ABS
4.12e4

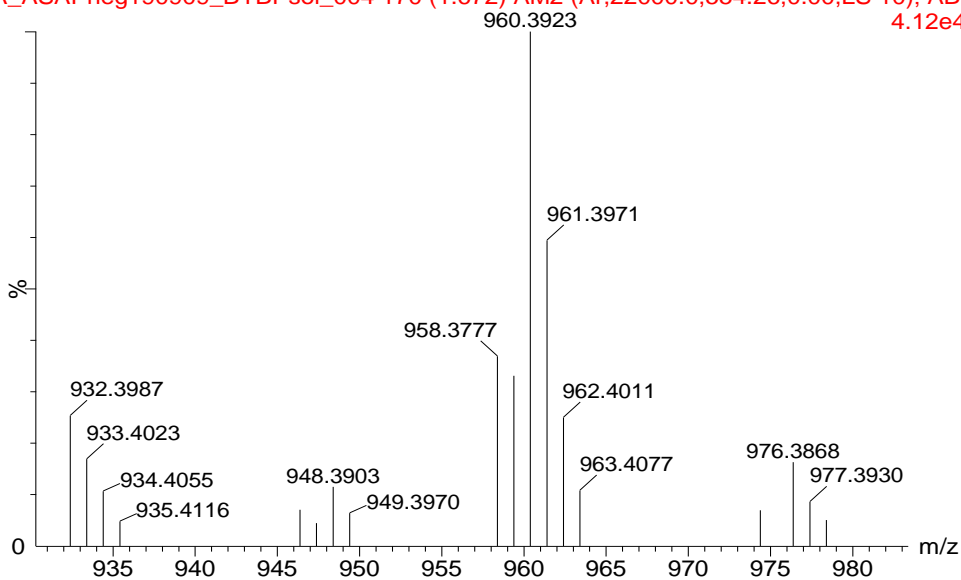


Fig. F-12 ASAP(-) mass spectrum of BP supernatant under optimized conditions showing pentamer and oxygenated pentamer at 961.3971 and 976.3868, respectively

ASAP(-) sen mode MS, lockspray, Probe T=300oC, source 100oC, t=0 IPwCap, BY
JA_ASAPneg190909_BYBPsol_004 281 (2.743) AM2 (Ar,22000.0,554.26,0.00,LS 10); Cm (276:28
7.67e3

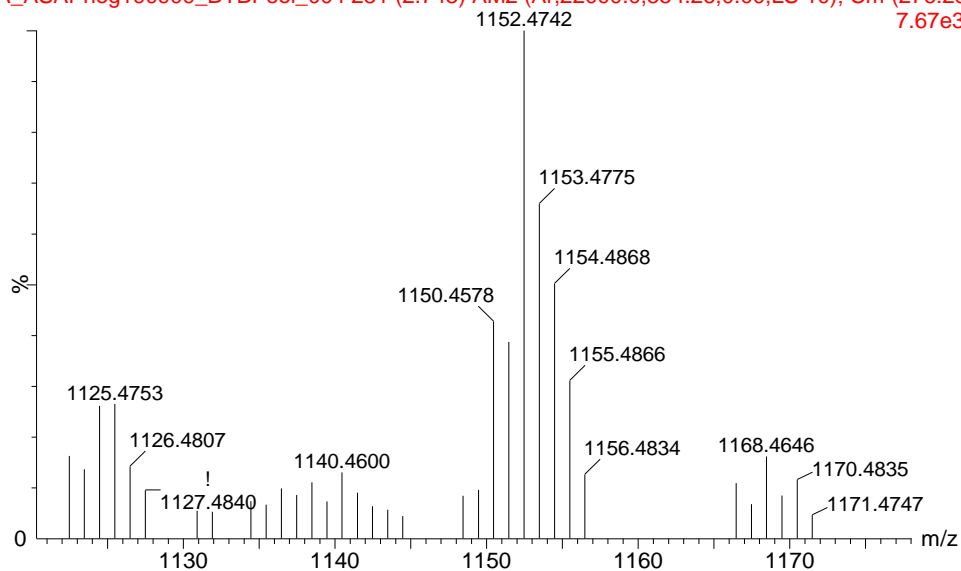


Fig. F-13 ASAP(-) mass spectrum of BP supernatant under optimized conditions showing hexamer and oxygenated hexamer at 1153.4775 and 1168.4646, respectively

ASAP(-) sen mode MS, lockspray, Probe T=300oC, source 100oC, t=0 IPwC
JA_ASAPneg190909_BYBPsol_004 217 (2.135) AM2 (Ar,22000.0,554.26,0.00,LS 10); ABS
434

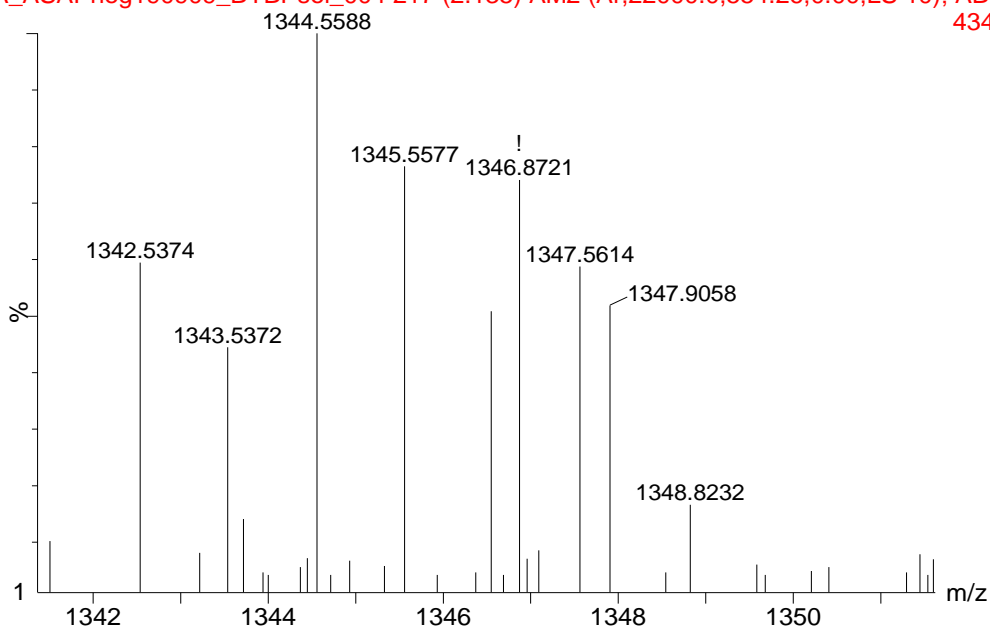


Fig. F-14 ASAP(-) mass spectrum of BP supernatant under optimized conditions showing heptamer at m/z = 1345.5577

Appendix G: SPE Experiments – preamble for real wastewater treatment

One of the objectives of the study was to attempt the application of synthetic wastewater-derived optimized parameters to real wastewater. However, the onset of Covid-19 and related remote working mode necessitated a stop to this objective. Before the University closure, a SPE protocol was developed (Appendix G) and applied to the extraction of the target compounds. This showed recoveries between of 74 ± 2 and $88\pm 0.3\%$ for PHBA and BP, respectively. The protocol shows prospects for application to a real wastewater scenario. It is hoped, this effort may be continued by a curious mind.

Appendix H: SPE protocol and recoveries

SPE protocol

A SPE protocol previously developed within the group was used modified as presented below:

- Introduce a SPE cartridge (Hydrophilic-lipophilic balance, HLB cartridges were used for this study) onto the vacuum manifold, and close tight any opening not holding a cartridge
Preconditioning
- Precondition the cartridge with 10 ml ACN and 5 ml methanol/distilled water (1:1)
Equilibration
- Equilibrate the cartridge with 10 ml distilled water
Loading
- Wait for 15 minutes under vacuum and pass the water sample through the cartridge at a flow rate between 3 and 6 ml/min using a vacuum manifold. Ensure the flow does not cease through the extraction time
Washing
- Wash the cartridge with 5 mL distilled water (0.01 M HCl) and then with 5 ml methanol/distilled water (0.01 M HCl) (5:95)
- Use air to expel the liquid and dry the cartridge under vacuum for 30 minutes.
Elution
- Elute the cartridge with 20 ml ACN in four aliquots of 5 mL each
Evaporation
- Evaporate all ACN from the sample by passing a gentle stream of nitrogen with sample immersed in water bath heated to between 30°C and 40°C
- Once the ACN is evaporated, dissolve compounds with 1 mL of ACN

Following the above protocol, compounds recovery in mix-5 with synthetic wastewater initially containing $40\ \mu\text{M}$ of each compound was determined.

Table G-1 Recovery of compounds in mix-5 following SPE

% (v/v) organic solvent wash	Acet		PHBA		MP		PP		BP	
	% recovery	STD	% recovery	STD	% recovery	STD	% recovery	STD	% recovery	STD
5%	86.7	0.1	74	2.0	80.7	0.7	85	3	87.7	0.30
30%	14.8	1.3	69.5	0.4	81	5	86	5	88	2

VITA AUCTORIS

NAME: Baturh Yarkwan

PLACE OF BIRTH: Jaki, Ishangev-Ya, Kwande LG, Benue State, Nigeria

DATE OF BIRTH October, 1980

EDUCATION Ph.D., Chemistry and Biochemistry
University of Windsor
Windsor, Ontario, Canada 2021
M.Sc., Industrial Biochemistry and Biotechnology
University of Nigeria,
Nsukka, Enugu State, Nigeria, 2009
B.Tech. (Hons.) Biochemistry (major) Microbiology (Minor)
Federal University of Technology,
Minna, Niger State, Nigeria, 2004